INITIAL LABORATORY STUDY OF THE SHEAR STRENGTH PROPERTIES OF COMPACTED, HIGHLY PLASTIC CLAYS USED FOR HIGHWAY EMBANKMENT CONSTRUCTION IN THE AREA OF HOUSTON, TEXAS

Alexander W. Gourlay and
Stephen G. Wright

A Report on Laboratory Testing Performed Under Interagency Contract Nos. (82-83) 2187 and (84-85) 1026

Conducted For

TEXAS STATE DEPARTMENT OF HIGHWAYS AND
PUBLIC TRANSPORTATION-DISTRICT 12

CENTER FOR TRANSPORTATION RESEARCH
BUREAU OF ENGINEERING RESEARCH
THE UNIVERSITY OF TEXAS AT AUSTIN
SEPTEMBER 1984

INITIAL LABORATORY STUDY OF THE SHEAR STRENGTH PROPERTIES OF COMPACTED, HIGHLY PLASTIC CLAYS USED FOR HIGHWAY EMBANKMENT CONSTRUCTION IN THE AREA OF HOUSTON, TEXAS

Alexander W. Gourlay
Stephen G. Wright

A Report on Laboratory Testing
Performed Under
Interagency Contract Nos.
(82-83)2187
and
(84-85)1026

Conducted for

Texas
State Department of Highways and Public Transportation
District 12

by the

CENTER FOR TRANSPORTATION RESEARCH
BUREAU OF ENGINEERING RESEARCH
THE UNIVERSITY OF TEXAS AT AUSTIN

September 1984

The contents of this report reflect the views of the authors, who are responsible for the facts and the accuracy of the data presented herein. The contents do not necessarily reflect the official views or policies of the Federal Highway Administration. This report does not constitute a standard, specification, or regulation.

There was no invention or discovery conceived or first actually reduced to practice in the course of or under this contract, including any art, method, process, machine, manufacture, design or composition of matter, or any new and useful improvement thereof, or any variety of plant which is or may be patentable under the patent laws of the United States of America or any foreign country.

PREFACE

A number of embankment slopes have been constructed in District 12 of the Texas State Department of Highways and Public Transportation (SDHPT) using a highly plastic clay, locally referred to as "Beaumont" clay. Many of these embankments have experienced significant problems with slides occurring a number of years after construction. In June of 1983 an Interagency Contract was initiated between the Texas SDHPT and The Center for Transportation Research (CTR) for CTR to perform a series of laboratory tests to measure the shear strength properties of Beaumont clay from selected embankments which had failed. A first contract was completed 31 August 1983 and a new contract was approved 30 November 1983 to continue the laboratory testing program. Results of the laboratory tests performed under the first and a portion of the second contracts were presented in a special draft report to the SDHPT as part of the contract work; no formal reports were planned other than the draft report. However, the results of the study have been judged to be of sufficient use to warrant a more formal report, available for wider distribution. Accordingly, this current report is being printed. The current report is essentially identical to the earlier Interagency contract report. Later phases of the work performed under the interagency contracts have already been reported by Green and Wright (1986) in Research Report 436-1.

ABSTRACT

This report presents the results of the first series of tests performed to measure the long-term strength properties of "Beaumont" clay. The soil tested in this study was taken from several embankments which have experienced slope failures in District 12 of the Texas State Department of Highways and Public Transportation.

Results of compaction tests performed using several different compaction procedures and efforts, including ones used by the Texas SDHPT as well as ASTM standard procedures, are summarized. Effective stress shear strength parameters were determined using unconsolidated-undrained triaxial shear tests procedures, with pore pressure measurements. Specimen preparation and testing procedures, as well as results, are presented.

The data presented in this report has been used in subsequent studies by Stauffer and Wright (1984); this report constitutes the primary documentation of the shear strength data used in the studies by Stauffer and Wright. The work presented in this report also served as a the catalyst for Research Project 3-8-85-436, which involved much more detailed laboratory testing.

SUMMARY

This report presents the results of laboratory tests which have been performed to define the shear strength properties of highly plastic clay soils used for construction of embankments in District 12 and Houston Urban districts of the Texas State Department of Highways and Public Transportation. A number of embankment slopes which have been constructed of such highly plastic soils, locally referred to as "Beaumont" clay, have experienced significant problems with slides which occur a number of years after construction. In response to this problem, and recognition that very little was known about the long-term shear strength properties of the highly plastic soils involved, an Interagency Contract was initiated between the Texas SDHPT and The Center for Transportation Research in June of 1983 to perform laboratory tests to measure the shear strength properties of soils from selected embankments which had failed. The first contract was completed 31 August 1983 and a new contract was approved 30 November 1983 to continue the laboratory testing program. This report presents results of the laboratory tests performed under the first and a portion of the second contracts.

IMPLEMENTATION STATEMENT

The results of the testing presented in this report and work presented by Stauffer and Wright (1984) revealed that a significant discrepancy exists between the effective stress ("drained") shear strength parameters determined in conventional laboratory unconsolidated-undrained triaxial shear tests and those determined from actual slope failures. This discrepancy was the focus of a later Research Project 3-8-85-436, which led to the discovery that repeated wetting and drying would reduce the effective stress shear strength parameters to values less than those produced by simply wetting (and saturating) the soil once.

The effects of repeated wetting and drying are still not fully understood and cannot be predicted reliably. However, it is evident that conventional laboratory tests performed on specimens which have not been subjected to repeated wetting and drying may result in substantial overestimates of the long-term, effective stress, shear strength parameters applicable to the field. Further study of the effects of repeated wetting and drying on the strength properties of Beaumont clay are needed. The information on basic soil properties provide in this report should be useful to such future studies.

TABLE OF CONTENTS

LIST OF FIGURES

LIST OF TABLES

CHAPTER 1: INTRODUCTION

A relatively large number of embankments in south central Texas have experienced slides in recent years. During the last approximately two years, there have been over 25 such slides in highway embankments in the Houston area alone. The slides appear to have a number of commor features: they generally occur in embankments with side slopes ranging from 2.5:1 to 3:1 (horizontal:vertical); they generally occur between 15 and 20 years after the construction of the embankment; the slide surface is between three and five feet below the surface of the slope; and the material in which the slides have occurred is usually a highly plastic soil taken from borrow pits in the local Beaumont clay formation.

While a large number of embankments have been constructed of highly plastic clays in south central Texas and a number have experienced slides, almost no information could be found on the shear strength properties of such clays in the compacted, rather than natural, state. Accordingly, a laboratory testing program was initiated to determine the relevant strength properties. The program was specifically directed toward determining the effective stress shear strength parameters of compacted Beaumont clay using conventional laboratory triaxial shear tests. This report presents the initial results of the laboratory testing program carried out at The University of Texas at Austin.

Soil was recovered for use in the testing program from two embankments where slides had occurred. The composition of the fill in

both embankments was extremely variable over short distances. In each embankment there appeared to be two distinct clays: a medium plastic clay and a highly plastic clay. It was decided that the efforts of the investigation would be concentrated on the two distinctly different soils from one of the two embankments which were sampled.

Specimens were compacted in the laboratory using procedures chosen to produce what were judged to be representive compaction conditions for the soil in the embankments. A series of conventional consolidated-undrained ($\bar{R}$) triaxial shear tests with pore water pressure measurements was performed to establish effective stress shear strength parameters for the two soils. One consolidated-drained (S) triaxial shear test was performed on a specimen of the more highly plastic clay to confirm the results from the undrained shear tests. In addition, another specimen of the highly plastic clay was subjected to ten cycles of consolidation and swell and then sheared under undrained ($\bar{R}$) conditions to simulate the effects of repeated shrinkage and swelling which occurs due to wetting and drying on the face of an embankment.

In Chapter 2, the two embankments and slides which were chosen for close investigation are described. The procedures which were used to recover soil from the embankments for use in the testing program are presented in Chapter 3. In Chapter 4, the index properties of the soils which were sampled are summarized. The compaction properties of two soils and the methods used to estimate the initial compaction conditions in the embankments are presented in Chapter 5. Two methods of compaction were studied to determine a procedure for compacting the triaxial test

specimens; the two methods and the results of these studies are presented in Chapter 6. In Chapter 7, the properties of the specimens immediately after compaction are examined. In Chapter 8, the shear test apparatus, methods used to set-up and consolidate the specimens in the triaxial cells, and the properties of the specimens after consolidation are presented. The procedures for triaxial shear testing and the results of the shear tests, including effective stress shear strength envelopes, are presented in Chapter 9. Finally, in Chapter 10, the effective stress strength parameters which were measured in the laboratory are compared with the values back-calculated from an analysis of one of the embankment slides; consideration is given to factors which might account for discrepancies between the measured and back-calculated strength parameters, and areas of research are suggested which may help to further explain the field behaviour of these compacted clays.

CHAPTER 2: SITE IDENTIFICATION AND DESCRIPTION

2.1. BACKGROUND

A preliminary objective of this investigation was to identify and select for further investigation and sampling embankments which had failed a number of years after construction. In recent years, over 25 such long-term embankment failures have been identified in the Houston, Texas area. The majority of these slides have been reworked in some manner by the Texas State Department of Highways and Public Transportation (the Texas SDHPT) in an attempt to prevent further sliding from occurring. These efforts have most commonly taken the form of recompaction, or lime-stabilization followed by recompaction. For the purposes of this investigation, such sites had to be excluded from consideration since a lime-stabilized soil would not be representative of the soil which had originally failed, and any reworking of the slope would make the mode and extent of the original failure uncertain.

An initial inspection tour of approximately eight embankment failures was made in February of 1983 by representatives of the Texas SDHPT, Federal Highway Administration, and The Center for Transportation Research (The University of Texas), at which time samples were taken for moisture content and Atterberg limit determinations. It was hoped that

this information would help to identify the "problem soils" in each embankment and make apparent any recurrent features of the slides.

Tests were performed by the Texas SDHPT and results provided for use in this study. The tests indicated the presence of clay soils in the embankments ranging from medium to high plasticity. The plastic limits fell within a relatively narrow band with an average of approximately 20 percent, while the plasticity indices varied from 33 to 53. The moisture contents of the samples which were taken showed a significant range of from 25 percent to 43 percent, with an average value of 31 percent.

It has been recognized that many of the surficial soils in the greater Houston area have a significant swell potential (Carothers, 1965, and United States Department of Agriculture, Soil Conservation Service, 1976). It was apparent that clay soils used for embankment fill in this region could behave in a similar fashion.

2.2. SITE SELECTION

Three embankments were selected for further investigation, largely on the basis of the Atterberg limits determined by the Texas SDHPT. The three embankments appeared to contain fill ranging from the highest to lowest plasticity of those examined in the intial inspection tour, were not covered with rip-rap, and were not thought to have been recompacted or reworked; this last factor was particularily essential to the measurement of slide geometries which would be used to

back-calculate the mobilized soil strengths at the time of failure. The sites selected were:

1. IH 610 South and Scott Street, NE Quadrant
2. SH 225 and SH 146, SW Quadrant
3. SH 225 and SH 146, NW Quadrant.

On March 15, 1983 these three sites were revisited with the intention of gathering information on slope geometry and obtaining further soil samples, including a relatively large volume of soil for the shear strength testing program on which this report is based.

When soil from the SH 225 and SH 146, NW Quadrant embankment was initially examined in the laboratory, it was noted that some samples of soil contained small lumps of a whitish material. It was thought that some degree of lime-stabilization might have taken place during construction and, for this reason, no soil from this site was used in the shear strength testing program. It was later found that the whitish material was actually a calcareous deposit often found in the Beaumont clay. In this report, however, the SH 225 and SH 146, NW Quadrant, site is not given any further consideration although Stauffer (1984), in his more general investigation of embankment failures in Texas, has reported slope geometries, index properties, and back-calculated shear strength parameters for the SH 225 and SH 146, NW Quadrant embankment failure.

2.2.1. IH 610 AND SCOTT STREET

The embankment in the north-east quadrant of the IH 610 and Scott Street interchange had failed in two areas. Figure 2.1 was redrawn from field sketches and indicates the extent of the failures. There was an older, well-defined shallow slide (on the left in Fig. 2.1) from which all the soil for the shear testing was taken, and an adjacent area that appeared to be slumping and on the verge of failing. By November 1983, the slumping had become severe and soil was being forced onto the roadway, although there was still no well-defined failure ("slip") plane.

On the portion of the slope which was slumping, rolls and dips were evident just down the slope from two cracks running parallel to the roadway. The cracks varied in width from one to three inches and did not appear to be more than one foot deep. The grass on the section which was slumping varied in color and thickness.

There was a heavy covering of weeds and other vegetation on the older slide mass, indicating a significantly different soil condition. It is possible that the disturbed soil was absorbing rain water that would normally have been shed by the slope. Some minor reworking of the lower portion of the older slide had been performed to prevent the soil from spilling onto the roadway.

Moisture content samples were taken from two hand-augered holes made at the locations shown in Fig. 2.1. The resulting moisture content and soil profiles are shown in Fig. 2.2. Although it is difficult to draw any significant conclusions from such a small body of data, it does

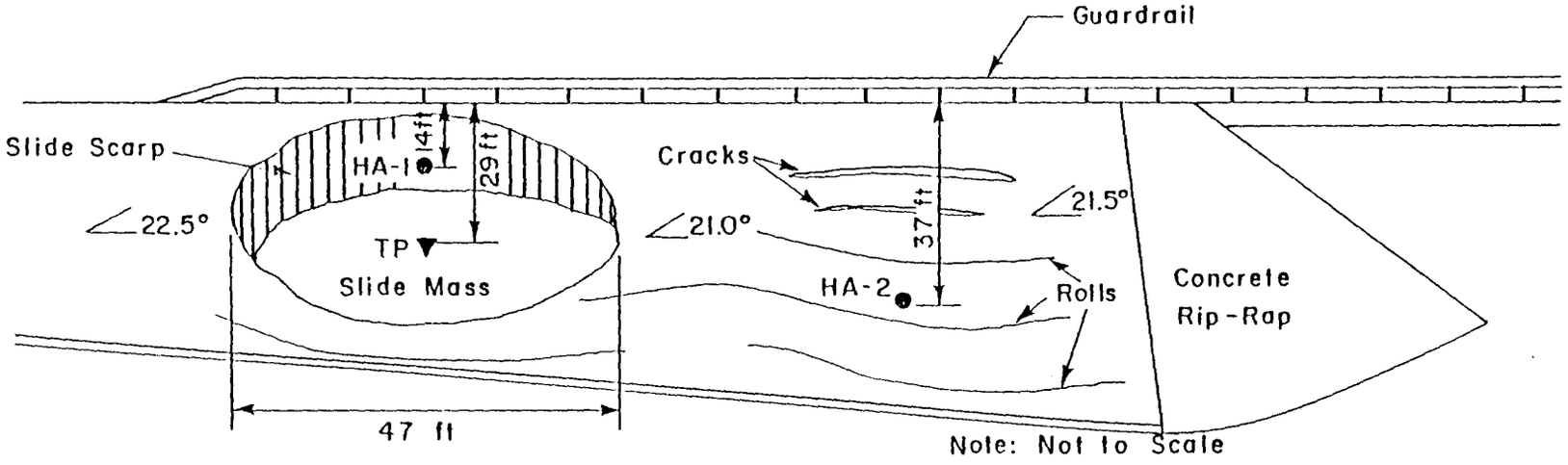

● HA Hand-augered Borehole
▼ TP Test Pit
21.0° Slope Angle Measurement

Fig. 2.1 Sketch of IH 610 and Scott Street (NE quadrant) Embankment Showing Extent of Slope Movement and Sampling Locations (redrawn from field sketch, 15 March 1983)

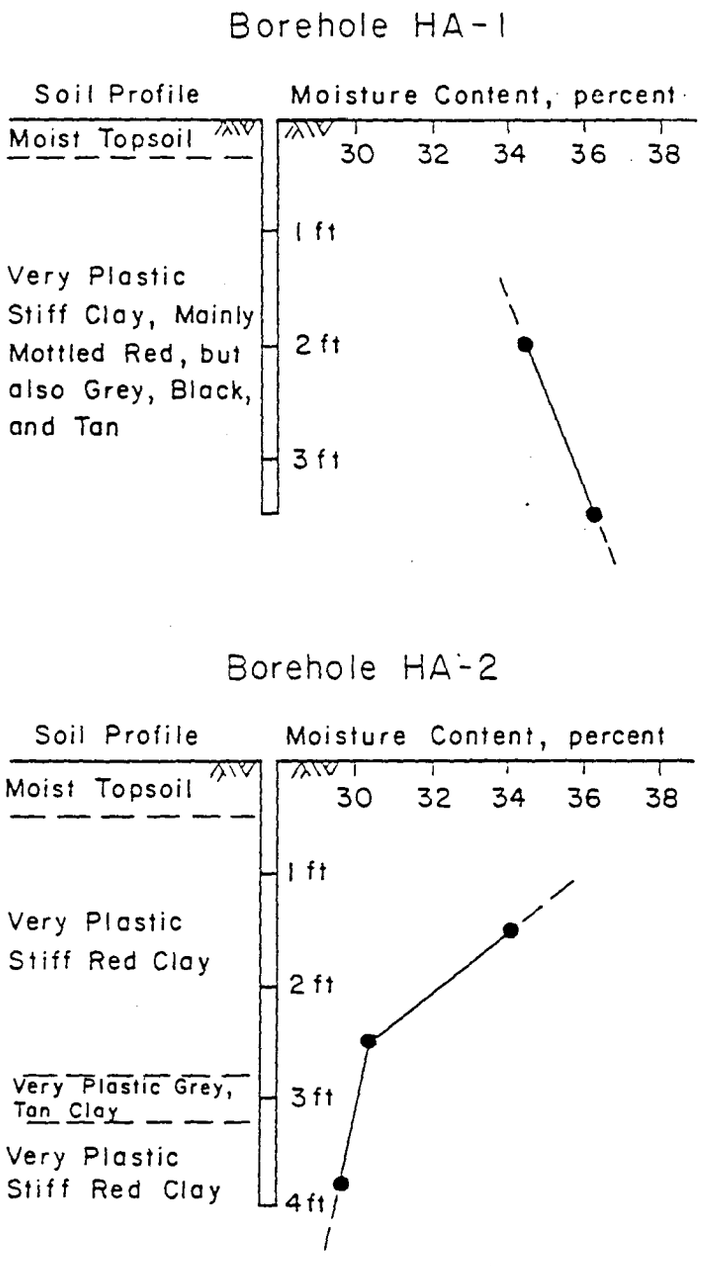

Fig. 2.2 Soil and Moisture Content Profiles for Two Hand-Augered Boreholes at IH 610 and Scott Street

appear that the average moisture content in the older slide mass (34 to 36 percent) was several percent higher than in the section of the slope which was currently slumping (with moisture contents ranging from 30 to 34 percent).

Stauffer (1984) presents slope geometry information for the IH 610 and Scott Street embankment. Figure 2.3 shows an estimated cross-section of the older slide mass as measured in March 1983. The field evidence lends support to the existence of a single failure surface in this particular case.

Information provided by the Texas SDHPT indicates that the embankment was constructed in 1966 and that it was composed of "Common Roadway Excavation and Fill (Clayey Soil)". Measurements taken in March 1983 indicate that the embankment is approximately 20 feet high, with side slopes varying between 2.4:1 and 2.6:1 in the vicinity of the slide.

2.2.2. SH 225 AND SH 146, SW QUADRANT

The embankment in the south-west quadrant of the SH 225 and SH 146 interchange contained one well-defined slide. Figure 2.4 was redrawn from field sketches and shows the position and the extent of the slide in relation to the embankment. Figure 2.5 shows an estimated cross-section through the slide and suggests that, although the initial failure may have occurred on a single surface, the scarp of the slide appears to have subsequently moved up the slope in a progressive manner.

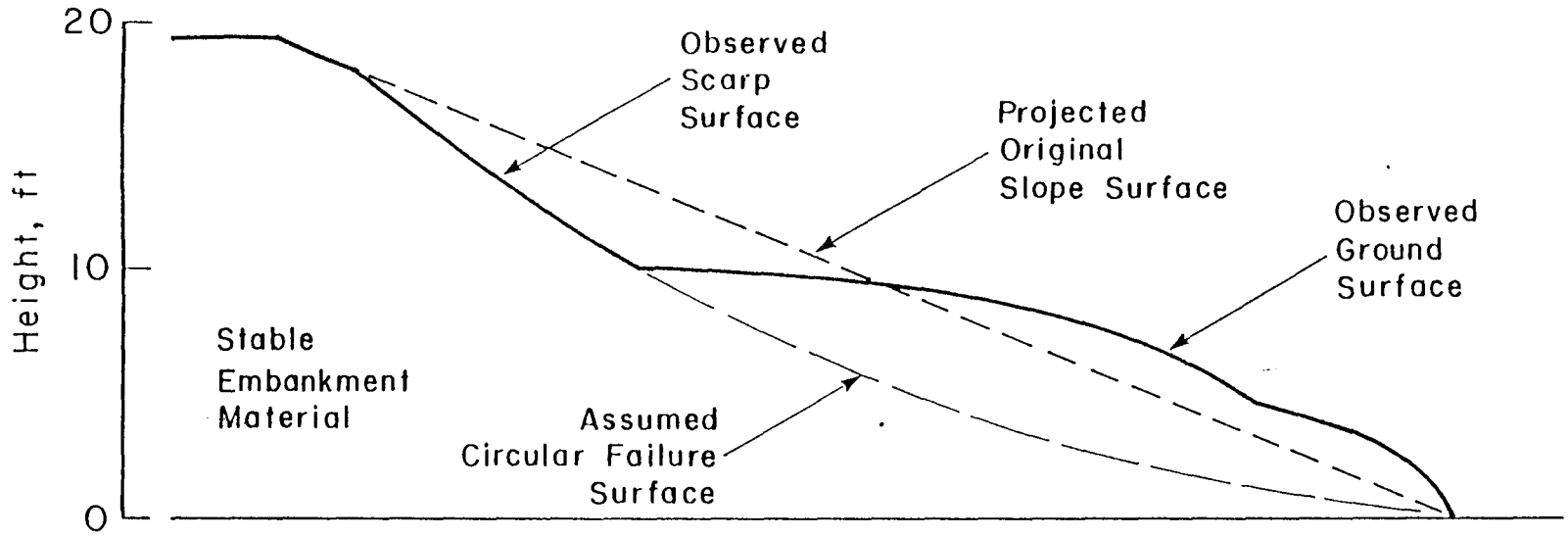

Fig. 2.3 Cross-section of Embankment Slide at Ill 610 and Scott Street

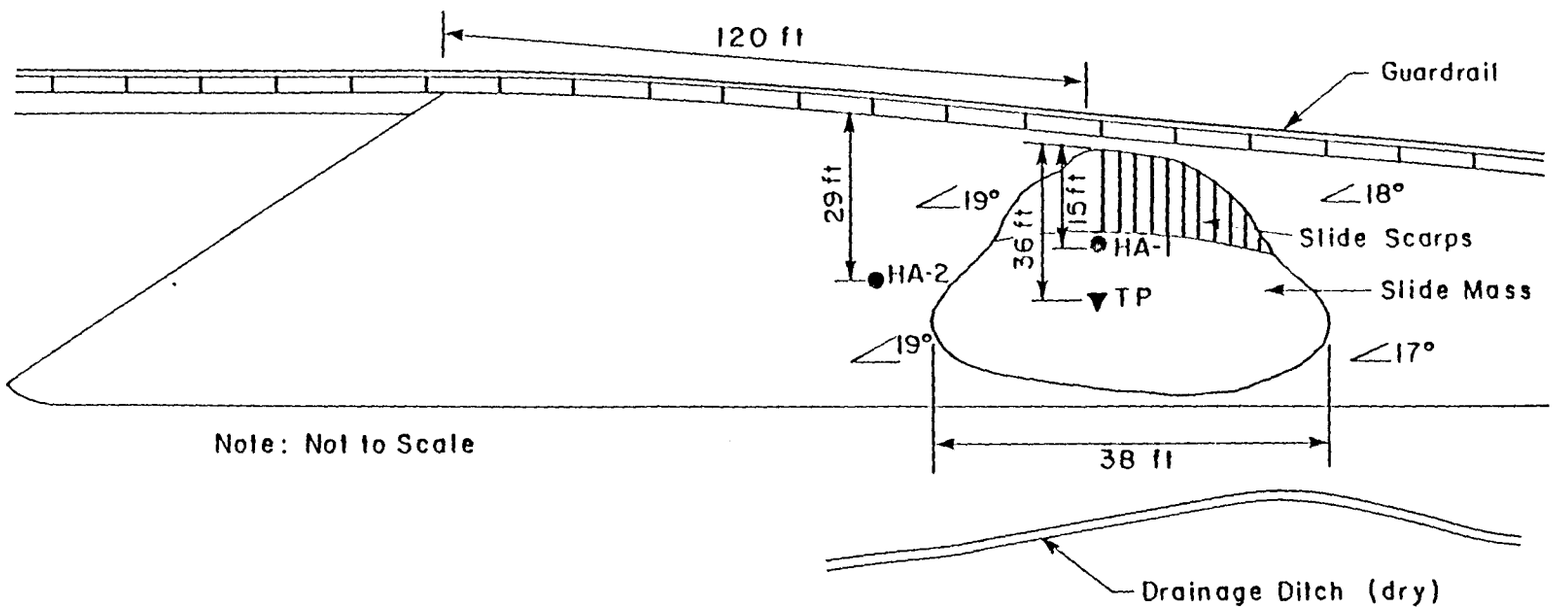

● HA Hand-augered Borehole
▼ TP Test Pit
∠19° Slope Angle Measurement

Fig. 2.4 Sketch of SH 225 and SH 146 (SW Quadrant) Embankment Showing Extent of Slope Movement and Sampling Locations (redrawn from field sketch, 15 March 1983)

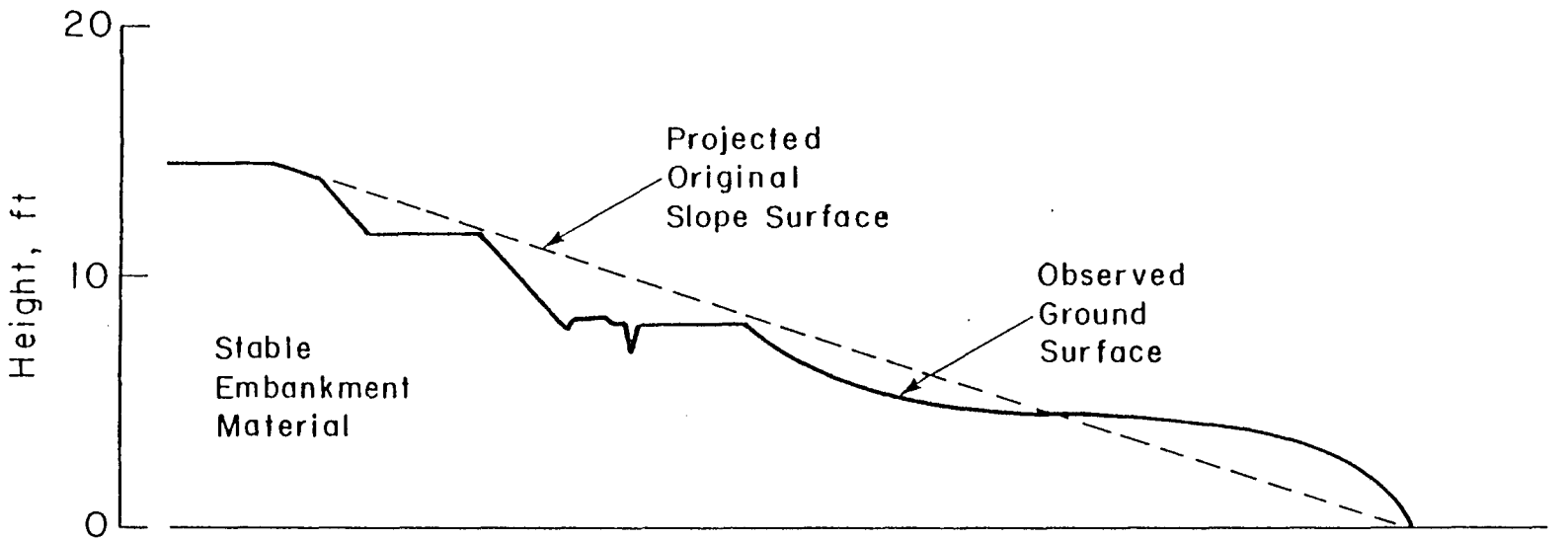

Fig. 2.5 Cross-section of Embankment Slide at SH 225 and SH 146 (SW Quadrant)

Two hand-augered holes were made in and near the slide mass on this embankment, at the locations shown in Fig. 2.4. The moisture content and soil profiles at these locations are presented in Fig. 2.6. The moisture contents do not show any significant trends, although the average moisture content in the slide mass was approximately 28 percent which is significantly lower than that found in the IH 610 and Scott Street embankment.

The base of the slide was situated well away from any roadway, so there had been no immediate need to repair the slide; the slide appeared essentially undisturbed. There was also no evidence to suggest that the slope had failed previously and been recompacted. The soil did not appear to have been lime-stabilized during construction. The grass growth was relatively uniform over the whole slope and there were signs that the embankment was well-maintained.

Information provided by the Texas SDHPT indicates that the embankment was constructed in 1952 and that it was again composed of "Common Roadway Excavation and Fill". Measurements taken in the vicinity of the slide in March 1983 indicated slopes ranging between 2.9:1 and 3.2:1, with an embankment height of approximately 15 feet.

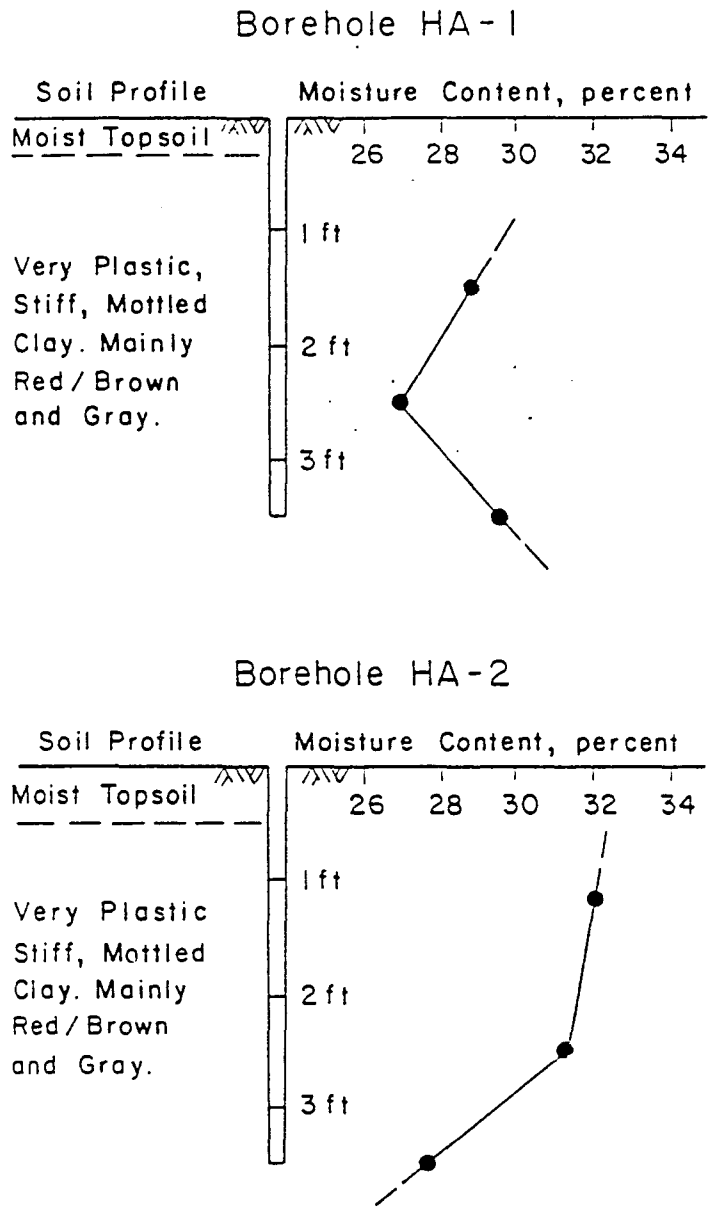

Fig. 2.6 Soil and Moisture Content Profiles for Two Hand-Augered Boreholes at SH 225 and SH 146 (SW Quadrant)

CHAPTER 3: SAMPLING PROCEDURES

Test pits were excavated in each of the embankments at the locations noted on Figures 2.1 and 2.4 and a large quantity of soil was taken for testing in the laboratory. The sampling pits were approximately 3-1/2 feet deep and penetrated several layers of material in the slide mass. Approximately four cubic feet of clay was removed from each sampling pit; the clay was placed in canvas sacks and labelled with the apparent material type and position in the excavation sequence.

In addition to the test pits, two hand-augered boreholes were made in and near the slide mass at each site to depths of approximately 3-1/2 feet. The logs of these boreholes were presented in Figures 2.2 and 2.6 for the two sites and indicate similar variations in clay type to those found in the sampling pits. Three or four small samples were taken from each borehole at depths judged to be representative of different strata. The samples were carefully sealed in plastic bags.

The borehole samples, as well as some samples which had been taken from the sampling pits and stored in plastic bags, were returned to the geotechnical laboratories of The University of Texas at Austin. Moisture contents and Atterberg limits were determined for these samples almost immediately after they were received in the laboratory. The larger quantities of soil taken from the sampling pits and stored in canvas

bags were allowed to air-dry in the laboratory for approximately two months until the shear testing program was started.

The most notable aspect of the soil observed in the sampling process was the extreme variability over short depths. Although the clay was consistently very sticky, it ranged from brown and tan to grey and black; the tan and black clays were, however, present more as traces than as identifiable strata. Care was taken to obtain at least enough of each of the material types for moisture content determinations; large quantities of the brown and grey clays were recovered.

Although the grey clays at the two sites appeared similar, the brown clays from the two sites were easily distinguished from one another. The clay from the IH 610 and Scott Street embankment was definitely redder and is therefore referred to as "red" clay in the remainder of this report; the browner clay from the SH 225 and SH 146, SW Quadrant site is referred to as "brown" clay. The grey clays from the two sites have not been differentiated on the basis of color, although care has been taken to keep separate the soil from the different embankments.

As the shear testing program progressed, it became necessary to return to the IH 610 and Scott Street site to obtain more of the red clay. Thus, on 5 August 1983, approximately eight cubic feet of red clay was extracted from a pit immediately adjacent to the excavation that had been made in March. Quantities of the red clay were taken from above and below an intervening grey layer; the samples of red clay from the two sampling trips were very similar.

CHAPTER 4: INDEX PROPERTIES

4.1. INTRODUCTION

A series of index property tests was carried out to identify the soils obtained from the embankments at IH 610 and Scott Street, and SH 225 and SH 146 (SW Quadrant). These tests consisted of Atterberg limit determinations and grain size analyses. All tests were carried out to ASTM specifications (ASTM, 1982); the relevant standards are D 422 for grain size analysis by hydrometer, D 423 for the liquid limit, and D 424 for the plastic limit. Results of these index property tests are presented and discussed in this chapter.

4.2. ATTERBERG LIMITS

For the purposes of this study, there appeared to be four materials to examine: a red and a grey clay from IH 610 and Scott Street and a brown and a grey clay from SH 225 and SH 146 (SW Quadrant). Liquid and plastic limits were determined using the air-dry fraction of each of these soils passing the No.40 sieve. Plasticity indices were also calculated. The results are presented in Table 4.1. Stauffer (1984) has presented similar data obtained on soils from embankment failures throughout Texas.

Table 4.1

Results of Index Property Tests

Site	Date of Sampling	Clay Color	PL (%)	LL (%)	PI (%)	Activity A_c
IH 610 & Scott Rd	3/16/83	Red	19.7	71.4	51.7	0.76
IH 610 & Scott Rd	8/05/83	Red	21.1	72.7	51.6	0.75
IH 610 & Scott Rd	3/16/83	Grey	14.6	53.8	39.2	0.80
IH 610 & Scott Rd	8/05/83	Grey	18.0	55.2	37.2	0.75
SH225 & SH146 (SW)	3/16/83	Brown	21.2	70.4	49.2	0.78
SH225 & SH146 (SW)	3/16/83	Grey	20.1	55.8	35.7	—

It is evident from Table 4.1 that the red clay from IH 610 and Scott Street and the brown clay from SH 225 and SH 146 (SW Quadrant) have similar index properties, and that the grey clays from the two sites also appear similar. There is a clear distinction, with regard to plasticity, between the red/brown clay and the grey clay, and this distinction can be made for both sites. The red and brown clays, with an average liquid limit of 70 percent, would be classified as highly plastic (CH under the Unified Soil Classification System), while the grey clays, with an average liquid limit of 50 percent, would only just fall into the high plasticity category (but would again be classified as CH soils).

It would be improper to use color, alone, as a basis for identification of the clays since soils can change in color due to the oxidation of elements which are only present in minute proportions and do not affect the engineering properties of the soil. However, in this study, color has proved to be useful in identifying the clays of different plasticity.

Excellent correlation was found between the Atterberg limits measured on the IH 610 and Scott Street soils from the first and second sampling trips. Although this was to be expected considering the proximity of the two sampling pits, the confirmation was needed to justify the use of the soil from the second trip in the ongoing testing program. Periodically, the index properties of batches of soil processed for testing have been checked against these initial values.

4.3. GRAIN SIZE DISTRIBUTIONS

Hydrometer tests were performed to determine the grain size distributions for five of the six soils/sampling dates identified in Table 4.1. In accordance with standard practice (ASTM D 422), only that fraction of air-dried soil passing the No.10 sieve was used; the amount of soil which did not pass the No.10 sieve was small and consisted of hardened lumps rather than large sand-sized particles. At the end of the hydrometer tests, the proportion of the soil retained on a No.200 sieve was determined.

Grain size distribution charts for the soil from the IH 610 and Scott Street embankment are presented in Figures 4.1 and 4.2 for the red and grey clays, respectively. Grain size distributions are shown in each figure for soil samples obtained during the first and second sampling trips. There do not appear to be any significant differences in the grain size distributions of the soils from the different sampling pits. The grain size distribution for the brown clay from the SH 225 and SH 146 (SW Quadrant) site is presented in Fig. 4.3. The distribution is similar to those shown in Fig. 4.1 for samples of red clay from the IH 610 and Scott Street embankment.

The red clay appears to have a significantly finer grain size than the grey clay. Less than 5 percent, if any, of the red clay particles are larger than the No.200 sieve opening (0.075 mm), whereas approximately 15 percent of the grey clay particles seem to exceed this size. The results also indicate that 63 percent of the red clay particles are

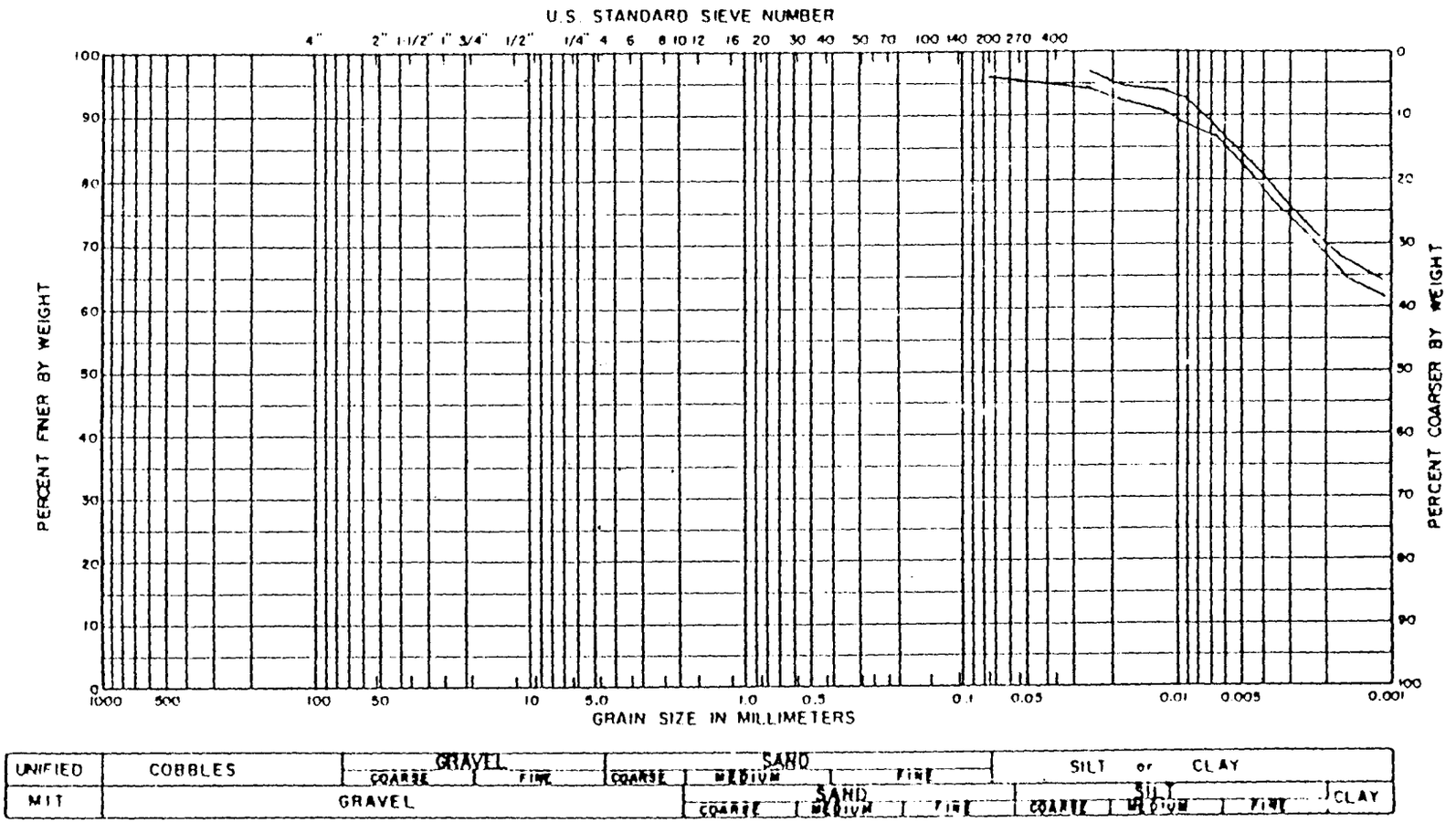

Fig. 4.1 Grain Size Distributions for Red Clay from IH 610 and Scott Street

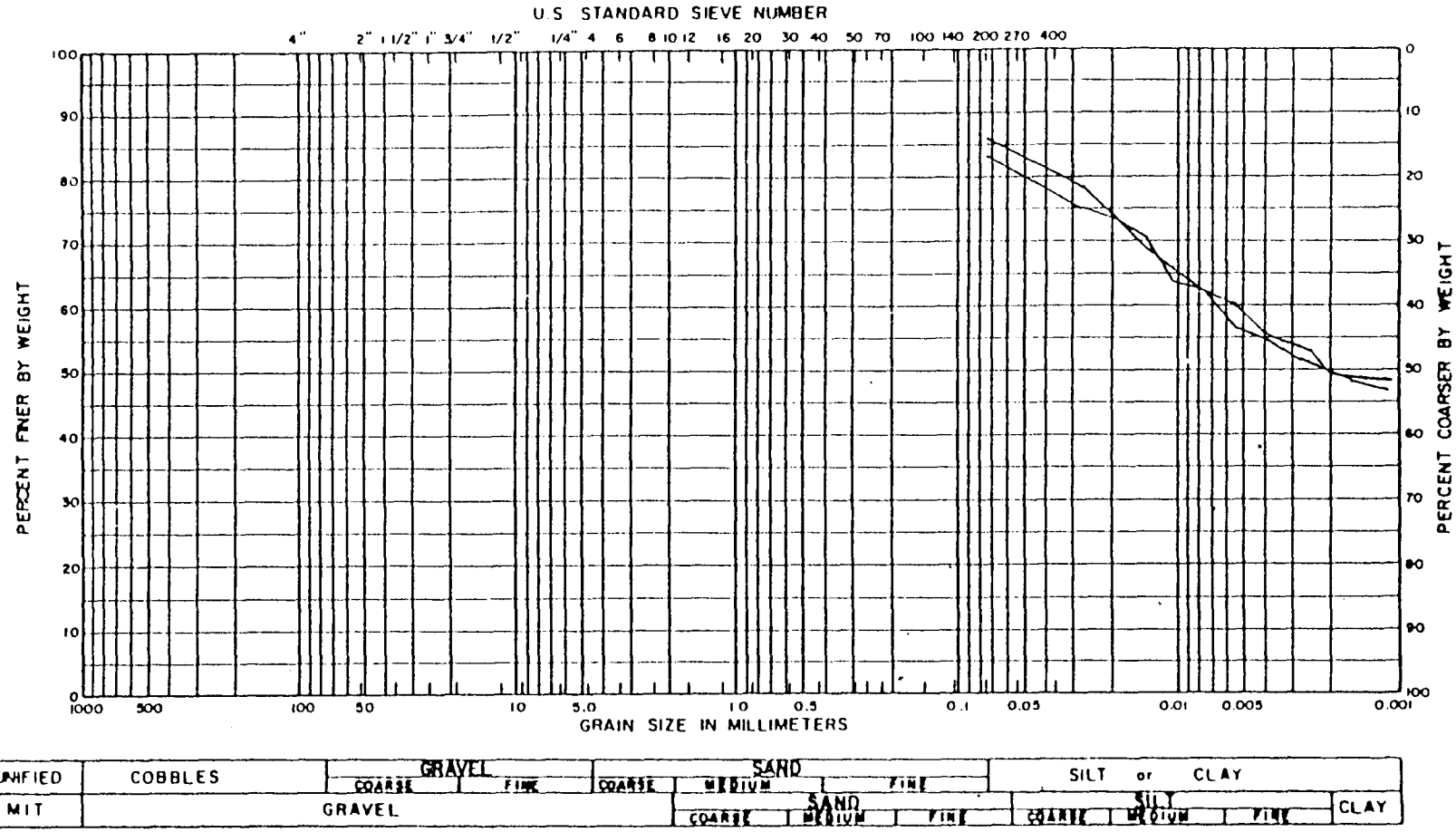

Fig. 4.2 Grain Size Distributions for Grey Clay from III 610 and Scott Street

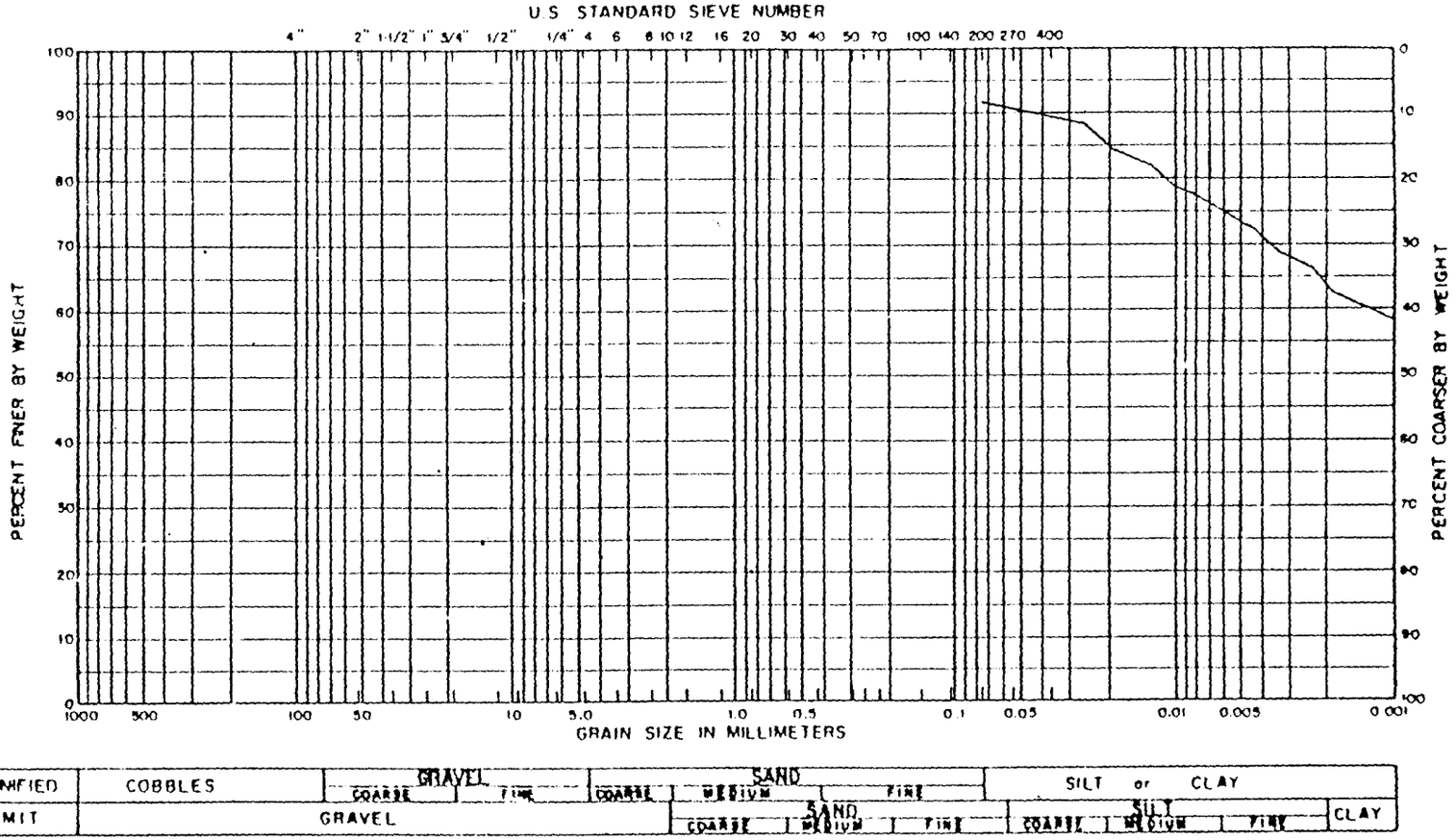

Fig. 4.3 Grain Size Disribution for Brown Clay from SH 225 and SH 146 (SW Quadrant)

finer than 0.001 mm, while the corresponding figure for the grey clay is only 47 percent. Therefore, although both soils are composed of mainly clay-sized particles, the grey clay has a moderately higher sand content. When the soils were being sampled, it was noted that the grey clay appeared to be slightly coarser than the red clay.

4.4. ACTIVITIES

The activity, defined as the ratio of the plasticity index of a soil to the percentage by weight of soil finer than 0.002 mm, was found to fall within a relatively narrow range of values for the clays in this study. The calculated activities are presented in Table 4.1.

The activities of the red, brown, and grey clays varied between 0.75 and 0.80 with no discernible distinction among the different materials. Stauffer (1984) has presented activity values for over 30 different soils taken from embankments which have failed in similar circumstances to those in this investigation; he found comparable results, although the range of activities broadened slightly (0.6 to 0.9).

4.5. COMPARISONS AND CORRELATIONS

The plasticity index and liquid limit results from the Atterberg

limit tests have been plotted on a plasticity chart presented in Fig. 4.4 for the red and grey clays from IH 610 and Scott Street, and the brown and grey clays from SH 225 and SH 146 (SW Quadrant). Stauffer (1984) reports the results of a series of Atterberg limit tests performed on soil samples obtained from a number of embankment and cutting slope failures in south central Texas. The Atterberg limits for these soils have also been plotted on the plasticity chart presented in Fig. 4.4.

There is generally a trend for the Atterberg limits of soils with the same geologic origin to plot in a band parallel to the A-line of the plasticity chart. It is interesting, although not necessarily significant, that the Atterberg limits of soil from similar embankment slides do indeed plot parallel to the A-line in Fig. 4.4.

It is commonly found in geotechnical practice that the problems associated with the behaviour of clay soils increase as the plasticity index of the soil increases. Compressibility increases with plasticity, as does susceptibility to expansive activity, but more significantly shearing resistance tends to decrease. Gibson (1953), Bjerrum and Simons (1960), and Mitchell (1976) have all produced results indicating a reduction in the effective stress angle of shearing resistance, $\bar{\phi}$, with increasing plasticity index. Their results have been redrawn and are presented in Figures 4.5, 4.6, and 4.7.

There appears to have been little work done to correlate the cohesion component of shear strength with index properties. This is perhaps attributable to a close relationship between cohesion and stress history. Atterberg limit tests on a thoroughly remolded soil sample

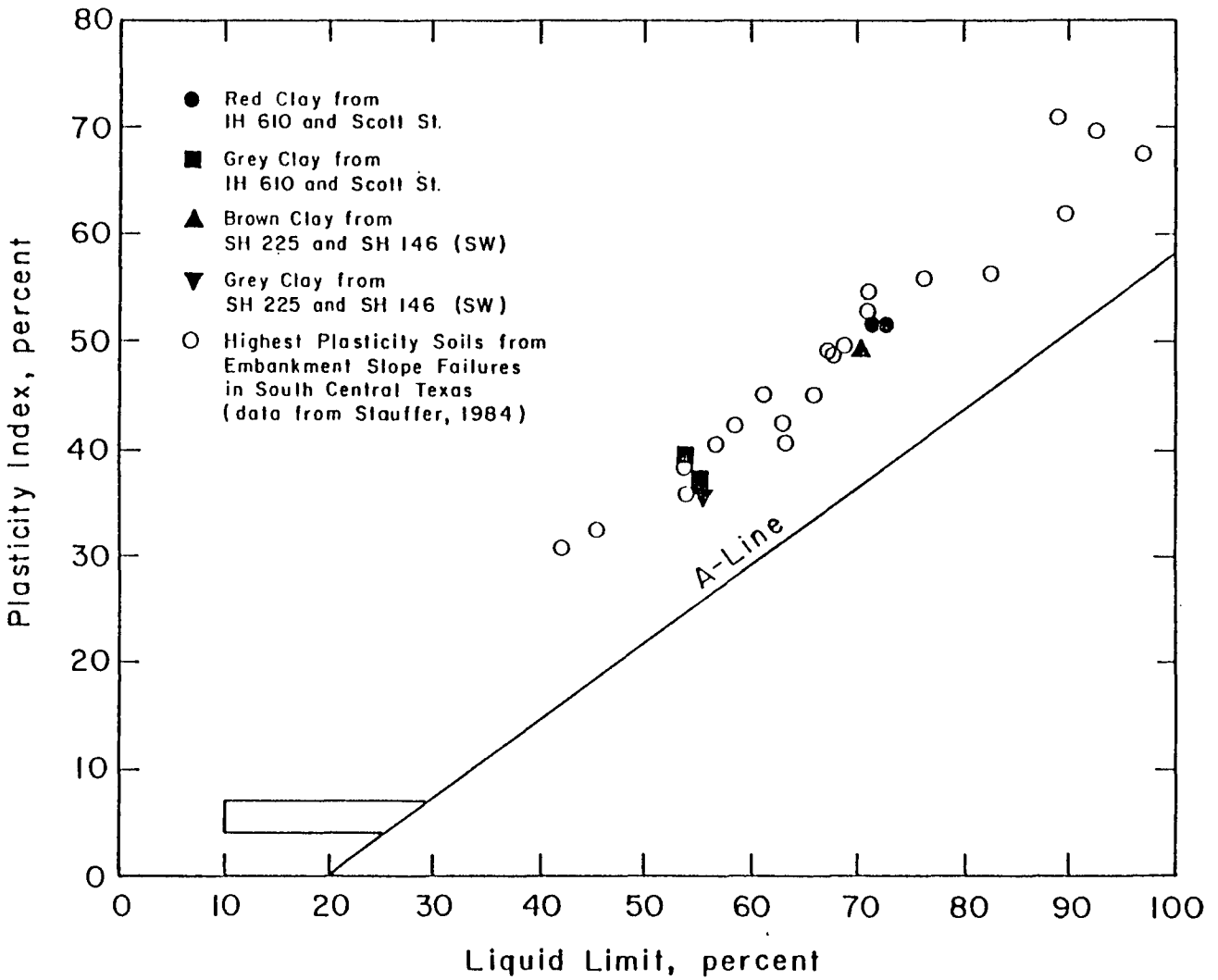

Fig. 4.4 Plasticity Characteristics of Soils obtained from Embankment Slope Failures throughout South Central Texas

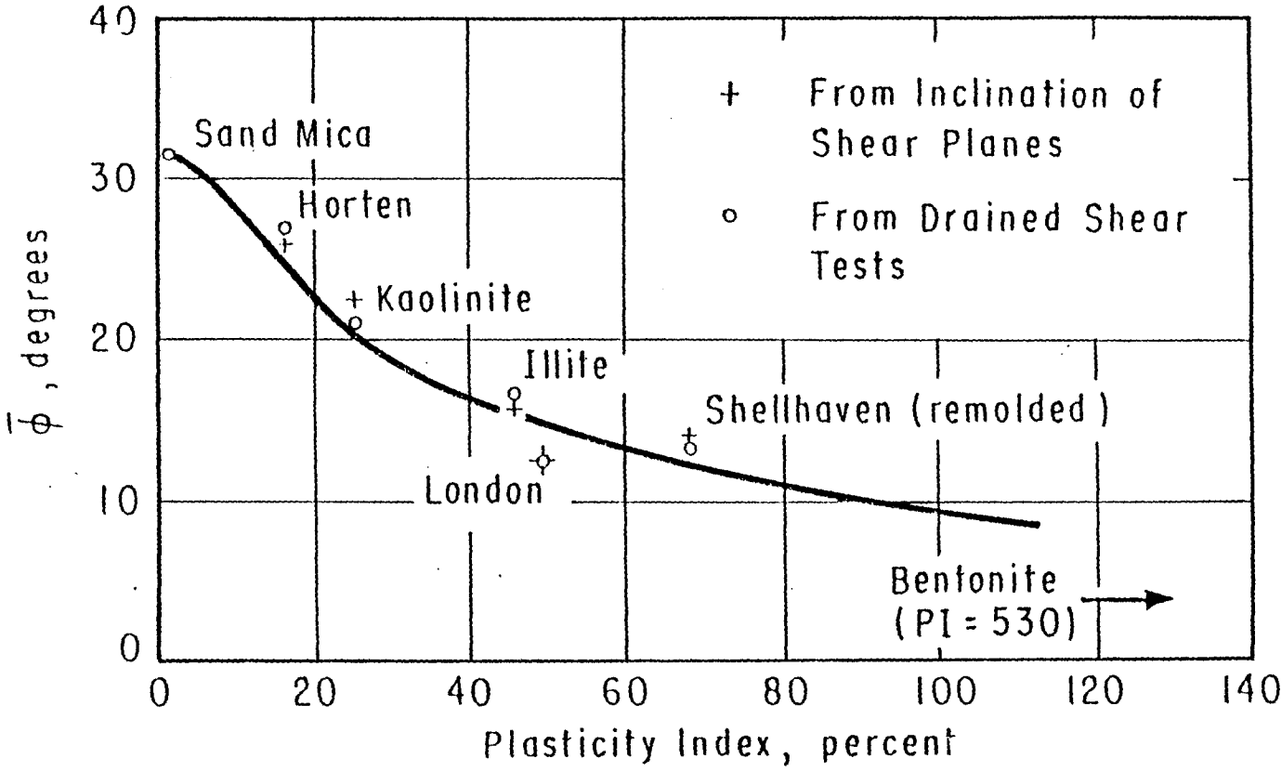

Fig. 4.5 Relationship between $\bar{\phi}$ and Plasticity Index (after Gibson, 1953)

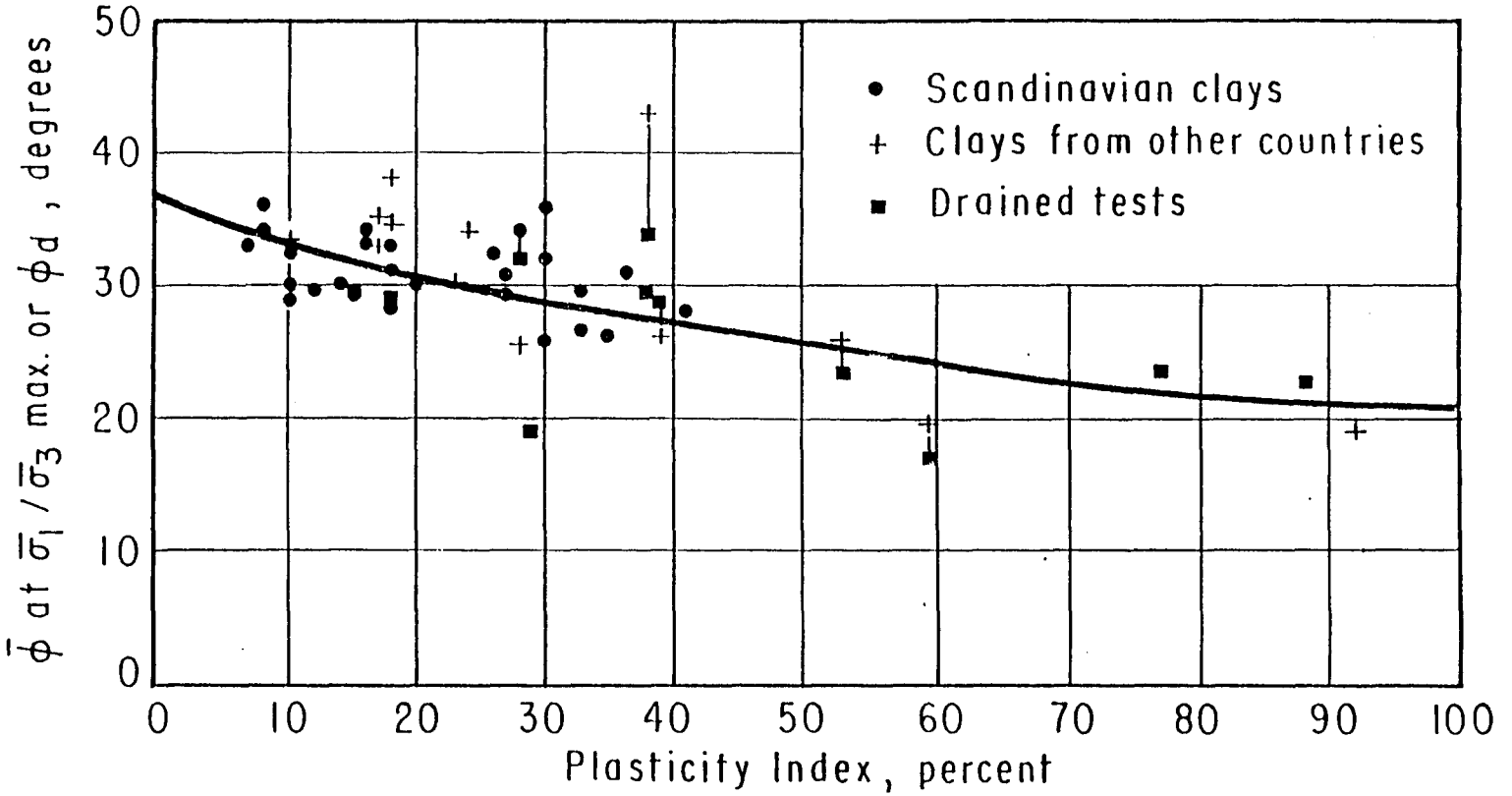

Fig. 4.6 Relationship between $\bar{\phi}$ Measured in Consolidated-Undrained and Consolidated-Drained Triaxial Shear Tests, and Plasticity Index (after Bjerrum and Simons, 1960)

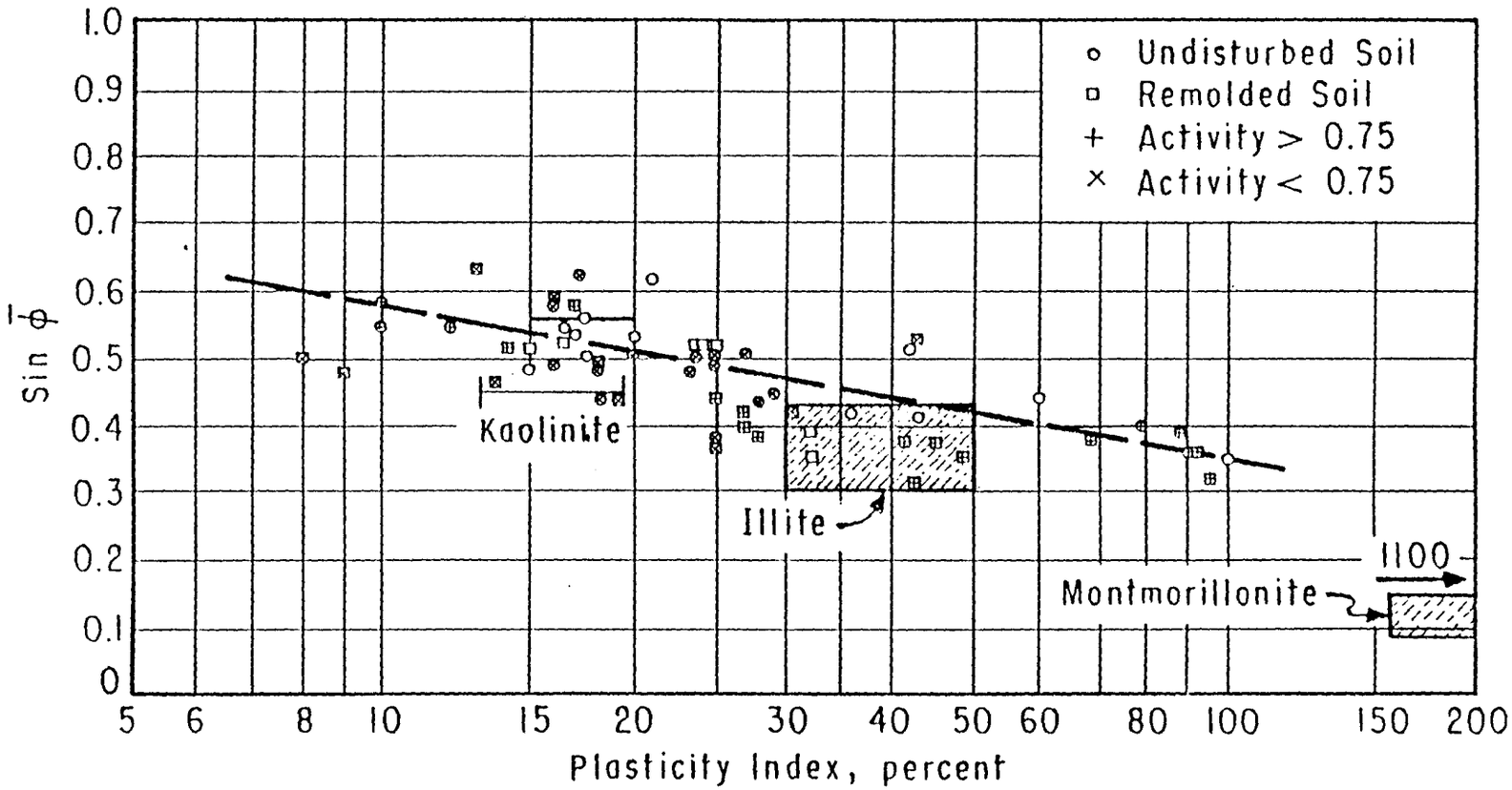

Fig. 4.7 Relationship between $\bar{\phi}$ and Plasticity Index (after Mitchell, 1976)

could not be expected to relate in any direct manner to this soil property.

4.6. CONCLUSIONS

The clays from the IH 610 and Scott Street, and SH 225 and SH 146 (SW Quadrant) embankments were determined to have plasticity indices ranging from 35 to 52 percent and liquid limits from 53 to 73 percent. Such soils can be categorized as moderately to very highly plastic and are frequently found to be moderately to highly expansive. The results of Atterberg limit tests on soils obtained during the second sampling trip were in good agreement with the results of tests on the soil from the first sampling trip. This new soil was therefore judged to be suitable for use in the shear testing program.

Grain size distributions showed that the red and brown clay particles were significantly finer than those of the grey clay; this factor would undoubtedly contribute to the differing Atterberg limits. The activities of the two clays were essentially identical and similar to those found in soil from failed embankments throughout Texas.

Based on the Atterberg limit results and the correlations between plasticity and the effective stress angle of shearing resistance, $\bar{\phi}$, the red clay from the IH 610 and Scott Street embankment appeared to represent the worst of the soils examined, with regard to shear strength and slope stability. It would be reasonable to expect a

lower effective stress angle of shearing resistance from the red clay than, say, the grey clay from the same site.

Since the object of the investigation was to measure in the laboratory the apparently low shear strengths associated with the embankment slides, the major emphasis of the testing program was placed on the red clay from the IH 610 and Scott Street embankment.

CHAPTER 5: CHOICE OF COMPACTION CRITERIA

5.1. BACKGROUND

In the early stages of this investigation, it was decided that the shear testing should, at least initially, be performed using specimens which were compacted in the laboratory. Although useful information would be obtained from the testing of undisturbed samples taken from one of the embankment slides, funds were not available to support such an undertaking.

It was thought that the use of specimens prepared in the laboratory would allow an investigation of some of the factors affecting the shear strength of the soils, which would not have been possible using undisturbed samples. In addition, it was believed that the shear strength obtained from soil specimens compacted in the laboratory would be very similar to the shear strength obtained from undisturbed samples. For example, Vaughan et al. (1979) have shown that differences in structure induced by laboratory dynamic, laboratory static, and field compaction techniques have no systematic influence on peak strength in terms of effective stress.

It was considered desirable that the laboratory specimens should reflect the densities and moisture contents which were achieved originally during construction of the embankments under consideration.

However, original construction records were not available and it was, therefore, necessary to establish the initial conditions in some other way.

Three approaches were identified to establish the compaction conditions at the time of construction. The three approaches are described in this chapter. Two of these approaches utilize Texas SDHPT laboratory test procedures (SDHPT Test Methods Tex-114-E and Tex-113-E); the third involves an estimation of the densities likely to be achieved, based on general geotechnical practice.

5.2. TEXAS SDHPT TEST METHOD TEX-114-E

5.2.1. OUTLINE OF PROCEDURE

Test Method Tex-114-E (Texas SDHPT, 1978) is described as a "Compaction Ratio Method for Selection of Density of Soils and Base Materials in Place." This laboratory procedure has been developed by the Texas SDHPT to determine optimum placement densities and moisture contents for soils used as base materials in highway construction.

A flow-chart summary of the procedure used in Test Method Tex-114-E is shown in Fig. 5.1. In the procedure a density, D_A, is defined in terms of a "compaction ratio", CR, and standardized measures of loose and dense density (represented by D_L and D_D respectively) by the following equation:

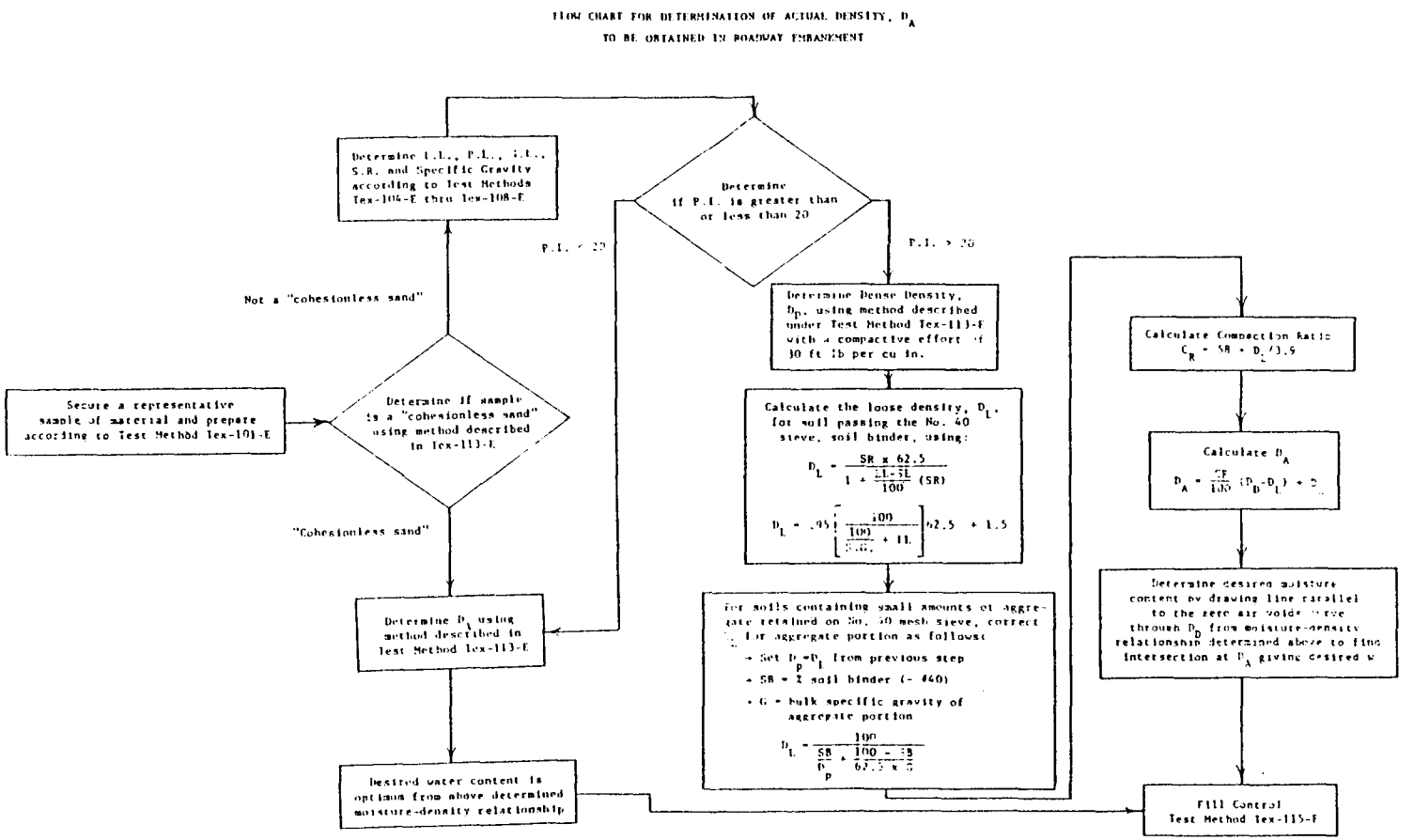

Fig. 5.1 Flow-Chart Summary of the Procedure used in Test Method Tex-114-E

$$D_A = \frac{CR}{100} (D_D - D_L) + D_L \qquad (5.1)$$

The ways in which each of the variables (CR, D_L, and D_D) is determined are examined separately in this section. The density, D_A, is termed an "actual" density in the Test Method. This density is subsequently selected by the Texas SDHPT as the dry density to be achieved during construction.

5.2.2. DEFINITION OF COEFFICIENTS

5.2.2.1. Dense Density, D_D

The dense density, D_D, is defined as the maximum dry density for the material tested in the laboratory in accordance with Test Method Tex-113-E ("Determination of Moisture-Density Relations of Soils and Base Materials", Texas SDHPT, 1978) using a compactive effort of 30 ft lb per cu in. To put this compactive effort in perspective, the compactive effort used in the Standard Proctor compaction procedure (ASTM D 698, or AASHTO T 99) is 7.16 ft lb per cu in. and the Modified Proctor (ASTM D 1557, or AASHTO T 180) compactive effort is 32.55 ft lb per cu in. The compactive effort specified in Tex-114-E for the determination of dense densities is, therefore, slightly lower than that of the Modified Proctor procedure.

Test Method Tex-113-E prescribes the use of specific compaction equipment which was not available in the laboratories of The University of Texas at Austin. Accordingly, alternate equipment was used for the present study. It was found that the desired compactive effort (30 ft lb per cu in.) could be achieved by using the Modified Proctor procedure with 23 blows per layer instead of the usual 25 blows per layer. The corresponding relationship between dry unit weight and compaction moisture content for the red clay from the IH 610 and Scott Street embankment is shown in Fig. 5.2. The maximum dry density (D_D) for this compactive effort is approximately 113.1 pcf and occurs at an optimum moisture content of 17.4 percent. This moisture content (17.4 percent) is approximately three percent lower than the plastic limit for the red clay.

The relationship between dry unit weight and compaction moisture content for the grey clay from IH 610 and Scott Street at a compactive effort of 30 ft lb per cu in. is presented in Fig. 5.3. The maximum dry density, D_D, for this compactive effort is approximately 115.6 pcf with an optimum moisture content of 15.8 percent. This moisture content (15.8 percent) is approximately two percent less than the average of the plastic limit values for the grey clay reported in Table 4.1.

5.2.2.2. Loose Density, D_L

According to Test Method Tex-114-E, the loose density, D_L, can be determined by one of three procedures, two of which are clearly intended for use with clayey soils and a third which appears more suited

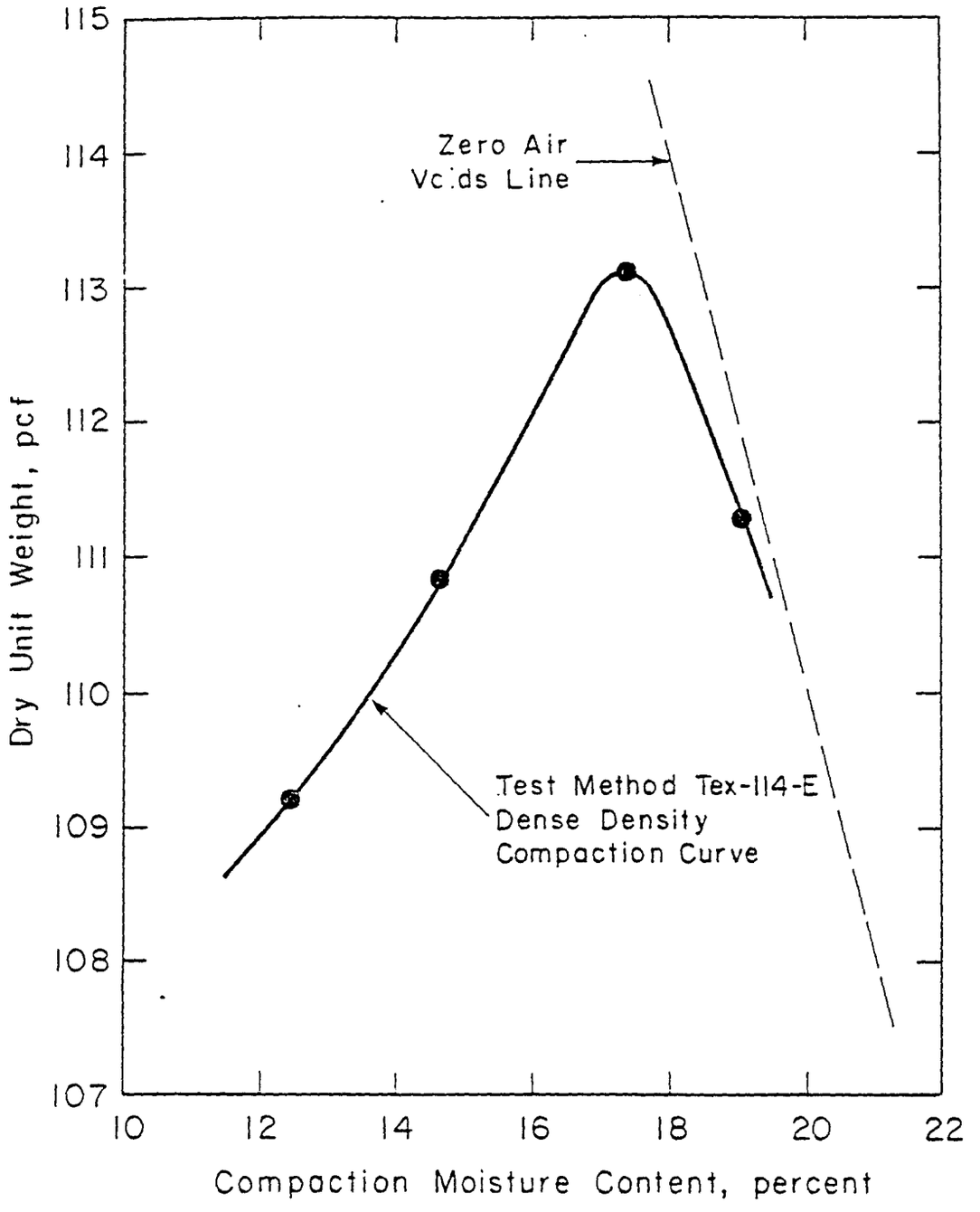

Fig. 5.2 Moisture-Density Relationship for Tex-114-E Dense Density (at a Compactive Effort of 30 ft lb per cu in) for Red Clay from IH 610 and Scott Street

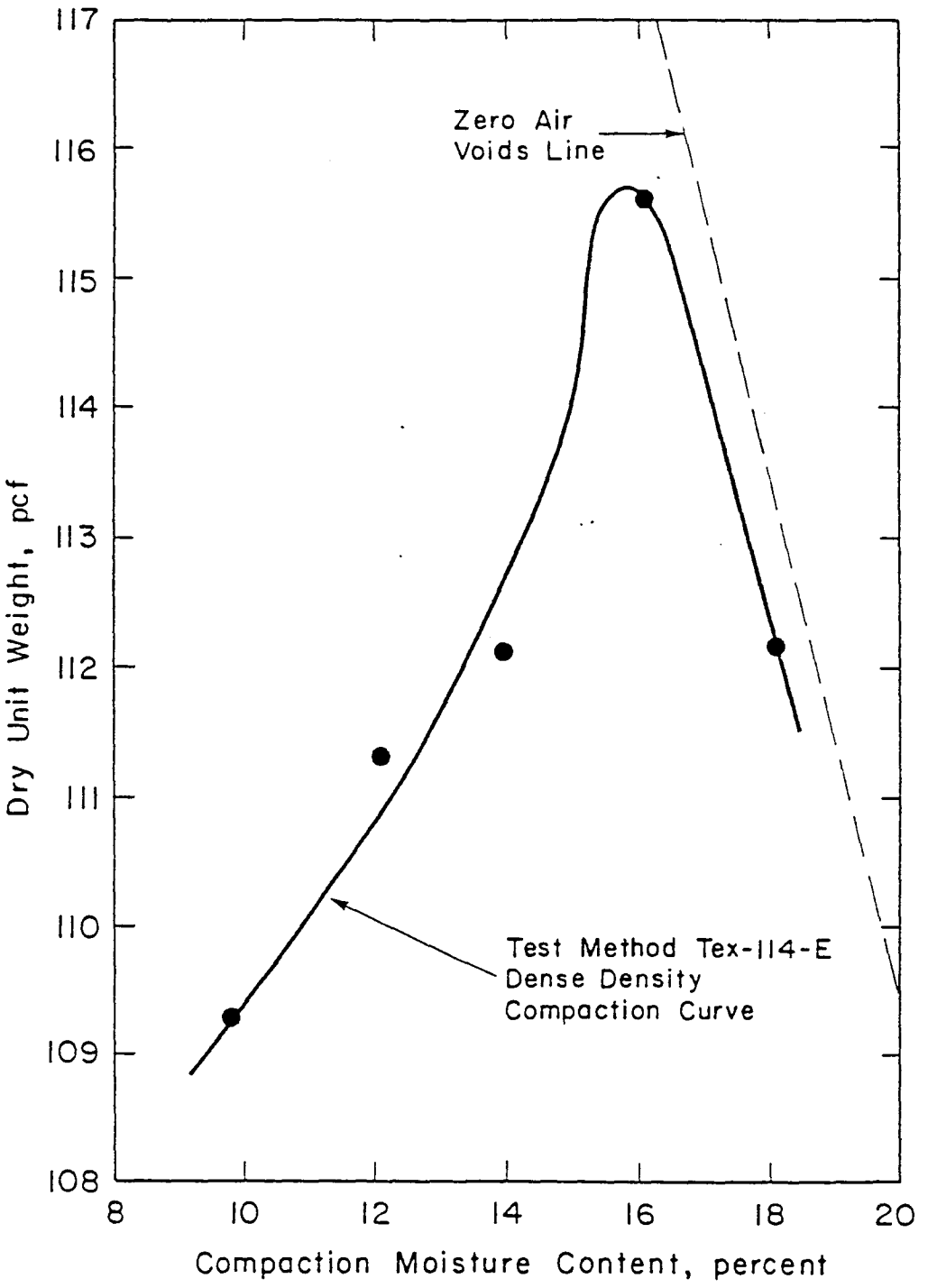

Fig. 5.3 Moisture-Density Relationship for Tex-114-E Dense Density (at a Compactive Effort of 30 ft lb per cu in.) for Grey Clay from IH 610 and Scott Street

to cohesionless materials. The three ways in which the loose density may be determined by Test Method Tex-114-E are as follows:

1. The loose density may be calculated using the shrinkage ratio (SR), the shrinkage limit (SL), and the liquid limit (LL) in the following relationship:

$$D_L = \frac{SR \times 62.5}{1 + \frac{LL - SL}{100}(SR)} \qquad (5.2)$$

where the shrinkage ratio, shrinkage limit, and liquid limit are expressed as percentages. The shrinkage ratio and shrinkage limit of a soil are determined using Test Method Tex-107-E, "Determination of Shrinkage Factors of Soils" (Texas SDHPT, 1978). The loose density, D_L, is first calculated using Equation (5.2) and then corrected for the effect of any aggregate fraction not included in the soil used to determine the liquid limit, shrinkage ratio, and shrinkage limit. The aggregate fraction is defined as the portion of the soil retained on a No.40 sieve.

2. The loose density of soil may be calculated using the specific gravity of solids (G_s), and liquid limit (LL) in the following empirical equation:

$$D_L = 0.95 \times 62.5 \times \left(\frac{100}{\frac{100}{G_s} + LL}\right) + 1.5 \qquad (5.3)$$

where the liquid limit is expressed as a percentage. The resulting value for D_L is adjusted for aggregate content in the same manner as in (1).

3. The loose density may be taken as the dry rodded unit weight of material determined by the procedure described in ASTM Standard C 29-55-T.

Approach (3) is clearly suited to cohesionless materials and, therefore, was not used to determine loose densities for the soils in this study. Either of the first two approaches could have been used as they are both suitable for cohesive soils; however, the soil properties needed to follow approach (2) had already been determined or could be easily estimated and it was decided that this approach would be used. For all soils under consideration in this study, the fraction of material retained on a No.40 sieve is zero or negligibly small. There is, therefore, no need to correct the calculated loose density values for the effect of this soil fraction.

Approach (2) was used to determine the loose densities using a value of 2.70 for G_s and average values of 72 percent and 55 percent for the liquid limits of the red and grey clays, respectively. The loose density, D_L, is calculated in this manner to be 56.0 pcf for the red clay and 66.0 pcf for the grey clay.

5.2.2.3. Compaction Ratio, CR

The compaction ratio, CR, is a measure of the relative looseness or denseness of a clay fill, in the same way that the Relative Density, D_R, for sand indicates the manner in which the actual void ratio relates to minimum and maximum achievable void ratios. In Test Method Tex-114-E the following empirical relationship is used to determine the compaction ratio:

$$CR = 58 + D_L/3.9 \qquad (5.4)$$

Using a loose density of 56.0 pcf for the red clay, and 66.0 pcf for the grey clay, from the IH 610 and Scott Street embankment, the compaction ratio is calculated to be 72.4 percent for the red clay and 74.9 percent for the grey clay.

5.2.3. CALCULATION OF DENSITY, D_A

The density, D_A, was calculated from Equation 5.1 for the red and grey clays from the IH 610 and Scott Street embankment. The calculated values for D_A as well as the values found for the parameters (D_D, D_L, and CR) used to calculate D_A are summarized in Table 5.1. By Test Method Tex-114-E, the densities are 97.3 pcf for the red clay and 103.2 pcf for the grey clay.

Table 5.1

Summary of Test Method Tex-114-E Variables
for the Red and Grey Clays from IH 610 and Scott Street

Clay	Dry Dense Density D_D (pcf)	Dry Loose Density D_L (pcf)	Compaction Ratio CR (%)	Actual Field Dry Density D_A (pcf)
Red	113.1	56.0	72.4	97.3
Grey	115.6	66.0	74.9	103.2

5.3. TEXAS SDHPT TEST METHOD TEX-113-E

The second approach used to estimate the initial field compaction conditions was based on determining maximum dry densities and corresponding optimum moisture contents using the procedure outlined in Test Method Tex-113-E (Texas SDHPT, 1978).

Test Method Tex-113-E, "Determination of Moisture-Density Relations of Soils and Base Materials," is a modification of the procedure outlined in the ASTM D 1557 and AASHTO T 180 standards. Test Method Tex-113-E employs a range in compactive efforts from 4 to 53 ft lb per cu in. depending on the type of soil. For clay soils, the Test Method specifies compactive efforts of 4, 5, or 6.6 ft lb per cu in. depending on the plasticity index of the soil. It would appear that consideration has been given to the determination of compactive efforts which realistically represent the field compaction conditions which are typically achieved with different clay soils.

The red and grey clays from the IH 610 and Scott Street embankment have plasticity index values of 52 percent and 38 percent, respectively. Test Method Tex-113-E indicates that "very plastic clays, subject to large volume change and with plasticity indices between 35 and 45," should be compacted using compactive efforts between 4 and 5 ft lb per cu in. Subgrade soils with plasticity indices greater than 45 should be compacted at 4 ft lb per cu in.

The equipment specified for Test Method Tex-113-E was not available. Accordingly, the compaction was performed using a Standard Proc-

tor-type mold and hammer, with the standard three lifts, but with a reduced number of blows per layer. It was felt that scale effects introduced by differences in mold and hammer-face sizes between the compaction procedures specified and actually used, would be insignificant since the relative (mold-to-hammer) sizes were similar. This conclusion is supported by the research of Holtz and Lowitz (1957) and Tamez (1957) which indicate that compaction test details can be varied over wide ranges without appreciably influencing the test results.

The red clay from the IH 610 and Scott Street embankment, which has a plasticity index of 52 percent, was compacted using the Standard Proctor procedure with 14 blows per layer instead of the standard 25 blows per layer. This compaction method corresponds to a compactive effort of 4.02 ft lb per cu in. which is very close to the value specified in Tex-113-E for a soil with a plasticity index greater than 45 percent. The relationship between dry unit weight and compaction moisture content for this compactive effort is presented in Fig. 5.4. The maximum dry unit weight for the red clay is 96.3 pcf at an optimum moisture content of 24 percent.

The grey clay from the IH 610 and Scott Street embankment, which has a plasticity index of 38 percent, was compacted using the Standard Proctor procedure with 17 blows per layer. This compaction method corresponds to a compactive effort of 4.88 ft lb per cu in. which is within the range specified in Tex-113-E for a soil with a plasticity index between 35 and 45 percent. The relationship between dry unit weight and compaction moisture content which was obtained for this compactive

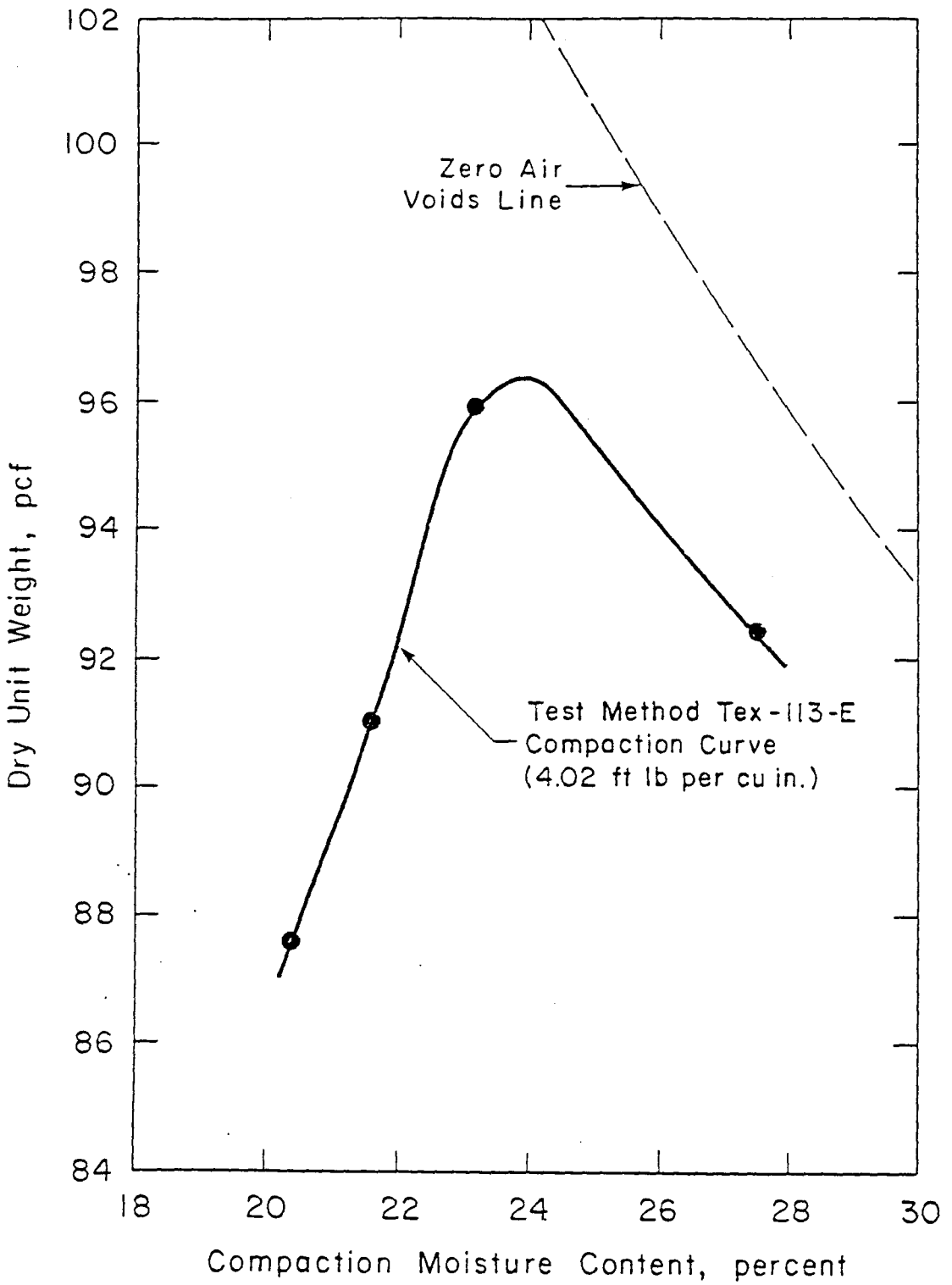

Fig. 5.4 Moisture-Density Relationship by Test Method Tex-113-E (at a Compactive Effort of 4.02 ft lb per cu in.) for Red Clay from IH 610 and Scott Street

effort is presented in Fig. 5.5. The maximum dry unit weight for the grey clay is 102.0 pcf at an optimum moisture content of 21 percent.

5.4. TYPICAL COMPACTION REQUIREMENTS

A third estimate of the probable field compaction densities for the embankments under consideration was made on the basis of the results of Standard Proctor compaction tests and what appears to be conventional engineering practice based on several sources. Sowers (1979) presents typical compaction requirements for various soil types based on the Unified Soil Classification System. For soils classified as CH, which include the red and grey clays from the IH 610 and Scott Street embankment, Sowers' recommendations indicate that compaction to between 93 and 97 percent of the Standard Proctor maximum dry density is necessary for fills requiring some degree of strength or incompressibility. The NAVFAC DM-7.2 Design Manual (United States Department of The Navy, 1982) contains recommendations on appropriate compaction conditions for various types of fills. It indicates that, for embankments less than 50 feet high, the minimum compacted dry density should be 95 percent of the Standard Proctor maximum. The Earth Manual (United States Bureau of Reclamation, 1963) presents criteria for the control of compacted dam embankments. Again, it appears that a dry density which is 95 percent of the Standard Proctor maximum is satisfactory for small embankments. Therefore, in general, it would seem reasonable to expect that a typical highway embankment consisting of a highly plastic clay fill should be

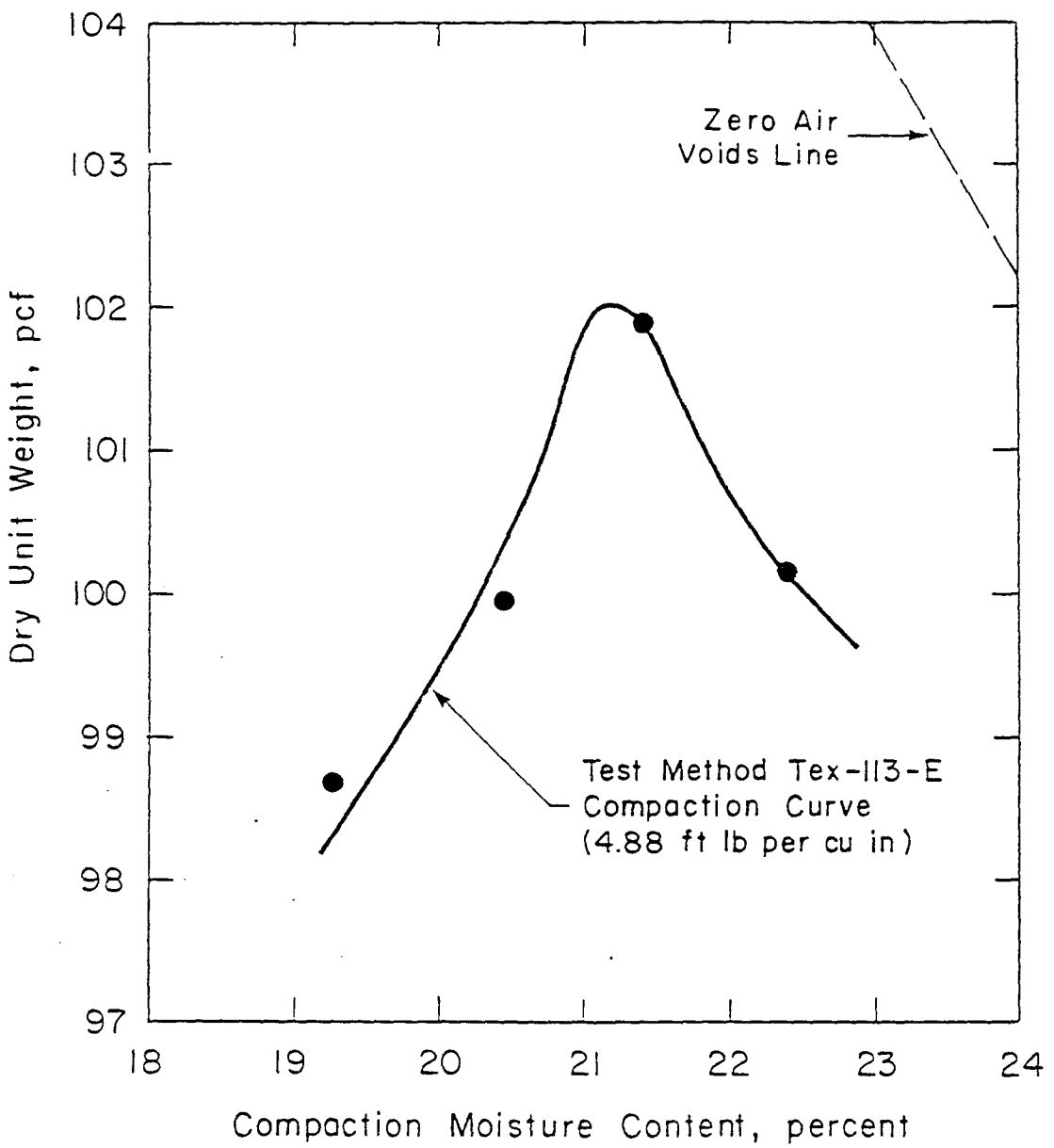

Fig. 5.5 Moisture Density Relationship by Test Method Tex-113-E (at a Compactive Effort of 4.88 ft lb per cu in.) for Grey Clay from IH 610 and Scott Street

compacted to a density of at least 95 percent of the Standard Proctor maximum dry density.

Figures 5.6 and 5.7 show the relationships obtained between dry unit weight and compaction moisture content from Standard Proctor compaction tests performed on the red and grey clays, respectively. The maximum dry unit weights were found to be approximately 100 pcf for the red clay and 105 pcf for the grey clay. Based on the discussion in the previous paragraph, it seems that a dry density of 95 percent of these maximum densities would be appropriate for the embankments of interest. For the red and grey clays, 95 percent of the maximum dry density is represented by dry densities of 95 pcf and 100 pcf, respectively.

5.5. CONCLUSIONS

Three independent methods of establishing probable field compaction densities have been presented and used in this Chapter. The compaction curves used to make these estimates are summarized in Figures 5.8 and 5.9.

Probable field densities arrived at by these three procedures are summarized in Table 5.2. The range in dry density estimates arrived at by these three procedures is only 2 pcf for the red clay and 3 pcf for the grey clay. The densities arrived at by the three procedures are remarkably similar. Although it is unlikely that, within reasonable limits, the compacted density will greatly affect the measured soil

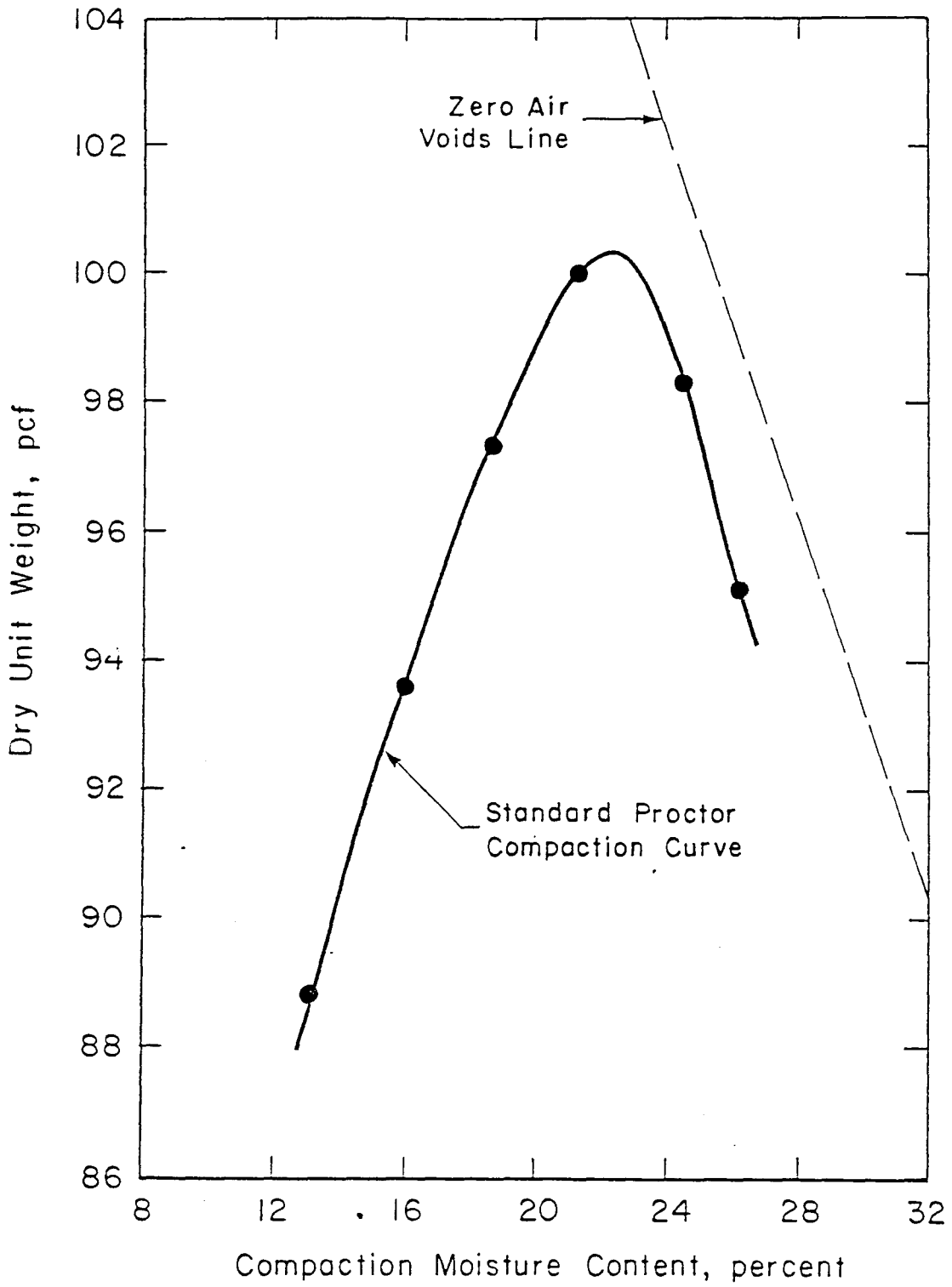

Fig. 5.6 Standard Proctor Moisture-Density Relationship for Red Clay from IH 610 and Scott Street

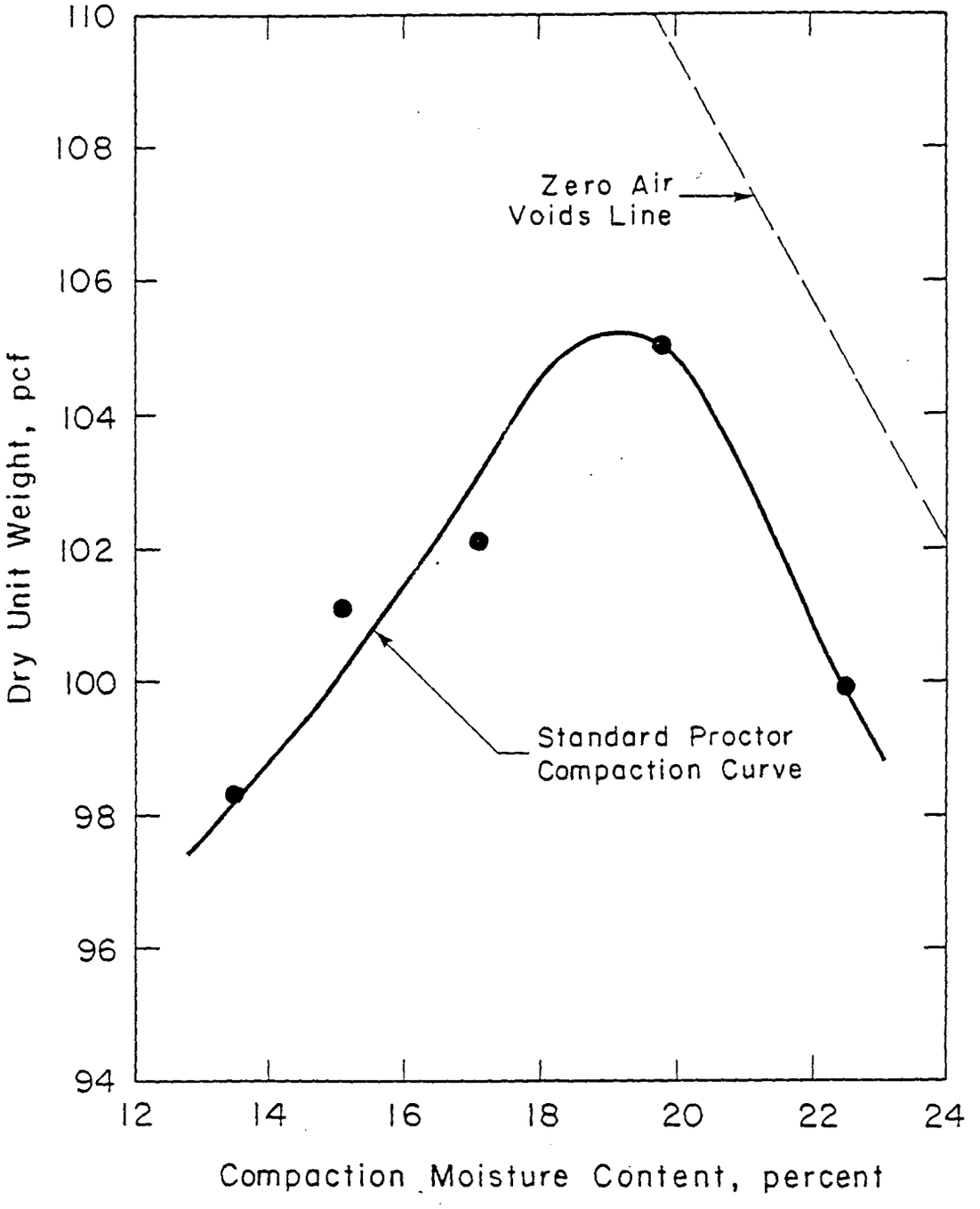

Fig. 5.7 Standard Proctor Moisture-Density Relationship for Grey Clay from IH 610 and Scott Street

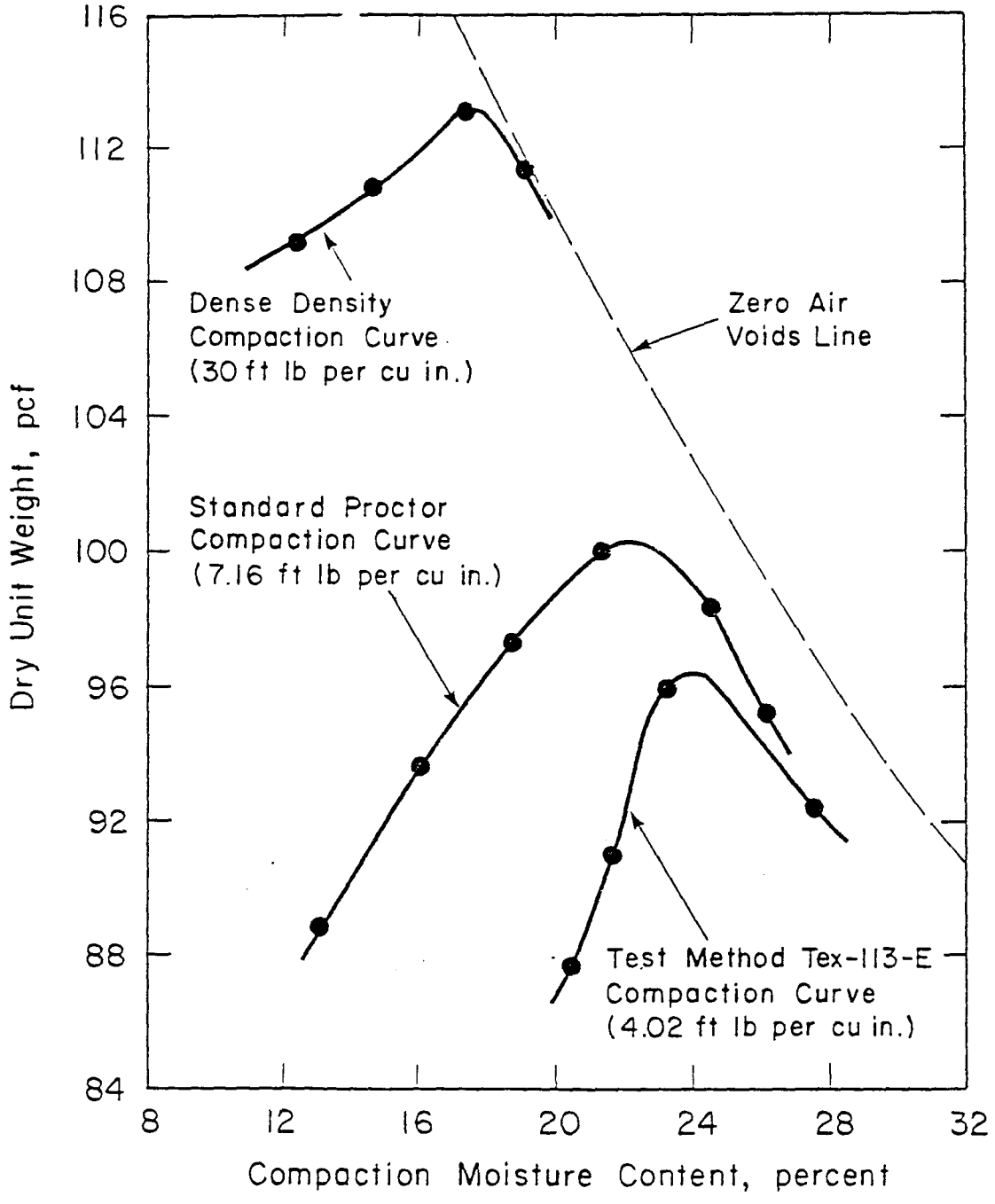

Fig. 5.8 Summary of Moisture-Density Relationships Determined for Red Clay from IH 610 and Scott Street

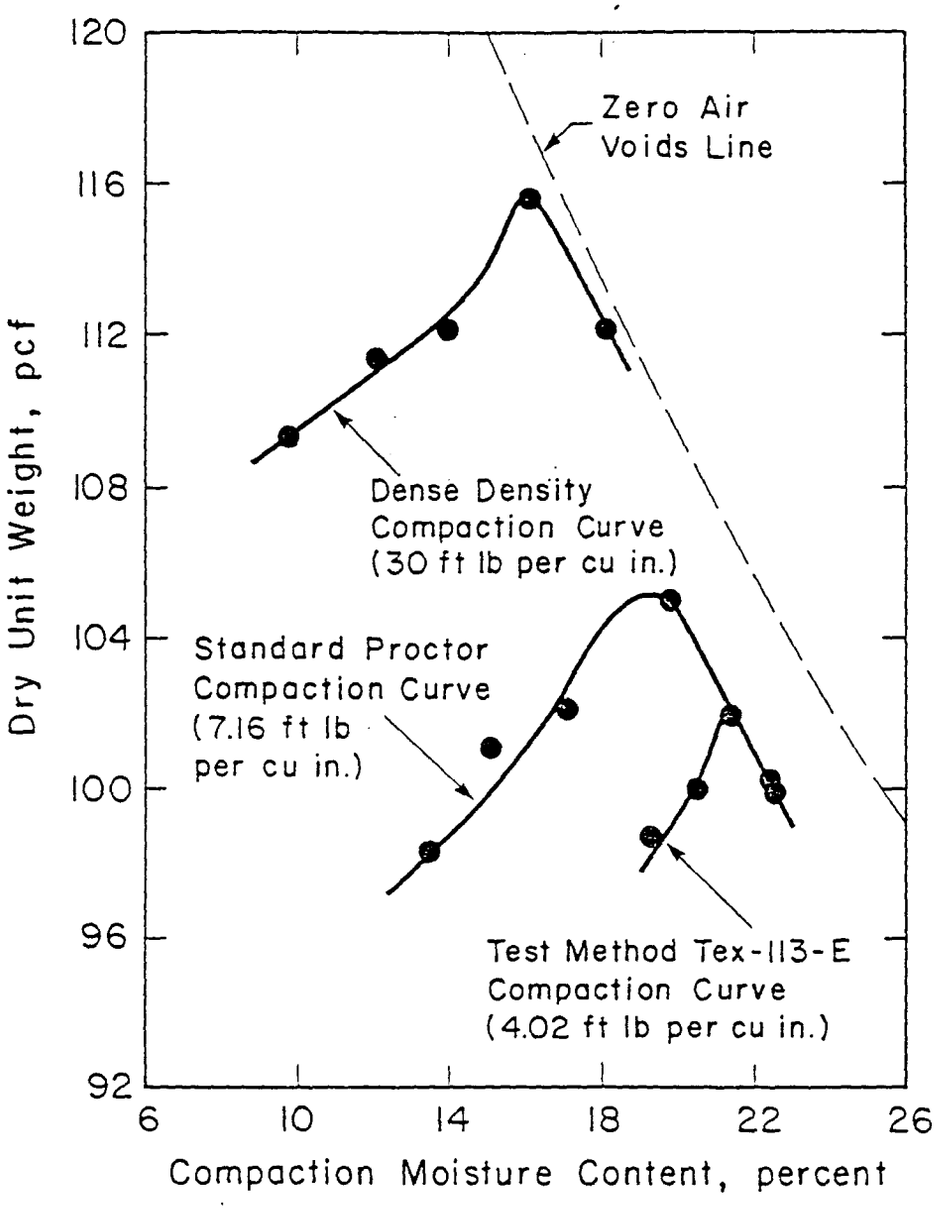

Fig. 5.9 Summary of Moisture-Density Relationships Determined for Grey Clay from IH 610 and Scott Street

Table 5.2

Summary of Estimates of the Initial Dry Density for the Red and Grey Clays from the IH 610 and Scott Street Embankment

Estimation Method for Dry Density, γ_d, at time of construction	Red Clay γ_d (pcf)	Gray Clay γ_d (pcf)
Test Method Tex-114-E	97	103
Test Method Tex-113-E	96	102
95% Standard Proctor	95	100

strength, it is reassuring that the three independent estimates of initial dry unit weight are so similar for each clay:

Although the differences among the "field" densities arrived at by the three procedures were small, it was decided that the triaxial shear test specimens should be compacted to the maximum dry density and optimum moisture content found using Test Method Tex-113-E. Personnel of the Texas SDHPT had recommended Test Method Tex-113-E as being representative of the compaction which would actually be achieved in the field. The "target" compaction levels for the soils from the IH 610 and Scott Street embankment were therefore chosen to be a maximum dry density of 96.3 pcf at a moisture content of 24 percent for the red clay, and a maximum dry density of 102.0 pcf at a moisture content of 21 percent for the grey clay.

CHAPTER 6: SPECIMEN PREPARATION PROCEDURES

6.1. INTRODUCTION

In order to proceed with the triaxial shear testing program, it was necessary to produce 1-1/2 inch diameter, 3 inch high specimens of the red and grey clays at the maximum dry densities and optimum moisture contents chosen in Chapter 5. The manner in which the specimens were actually compacted was not judged to have a significant effect on their shearing properties as long as the preparation procedure did not encourage the formation of large voids, planes of weakness, or other non-homogeneities. The problem was therefore to find a procedure which allowed reproducible density and which would produce uniform specimens which were free of large voids at a compactive effort below Standard Proctor.

All the triaxial specimens were compacted in a mold. The mold had been designed and made specifically to produce 1-1/2 inch diameter, 3 inch high triaxial specimens. Two procedures were investigated and evaluated for compacting specimens in the mold: a dynamic method using a falling-weight hammer to compact the soil and a kneading method involving the use of a pressure-controlled ram to compact the soil. This latter procedure was judged to more closely reproduce the kneading action of field compaction equipment.

6.2. SOIL PREPARATION

All testing in this program was carried out beginning with soil air-dried to a moisture content of approximately 6 percent. Large lumps of dry, hard clay were broken apart with a hammer and the resulting fragments sorted to produce quantities of the red and grey clays. These fragments were pulverized and then finally processed in a mechanical grinder to a particle size passing the No.10 sieve.

The results of grain size analyses performed on the IH 610 and Scott Street soils were presented in Chapter 4. It appears that approximately 95 percent of the red clay particles and 85 percent of the grey clay particles are smaller than the No.200 sieve opening. Furthermore, both clays contain negligible sand fractions. Therefore it seems reasonable to assume that the grinding of the clays during the preparation process would have had little, if any, effect on the mechanical composition of the two clays.

Quantities of the air-dried, pulverized soil were placed in a Lancaster "Counter Current Batch Mixer" and sufficient water was added to bring the moisture content of the soil to within 2 or 3 percent of the target value (24 percent for the red clay and 21 percent for the grey clay). The soil was then sealed in plastic bags and stored in a moist room for at least 24 hours to allow the clay to absorb the moisture. After this period of hydration, the moisture content of the soil was determined and, just before the specimens were compacted, the soil was

placed in the Lancaster mixer for a second time and sufficient water was added to bring the moisture content up to the target value.

This two-stage mixing process proved to be the only reliable way of obtaining soil at a moisture content within 1 or 2 percent of the desired value. During the final mixing, water was sprayed in a fine mist onto the soil as it was churned by the mixer. The amount of water which was added was sometimes very small and it is unlikely that the mixing process distributed this water evenly throughout the soil.

The moisture content control proved to be adequate, but not exceptional. Results will be presented in Chapter 7 to show that the moisture contents of the majority of the triaxial specimens compacted from the red clay were within 2 percent of the optimum moisture content (24 percent) although a small number deviated by as much as 3 percent.

6.3. SPECIMEN COMPACTION

The same compaction mold was used to compact specimens with the hammer procedure and the kneading procedure. The mold consists of an open-ended split brass cylinder with an inside diameter of 1-1/2 inches and a height of 3 inches. The brass cylinder is in three equal segments which can be secured tightly in a recessed base plate and held together at the top by a collar which locks onto pins on the outside of the three segments. Restraint at mid-height of the cylinder is provided by a circular clamp which holds the segments tightly against each other.

6.3.1. HAMMER COMPACTION

The method of hammer compaction used in this study has been developed through a number of years in the geotechnical laboratories of The University of Texas at Austin. The required equipment was readily available and the researchers were experienced in its use.

A standard hammer was used to compact all specimens. It consists of a 2.15 lb steel weight mounted on shaft in such a way that it can be dropped vertically. The weight impacts on a 1.46 inch diameter cast acrylic foot which is placed in contact with the loose soil in the mold. The diameter of the foot is slightly less than the inside diameter of the mold; therefore, the compactive effort is distributed across the entire cross-section of the specimen.

The density of a specimen is controlled by varying the number of hammer blows per layer, the height of hammer fall, and the number of layers or lifts used to compact the specimen. Experience indicated that the optimum number of lifts for a 3 inch high specimen was approximately ten; with more, it becomes difficult to control the layer thickness accurately and with less, the soil in each lift may not be compacted evenly.

Theoretically, a compactive effort of 4.02 ft lb per cu in. was needed to compact specimens of the red clay to the "target" density of 96.3 pcf. It was calculated that, with two blows per layer, the hammer would have to be dropped from a height of approximately 5.9 inches to produce this compactive effort (4.02 ft lb per cu in.) for the small triaxial specimens of red clay. Similarily, it was calculated that the

height of fall would have to be approximately 7.2 inches to produce the compactive effort of 4.88 ft lb per cu in. needed to achieve the target density for the grey clay. However, it is likely that there is a significantly greater kneading effect with the Proctor compaction method than with the method used to compact the triaxial specimens since the hammer fits tightly inside the mold for the triaxial specimens. The height of fall needed to be adjusted somewhat for both the red and grey clays to produce specimens at the target densities of 96.3 pcf and 102.0 pcf, respectively.

In order to estimate the height of hammer fall needed to produce specimens at the target densities, a series of specimens of red and grey clay were compacted with the hammer being dropped from different heights. It was found that the reproducible results were obtained with two blows per layer and ten layers for all specimens. Figures 6.1 and 6.2 show the variations in dry unit weight, γ_d, with the height of hammer fall for a number of specimens of red and grey clay, respectively. From these results, it was determined that the hammer would have to be dropped from a height of approximately 9 inches to achieve the target density for the red clay and approximately 6-1/2 inches to achieve the target density for the grey clay. For reasons which will be explained in Chapter 7, a range of hammer heights were later used for the compaction of the red clay specimens; these heights ranged from 8 to 9-1/2 inches.

The hammer compaction procedure generally worked well; at a given moisture content it proved possible to repeatedly compact specimens to similar densities. However, the external surfaces of the specimens

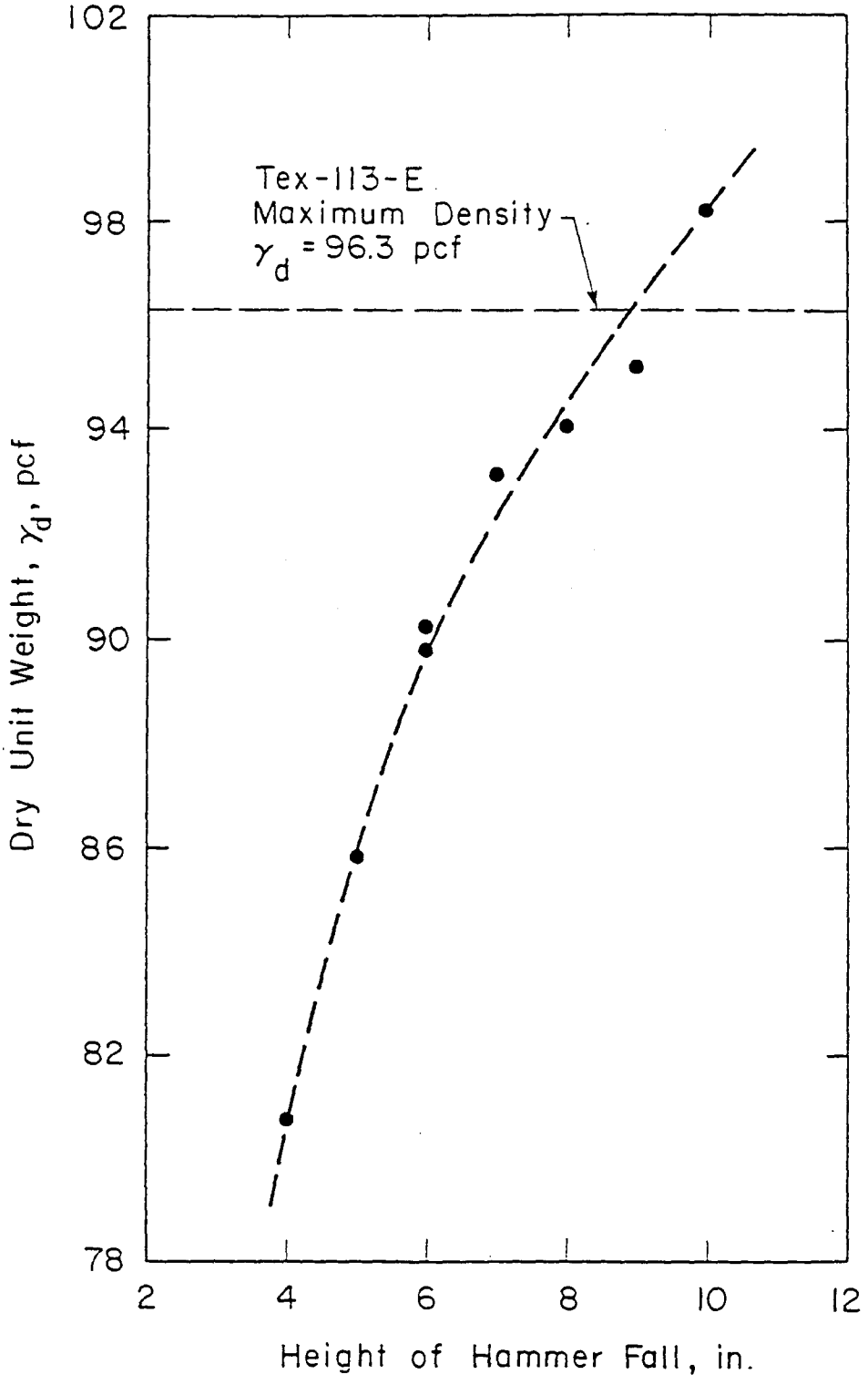

Fig. 6.1 Variation in Dry Unit Weight, Computed at the Target Moisture Content, with Height of Hammer Fall for Triaxial Specimens of Red Clay from IH 610 and Scott Street

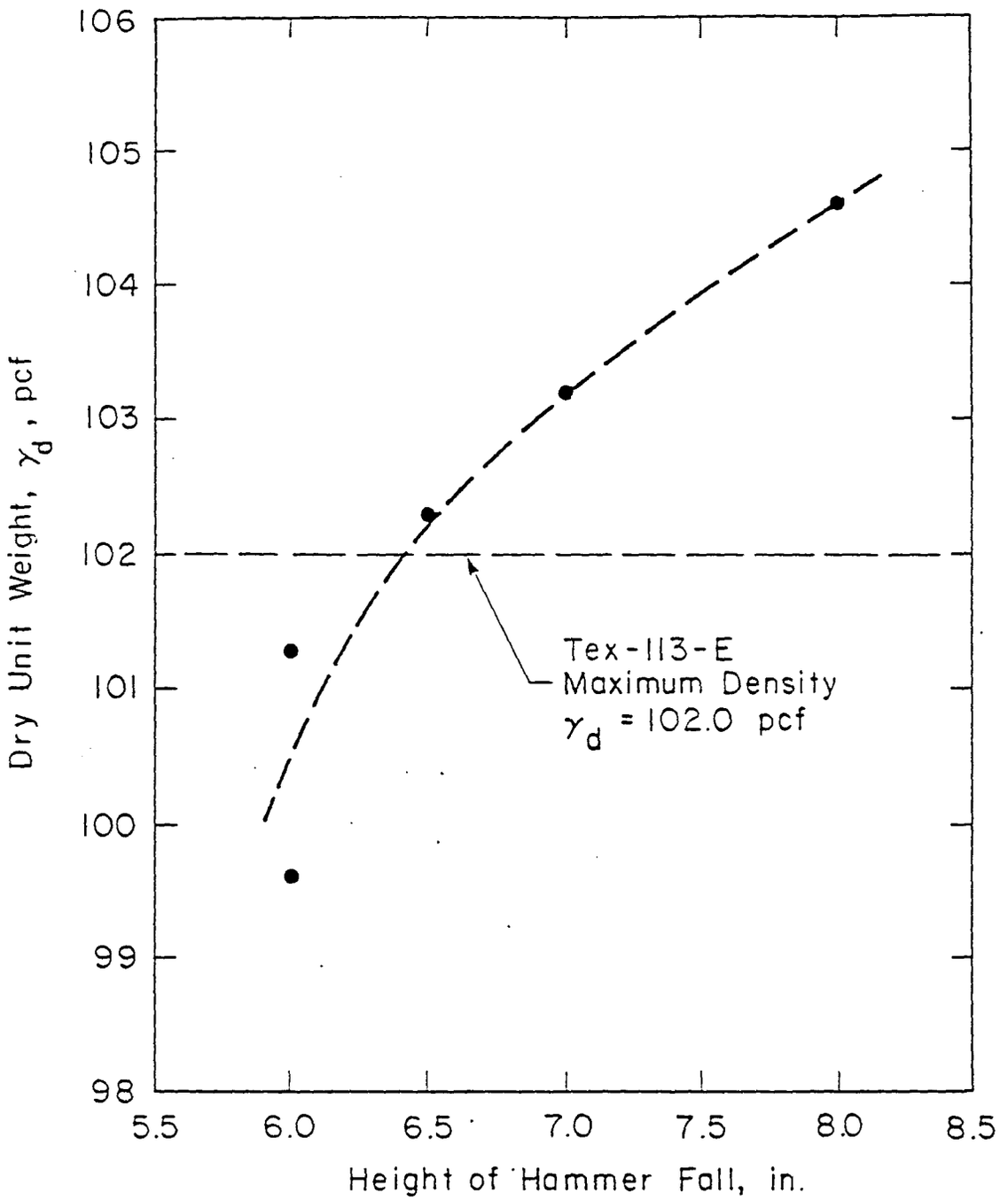

Fig. 6.2 Variation in Dry Unit Weight, Computed at the Target Moisture Content, with Height of Hammer Fall for Triaxial Specimens of Grey Clay from IH 610 and Scott Street

exhibited pronounced voids. There is little evidence to suggest that these voids extended into the inside of the samples, or that their presence on the outside significantly influenced the shear strength of the specimens

The size of the external voids seemed to depend on the condition of the soil which was placed in the mold. The soil tended to form large clods when being mixed and the size of the clods increased with the mixing time. At the low compactive efforts being used to form the specimens, the clods did not appear to be completely broken down by the compaction. The failure of the clods to break down seems to have been more pronounced in the soil placed against the faces of the mold; it is presumed that the internal clods had more freedom to deform and would therefore have squeezed together to form a more homogeneous structure than external appearances might have suggested. There was certainly never any sign of the existence of internal voids when the specimens were cut apart, although the cutting action could have smeared over any such openings.

It was felt that a different compaction method might be more effective at breaking down the clods. For this reason, the kneading compaction procedure was developed and evaluated.

6.3.2. KNEADING COMPACTION

The kneading compaction procedure was used to compact triaxi-

al-sized specimens of the red clay from the IH 610 and Scott Street embankment. It was thought that the manner in which kneading repeatedly shears the soil structure would help to break down the clods of soil which formed during the mixing process.

The kneading compaction apparatus used in this study consisted of a Bellofram air cylinder, with approximately one half inch of travel, and an air pressure regulation system. The apparatus is depicted schematically in Fig. 6.3. By controlling the air pressure acting on one side of a semi-rigid neoprene diaphragm inside the Bellofram cylinder, the force needed to displace the piston and, thus, the stress applied to the soil, were controlled.

During compaction, the tip of the ram was pressed against the loose soil in the mold and force was applied by hand to the casing of the cylinder until the piston just began to retract into the cylinder. At this point, the maximum contact pressure was being exerted by the ram or "foot."

The variables influencing the density of specimens compacted with the kneading procedure were the number of soil lifts, the air pressure in the Bellofram air cylinder, the number of "tamps" per layer, and the duration of each tamp. It was possible to feel when the maximum contact pressure had been applied since the piston would begin to retract into the cylinder; the time for which the maximum contact pressure is maintained is known as the "dwell" time. The force applied to the casing of the cylinder was then released and the foot was moved to another position.

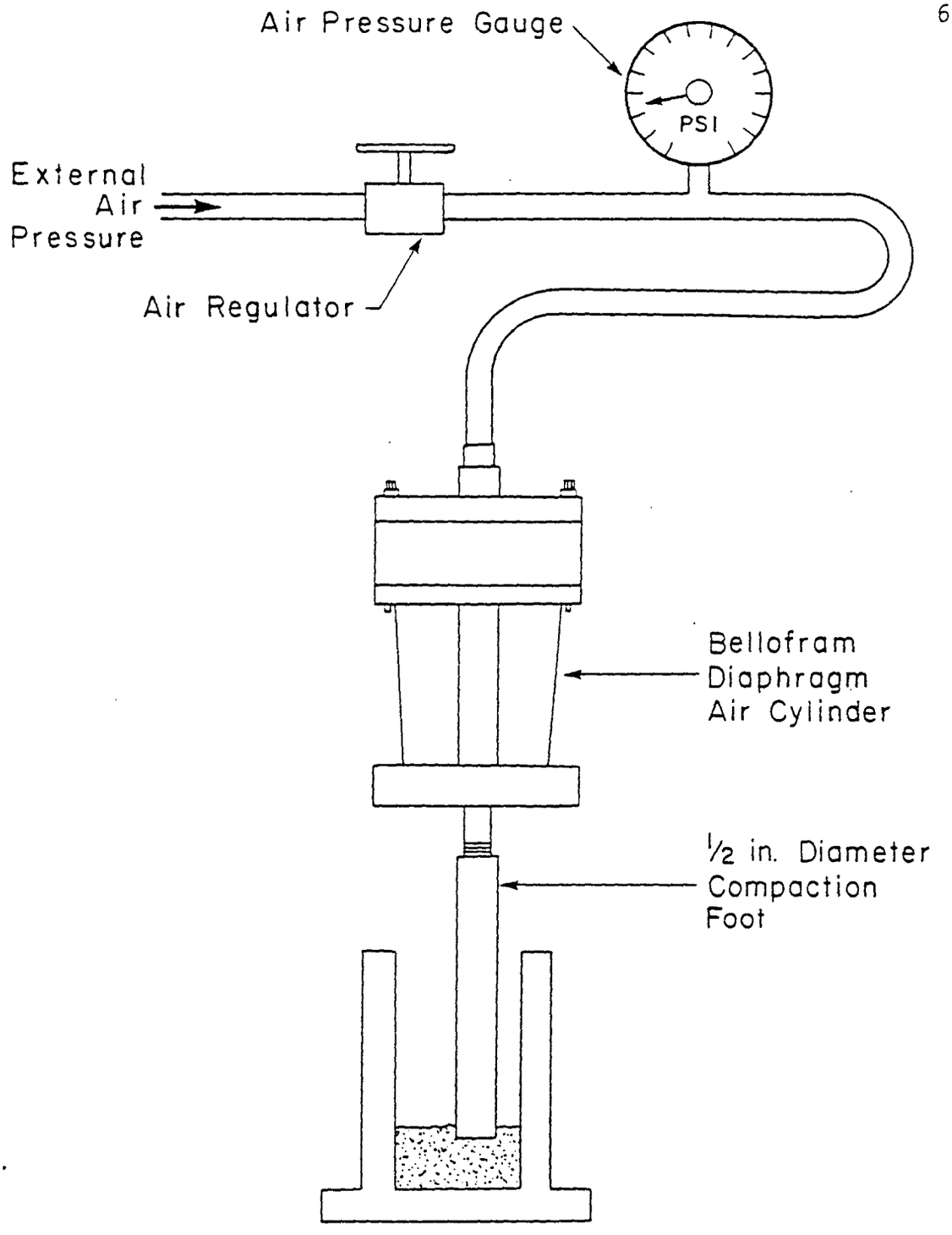

Fig. 6.3 Schematic Representation of
Kneading Compaction Apparatus

Specimens were formed with 5, 7, 8, 10, or 15 layers; it was found that the compacting effect of the foot did not penetrate more than 1/3 inch below the surface of the soil and it was therefore necessary to compact the specimens in at least ten lifts. As an absolute minimum, seven tamps per layer were needed to compact across the entire cross-sectional area of the specimen, although a more even distribution was achieved with ten tamps per layer. Specimens were compacted using dwell times of less than one second and approximately three seconds; the different dwell times did not appear to affect the structure of the specimens. Air pressures in the Bellofram air piston ranging from 8 to 12 psi were used; the homogeneity of specimens formed with the higher pressure was significantly better than that achieved with the lower air pressure.

Specimens produced with the kneading compaction procedure, which had dry unit weights close to the target value, also had voids which were at least as large as those produced by the hammer compaction procedure. Air pressures in the Bellofram air piston significantly greater than 12 psi would have been needed to completely break down the clods and the dry unit weights of specimens compacted in this manner would have been unacceptably high. The kneading compaction procedure was no more effective than the hammer compaction procedure in reducing voids in the specimens. Therefore, the kneading compaction procedure was not given further consideration in this study.

6.4. CONCLUSIONS

It was decided that the voids on the external surfaces of the specimens would not significantly affect their shearing strengths. If the effective stress shear strength parameters measured later in the laboratory turned out to be lower than the parameters back-calculated from observations of slides in the embankments under consideration, the effect of the voids might be suspected and could be examined more closely.

The hammer compaction procedure was chosen because it appeared to produce specimens with slightly smaller voids, was easier to perform, and gave more reproducible results than the kneading compaction procedure. All the specimens which were used in the shear testing program were prepared using the hammer compaction procedure.

Early in the testing program it was discovered that the quality of specimens was significantly improved if the clods were broken up before being placed in the mold. The most effective procedure for breaking the clods was found to involve extruding the soil through a No.10 sieve with a pestle. The extruded "strings" were then broken apart and arranged as evenly as possible in the bottom of the mold. The surface voids of specimens compacted using this method were much smaller than those found in the other hammer-compacted specimens.

The first two triaxial specimens formed from the red clay were compacted without benefit of the extrusion technique. However, the soil for every specimen after the first two was broken down before being

placed in the mold. It will be shown in Chapter 9 that the first two specimens exhibited strengths which fell towards the lower bound of the Mohr-Coulomb shear strength envelope; it is not known whether this observation is a coincidence or whether it indicates that the large voids did indeed affect the shear strength of these specimens.

CHAPTER 7: PROPERTIES OF AS-COMPACTED SPECIMENS

7.1. INTRODUCTION

Nine 1-1/2 inch diameter, 3 inch high compacted specimens of red clay from the IH 610 and Scott Street embankment were tested in the triaxial shear test program. Four similar specimens of grey clay from the IH 610 and Scott Street embankment were prepared and tested. In this chapter, the as-compacted properties of specimens prepared with red clay are presented. Although the grey clay was also tested, the major emphasis of the investigation was placed on the red clay and, therefore, a much more extensive body of data is available for this soil.

The dry unit weight and moisture content of each specimen were estimated at the time of compaction and subsequently determined more accurately at the end of the triaxial shear tests. At the end of each test, the specimen was recovered from the triaxial cell, weighed, and then oven-dried to determine the final moisture content and weight of dry soil. Since the weight of each specimen at the time of compaction had previously been measured, it was possible to calculate directly the initial moisture contents and dry unit weights. In this chapter, the ranges of the initial values of the dry unit weight, moisture content, and degree of saturation of the nine triaxial specimens compacted with red clay are presented.

Many more specimens were compacted than were actually subjected to triaxial shear testing. A number of unconfined compression tests were carried out on these spare specimens to gain an approximate estimate of the short-term, undrained shear strength of the red clay. Results from the unconfined compression tests are also presented in this Chapter.

7.1.1. NOMENCLATURE FOR SPECIMEN IDENTIFICATION

Individual specimens are identified by numbers or letters including a prefix to indicate the location in which the specimens were sheared. Specimens were sheared in laboratories in the basement and sixth floor of Ernest Cockrell Jr. Hall, leading to the prefixes "B" and "6", respectively. Specimens were numbered in the sequence in which they were installed in the triaxial cells at each location. For example, specimens B.1 and 6.1 were the first specimens set-up in the basement and sixth floor laboratories, respectively. There were minor differences in test procedure at the two locations caused by differences in equipment; for example, it was possible to measure volume change during consolidation with the equipment in the sixth floor laboratory, but not with the equipment in the basement laboratory.

7.2. UNCONFINED COMPRESSIVE STRENGTH

Unconfined compression tests were performed on nine specimens of

red clay, which ranged in dry unit weight from 81 pcf to 98 pcf. The moisture contents of these specimens at the time of compaction ranged from 23.2 percent to 24.2 percent. The tests were performed in accordance with ASTM Standard D 2166 at a strain rate of approximately one percent per minute.

The unconfined compressive strengths (q_u) have been plotted versus the initial dry unit weights of each of the specimens in Fig. 7.1. The results show clearly that the unconfined compressive strength increases from approximately 2000 psf at a dry density of 81 pcf to almost 5000 psf at a dry density of 98 pcf. It would, therefore, be reasonable to expect that compaction conditions would have a significant effect on the undrained, short-term strength of the IH 610 and Scott Street red clay.

7.3. MOISTURE CONTENT AND DRY DENSITY CONTROL

The height and diameter of each specimen were measured with a stand-mounted caliper and the average values of four independent measurements of each dimension were used to calculate the specimen volume. The wet weight of each specimen was also determined to the nearest one one-hundredth of a gram. The total unit weight, γ, of each specimen was determined by dividing the wet weight of the specimen by the volume of the specimen.

The dry unit weight (also referred to as the dry density), γ_d, was computed from the relationship:

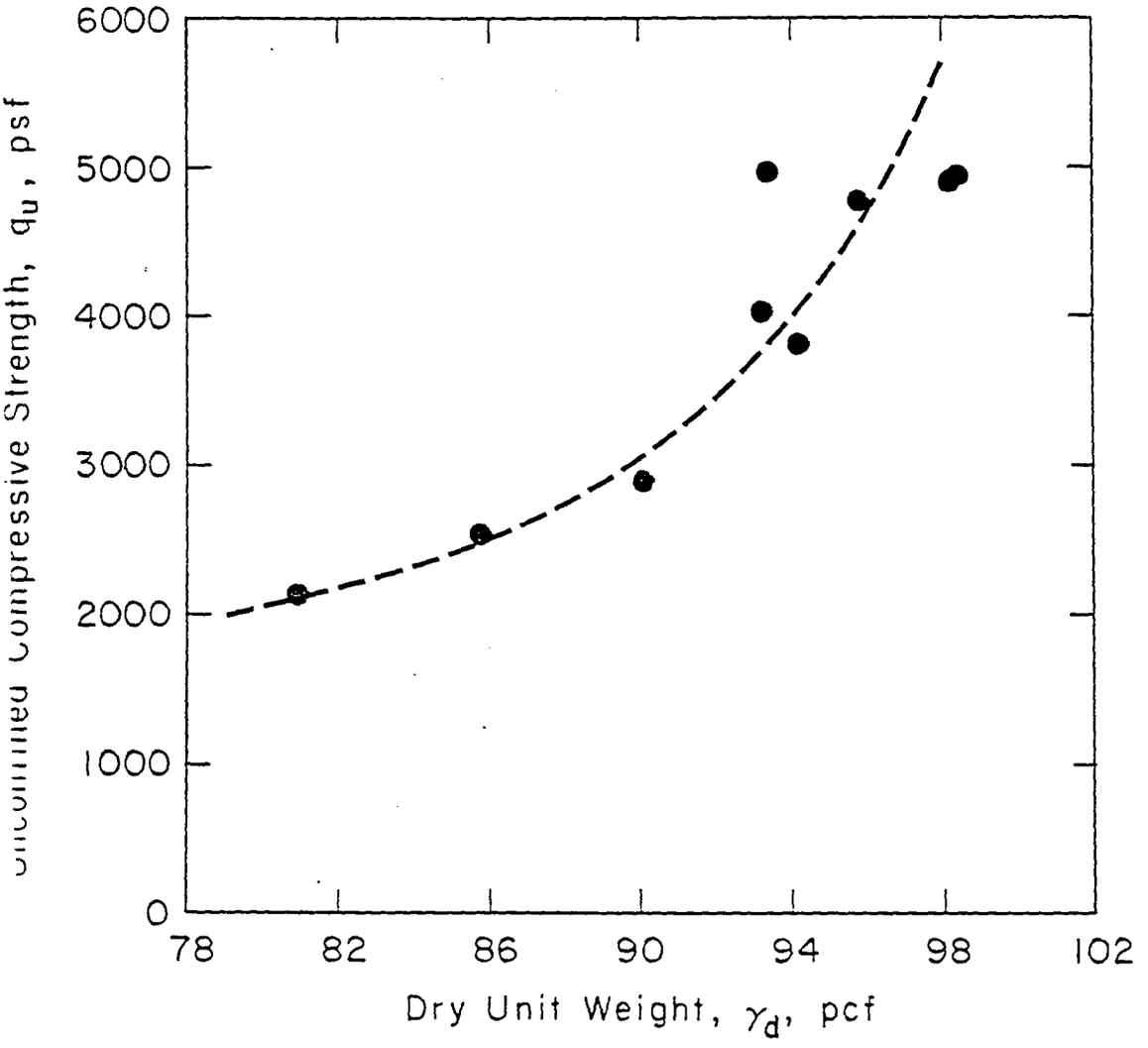

Fig. 7.1 Variation of Unconfined Compressive Strength with Dry Unit Weight for Nine Specimens of Red Clay from IH 610 and Scott Street

$$\gamma_d = \frac{\gamma}{1 + \omega} \qquad (7.1)$$

where ω is the moisture content of the specimen, expressed as a decimal. At the time of compaction the average moisture content of each specimen was not known precisely. In some cases, the moisture content of a small sample of soil from a particular batch had been determined after the final mixing. In other cases, the final mixing occurred just before compaction and water had been added to increase the moisture content of the soil to the "target" values of 24 percent for the red clay or 21 percent for the grey clay. In such situations, it was assumed that the specimens were being compacted at the "target" moisture content, while the actual moisture content may have been significantly different. Also, the moisture content of the soil may have been reduced by the compaction process. Accordingly, an estimated moisture content rather than a measured one was used to compute dry density values at the time of compaction. If the computed dry density of a specimen varied significantly from the "target" dry density, it was assumed that an insufficient or excessive compactive effort had been used since the moisture content of the soil was presumed to equal the "target" value. In such instances, the specimen was discarded and the height of hammer fall was adjusted before another specimen was compacted from the same batch of soil. The height of hammer fall was therefore varied from one specimen to another in an attempt to attain the target density.

The initial dry unit weights of the nine specimens of red clay which were subsequently tested in the triaxial shear testing program are plotted versus compaction moisture content in Fig. 7.2. Different symbols represent specimens compacted with different heights of hammer fall; the heights ranged from 8.0 to 9.5 inches. The moisture content and dry density values are those calculated after the dry weight of soil in each specimen had been determined at the end of each shear test.

The results in Fig. 7.2 show that the variation of the height of hammer fall produced a relatively narrow range of dry unit weights, despite variations in the compaction moisture content. The range in dry unit weights is only 2.5 pcf. Since the original field compaction conditions can only be estimated and it is likely that there is considerable variation throughout the embankment in the degree of compaction which was achieved, the range in laboratory dry densities is judged acceptable.

The moisture contents of the specimens varied significantly, despite the care taken to achieve the desired value of 24 percent, selected and described in Chapter 5. While four of the specimens had initial moisture contents within 1 percent of the target value of 24 percent, another four of the nine specimens had moisture contents which were more than 2 percent greater or lower than the target value. However, the variations in compaction moisture content did not appear to have affected significantly the final moisture content and dry unit weight of the specimens when fully saturated and consolidated, as will be shown in Chapter 8.

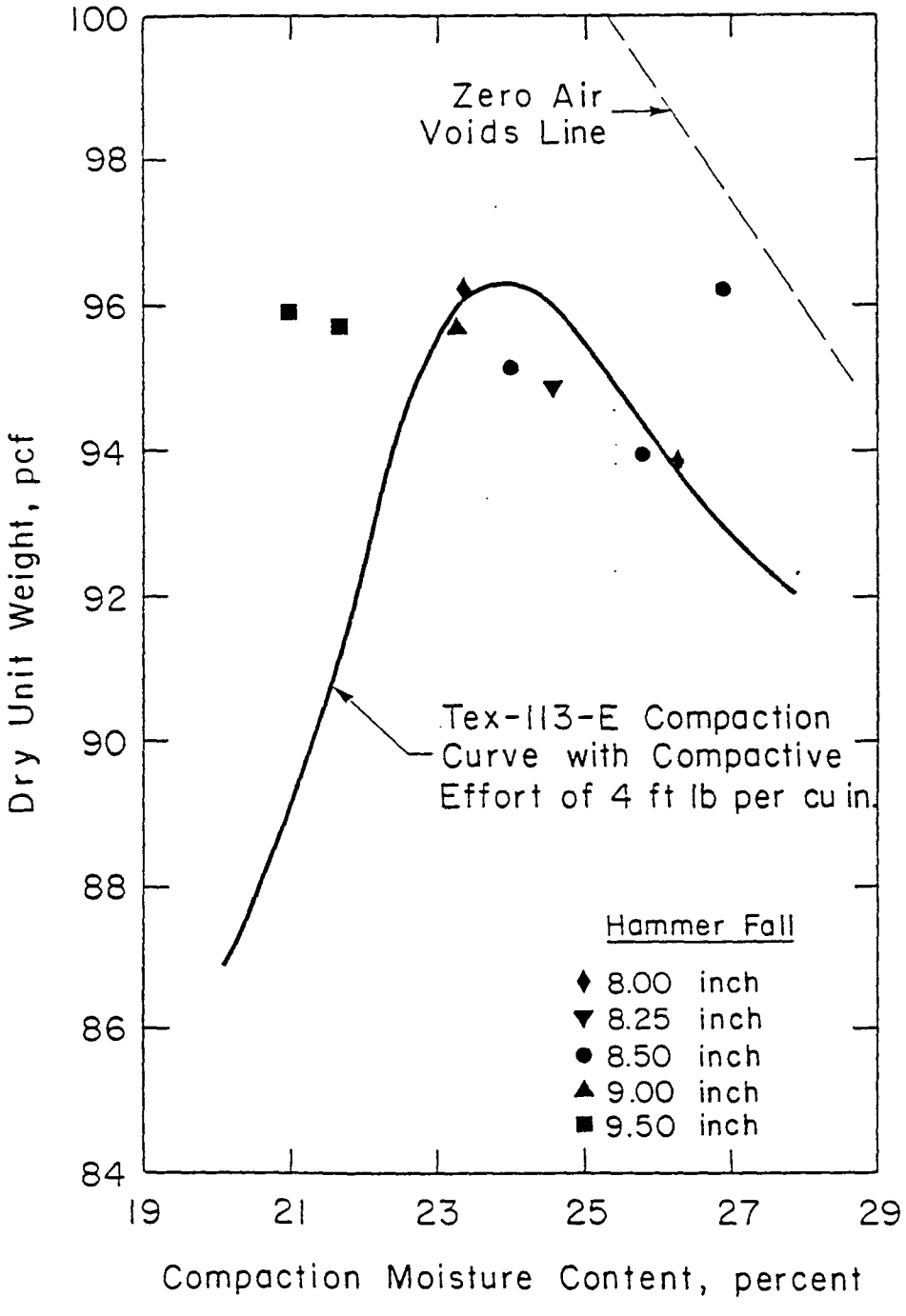

Fig. 7.2 Variation of Dry Density with Moisture Content at Different Compactive Efforts for Nine Specimens of Red Clay from IH 610 and Scott Street

7.4. INITIAL DEGREE OF SATURATION

The degree of saturation S_r (the ratio of volume of pore water to total volume of voids) was calculated for each specimen from the expression:

$$S_r = \frac{\omega G_s \gamma_d}{G_s \gamma_w - \gamma_d} \tag{7.2}$$

where ω is the moisture content, G_s is the specific gravity of solids, γ_d is the dry unit weight of the soil, and γ_w is the unit weight of water. Throughout this investigation, the specific gravity of solids for the red and grey clays was assumed to be 2.70.

The initial degree of saturation of the triaxial specimens was calculated using the initial moisture contents and initial dry unit weights which were calculated after the dry weight of the specimen had been determined at the end of each test. The degree of saturation is plotted versus the compaction moisture content for nine specimens of red clay from the IH 610 and Scott Street embankment in Fig. 7.3. The figure clearly shows that the initial degree of saturation increases as the compaction moisture content increases.

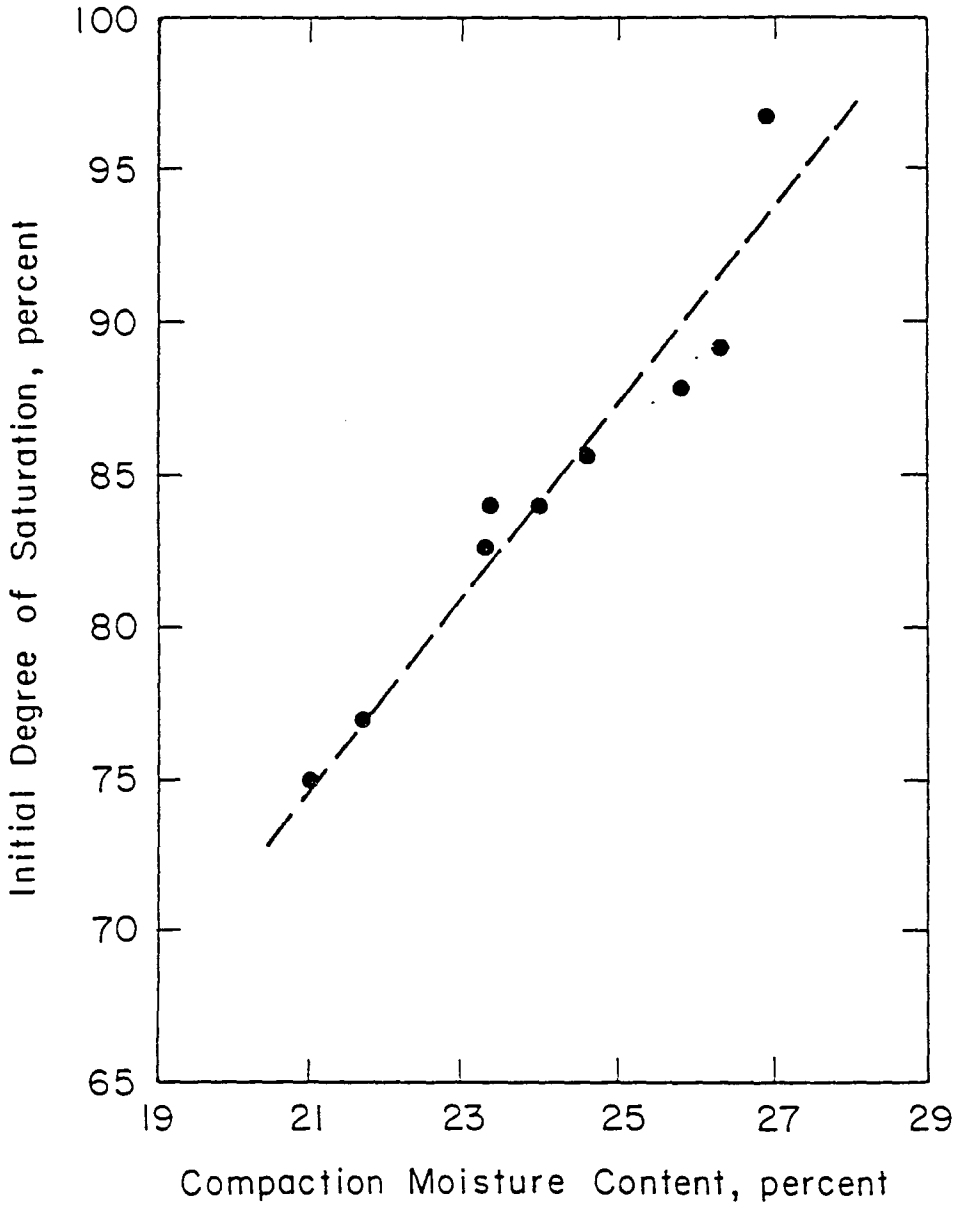

Fig. 7.3 Variation of Initial Saturation with Compaction Moisture Content for Nine specimens of Red Clay from IH 610 and Scott Street

CHAPTER 8: SET-UP AND CONSOLIDATION OF TRIAXIAL SPECIMENS

8.1. INTRODUCTION

Twelve consolidated-undrained ($\bar{R}$) triaxial shear tests with pore pressure measurement and one consolidated-drained (S) triaxial shear test were performed to determine effective stress shear strength parameters. Tests were performed on hammer-compacted specimens of the red and grey clays from the IH 610 and Scott Street embankment. In this and successive chapters, any discussion of soil or specimen properties will be in reference to the red clay from the IH 610 and Scott Street embankment unless the soil is identified otherwise. The triaxial test equipment and the procedures which were used to set-up and consolidate specimens in triaxial cells are described in this chapter. The properties of the specimens after consolidation and saturation are also presented.

8.2. TEST APPARATUS

The triaxial shear tests were performed in two laboratories; the equipment in each laboratory is described briefly in this section. The equipment was all capable of producing high quality test data and it is

not thought that differences in apparatus affected the shear strength data in any significant manner.

8.2.1. SIXTH FLOOR LABORATORY

The apparatus used in the sixth floor laboratory has been described in some detail by Deming (1982) and Paster (1981). The cell and pore water pressures were applied through air-over-water interfaces. The pressurized air system in the laboratory was regulated to provide the desired air pressures. Figure 8.1, which has been reproduced from Deming's thesis, shows the general arrangement of the triaxial cell which was used. The cell was filled with deaired water and was connected through approximately two feet of 1/8 inch diameter tubing to an external accumulator which contained the air-over-water interface for the cell pressure.

A device for measuring pore water pressures and volume changes during consolidation and shear was connected to the "pore pressure line" which runs through the base pedestal to the bottom of the specimen. The pore pressure and volume change device is similar to the one developed by Chan and Duncan (1966). The air-over-water interface which was used to control the back pressure was an integral part of the pore pressure and volume change device.

Pore water pressure and cell pressure were measured with a single low compliance Validyne Model DP15 pressure transducer with appropriate valves to allow each pressure to be measured independently of the

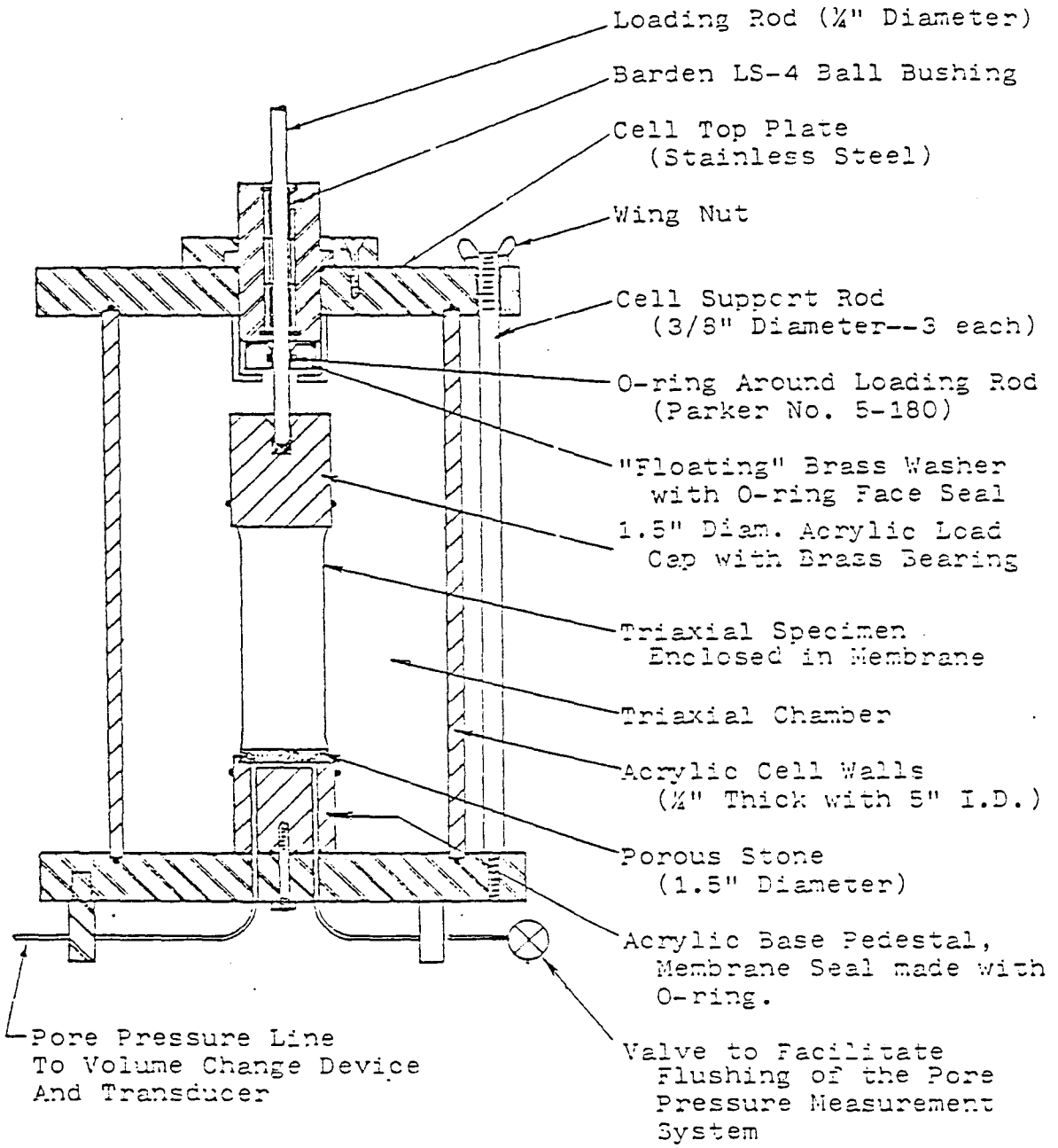

Fig. 8.1 Cross-Section Drawing of Triaxial Cell in Sixth Floor Laboratory (after Deming, 1982)

other. The electrical output from the transducer was fed to a carrier demodulator and then to a digital voltmeter.

A Wykeham Farrance loading press (Model 10021) was used to shear the specimens at a constant rate of axial deformation. Axial loads were measured using a Transducers Inc. (Model BTC-FF62-CS-100) electronic load cell. The electrical output from the load cell was fed to a digital voltmeter.

8.2.2. BASEMENT LABORATORY

The apparatus which was used in the basement laboratory was similar to that in the sixth floor laboratory. The cell and pore water pressures were applied through air-over-water interfaces. The triaxial cells were slightly smaller than those in the sixth floor laboratory but had the same design features. A Validyne Model DP15 pressure transducer was mounted on the outside of the cell and connected to one of the two pore pressure lines, which run through the base pedestal to the bottom of the specimen, to measure pore water pressures. The electrical output from the pore pressure transducer was recorded using a digital voltmeter. The other pore pressure line was connected to a pressurized air-over-water interface which could be used to control the pore pressures within the specimen. The pore pressure lines were flushed by bleeding water and air through a relief valve in the transducer.

The accumulators which contained the air-over-water interfaces for the application of cell and back pressures were mounted on a separate

panel board. The air pressures acting on each of these interfaces were regulated using controls on the panel board and were measured with an air pressure gauge mounted on the panel board.

All specimens were sheared using Wykeham Farrance loading presses; these presses were the same as those used in the sixth floor laboratory. The axial load was measured with a proving ring. A dial gauge was used to measure axial deformation.

8.2.3. CALIBRATION OF EQUIPMENT

Each of the measuring systems used in this study was calibrated against a "standard" system which was judged to give accurate and reproducible results. The calibration factors were checked for each system.

The standard system which was used for the calibration of the proving rings was the Transducers Inc. electronic load cell which was also used to measure axial loads in the sixth floor laboratory. This load cell was itself calibrated using a series of known dead-weights. A linear regression analysis was performed to determine a calibration factor for each proving ring over the range of expected loads.

The standard system which was used to calibrate pressure measuring systems was a Wallace and Tiernan Series 1500 pressure gauge, which is rated by the manufacturer as being accurate to 0.13 psi. The calibration of pressure transducers was achieved by connecting them to a triaxial cell filled with water in which the pressure was raised and lowered over the ranges expected to be reached during the testing of the speci-

mens. The same transducer/demodulator/voltmeter combinations were used during the shear testing as during the calibration. A linear regression analysis was performed on the calibration measurements to determine the calibration factors for each transducer. The response of the transducers was always sufficiently linear to justify the use of a linear calibration line.

The pressure gauges which were used to measure the applied cell pressures in the basement laboratory were calibrated at the same time and in the same manner as the pressure transducers. The calibration factors for each of the pressure gauges were also determined by a linear regression analysis. These calibration factors were predictably very close to unity, i.e. a gauge reading of 1 psi corresponded to an actual pressure of 1 psi.

8.3. PROCEDURE FOR INSTALLATION OF SPECIMENS IN CELLS

The procedures used to set-up specimens in the triaxial cells were essentially the same in the basement and sixth floor laboratories. The compacted specimens were stiff and there appeared to be little possibility of a specimen being mechanically disturbed as it was set-up in a cell.

The pore pressure lines leading to the base pedestal of the triaxial cell and the porous stone on the pedestal were saturated with deaired water before the specimen was placed on the pedestal. Two rolled-up membranes were placed over the pedestal and sealed independ-

ently with rubber O-rings in such a way that they could be rolled upward at a later stage. The porous stone was then covered with a disk of filter paper and the specimen placed on the filter paper. The top cap was placed on the upper surface of the specimen. A vertical filter paper drain was prepared from Whatman No.1 Chromatography Paper, moistened, and wrapped around the specimen. The filter paper was cut in alternating vertical strips to cover approximately 50 percent of the perimeter of the specimen and overlapped the edge of the porous stone at the base of the specimen.

After the filter paper drain had been oriented and smoothed, the first of the two membranes was rolled up the sides of the specimen and over the top cap. The drainage valve to the base of the specimen was then opened and deaired water was introduced between the specimen and the membrane. The membrane bulged outwards due to the hydrostatic pressure of this free water. The membrane was gently "massaged" to release air trapped in the external voids of the specimen. The second membrane was then rolled slowly over the first membrane. The rolling constriction provided by the second membrane forced the free water and air trapped inside the first membrane to flow upward past the top cap. When the excess water and free air had been forced out, the first membrane was sealed against the lower portion of the top cap with an O-ring. The second membrane was then rolled over this seal and secured against the upper portion of the top cap with another O-ring.

The wall and top plate of the cell were assembled and secured. The loading rod was liberally coated with silicon oil, carefully pushed

through the ball bushing assembly in the top plate of the cell, and seated in the top cap. The triaxial cell was then filled with deaired water. At this stage, the pore pressure lines were again flushed with deaired water.

When the cell was full of water, it was connected to the lines which would be used to control the consolidation phase of the test. In the sixth floor laboratory, the air line used to control the cell pressure was connected to the accumulator mounted on the side of the cell and the pore pressure line was connected to the volume change device. The volume change device had been previously deaired. In the basement laboratory, the cell and pore pressure lines were connected to the accumulators containing the air-over-water interfaces.

8.4. PROCEDURE FOR CONSOLIDATION AND SATURATION OF SPECIMENS

Once specimens were set-up in the triaxial cells, they were consolidated and saturated. The procedures used for consolidation and saturation are described in this section.

8.4.1. CONSOLIDATION OF SPECIMENS

Specimens were consolidated to final effective consolidation pressures ranging from 1.1 to 19.4 psi for the red clay and from 1.1 to 20.2 psi for the grey clay. The value of the desired final effective

consolidation pressure dictated the consolidation procedure. In tests with final effective consolidation pressures of less than 2 psi, a special procedure was used which will be described in the following section. In tests with a final effective consolidation pressure of 5 psi or more, the specimen was first subjected directly to an effective confining pressure of 5 psi. This was achieved by applying a pressure of 10 psi to the cell fluid and a pressure of 5 psi to the pore fluid. The pore fluid pressure during consolidation is typically referred to as a "back pressure" and the term "back pressure" will be used subsequently in this report. After the initial cell and back pressures of 5 and 10 psi, respectively, had been applied, the cell pressure and back pressure were raised in equal increments every two or three days until full saturation was achieved. The manner in which the saturation of a specimen was estimated is described in a following section.

In tests where the final effective consolidation pressure was to be greater than 5 psi, the procedure described above was followed until full saturation was achieved. At that stage, the cell pressure was raised a sufficient amount to increase the effective confining pressure to the desired final effective consolidation pressure. In the sixth floor laboratory, pore water volume changes were recorded to determine when primary consolidation had finished. The specimen was then sheared.

Back pressure increments were limited to 5 psi to ensure that specimens were not inadvertently subjected to effective confining pressures which were higher than the desired final effective consolidation pressure. In an unsaturated specimen, the pore pressures within the spe-

cimen only rise to the level of the recently applied back pressure gradually and, as a result, some portions of the specimen are subjected to significantly higher effective confining pressures than other portions. It was judged that the significance of this effect would be minimized by limiting the increments in back pressure to 5 psi.

8.4.1.1. Procedure for Consolidation to Low Final Pressures

The manner in which the cell and back pressures were controlled was slightly different in tests with final effective consolidation pressures less than 2 psi. In these tests, a single air pressure source acted on the air-over-water interfaces for both the cell pressure and the back pressure. The effective confining pressure was controlled by maintaining a selected difference in height between the two (cell pressure and back pressure) air-over-water interfaces. For example, the cell pressure interface would be situated approximately 28 inches above the back pressure interface to maintain an effective confining pressure of 1.0 psi. The final effective consolidation pressure was applied to the specimen as soon as it was installed in the triaxial cell. The single air pressure acting on both interfaces was then increased by 5 psi every two or three days until the specimen was fully saturated.

8.4.2. SATURATION OF SPECIMENS

The pore pressure coefficient, "B" (Skempton, 1954) was measured to determine whether a specimen was fully saturated. By assuming that the compressibility of the pore water is negligible compared to the compressibility of the soil structure of a specimen, Skempton was able to show that the pore pressure coefficient B is unity for a fully saturated soil. Skempton defined the coefficient B with the relationship:

$$B = \frac{\Delta u_a}{\Delta \sigma_3} \tag{8.1}$$

where $\Delta\sigma_3$ is an increment in the all-round confining pressure and Δu_a is the resulting change in pore pressure.

Saturation was determined by measuring the pore pressure coefficient B, or "B-value", for each specimen as follows: each time the cell pressure was raised by an amount $\Delta\sigma_3$, the specimen was isolated from the applied back pressure by the closure of the drainage valve and the resulting change in pore pressure, Δu_a, was measured. The change in pore water pressure was measured with the pore pressure transducer thirty seconds after the cell pressure had originally been raised.

Immediately after the pore water pressure was measured to determine the B-value, the back pressure was increased by the same amount as the cell pressure ($\Delta\sigma_3$) and the drainage valve was opened. The specimen was then allowed to equilibrate at the same effective confining pressure as had been applied prior to the initial increase in the cell pressure.

The B-value was calculated using Equation (8.1) each time the cell and back pressures were raised. If the B-value was 0.99 or greater, the specimen was considered to be fully saturated. It was found that back pressures ranging from 20 to 30 psi were needed to achieve saturation. The first B-value measured after the installation of a specimen in a triaxial cell typically ranged from 0.6 to 0.8. No distinct trend was observed between the initial degree of saturation of a specimen and the initial B-value.

8.5. SPECIMEN PROPERTIES AFTER CONSOLIDATION

Properties of specimens after consolidation and saturation in the triaxial cells are considered in this section. Results for changes in moisture content, dry unit weight, pore water volume, and degree of saturation are presented. The consolidation characteristics of the specimens are also considered. Seven conventional consolidated-undrained ($\overline{R}$ or $\overline{CU}$) tests with pore pressure measurement, one consolidated-drained (S or CD) test, and one consolidated-undrained test in which the consolidation pressure was varied cyclically, were performed on specimens of red clay from the IH 610 and Scott Street embankment. The cyclically-consolidated specimen is considered in a separate section of this chapter, as this specimen exhibited significantly different properties than comparable specimens which were consolidated conventionally.

8.5.1. MOISTURE CONTENT

In all of the consolidated-undrained tests, the moisture contents of the specimens at the end of consolidation were assumed to be exactly the same as those measured at the end of shear since no drainage was allowed during shear. In the one drained test, where drainage was allowed during shear, the moisture content at the end of consolidation was back-calculated using the measured moisture content at the end of shear and the measured pore water volume change during shear. The moisture contents at the end of consolidation are plotted versus the final effective consolidation pressures in Fig. 8.2 for both the drained and undrained tests. The range and average value of the compaction moisture contents are also shown. It is evident that all of the specimens absorbed additional water during the consolidation phase and that generally the increase in moisture content was greater for specimens subjected to lower effective confining pressures.

The results shown in Fig. 8.2 all seem very reasonable. That is, it is reasonable to expect an increase in moisture content for all the specimens, regardless of confining pressure, due to the saturation of the specimens prior to or in conjunction with the consolidation process. Also, it is reasonable to expect that a higher effective confining pressure would result in a more compact soil structure and a correspondingly lower moisture content.

The moisture contents at the end of consolidation of the laboratory specimens are similar to the moisture contents which were measured

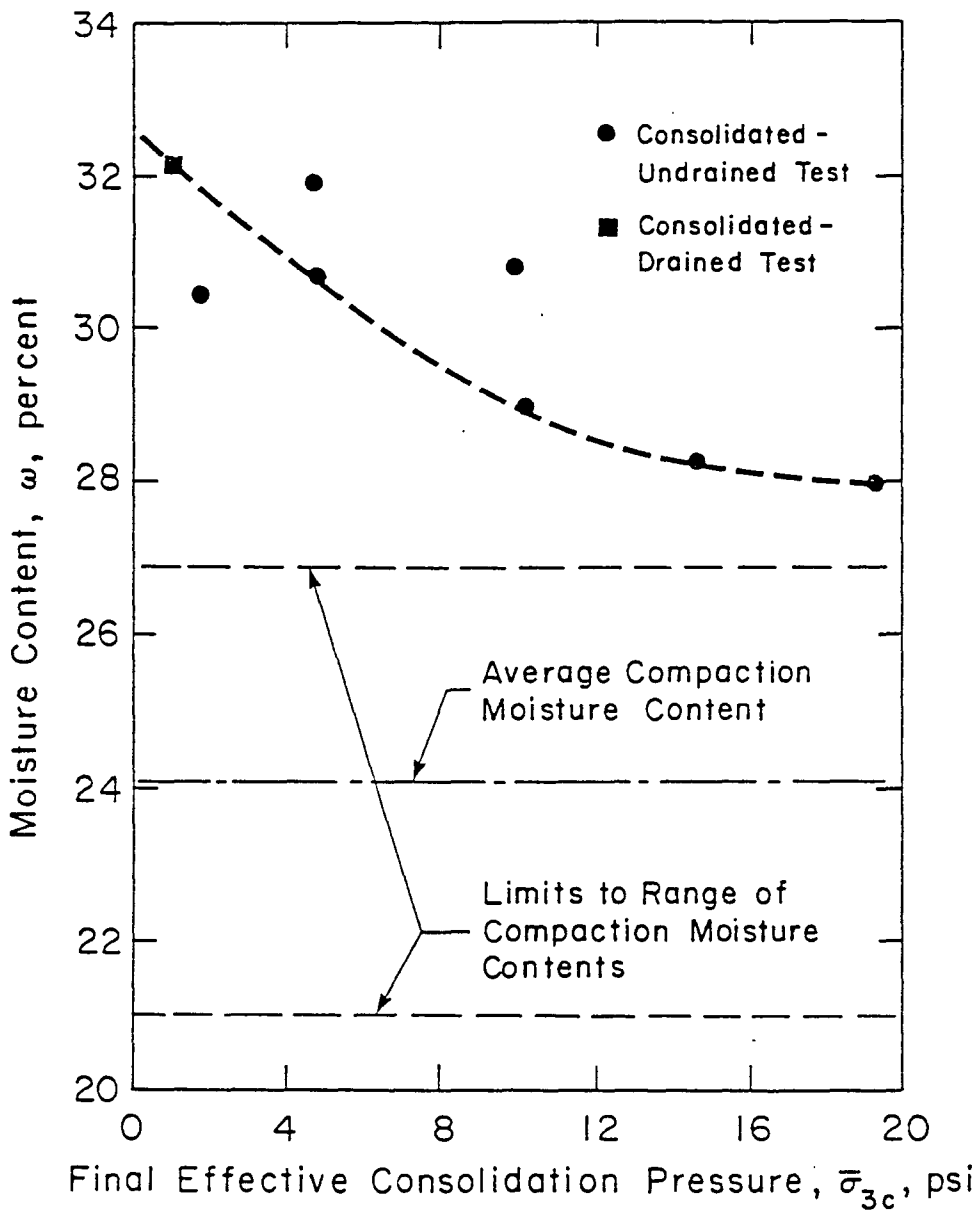

Fig. 8.2 Variation of Moisture Content at End of Consolidation with Final Effective Consolidation Pressure for 8 Specimens of Red Clay from IH 610 and Scott Street

in the IH 610 and Scott Street embankment and presented in Chapter 2. At a depth of three feet in the embankment, where the effective confining pressure would be approximately 2 psi, the measured moisture content in a section of the embankment which had not been disturbed by a slide was approximately 30 percent. At the same effective confining pressure in the laboratory, the moisture content of a fully saturated specimen appears to range from approximately 30 percent to 32 percent based on the results shown in Fig. 8.2. The close similarity between the field moisture contents and the moisture contents measured in the triaxial specimens indicates that the embankment material was almost fully saturated and that the compaction and consolidation procedures used in the laboratory were probably reasonable.

8.5.2. DRY UNIT WEIGHT

The dry unit weight at the end of consolidation was calculated for each of the eight specimens under consideration in this section. The variation of the final dry unit weight with the final effective consolidation pressure for each specimen is plotted in Fig. 8.3. The data show that lower confining pressures result in lower dry unit weights.

With the exception of the specimen B.1, which was consolidated at an effective pressure of 19.4 psi, all the specimens swelled during the consolidation phase. This observation is in agreement with the increases in moisture content shown in Fig. 8.2 and indicates that the

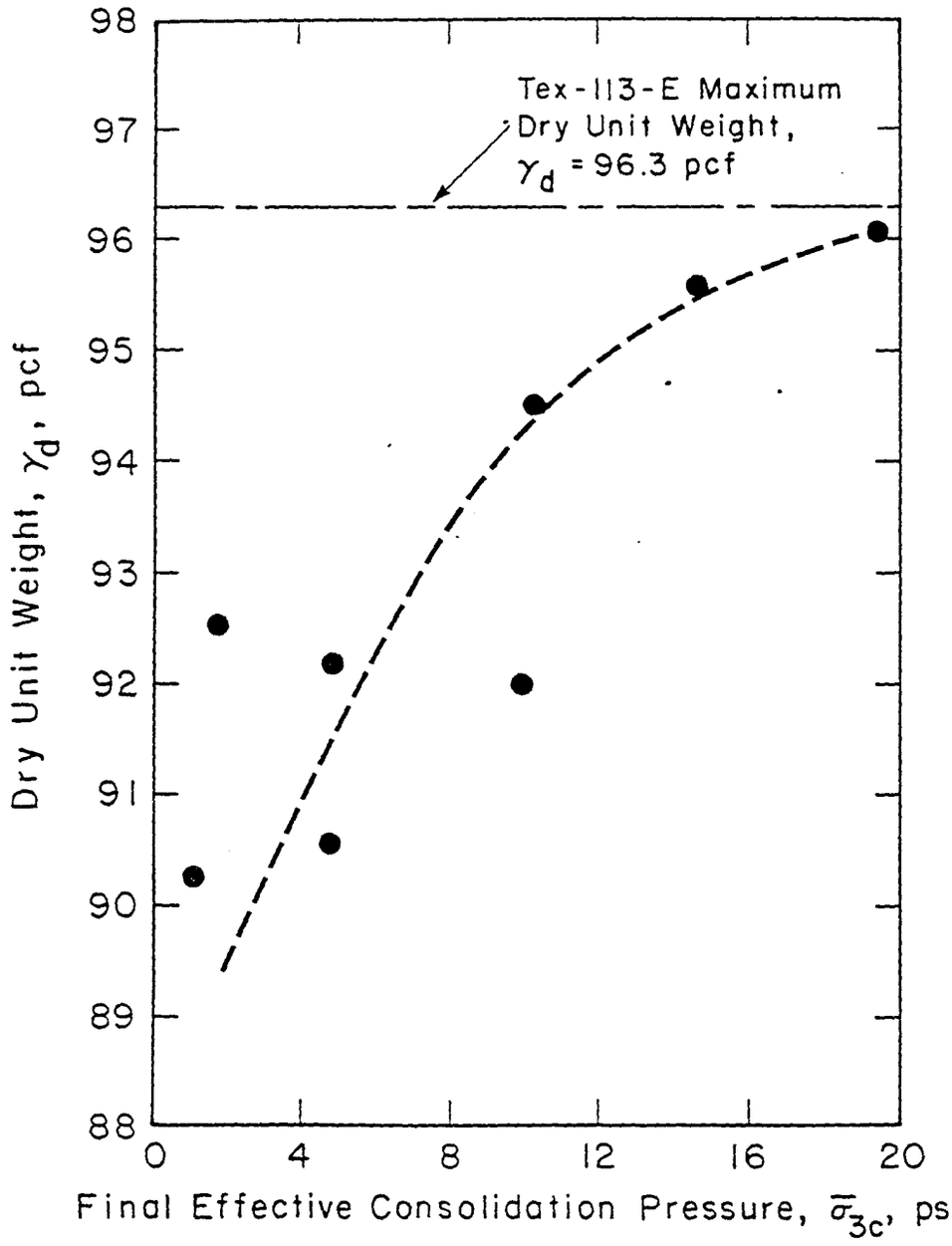

Fig. 8.3 Variation of Dry Unit Weight at End of Consolidation with Final Effective Consolidation Pressure for Eight Specimens of Red Clay from IH 610 and Scott Street

dry unit weight of the embankment fill is likely to have decreased since the time of compaction.

8.5.3. VOLUME CHANGE DURING CONSOLIDATION

The volume of water which had to have flowed into or out of a specimen to cause the change in moisture content from the value at the time of compaction to the value at the end of consolidation was calculated for all the triaxial specimens. The calculated volume changes, represented by solid symbols, are plotted versus the final effective consolidation pressure, $\bar{\sigma}_{3c}$, in Fig. 8.4.

The volume of water which flowed into or out of a specimen during consolidation and saturation was measured using a volume change device for all specimens tested in the sixth floor laboratory. The net measured increases in pore water volume, represented by open symbols, for three specimens tested in the sixth floor laboratory are also presented in Fig. 8.4. These values can be seen to vary significantly from the values which were calculated from the changes in moisture content of the same three specimens.

The results presented previously in Fig. 8.3 indicate that specimens which were consolidated at low effective confining pressures tended to swell more than specimens at higher confining pressures. Thus, it is reasonable to expect that the increase in pore water volume would be greater for specimens consolidated at low effective confining pressures. However, the results shown in Fig. 8.4 do not conclusively support the

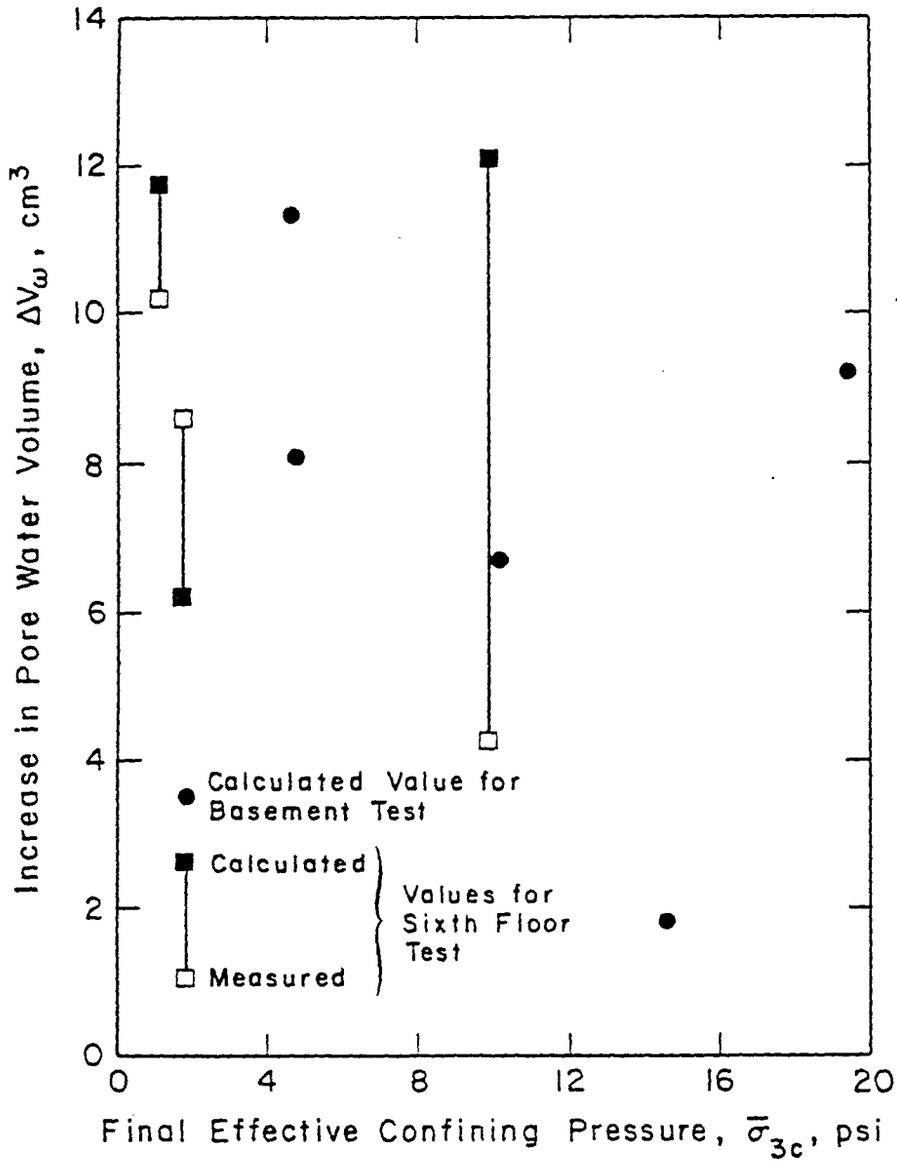

Fig. 8.4 Calculated and Measured Increases in Pore Water Volume during Consolidation for Eight Specimens of Red Clay from IH 610 and Scott Street

existence of such a trend. One reason for the differences between the calculated and measured volume changes may be that, while each specimen was being installed in a triaxial cell, free water was allowed to flow between the membrane and the specimen. It is likely that the specimens absorbed a significant volume of water as a result of this set-up procedure. If the pore water volumes increased while specimens were being installed in the triaxial cells, the increases in pore water volume measured during consolidation would be expected to be less than those calculated from the changes in moisture content. The results presented in Fig. 8.4 indicate that this effect was observed in two of the three tests where volume changes were measured.

8.5.4. FINAL DEGREE OF SATURATION

The final degree of saturation at the end of consolidation could not be calculated directly because the volume of the specimen at the end of consolidation was not known accurately. Although initial volumes were measured at the time of compaction and volume changes during consolidation were measured or calculated for each specimen as shown in the previous section, the volume change data do not appear to be reliable. Thus, the volume and degree of saturation of each specimen at the end of consolidation were not calculated directly.

As it was not possible to calculate directly the degree of saturation at the end of consolidation, this value has been inferred from measurements of the pore pressure parameter B (Skempton, 1954); the

method used to determine the "B-value" was described earlier in this chapter. The consolidation and saturation phase of a test was not concluded until a B-value of 0.99 or greater was obtained. Therefore, it has been assumed that the degree of saturation at the end of consolidation was 100 percent for all specimens.

8.5.5. CHANGES DUE TO CYCLIC CONSOLIDATION

In an attempt to simulate alternate cycles of drying and wetting near the face of an embankment, the effective confining pressure for one test (6.5) was varied from 1.1 psi to 20 psi for ten full cycles. The specimen was allowed to reach complete equilibrium under each stress state (consolidation or swell). The duration of each full cycle of consolidation and swell was approximately six days. The ten cycles of consolidation and swell were completed in 75 days.

During saturation and ten cycles of consolidation and swell, the moisture content of the specimen increased from 26.3 percent at the time of compaction to 30.7 percent at the final effective confining pressure of 1.1 psi. This final value (30.7 percent) compares favorably with the results presented in Fig. 8.1 for the other eight specimens compacted with red clay from the IH 610 and Scott Street embankment.

The final dry unit weight of the specimen was 92.1 pcf which is 1.7 pcf lower than the value at the time of compaction. The specimen therefore swelled even though the cyclic variation in consolidation pressure might have been expected to densify the specimen. The final dry

unit weight of the specimen was only slightly higher than the dry unit weights (shown in Fig. 8.2) of specimens which were consolidated in one stage to similar final effective confining pressures.

CHAPTER 9: SHEAR TEST PROCEDURES AND RESULTS

9.1. INTRODUCTION

Twelve consolidated-undrained ($\bar{R}$) triaxial shear tests with pore pressure measurement and one consolidated-drained (S) triaxial shear test were performed to determine effective stress shear strength parameters. Tests were performed on compacted specimens of the red and grey clays from the IH 610 and Scott Street embankment. The procedures which were used in these triaxial shear tests, and the methods which were used to reduce the test data, are presented in this chapter. Stress-strain curves, effective stress paths, and shear strength envelopes are presented and discussed. Each shear test performed is summarized in Table 9.1; specimen properties are also summarized.

9.2. PROCEDURE FOR TRIAXIAL SHEAR TESTING

Specimens were sheared after they had reached full saturation and complete equilibrium under the final effective consolidation pressure, as described in Chapter 8. Based on volume change data during consolidation, it was estimated that all specimens would be fully consolidated and that all pore water pressures would have fully equilibrated within 2 days of the application of the final increment in effec-

Table 9.1

Summary of Specimen Properties and Shear Conditions for all Triaxial Shear Tests Performed in this Investigation

Test	Type of Test	Clay	Final Effective Consolidation Pressure $\bar{\sigma}_{3c}$ (psi)	Moisture Content (%)		Dry Density (pcf)		Duration	
				initial	after consol.	initial	after consol.	Consol. (days)	Shear (days)
B.1	$\overline{CU}$	Red 610/Scott	19.4	21.0	27.9	95.9	96.1	8	12
B.2	$\overline{CU}$	Red 610/Scott	4.8	24.6	30.7	94.9	92.2	6	7
B.3	$\overline{CU}$	Red 610/Scott	4.7	23.3	31.9	95.7	90.6	13	11
B.4	$\overline{CU}$	Red 610/Scott	10.2	24.0	29.0	95.1	94.5	11	15
B.5	$\overline{CU}$	Red 610/Scott	14.6	26.9	28.3	96.2	95.6	16	8
B.6	$\overline{CU}$	Grey 610/Scott	5.4	21.8	25.4	101.9	100.0	13	16
B.7	$\overline{CU}$	Grey 610/Scott	20.2	21.3	24.1	100.8	102.1	13	16
6.1	$\overline{CU}$	Red 610/Scott	9.9	21.7	30.8	95.7	92.0	11	15
6.2	$\overline{CU}$	Red 610/Scott	1.7	25.8	30.4	94.0	92.5	14	9
6.3	CD	Red 610/Scott	1.1	23.4	32.1	96.2	90.2	15	15
6.4	$\overline{CU}$	Grey 610/Scott	10.4	21.3	25.2	101.4	100.3	17	8
6.5	cyclic $\overline{CU}$	Red 610/Scott	1.1	26.3	30.7	97.4	92.1	75	10
6.6	$\overline{CU}$	Brown 225/146	1.1	23.3	29.3	99.0	94.1	14	13
6.8	$\overline{CU}$	Grey 610/Scott	1.1	20.7	26.2	102.0	98.8	14	11

tive consolidation pressure. Accordingly, the shear testing of a specimen generally was started two days after the final increment in effective confining pressure had been applied.

9.2.1. INSTALLATION OF TRIAXIAL CELL IN LOADING PRESS

After the consolidation and back-pressure saturation of a specimen had been completed, the triaxial cell was carefully transferred to the lower platen of the loading press. The platen was raised manually a sufficient distance to allow the loading rod, which was restrained but subjected to an unbalanced uplift force proportional to the cell pressure, to come into contact with the proving ring or load cell. The loading rod was then released and the platen was raised slowly at a steady rate to determine the loads due to the uplift force on the loading rod and frictional forces in the seal/bushing arrangement through which the loading rod passed. The load recorded by the proving ring or load cell due to these effects was later subtracted from the loads measured during the shear test.

After the force due to friction and uplift had been measured, the loading rod was seated in the top cap of the specimen. As the platen was raised slowly, a distinct increase in the load registered by the proving ring or load cell indicated that the loading rod was firmly seated in the top cap.

9.2.2. RATE AND DURATION OF SHEAR

The rate of shear in the consolidated-undrained ($\bar{R}$) triaxial shear tests was chosen to ensure that any pore pressures generated during shear could fully equilibrate. The rate at which pore pressures equilibrate within a specimen is a function of the coefficient of consolidation, c_v, of the specimen and the effective maximum drainage path length within the specimen. The length of the effective maximum drainage path is governed, in part, by the drainage conditions on the boundaries of the specimen.

The coefficient of consolidation should be measured during the consolidation of a fully saturated specimen. However, since only those specimens with final effective consolidation pressures greater than 5 psi were consolidated once they were fully saturated, there is only a limited body of data available for the evaluation of coefficients of consolidation.

Useful consolidation data exist for three tests: two tests (B.1 and 6.1) on specimens of red clay at final effective consolidation pressures of 19.4 and 9.9 psi, respectively, and one test (6.4) on a specimen of grey clay at a final effective consolidation pressure of 10.4 psi.

9.2.2.1. Determination of Coefficients of Consolidation

All triaxial tests in this investigation were carried out with

drainage from one end (via the porous stone at the base) and the radial boundary (via the lateral filter paper drain) of the specimen. Bishop and Henkel (1962) suggested that, for these drainage conditions, the coefficient of consolidation, c_v, can be calculated from the following equation:

$$c_v = \frac{\pi H^2}{81\ t_{100}} \tag{9.1}$$

where H is half of the average height of the specimen during consolidation and t_{100} is the time needed to complete primary consolidation.

Therefore, the coefficient of consolidation, c_v, of a specimen can be determined if the time required to complete primary consolidation, t_{100}, can be estimated from the consolidation data. Three approaches for determining t_{100} are presented below. The first approach was proposed by Bishop and Henkel (1962) and the second approach was proposed by Taylor (1948). These two approaches use graphical constructions on plots of consolidation data (in this case, the decrease in specimen height or volume during consolidation) versus the square root of time. The third approach involves the use of a plot of consolidation data versus the logarithm of time.

9.2.2.1.1. Bishop and Henkel's Approach for the Determination of t_{100}: Bishop and Henkel used a simple graphical construction on a plot of height or volume change versus the square root of time to determine t_{100}. They assumed that the effects of secondary consolidation were negligible and, therefore, that it is possible to draw a horizontal line

which is asymptotic to the final portion of the consolidation curve. The time corresponding to the intersection of an extension of the initial linear segment of the consolidation curve and the horizontal line is assumed to be t_{100}.

The consolidation data from Tests B.1 (decrease in height of specimen) and 6.4 (decrease in volume of specimen) are plotted versus time on a square root scale in Figures 9.1 and 9.2, respectively. It will be shown in a later section that the consolidation data from Test 6.1 were difficult to interpret and, therefore, were not considered at this stage.

The consolidation curves plotted in Figures 9.1 and 9.2 do not appear to become asymptotic to a horizontal line at large times. However, in order to use Bishop and Henkel's method, a horizontal line has been drawn through the last datum point. The graphical constructions shown in Figures 9.1 and 9.2 indicate that the time needed to complete primary consolidation, t_{100}, is approximately 11 minutes for the specimen of red clay in Test B.1 and 25 minutes for the specimen of grey clay in Test 6.4.

9.2.2.1.2. Taylor's Approach for the Determination of t_{100}: Taylor (1948) proposed a method for the determination of the time required to complete primary consolidation, t_{100}, from consolidation data which makes use of the fact that, for degrees of consolidation less than approximately 60 percent, the strains in a specimen caused by consolidation should be proportional to the square root of time. If this cond-

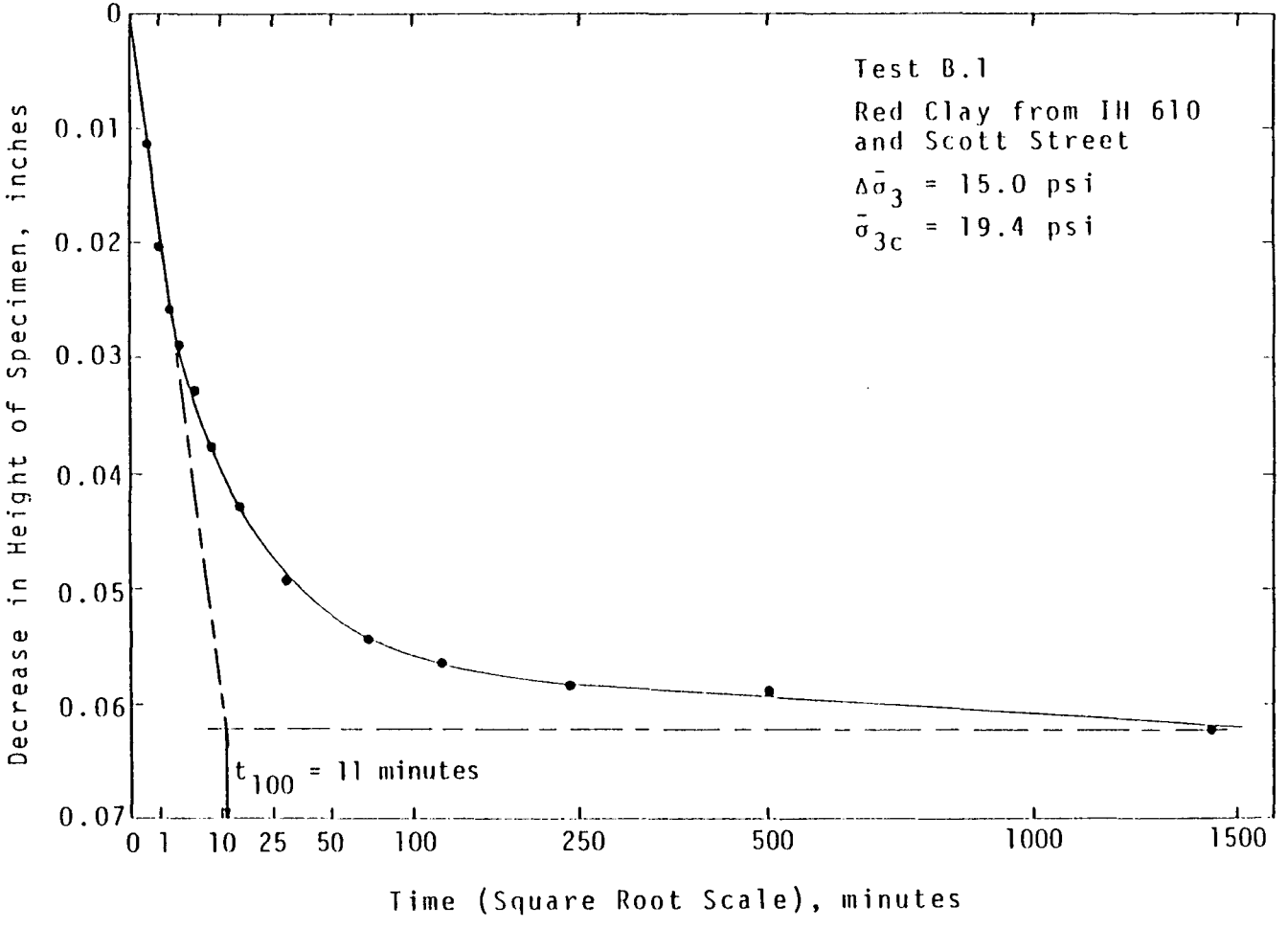

Fig. 9.1 Bishop and Henkel's Construction for the Determination of the End of Primary Consolidation, Shown on a Plot of the Decrease in Specimen Height Versus Time (on a Square Root Scale) for Test B.1.

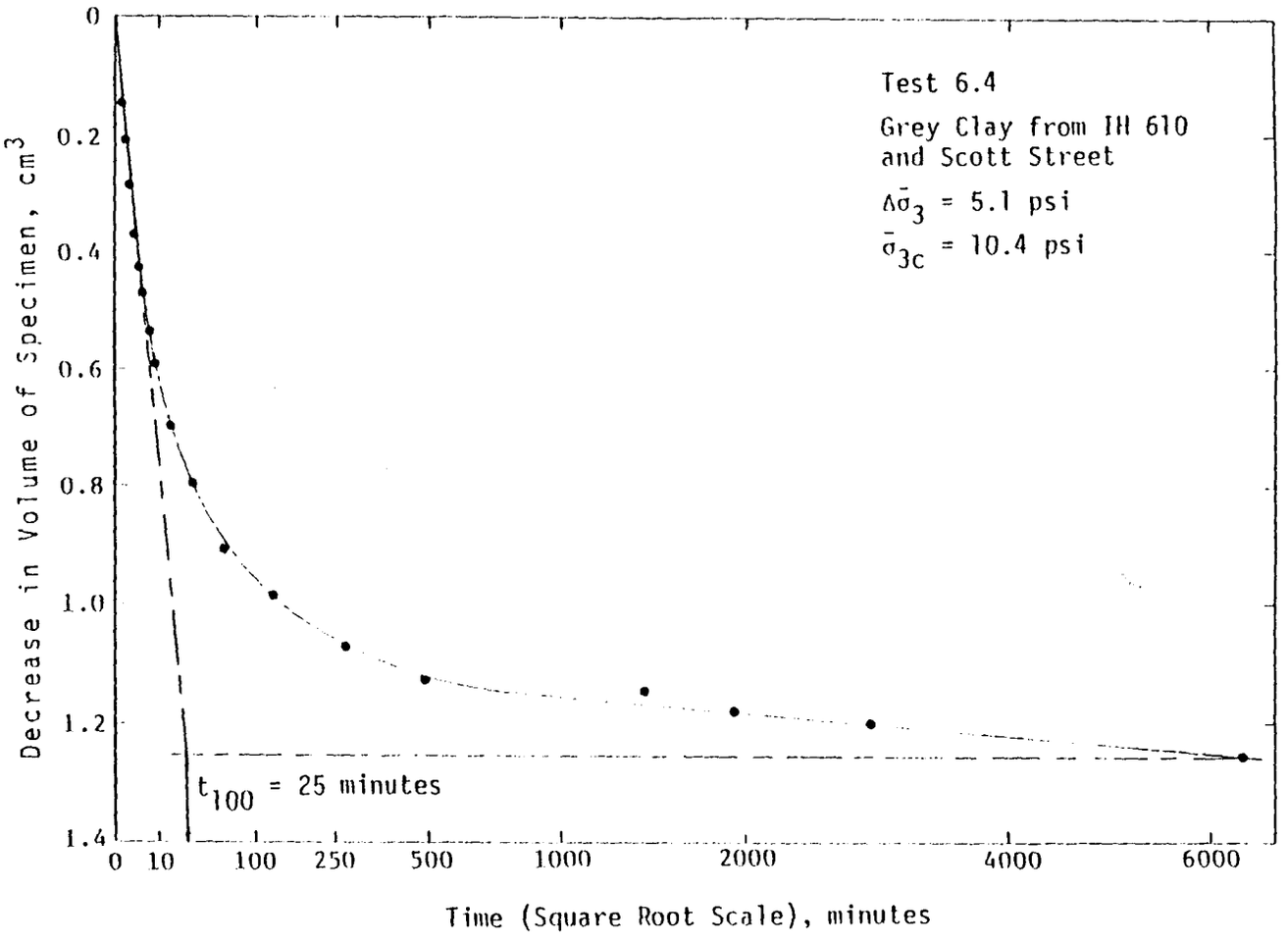

Fig. 9.2 Bishop and Henkel's Construction for the Determination of the End of Primary Consolidation, Shown on a Plot of the Decrease in Specimen Volume Versus Time (on a Square Root Scale) for Test 6.4.

dition exists, the initial portion of a consolidation curve plotted versus time on a square root scale should be linear.

Taylor showed that the decrease in height or volume of a specimen corresponding to the completion of 90 percent of primary consolidation, s_{90}, could be determined by the point of intersection of the consolidation curve and a line from the origin with abscissae 1.15 times greater than the abscissae of the initial linear segment of the consolidation curve. Taylor's graphical construction for the determination of s_{90} is shown in Figures 9.3 and 9.4 for Tests B.1 and 6.4, respectively.

The decrease in height or volume of a specimen corresponding to the completion of 100 percent of primary consolidation, s_{100}, is determined from the following relationship:

$$s_{100} = \frac{10}{9} s_{90} \qquad (9.2)$$

The time, t_{100}, corresponding to the completion of 100 percent of primary consolidation is taken as the time corresponding to s_{100} on the consolidation curve. Using the constructions shown in Figures 9.3 and 9.4, and Equation (9.3), it has been estimated that t_{100} is approximately 6 minutes for the specimen of red clay in Test B.1 and 11 minutes for the specimen of grey clay in Test 6.4.

9.2.2.1.3. Logarithm of Time Approach for the Determination of t_{100}: The third approach which is commonly used to estimate the time required to complete primary consolidation, t_{100}, involves the plotting of consolidation data versus time on a logarithmic scale. The relationships

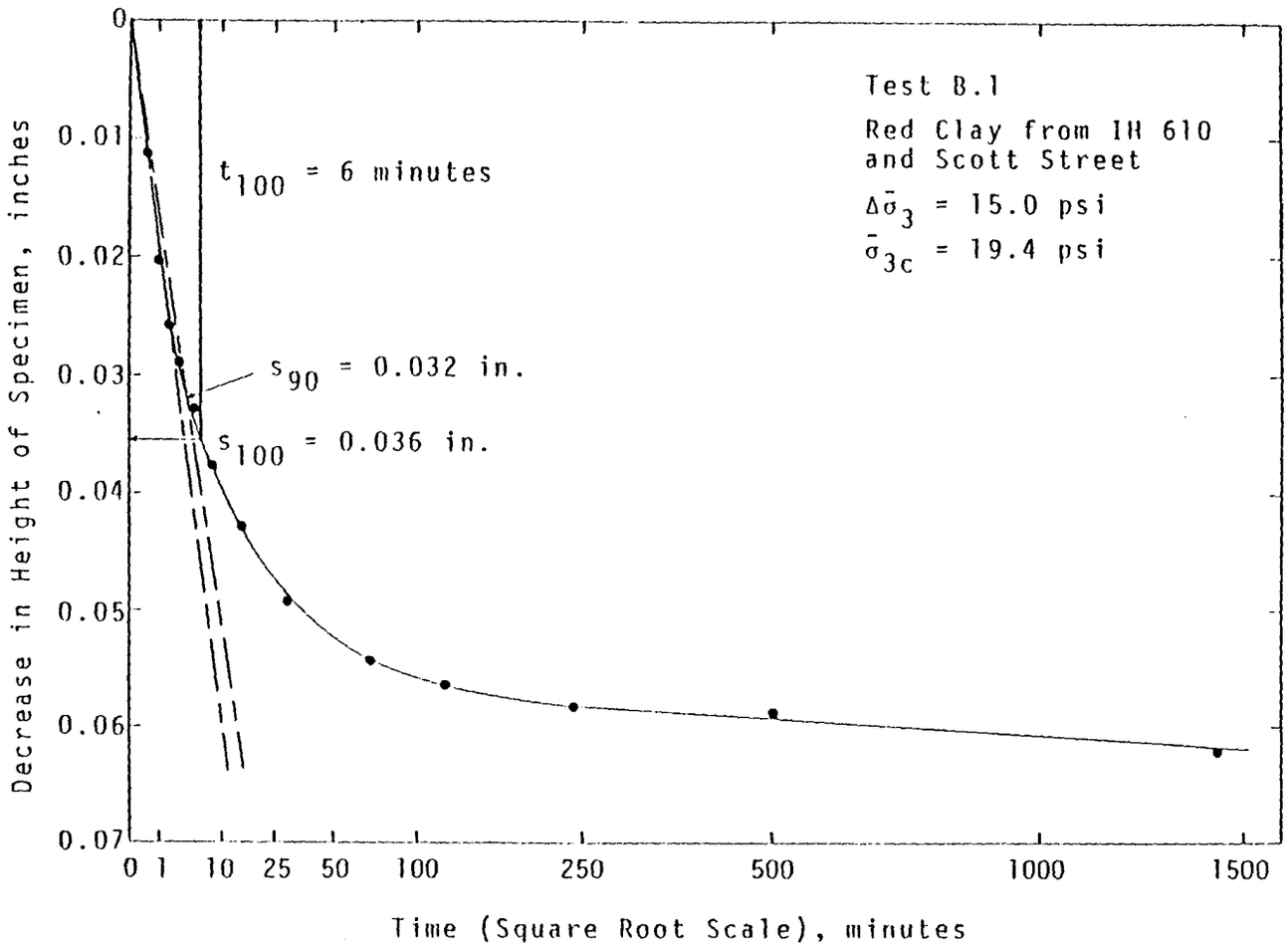

Fig. 9.3 Taylor's Construction for the Determination of the End of Primary Consolidation, Shown on a Plot of the Decrease in Specimen Height Versus Time (on a Square Root Scale) for Test B.1.

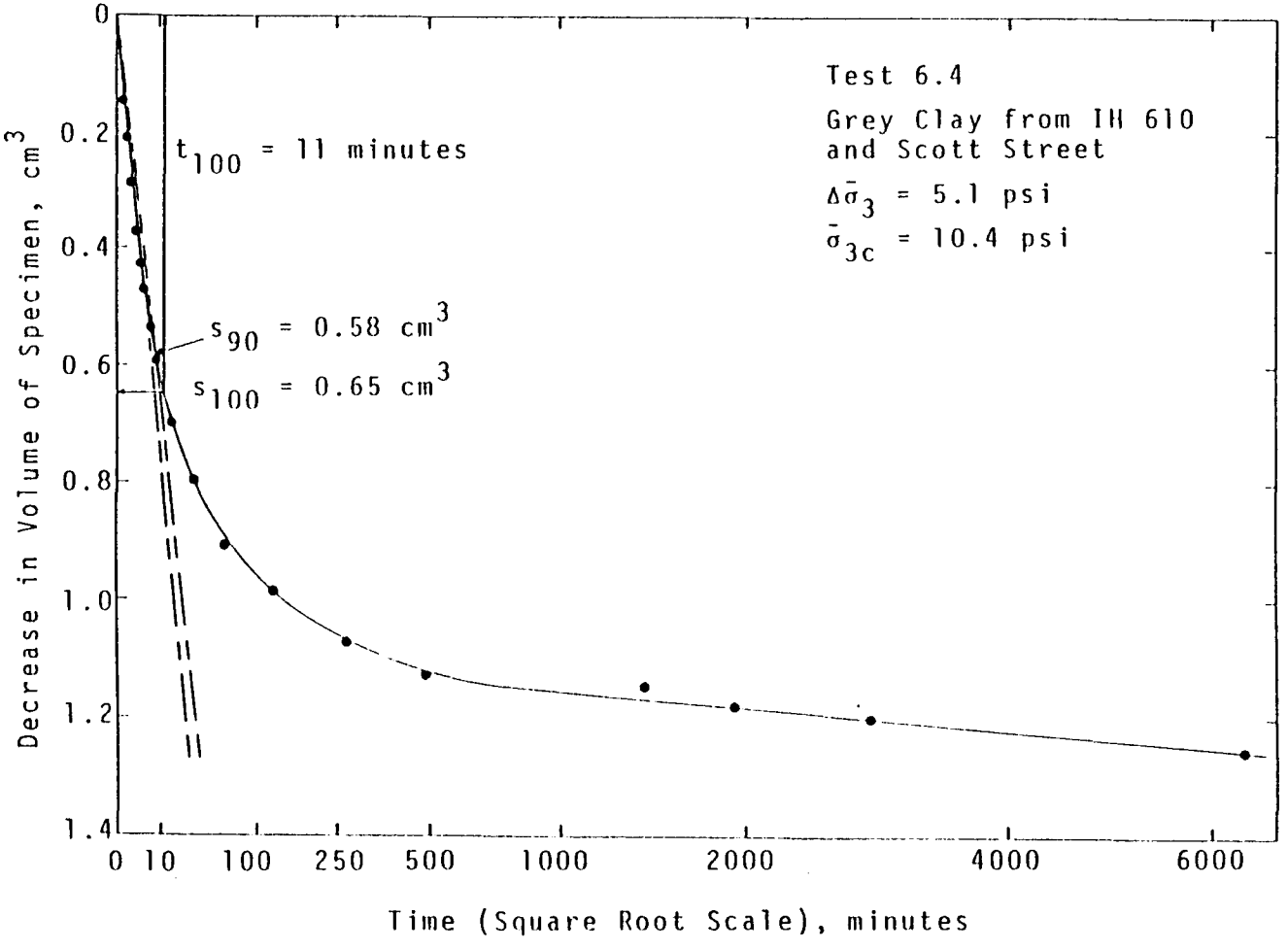

Fig. 9.4 Taylor's Construction for the Determination of the End of Primary Consolidation, Shown on a Plot of the Decrease in Specimen Volume Versus Time (on a Square Root Scale) for Test 6.4.

between the decrease in height of a specimen (Test B.1) and the decrease in pore water volume of a specimen (Test 6.4), and the logarithm of time, are presented in Figures 9.5 and 9.6, respectively.

It is clear that the consolidation curves in Figures 9.5 and 9.6 are divided into two distinct portions; these two portions are frequently assumed to correspond to primary and secondary consolidation. A graphical construction has been used (and is shown in Figures 9.5 and 9.6) to find the time, t_{100}, at which primary consolidation was essentially complete. The constructions indicate that t_{100} is approximately 70 minutes in Test B.1 (red clay) and 200 minutes in Test 6.4 (grey clay).

9.2.2.1.3.1. Consolidation Data from Test 6.1: As previously noted, volume changes and height changes during consolidation were recorded in Test 6.1, although the data were not used to determine t_{100}. The final increment in effective confining pressure applied in Test 6.1 was 4.9 psi. The relationships between the decrease in volume and the decrease in height during consolidation, and time, are plotted in Fig. 9.7. It has not been possible to make a graphical construction to determine t_{100} due to the irregular shapes of the two consolidation curves shown in Fig. 9.7. However, the similarity in the shapes of the two curves indicates that it should be reasonable to use either the change in height or the change in volume of a specimen to determine t_{100}.

9.2.2.1.4. Summary of t_{100} Values: The time required to complete primary consolidation, t_{100}, was estimated by three different approaches

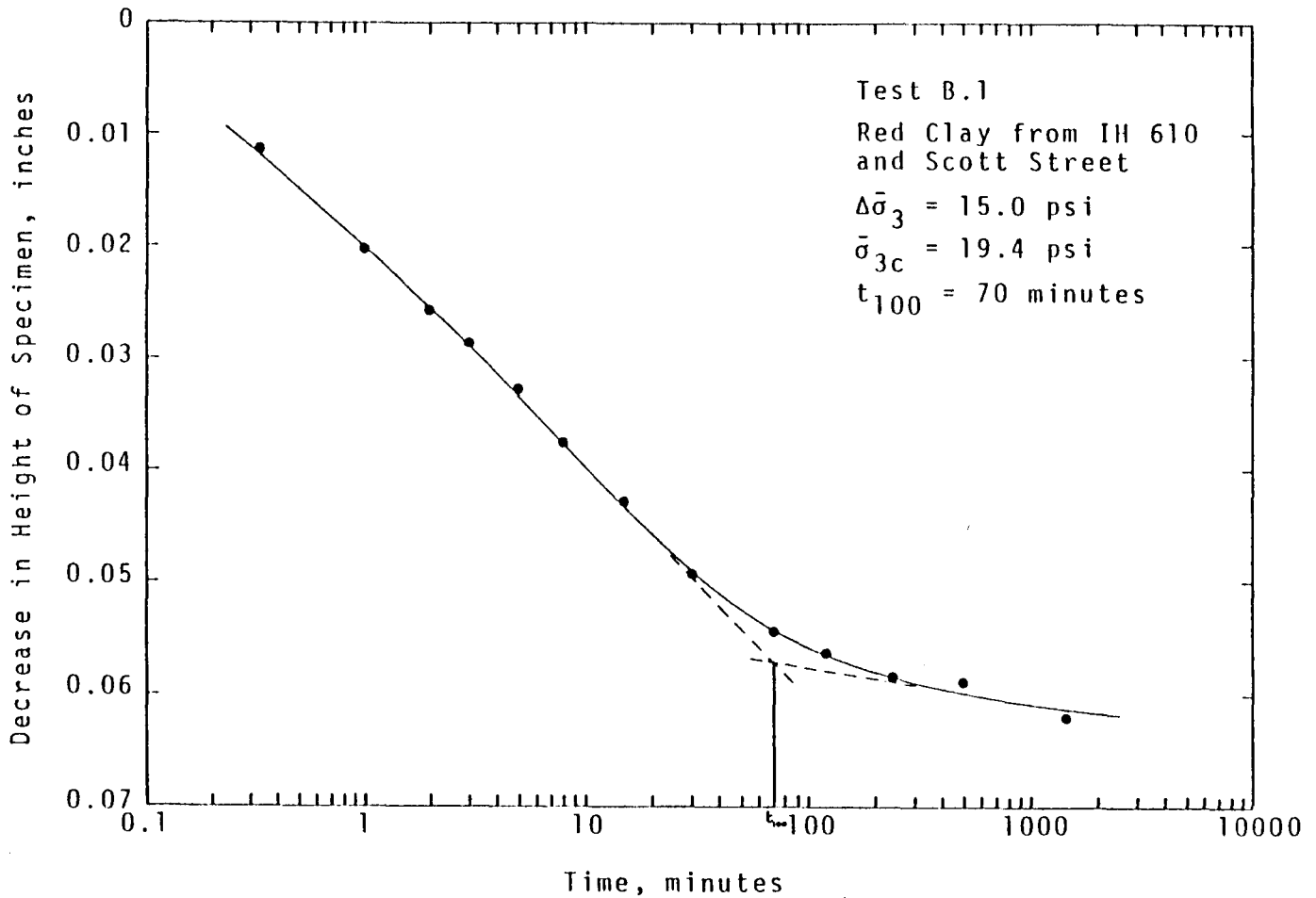

Fig. 9.5 Logarithm of Time Construction for the Determination of the End of Primary Consolidation, Shown on a Plot of the Decrease in Specimen Height Versus Time (on a Logarithmic Scale) for Test B.1.

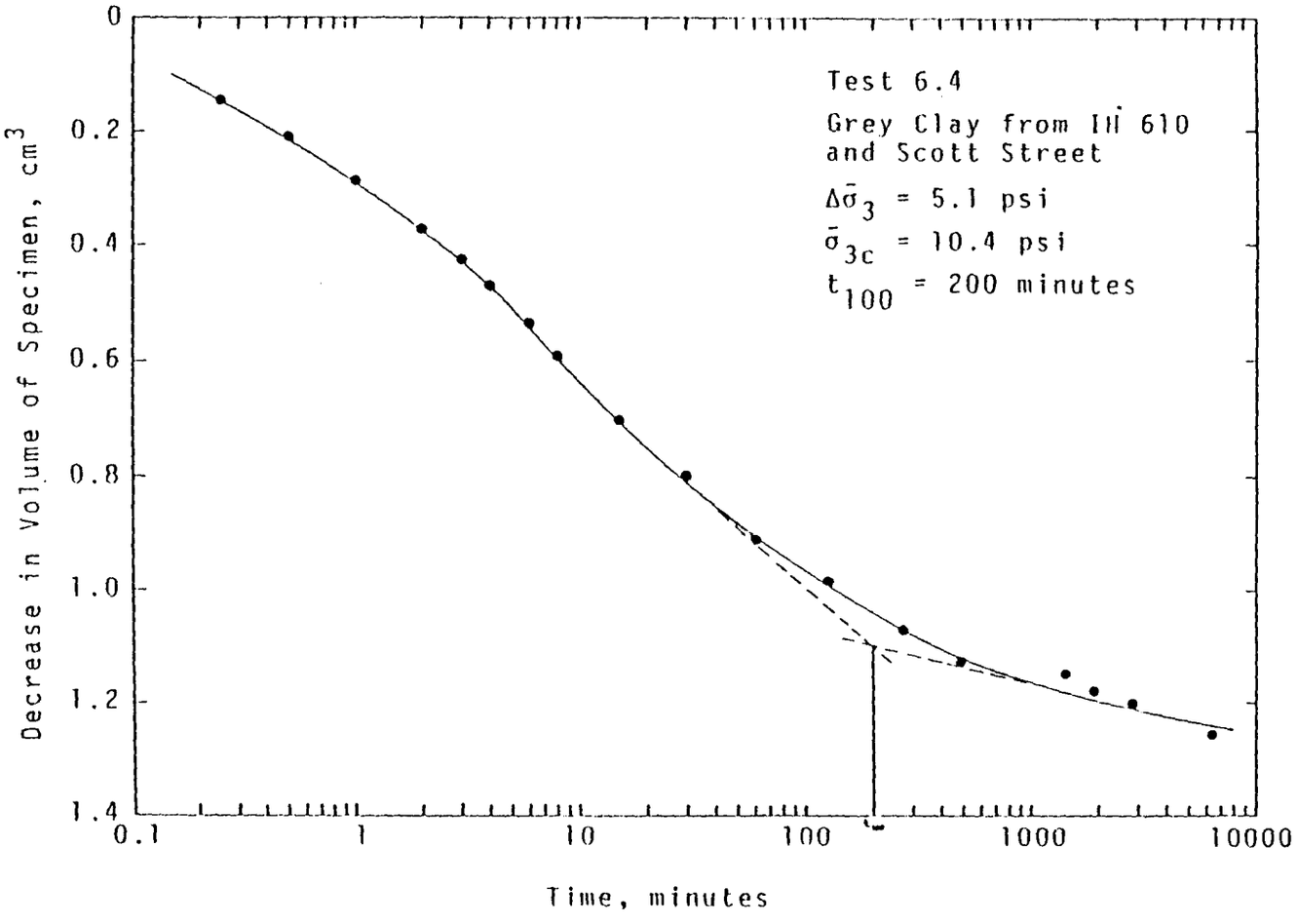

Fig. 9.6 Logarithm of Time Construction for the Determination of the End of Primary Consolidation, Shown on a Plot of the Decrease in Specimen Volume Versus Time (on a Logarithmic Scale) for Test 6.4.

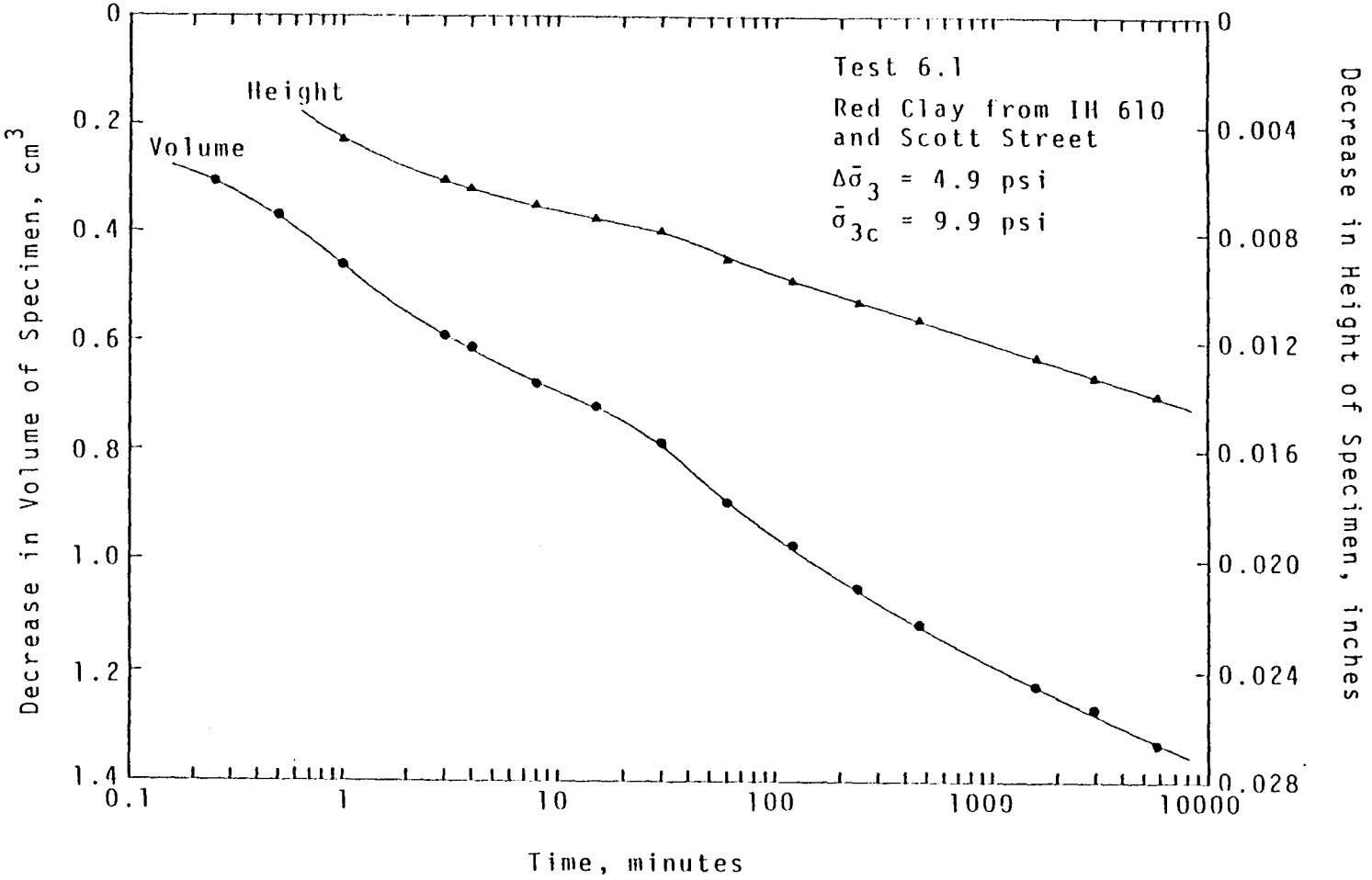

Fig. 9.7 Decrease in Pore Water Volume and Height of Specimen in Test 6.1 as a function of Time, during Final Consolidation Stage

for the specimen of red clay in Test B.1 and the specimen of grey clay in Test 6.4. These estimates are summarized in Table 9.2. The values range from 6 to 70 minutes for the red clay (Test B.1) and from 11 to 200 minutes for the grey clay (Test 6.4). In each case, the smallest and largest estimates were found using Taylor's approach and the logarithm of time approach, respectively.

9.2.2.1.5. Summary of Coefficient of Consolidation Values: The coefficient of consolidation values which correspond to each estimate of t_{100} can be found using Equation (9.1), which was proposed by Bishop and Henkel (1962). These values ranged from 0.0012 to 0.0145 $in.^2$/minute for red clay based on the results of Test B.1 and from 0.0004 to 0.0079 $in.^2$/minute for the grey clay based on the results of Test 6.4.

9.2.2.2. Times to Failure

Blight (1963) presented the following equation for calculating the minimum time to failure, t_f, corresponding to a degree of pore pressure equilibration of 95 percent, in an undrained triaxial shear test with all-round drainage:

$$t_f = \frac{0.07\ H^2}{c_v} \tag{9.3}$$

where H is half the average height of the specimen during shear and c_v is the coefficient of consolidation. It has been assumed that the condition

Table 9.2

Summary of t_{100} Values Estimated by Three Approaches using Consolidation Data from Tests B.1 and 6.4

Test	Estimated t_{100} (minutes)		
	Bishop and Henkel	Taylor	Logarithm of Time
B.1 (red clay)	11	6	70
6.4 (grey clay)	25	11	200

of drainage from one end and the radial boundary of the specimen is sufficiently close to the condition of all-round drainage to justify the use of Equation (9.3).

Equation (9.3) was used to estimate the minimum time to failure, t_f, in each consolidated-undrained ($\bar{R}$) test. The calculated minimum times to failure vary from 11 to 127 minutes for the specimen of red clay in Test B.1 and from 20 to 360 minutes for the specimen of grey clay in Test 6.4. The wide range in these estimates reflects the problems associated with the determination of an appropriate value for the coefficient of consolidation.

9.2.2.3. Determination of Rate of Shear

Because the results of the calculations for the times to failure, t_f, involved a great deal of uncertainty, a slower and, therefore, more conservative rate of shear was chosen. The slowest rate of deformation which could be achieved with the Wykeham Farrance loading presses was 0.0017 inches per hour and this rate was used for all the triaxial shear tests. This rate corresponds to an axial strain rate of approximately 0.06 percent per hour for a three inch high specimen. It will be shown in subsequent sections of this chapter that the axial strains at "failure" in the consolidated-undrained ($\bar{R}$) tests were, fairly consistently, approximately 1 percent. The chosen rate of shear, in conjunction with this strain at failure, corresponds to a time to failure of approxi-

mately 1060 minutes. This value is significantly greater than theminimum times to failure suggested by the analyses of the consolidation data.

9.2.2.4. Test Procedure During Shear

Specimens were sheared to maximum axial strains ranging from 10 to 18 percent. Sufficient strain was allowed to determine the effective stress shear strength parameters and to determine if there was a significant loss of strength at large strains. The shear portion of the triaxial tests usually lasted from one to two weeks.

The axial load, pore water pressure, and axial deformation were measured and recorded at regular intervals. Readings were taken approximately every hour during the first 12 hours, every 4 four hours during the next 12 hours, and subsequently every 6 to 12 hours. The rate at which the axial load increased was observed to ensure that a set of readings were obtained at approximately the stage in the test when the maximum axial load was reached. A test was discontinued when the distortion of a specimen was judged to be so large that significant innaccuracies would be produced in the cross-sectional area of the specimen and corresponding stresses which were computed using this cross-sectional area.

9.2.3. DRAINAGE CONDITIONS AND PORE PRESSURE MEASUREMENT

During shear in the consolidated-undrained ($\overline{R}$) tests, drainage

of the specimen was prevented by the closure of a drainage valve and pore water pressures were measured. At the start of shear, the pore water pressure was equal to the final back pressure at the end of consolidation. For the consolidated-drained (S) test which was performed, the back pressure at the end of consolidation was maintained throughout the shearing stage of the test and the specimen was allowed to drain as it was sheared. The pore pressure which was measured with the pore pressure transducer was constant throughout the shearing stage of the consolidated-drained (S) test.

9.2.4. END OF TEST PROCEDURE

At the end of a shear test, the loading press was turned off. In the drained test, the drainage valve to the base of the specimen, which had been open throughout the test, was closed. At the end of an undrained test, the drainage valve was left in the closed position. The cell water was then vented to atmospheric pressure and drained from the cell. The cell was then dismantled. The specimen was removed from the base pedestal, carefully stripped of membranes and filter paper, and cut into three approximately equal segments. These segments were individually weighed and oven-dried to determine the final moisture content distribution throughout the specimen and the dry weight of the specimen.

9.3. DATA REDUCTION PROCEDURES

Readings taken during the consolidated-undrained ($\overline{R}$) tests were reduced and plotted using a computer program, RBARPLT, which was written by Dr. Stephen G. Wright. The use of the computer to reduce the test data greatly increased the speed and accuracy of data reduction.

For each test, a computer data file was created which contained comments on the specimen properties and test procedures, calibration coefficients for the "raw" laboratory readings, various parameters used to reduce the data, and each set of laboratory readings. A set of laboratory readings consisted of instrumentation readings for the axial deformation, axial load, and pore water pressure measured at the same instant. The calibration coefficients for a group of readings consisted of a "zero value" and a "calibration factor". For example, the load cell reading which was recorded when the uplift and frictional forces on the loading rod were measured would be the axial load "zero value" and the slope of the relationship between force and voltage which was obtained when the load cell was calibrated (5.007 lb per mV) would be the axial load "calibration factor".

The computer program computed and applied corrections to the principal effective stresses to account for the effects caused by the stiffness of the rubber membranes and the strength of the vertical filter paper drain. The corrections were performed in accordance with the recommendations of Duncan and Seed (1965). The combined thickness of the two membranes (0.0054 in.), the Young's modulus of the membrane material

(135 psi), the proportion of the circumference covered by the filter paper drain (50 percent), and the strength of the filter paper drain (0.165 lb per in.) were included as parameters in the data file.

9.4. SHEAR TEST RESULTS

A primary objective of this investigation was to determine the effective stress shear strength parameters in the laboratory for the clays (red and grey) from the IH 610 and Scott Street embankment. Stress-strain curves, effective stress paths, and Mohr-Coulomb shear strength envelopes are presented in this section. The shearing behaviour of the red and grey clays is also discussed. The results of a single consolidated-undrained ($\bar{R}$) test on a specimen of brown clay from the SH 225 and SH 146 (SW Quadrant) are presented. The triaxial shear test results are presented in the form of summary plots generated by the computer program; the results for individual tests are presented in Appendix A for the red clay specimens, Appendix B for the specimen of brown clay, and Appendix C for the grey clay specimens.

9.4.1. RED CLAY FROM IH 610 AND SCOTT STREET

Seven consolidated-undrained ($\bar{R}$) triaxial shear tests were performed on the red clay from the IH 610 and Scott Street embankment at final effective consolidation pressures ranging from 1.7 to 19.4 psi.

This range of consolidation pressures was chosen to represent the low overburden pressures acting on the shallow slide surface which was observed in the IH 610 and Scott Street embankment and to determine whether the effective stress shear strength envelope exhibited curvature at low confining pressures. A consolidated-drained (S) and a cyclically consolidated-undrained ($\bar{R}$) triaxial shear test were also performed on the red clay. The results of these tests are also presented in this section.

9.4.1.1. Stress-Strain Relationships

The relationships between principal stress difference, $(\sigma_1-\sigma_3)$, and axial strain for seven compacted specimens are presented in Fig. 9.8. The stress-strain curves in Fig. 9.8 indicate that in three tests (B.1, B.3, and 6.1), there was no decrease in principal stress difference at large strains and that the reduction which was measured in the other tests was not significant.

The stress-strain curves in Fig. 9.8 show that the principal stress difference reached almost its maximum value at a strain of less than 1 percent in all the tests, regardless of the final effective consolidation pressure. There was some further increase in the principal stress difference at large strains in four of the seven tests (B.2, B.3, B.4, and B.5), which is thought to be due in part to the excessive distortion of the specimens at strains greater than approximately 6 percent, leading to innaccuracies in the computed cross-sectional areas of

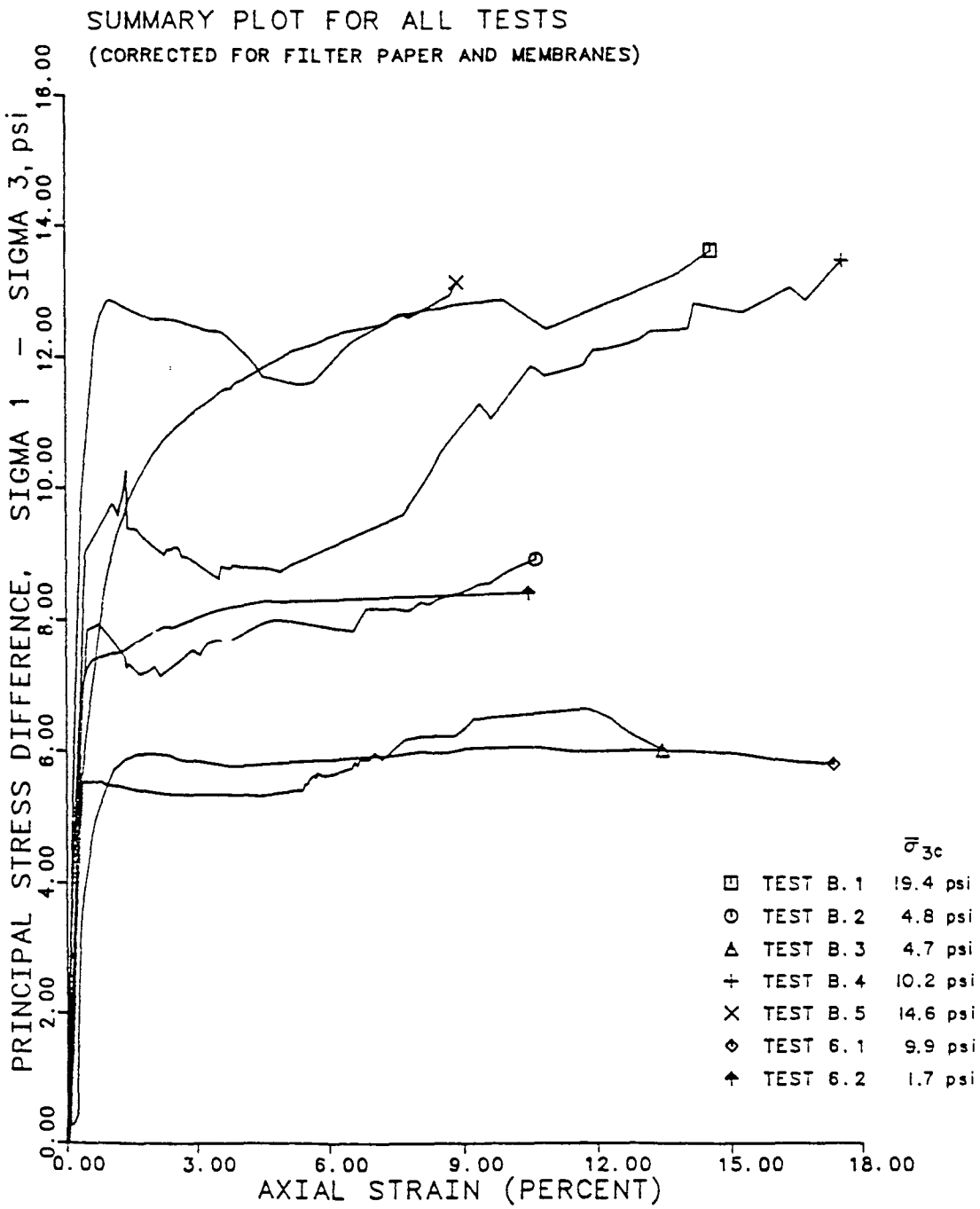

Fig. 9.8 Stress-Strain Relationships from Seven Consolidated-Undrained ($\bar{R}$) Triaxial Tests on Red Clay from IH 610 and Scott Street

the specimens. The minor fluctuations in the principal stress difference which are evident in the stress-strain curves from tests conducted in the basement laboratory (test prefix "B") are thought to have been caused by a faulty thermostat in that laboratory which caused very noticeable fluctuations in the room temperature.

9.4.1.2. Effective Stress Paths

The effective stress paths which were obtained from the seven consolidated-undrained ($\bar{R}$) triaxial shear tests performed on the laboratory-compacted specimens are presented in Fig. 9.9. The effective stress paths are plotted on a modified Mohr-Coulomb diagram showing the principal stress difference, $(\sigma_1-\sigma_3)$, versus the minor principal effective stress, $\bar{\sigma}_3$. The principal stress difference at the start of each test is zero since all the test specimens were consolidated isotropically. The minor principal effective stress at the start of shear was exactly the same as the final effective consolidation pressure applied to a specimen at the end of the consolidation phase of a test.

The <u>total</u> minor principal stress (confining pressure), σ_3, remained essentially constant during shear. However, the pore water pressures changed and, thus, the <u>effective</u> minor principal stresses shown in Fig. 9.9 changed during shear in each test. In all cases, the pore water pressures increased during the initial stages of shear. Thus, the effective stress paths move toward the left in Fig. 9.9 for the early stages of shear (lower values of $\sigma_1-\sigma_3$). This behaviour is indicative of

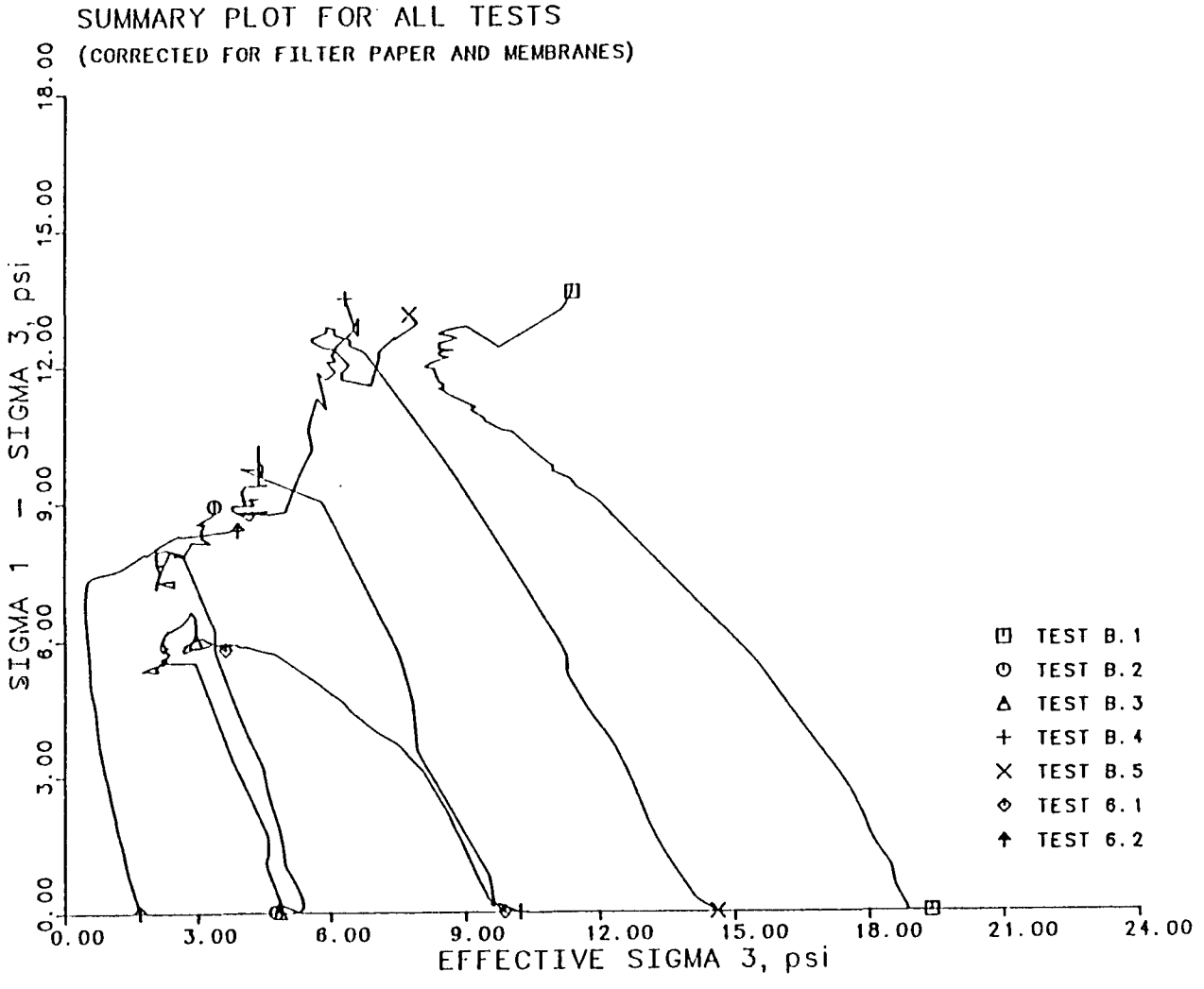

Fig. 9.9 Stress Paths from Seven Consolidated-Undrained (R) Triaxial Tests on Red Clay from IH 610 and and Scott Street

a tendency for contraction of the soil structure under shear and a compression of the pore fluid.

In the later stages of shear (higher values of $\sigma_1-\sigma_3$) in each test, the pore water pressures often began to decrease. This is reflected by the movement of the stress paths to the right in Fig. 9.9 in the latter stages of the tests. This behaviour indicates that the pore pressures were decreasing due to a tendency for dilation of the soil structure after the peak strength was reached; it is likely that there was a reorganization of the soil structure around the failure zone to accomodate the large deformations which were imposed on the specimens.

The pore water pressures developed in the initial stages of shear for tests performed at low effective consolidation pressures were slightly lower (stress paths were slightly steeper) than those for tests at higher effective consolidation pressures. Thus, confining pressure appeared to have a slight effect on the changes in pore water pressure during shear. The observation that higher confining pressures cause higher pore water pressures was to be expected.

The stress paths shown in Fig. 9.9 suggest that there may have been some effect of the compaction procedure which was used and the resulting structure of specimens. In Chapter 6, it was stated that specimens for Tests B.1 and 6.1 were compacted with soil which had <u>not</u> been extruded through the No.10 sieve and that the external voids in these specimens may have been slightly larger than in later specimens. The stress paths presented in Fig. 9.9 for tests B.1 and 6.1 appear to curve more distinctly to the left than those for other specimens. The more

distinct curvature to the left reflects relatively higher pore water pressures for the specimens used in these tests (B.1 and 6.1), possibly as a result of larger voids and a more compressible soil structure.

9.4.1.3. Effective Stress Shear Strength Envelopes

One of the principal objectives of this investigation was to determine the effective stress shear strength envelopes for the clays under consideration. A typical such shear strength envelope is illustrated on a Mohr-Coulomb effective stress diagram in Fig. 9.10. The Mohr's circles of stress drawn on the diagram shown in Fig. 9.10 represent the stress states for two triaxial specimens at "failure". The straight line shear strength ("failure") envelope is represented by the equation:

$$\tau = \bar{c} + \bar{\sigma} \tan \bar{\phi} \qquad (9.4)$$

where $\bar{\sigma}$ is the effective normal stress acting on the failure plane, τ is the shear stress on the failure plane (the "shear strength"), $\bar{c}$ is the effective stress cohesion value for the soil, and $\bar{\phi}$ is the effective stress friction angle for the soil. The effective stress shear strength parameters, $\bar{c}$ and $\bar{\phi}$, are used to define the effective stress shear strength envelope.

For the present study, it was found to be convenient to determine the effective stress shear strength parameters using a modified

er

ly

to

ys

s-

he

e-

he

ne

4)

is

ne

ve

ch

ar

ne

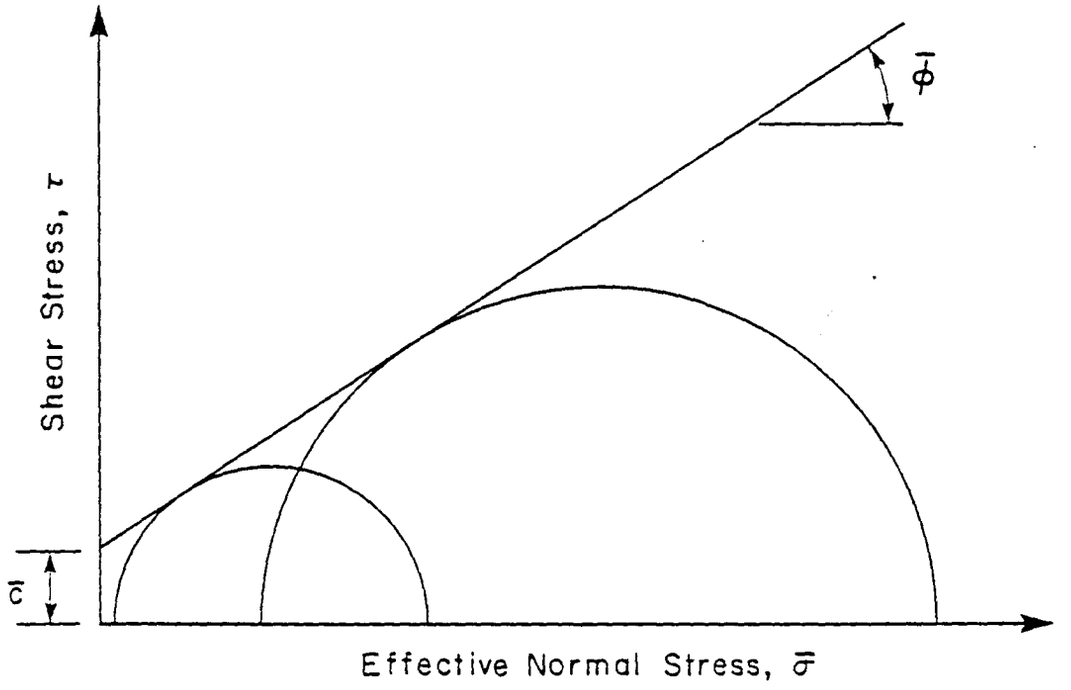

Fig. 9.10 Mohr-Coulomb Diagram Showing Mohr's Circles of Stress for Two Triaxial Specimens at Failure

Mohr-Coulomb diagram like the one presented in Fig. 9.11. With this diagram, the stress state at failure within a specimen is represented by a single point; a series of points showing succesive states of stress during shear form a "stress path." The effective stress shear strength envelope should be tangent to the effective stress paths on a modified Mohr-Coulomb diagram, just as the shear strength envelope is tangent to the Mohr's circles on a conventional Mohr-Coulomb diagram. If the Mohr-Coulomb shear strength envelope is a straight line, it can be shown that the effective stress shear strength parameters, $\bar{c}$ and $\bar{\phi}$, can be calculated from the intercept, d, and the slope, ψ, of the modified Mohr-Coulomb diagram with the following equations:

$$\bar{\phi} = \sin^{-1}\left(\frac{\tan\psi}{2 + \tan\psi}\right) \tag{9.5a}$$

$$\bar{c} = d\left(\frac{1 - \sin\bar{\phi}}{\cos\bar{\phi}}\right) \tag{9.5b}$$

The stress paths presented in Fig. 9.9 were used to determine the effective stress shear strength envelope. Consideration was given to the possibility that the shear strength envelope might exhibit some curvature at low effective confining pressures. However, the stress path for Test 6.2, performed at an effective consolidation pressure of approximately 1 psi, seems to exclude the possibility that the shear strength envelope curves sharply downward at very low confining pressures.

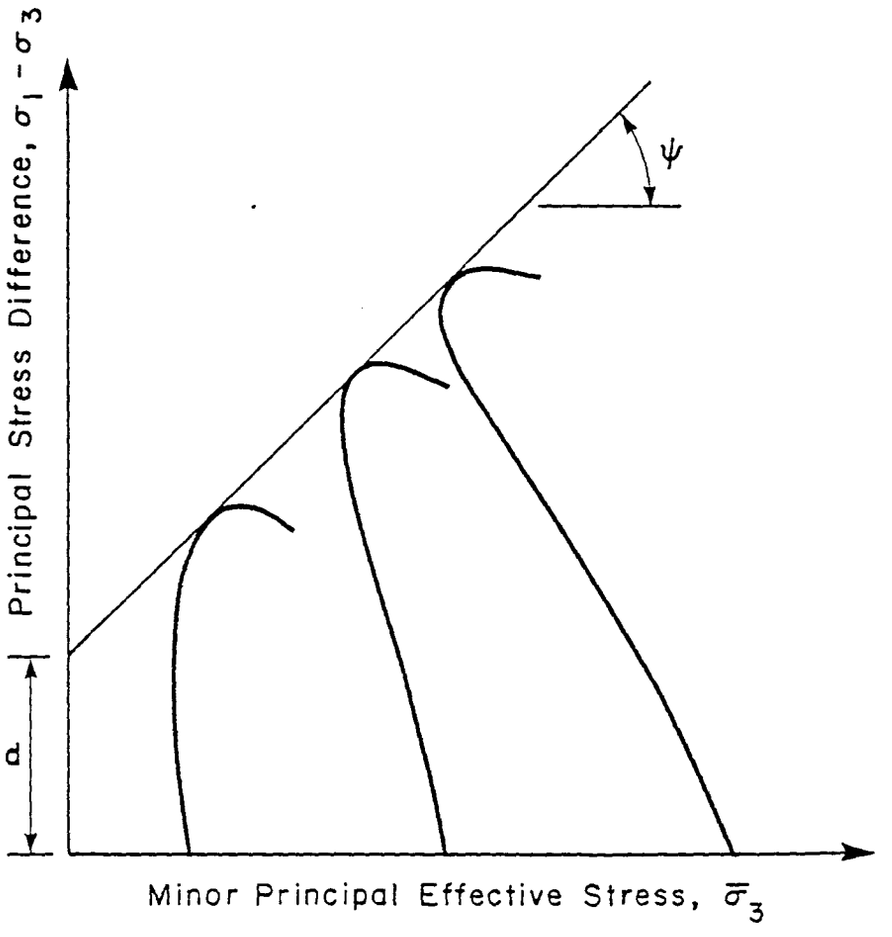

Fig. 9.11 Modified Mohr-Coulomb Diagram Showing Effective Stress Paths for Three Triaxial Specimens at Failure

In order to determine the shear strength envelope from the effective stress paths shown in Fig. 9.9, a straight line was fitted by a least-squares method of linear regression through the tangency points of the stress paths. This required an iterative process since the tangency point of a particular stress path could not be determined unless the slope of the shear strength envelope was known. The resulting modified Mohr-Coulomb shear strength envelope which was finally determined is presented in Fig. 9.12. The solid circles indicate the points of stress path tangency which represent "failure" for a particular test specimen. The intercept and slope parameters (d and ψ) were found to be 5.32 psi and 46.03 degrees, respectively. The corresponding effective stress shear strength parameters, $\overline{c}$ and $\overline{\phi}$, calculated using Equations (9.5a) and (9.5b), are 268 psf and 20.0 degrees, respectively. These values are thought to represent the most reasonable interpretation of the laboratory shear test results for the red clay.

In Fig. 9.13, additional "upper-bound" and "lower-bound" shear strength envelopes are drawn with the same slope as the line of best fit plotted in Fig. 9.12. For this extreme range of possible shear strength envelopes, the effective stress cohesion intercept varies from 156 to 348 psf.

The upper-bound and lower-bound shear strength envelopes represent two extreme interpretations of the family of stress paths measured in the undrained triaxial tests. The upper-bound envelope is defined with a reasonable degree of accuracy by the stress paths from Tests B.4, B.5, and 6.2. The position of the lower-bound envelope is controlled by

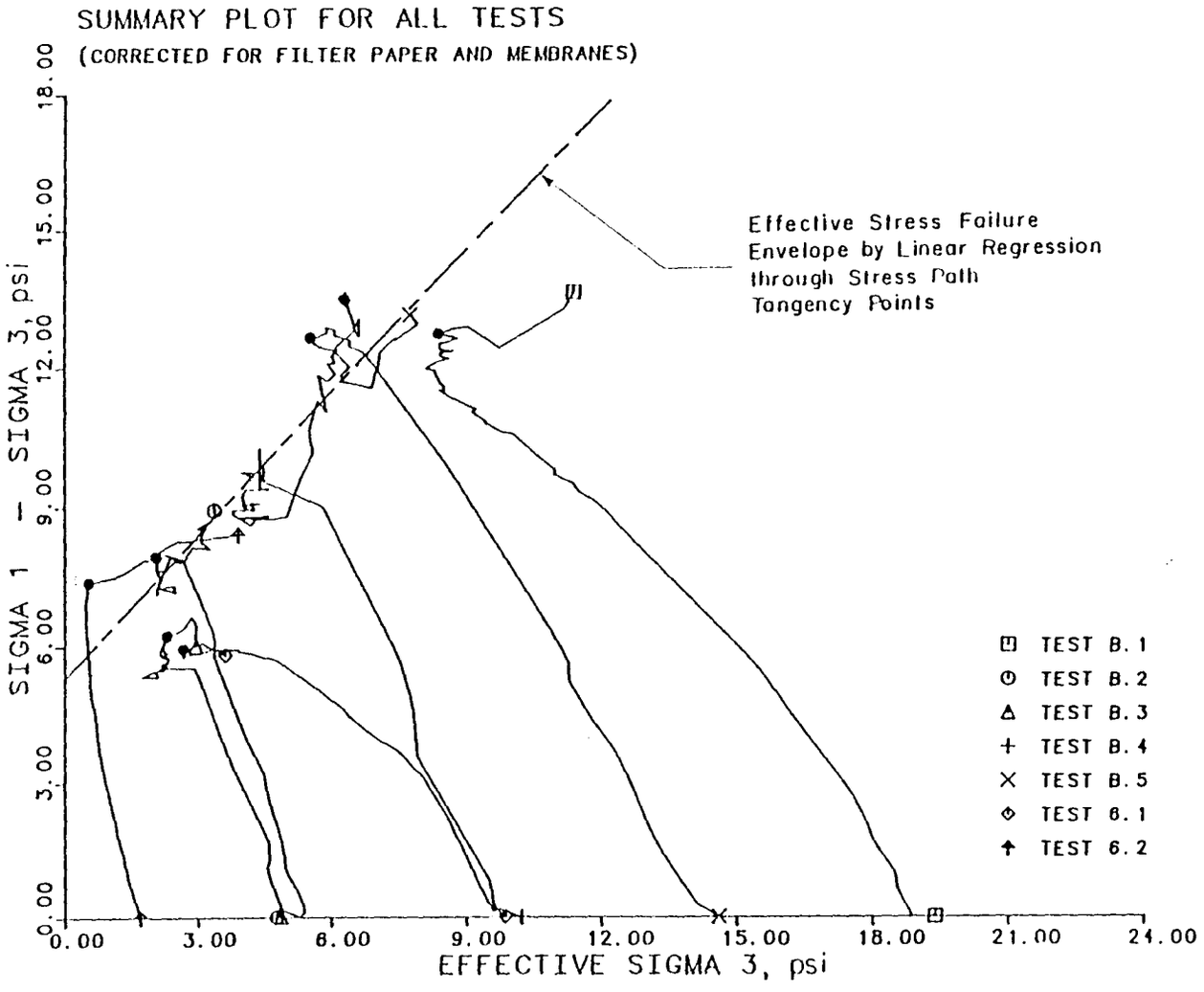

Fig. 9.12 Effective Stress Failure Envelope for Red Clay from III 610 and Scott Street

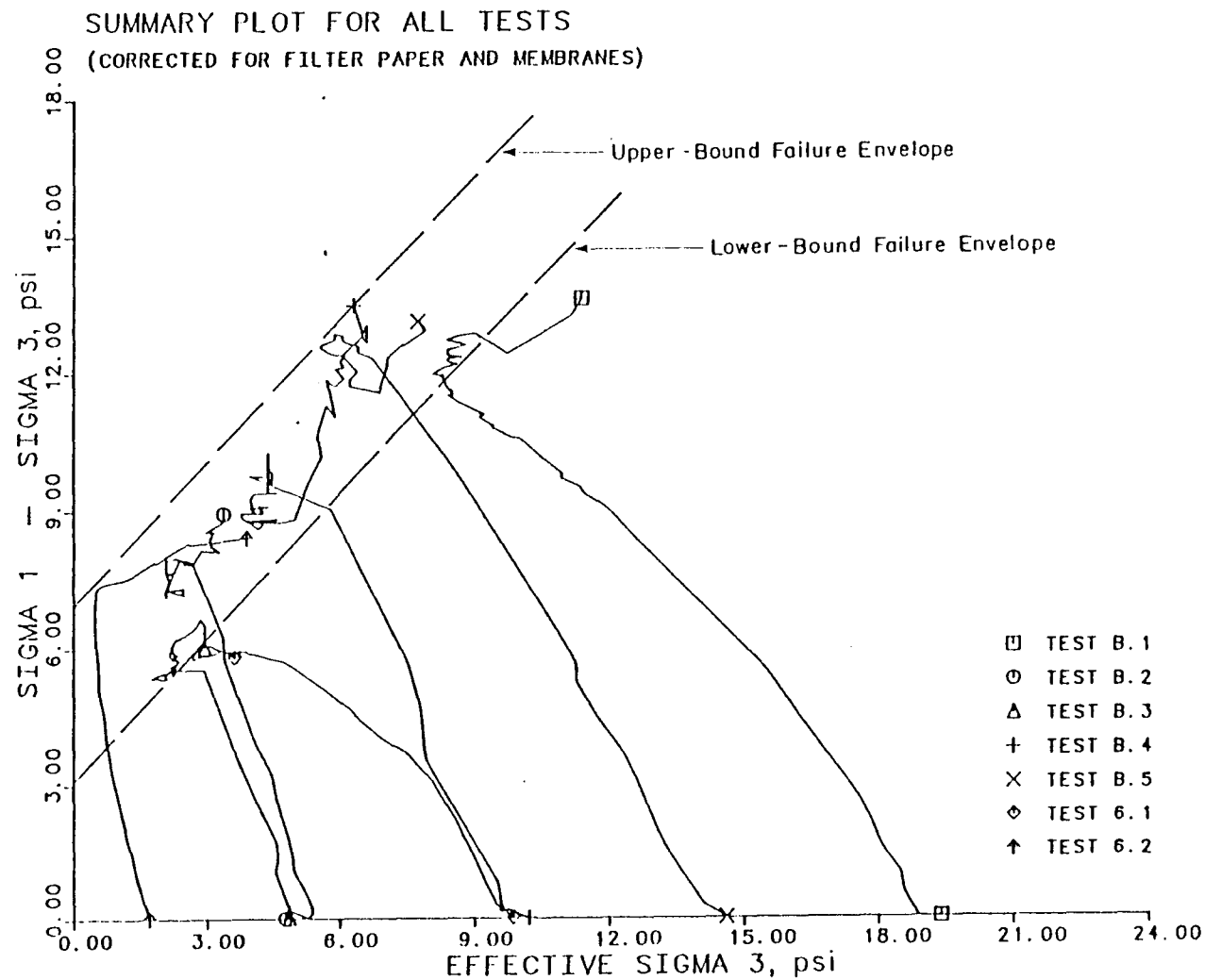

Fig. 9.13 Upper-Bound and Lower-Bound Failure Envelopes
for Red Clay from I-I 610 and Scott Street

the stress paths from Test B.1 and 6.1; it has already been suggested that these test specimens may have contained larger voids than the other specimens.

9.4.1.4. Consolidated-Drained Triaxial Shear Test

The single consolidated-drained (S) triaxial shear test was performed to verify the cohesion intercept ($\bar{c}$) value derived from the consolidated-undrained ($\bar{R}$) tests. The drained test (Test 6.3) was performed at a final effective consolidation pressure of 1.1 psi.

9.4.1.4.1. Selection of Loading Rate: The choice of the rate of shear in a drained test is governed by the need to allow excess pore pressures generated during shear to dissipate. Drained tests must generally be performed at slower rates than undrained tests.

The results of Bishop and Gibson (1963) can be used to show that, for the case of drainage from the radial boundary and only one end of a specimen, the minimum time to failure, t_f, required to ensure 95 percent pore water pressure dissipation in a drained triaxial test can be expressed in the following way:

$$t_f = \frac{0.56\ H^2}{c_v} \qquad (9.6)$$

where H is half the average height of the specimen during shear and c_v is the coefficient of consolidation measured during the final consolidation stage.

The drained test was performed at an effective consolidation pressure of 1.1 psi. Accordingly, there was no distinct consolidation phase after saturation and, thus, the coefficient of consolidation, c_v, was not measured for the specimen in the drained test. Instead, it was assumed that the smallest of the values for c_v which were estimated from the consolidation results in Test B.1 could be used to estimate the minimum time to failure in the drained test; Test B.1 was the only test on red clay for which reasonable consolidation data were available.

The smallest estimate of c_v for Test B.1, which was found using the logarithm of time approach, was 0.0012 in.^{2}/minute. Using this value of c_v and assuming that the average height of the specimen up to the time of "failure" was approximately 3 inches (which is a reasonable assumption at low axial strains), the minimum time to failure, t_f, is found to be approximately 1000 minutes (using Equation 9.6).

The stress-strain curve for the drained test (6.3), which is presented in Appendix A, shows that the specimen did not begin to take significant load until an axial strain of approximately 4 percent had been reached. It is possible that the loading rod was not seated firmly in the loading cap at the beginning of shear. Thus, it is difficult to state the actual strain at "failure" in this test, although it would not be unreasonable to assume a value of approximately 1 percent.

The rate of axial deformation which was used in Test 6.3 was 0.0017 inches per hour; this rate was the slowest which could be achieved with the Wykeham Farrance loading presses. If it is assumed that the axial strain at "failure" was 1 percent, the chosen rate of shear corresponds to a time to failure, t_f, of 1060 minutes which is slightly larger than the minimum value estimated using the consolidation results from Test B.1. It is likely that the use of consolidation data from Test B.1, at a final effective consolidation pressure of 19.4 psi, to estimate the time to failure in the drained test, at a final effective consolidation pressure of 1.1 psi, would result in a conservative estimate of the time to failure. Since the specimen in the drained test was less dense because of its lower effective consolidation pressure, it would be reasonable to expect faster pore pressure dissipation in a less dense specimen.

9.4.1.4.2. Test Results: The peak strength measured in a drained test can be represented by a single point on a modified Mohr-Coulomb diagram such as the one presented in Fig. 9.11. The peak strength measured in the drained test is plotted in Fig. 9.14 along with the effective stress paths from the undrained tests and the effective stress shear strength envelope determined from the undrained tests. The results indicate that there is very good agreement between the shear strengths of specimens tested under drained and undrained conditions. The decision to perform the majority of the triaxial shear tests under undrained conditions, therefore, is judged to be valid, and the existence of the cohesion intercept value ($\bar{c}$) is substantiated.

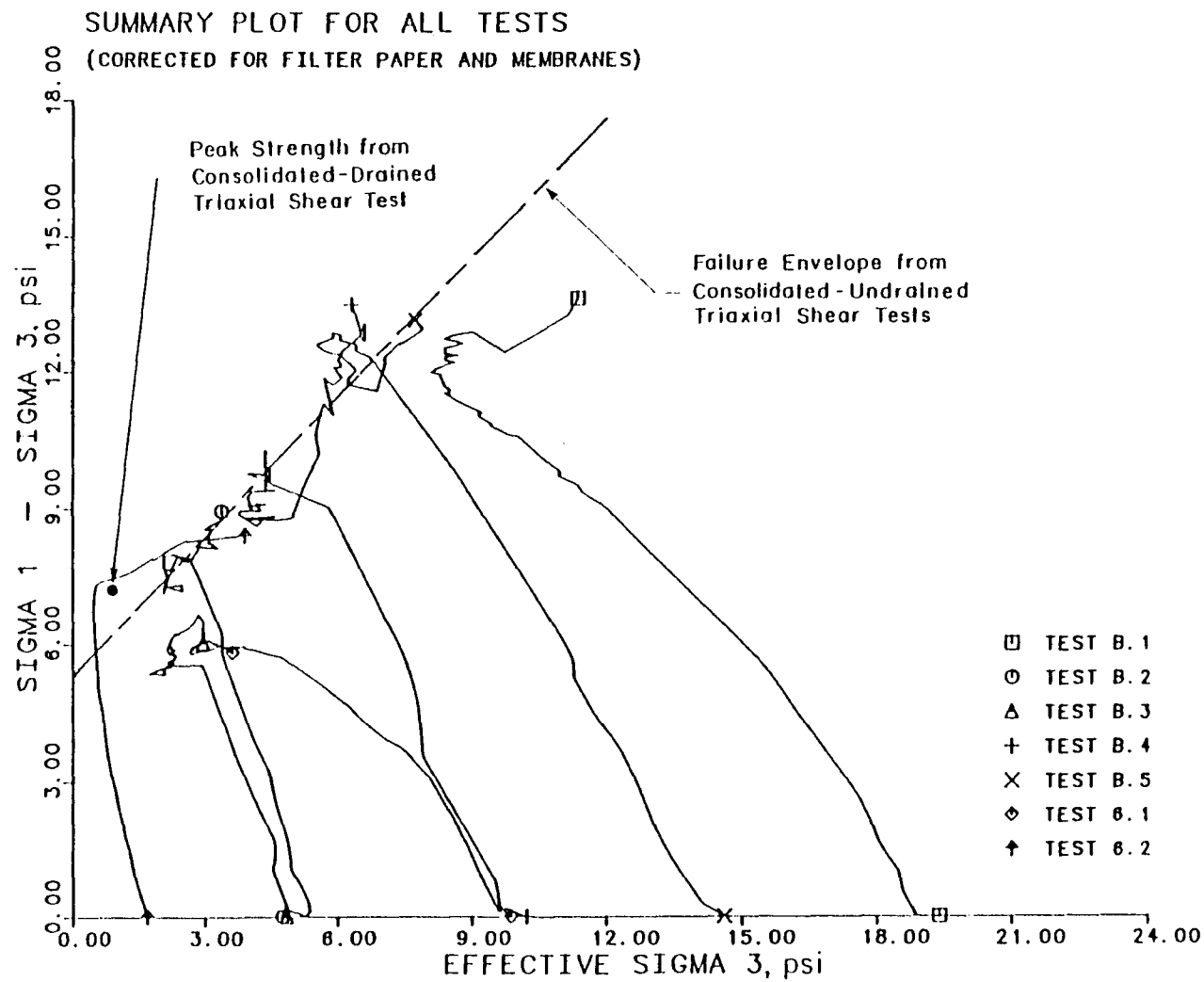

Fig. 9.14 Peak Strength Measured in Consolidated-Drained (S) Triaxial Test Plotted with Stress Paths from Undrained Tests on Red Clay from IH 610 and Scott Street

9.4.1.5. Cyclically Consolidated-Undrained Triaxial Shear Test

An undrained triaxial shear test was performed on the specimen which was subjected to ten cycles of consolidation and swell. In the consolidation phase of this test, the effective confining pressure on the specimen was alternated between 1.1 and 20 psi. The specimen was not loaded axially during the cyclic consolidation and swell stages of the test; but upon completion of these stages, the specimen was sheared at a final effective consolidation pressure of 1.1 psi. The final dry unit weight and moisture content of this specimen were not significantly different from the values observed in specimens which were consolidated in one stage to similar final effective consolidation pressures.

A modified Mohr-Coulomb diagram showing the stress path for the cyclically consolidated specimen (Test 6.5) is presented in Fig. 9.15. The effective stress paths from the tests where specimens were consolidated in the conventional manner are also shown for comparison. It is clear that the specimen subjected to cyclic consolidation and swell exhibited a strength which exceeded the strength suggested by the upper-bound shear strength envelope derived from the data for the other specimens (presented originally in Fig. 9.13.) Thus, it appears that the cyclic consolidation and swell caused some form of change in the soil which made the specimen stronger.

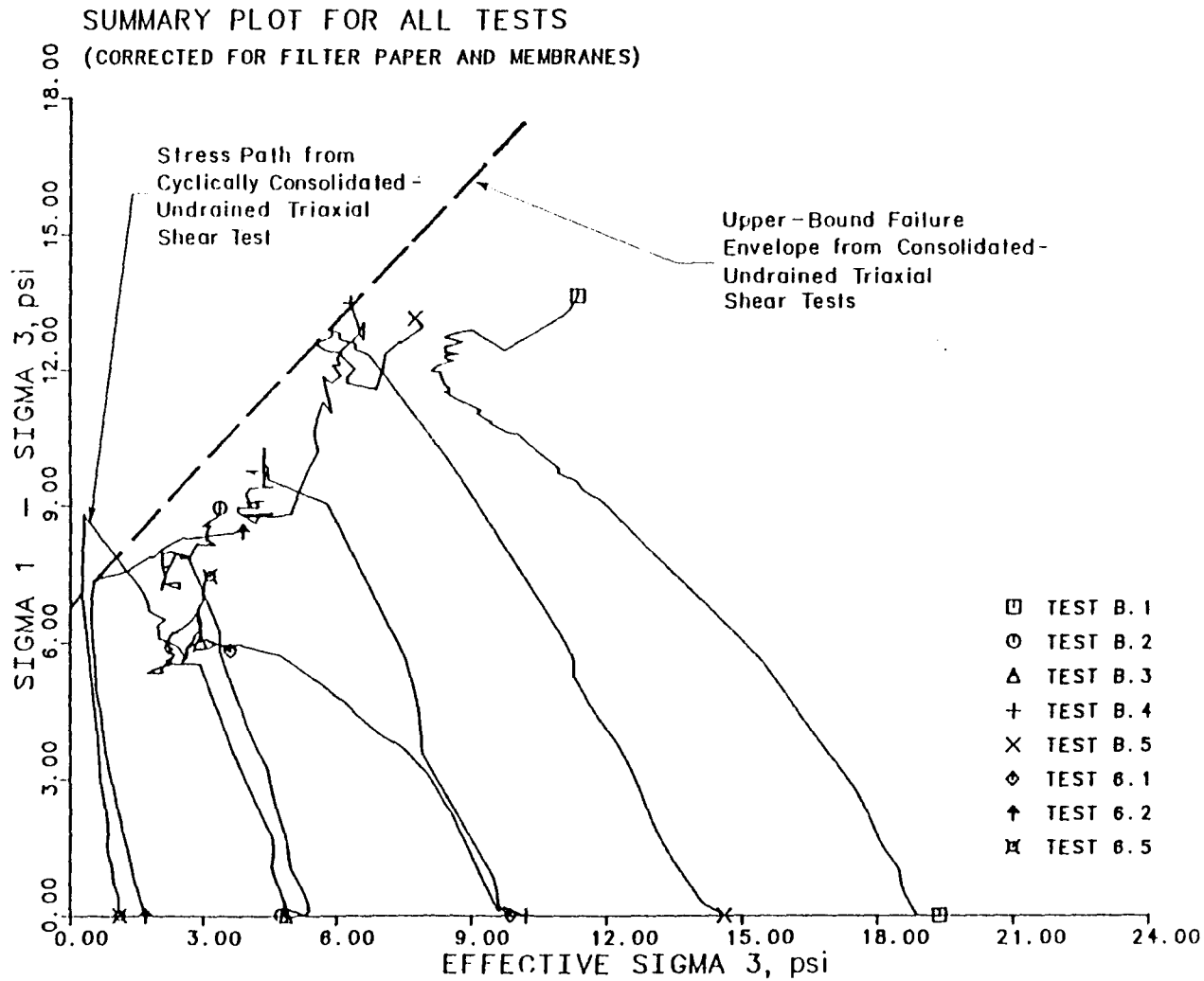

Fig. 9.15 Stress Path from Cyclically Consolidated-Undrained ($\bar{R}$) Test Plotted with Stress Paths from other Undrained Tests on Red Clay from IH 610 and Scott Street

9.4.2. BROWN CLAY FROM SH 225 AND SH 146 (SW)

A single consolidated-undrained ($\bar{R}$) triaxial shear test (Test 6.6) was performed on the brown clay from the SH 225 and SH 146 (SW Quadrant) embankment to determine if the brown clay had properties similar to those of the red clay. The results of the index property tests, which are reported in Chapter 4, indicated that the brown clay was similar to the red clay from the IH 610 and Scott Street embankment. Accordingly, the same compaction criteria were used for the preparation of the specimen of brown clay as had been developed for the red clay.

The specimen was compacted with a height of hammer fall equal to 8-1/2 inches. The initial moisture content and dry unit weight of the specimen were 23.4 percent and 99.0 pcf, respectively. Although the compaction moisture content was fairly close to the "target" value of 24.0 percent, the dry unit weight was 2.7 pcf higher than the "target" value of 96.3 pcf and 2.8 pcf higher than any actual compacted specimen of red clay tested in the triaxial program. Therefore, it would appear that the properties of this specimen of brown clay may be different from the properties of the red clay.

The specimen of brown clay was consolidated to a final effective pressure of 4.8 psi. The moisture content and dry unit weight of the specimen after consolidation and saturation were 29.3 percent and 94.1 pcf, respectively. Although the final moisture content compares reasonably well with the values obtained for specimens of red clay consolidated

to similar final effective pressures, the value of the final dry unit weight is almost 2 pcf higher than similar specimens of red clay.

A modified Mohr-Coulomb diagram showing the stress path for the consolidated-undrained ($\bar{R}$) triaxial shear test (6.6) performed on the specimen of brown clay is presented in Fig. 9.16. Effective stress paths and the upper-bound shear strength envelope for specimens compacted with red clay are also shown for comparison.

It appears from the results presented in Fig. 9.16 that the specimen compacted of brown clay from the SH 225 and SH 146 (SW Quadrant) embankment exhibited a strength which is slightly greater than the strength suggested by the upper-bound envelope for specimens of red clay. However, it is not possible to determine, based on the results of this one test, whether the brown clay is indeed "stronger" than the red clay or whether the high strength which was measured was a result of the somewhat higher initial density of the specimen.

9.4.3. GREY CLAY FROM IH 610 AND SCOTT STREET

Four consolidated-undrained ($\bar{R}$) triaxial shear tests were performed on the grey clay from the IH 610 and Scott Street embankment at final effective consolidation pressures ranging from 1.1 to 20.2 psi.

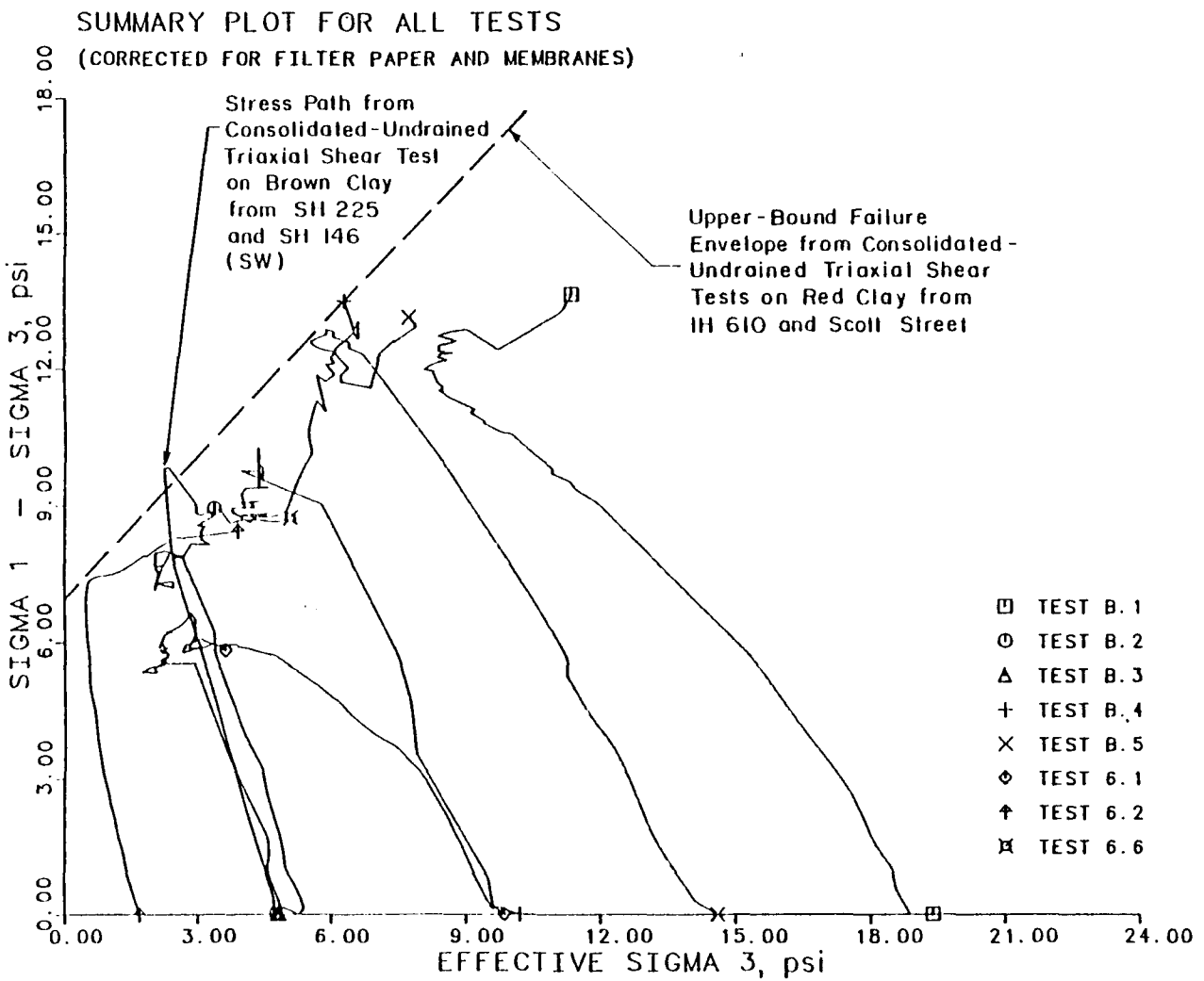

Fig. 9.16 Stress Path from Consolidated-Undrained ($\bar{R}$) Triaxial Test on Brown Clay from SH 225 and SH 146 (SW) Plotted with Stress Paths from Undrained Tests on Red Clay

9.4.3.1. Stress-Strain Relationships

The stress-strain curves, expressed in terms of principal stress difference, $(\sigma_1-\sigma_3)$, versus axial strain are plotted in Fig. 9.17. The stress-strain curve from the test (B.7) at the highest effective consolidation pressure of 20.2 psi is the only one which exhibits a gain in axial load throughout the test. The specimens in the three tests (6.8, B.6, and 6.4) performed at the lower final effective consolidation pressures of 1.1, 5.3, and 10.4 psi, respectively, all exhibited some reduction in principal stress difference after a peak principal stress difference was recorded, generally at strains of less than one percent. The maximum reduction in principal stress difference was approximately 25 percent of the peak value and occurred in the test (6.8) performed at the lowest final effective consolidation pressure.

9.4.3.2. Effective Stress Paths

The effective stress paths from the four consolidated-undrained ($\bar{R}$) tests performed on the grey clay are presented in Fig. 9.18. These stress paths exhibit similar characteristics to those presented for the red clay in Fig. 9.9. The pore pressures generally increased until the maximum principal stress difference was reached and then tended to decrease. This effect is likely to have been caused by a tendency for initial contraction of the soil structure followed by dilation.

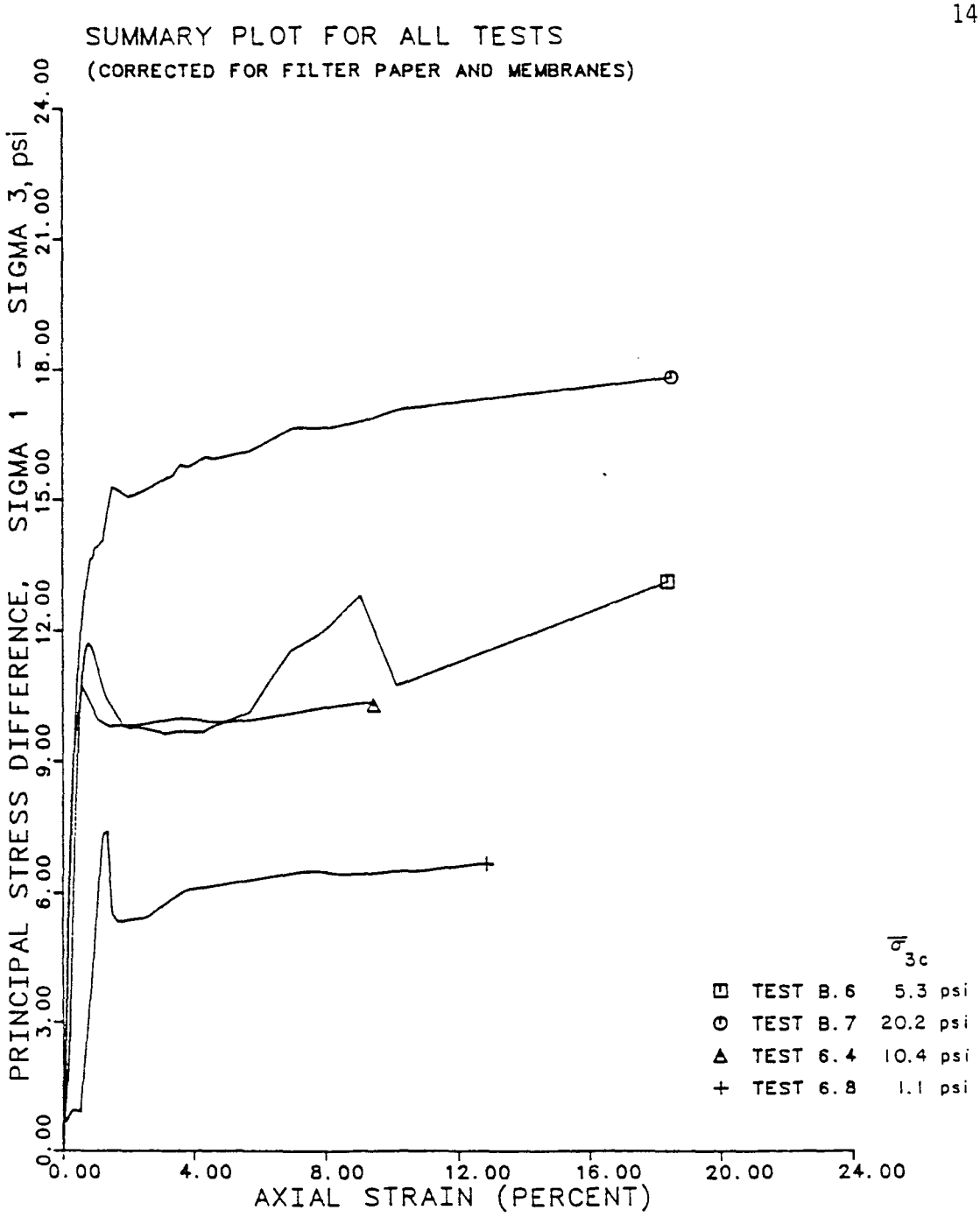

Fig. 9.17 Stress-Strain Relationships from Four Consolidated-Undrained ($\bar{R}$) Triaxial Tests on Grey Clay from IH 610 and Scott Street

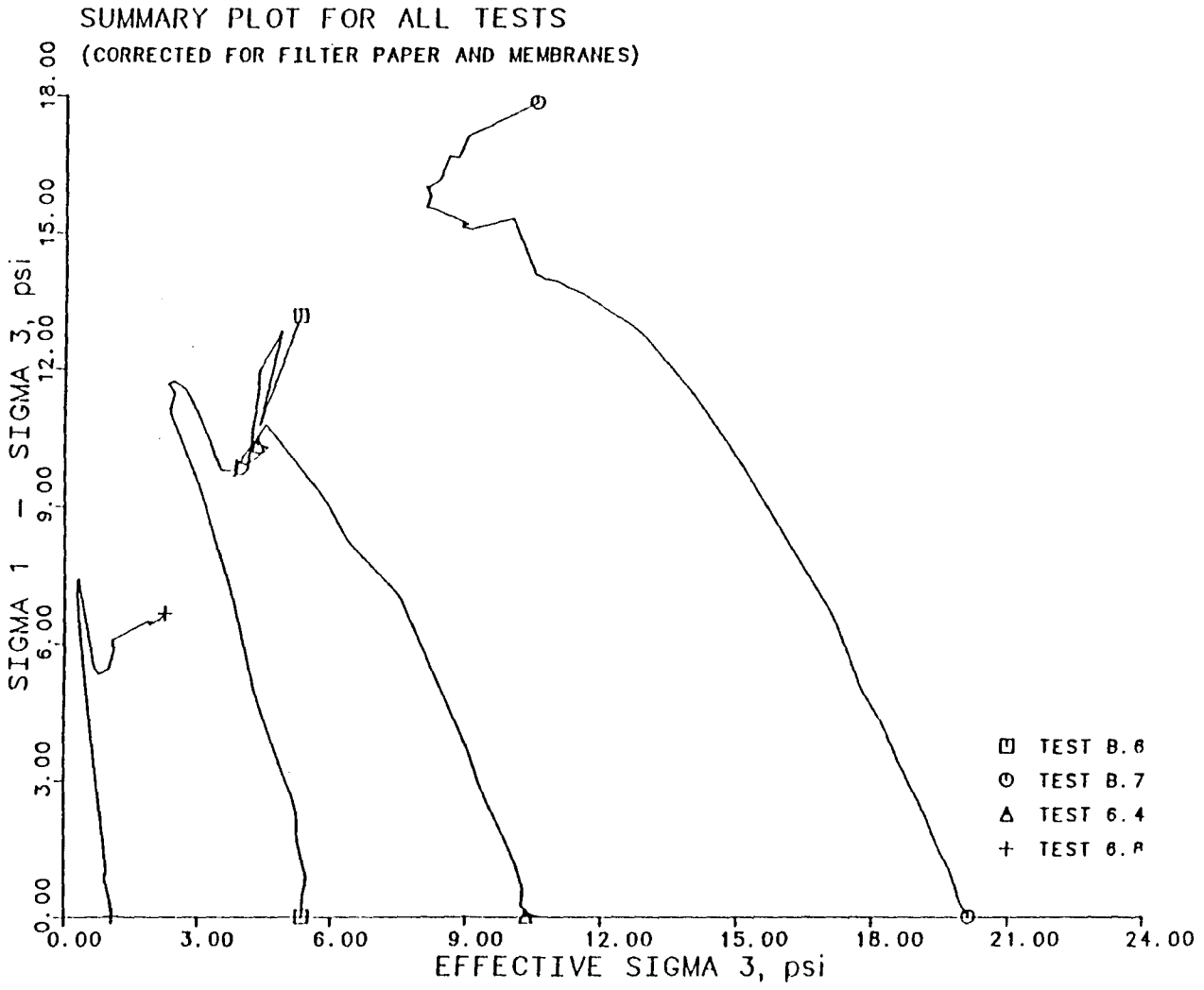

Fig. 9.18 Stress Paths from Four Consolidated-Undrained ($\bar{R}$) Triaxial Tests on Grey Clay from IH 610 and Scott Street

The initial portions of the stress paths plotted in Fig. 9.18 seem to become flatter as the effective consolidation pressure increases. This trend was also observed in the results of the tests performed on specimens compacted of red clay, but was not as clearly defined for the red clay as it was for the grey clay. It appears that the level of the effective consolidation pressure has a stronger influence on the shape of the stress paths than do any variations in structure of the specimens caused by the compaction procedure.

9.4.3.3. Effective Stress Shear Strength Envelope

The effective stress shear strength envelope for the grey clay was determined in the same manner as described earlier for the red clay. The stress path tangency points and the resulting shear strength envelope are presented on a modified Mohr-Coulomb diagram in Fig. 9.19. The corresponding effective stress shear strength parameters (calculated using Equations 9.5a and 9.5b) are $\bar{c}$ = 386 psf, and $\bar{\phi}$ = 19.7 degrees. The effective angle of internal friction, $\bar{\phi}$, for the grey clay is remarkably close to the value of 20.0 degrees which was determined for the red clay from the same embankment. The main difference between the two effective stress shear strength envelopes relates to the apparent cohesion intercept, $\bar{c}$, of each soil. The best estimate of the parameter $\bar{c}$ for the red clay is 268 psf and for the grey clay is 386 psf. Thus, it appears that the red clay was probably the "weaker" soil in the IH 610 and Scott Street embankment as originally anticipated.

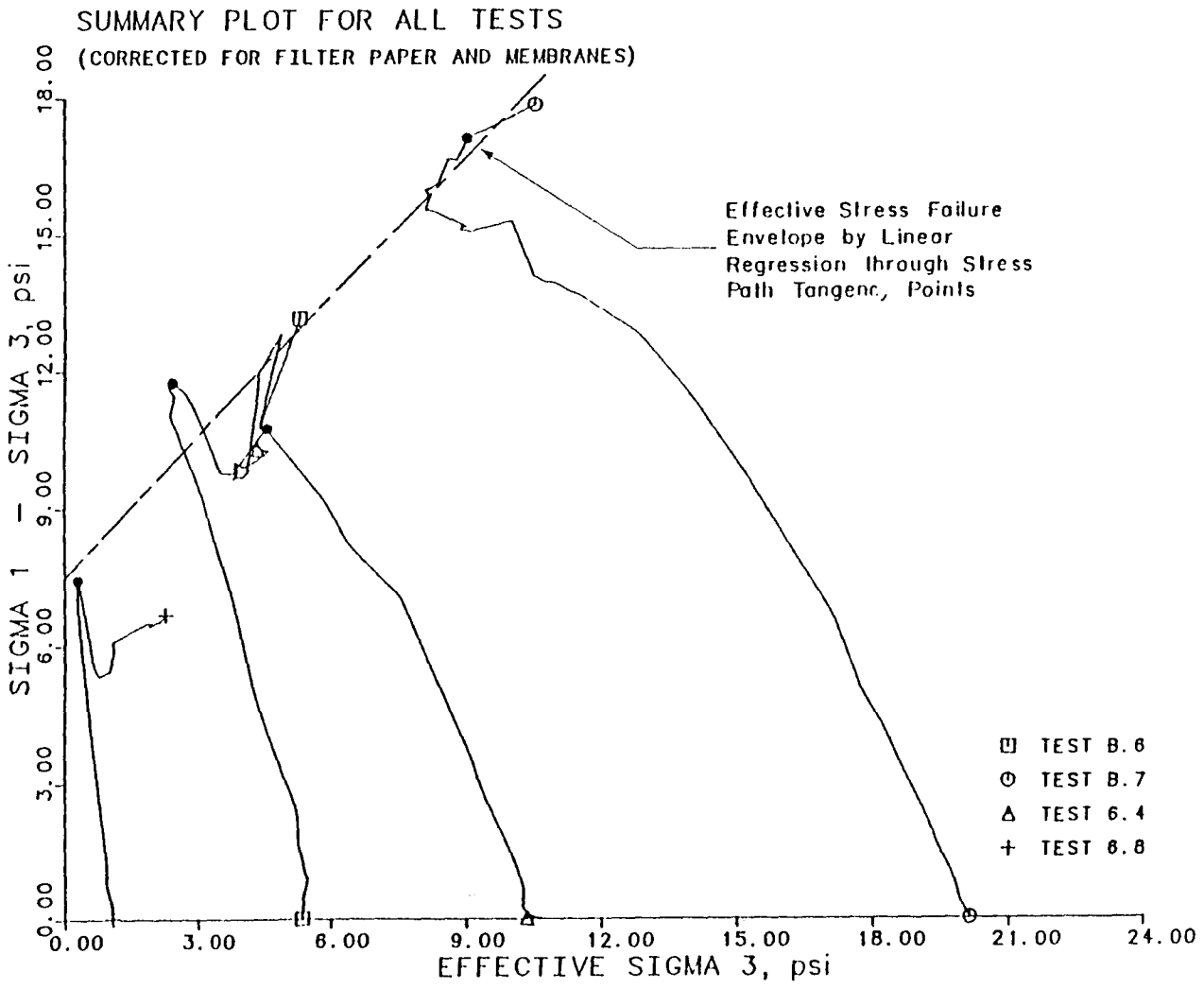

Fig. 9.19 Effective Stress Failure Envelope for Grey Clay from IH 610 and Scott Street

9.5. SUMMARY

The procedures used to perform triaxial shear tests on compacted specimens of red and grey clay obtained from the IH 610 and Scott Street embankment, have been presented in this chapter. Considerable care was taken during all stages of each test to ensure that the testing procedure was consistent from test to test and did not cause unrealistic strengths to be measured.

The shear test results enabled the effective stress shear strength envelopes for the red and grey clays to be identified with considerable confidence. It does not appear that the minor differences in equipment and procedure between the basement and sixth floor laboratories affected the results in any significant way. Furthermore, the similarity between the shear strength measured in the consolidated-drained (S) test and the effective stress shear strength envelope determined from the undrained shear tests, appears to support the choice of consolidated-undrained ($\overline{R}$) tests for the majority of the testing.

The effective stress shear strength envelopes for the red and grey clays appear to be linear at low effective confining pressures and can be defined in terms of effective stress cohesion and friction angle values. The effective stress angle of internal friction, $\overline{\phi}$, is 20.0 degrees for the red clay and 19.7 degrees for the grey clay. The effective stress cohesion, $\overline{c}$, is estimated to be approximately 270 psf for the red clay and 390 psf for the grey clay.

CHAPTER 10: CONCLUSIONS

10.1. SUMMARY OF RESULTS

A series of triaxial shear tests was performed on specimens of compacted clay taken from the site of a slide in an embankment at IH 610 and Scott Street in Houston, Texas. Seven specimens of red clay and four specimens of grey clay were tested under consolidated-undrained ($\bar{R}$) conditions. The results of these tests were used to define effective stress shear strength envelopes for the two (red and grey) clays. The effective stress shear strength parameters, $\bar{c}$ and $\bar{\phi}$, for the envelopes are summarized in Table 10.1.

A consolidated-drained (S) triaxial shear test was performed at a very low effective confining pressure on a specimen of red clay to verify the cohesion intercept value which had been indicated by the results of the consolidated-undrained ($\bar{R}$) tests. The peak strength of this specimen fell slightly above the strength indicated by the failure envelope derived from the consolidated-undrained tests, but was within the range of experimental scatter in the data for these tests. The results of the drained test therefore confirmed the existence of the effective stress cohesion intercept.

A specimen of red clay from the IH 610 and Scott Street embankment was subjected to ten cycles of consolidation and swell in order to

Table 10.1

Summary of Effective Strength Parameters
Determined in Laboratory Triaxial Shear Tests

Clay	$\overline{c}$ (psf)	$\overline{\phi}$ (degrees)
Red	270	20.0
Grey	390	19.7

simulate cycles of wetting and drying near the surface of an embankment. The specimen was then sheared under undrained conditions from an effective consolidation pressure of 1.1 psi. The strength of this specimen was significantly greater than the strength indicated by the upper bound envelope derived from the results of the conventionally consolidated specimens. Thus, it appears that the cyclic consolidation procedure produces stonger specimens than the conventional consolidation procedure.

10.2. COMPARISON OF LABORATORY AND FIELD STRENGTH PARAMETERS

Stauffer (1984) reports results of slope stability analyses performed on the slide in the IH 610 and Scott Street embankment. Stauffer assumed that the pore water pressures were zero in the embankment. He then calculated the averaged mobilized values of the effective stress shear strength paramters, $\bar{c}$ and $\bar{\phi}$, at the time of failure using the observed slide geometry and the fact that the factor of safety (F) must have been unity when the slide occurred.

Stauffer reports that the effective stress angle of internal friction, $\bar{\phi}$, determined using the back-calculation procedure is approximately 19 degrees. The effective stress cohesion intercept of the soil in the field appears to be approximately 7 psf. The value for the effective angle of internal friction (19 degrees) back-calculated by Stauffer agrees very well with the values of 20.0 and 19.7 degrees determined for

the red and grey clays, respectively, from the IH 610 and Scott Street embankment. Thus, the effective stress angles of internal friction measured in the laboratory tests appear to be good estimates of the value which can be mobilized in an embankment. However, the cohesion component of the shear strength back-calculated for the embankment by Stauffer is very small (approximately 7 psf), whereas the consolidated-undrained ($\bar{R}$) tests which were performed in the laboratory indicate the presence of a very substantial cohesion component (268 psf for the red clay and 386 psf for the grey clay). The existence of this cohesion intercept has been confirmed by both consolidated-undrained ($\bar{R}$) and consolidated-drained (S) triaxial shear tests performed at very low effective consolidation pressures. In fact, the principal reason for performing the triaxial tests at low effective stresses was to confirm the cohesion intercept measured in the laboratory.

Stauffer (1984) also calculated a factor of safety for the IH 610 and Scott Street embankment using the effective stress strength parameters which were measured in the laboratory for the red clay and presented in Table 10.1. He assumed that the pore water pressures were zero and reports a factor of safety of approximately 2.7 from his analysis. This ($F = 2.7$) indicates that the embankment should be stable while the fact that a slide has occurred indicates that it was not.

The assumption that the pore water pressures are zero may be unreasonable. However, another stability analysis performed using pore water pressures as high as 60 percent of the overburden pressure still yielded factors of safety of at least 1.3. Therefore, it does not appear

that the existence of high pore water pressures can be used to explain the discrepancy between the "predicted" stability of the embankment and its actual instability.

10.3. FACTORS AFFECTING LABORATORY RESULTS

There is a discrepancy between the value of the effective stress cohesion intercept measured in laboratory triaxial tests and the value back-calculated from the IH 610 and Scott Street embankment slide. Consequently, it does not appear that the field conditions are adequately represented by the compaction, consolidation, saturation, and shearing procedures employed for the triaxial tests in this study.

One explanation might be that the rates of shear in the triaxial tests were too high. However, the rates of shear in the undrained tests were much slower than conventional laboratory practice would normally dictate and it seems only remotely possible that a further reduction in the rate of shear would result in a lower effective stress cohesion intercept.

Another explanation for the discrepancy between the cohesion intercept measured in the laboratory and the value back-calculated from the embankment failure may be that the compaction method used to prepare the test specimens did not adequately reproduce conditions achieved in the field. However, it was noted during a recent examination of undisturbed 3 inch diameter Shelby tube samples from the IH 610 and Scott Street embankment that the consistency of the soil in these tubes was

very similar to the consistency of the compacted triaxial specimens at the end of shear. Furthermore, Vaughan et al. (1978) have published data indicating that variations in structure induced by field compaction, laboratory static compaction, and laboratory dynamic compaction (such as the hammer compaction used in this investigation) techniques have little effect on the effective stress shear strength envelopes measured in laboratory triaxial shear tests.

There is one other possible explanation of the discrepancy between the two values obtained for the cohesion intercept. Vaughan (1977) has drawn attention to the fact that the bulk strength of a fill will be influenced by the degree to which the fill material is broken down and remolded during compaction. The effect of the initial structure on shear strength will be largely controlled by the relative proportions of intact saturated clay lumps and the surrounding partly-saturated clay matrix. The greater the proportion of remolded clay, the closer will be the bulk strength to that of a thoroughly remolded sample of the same clay. However, as remolded strengths are generally lower than undisturbed strengths due to the loss of the strength contribution attributable to structural effects, the use of the throroughly remolded soil, as done in this study, should lead to an underestimate, rather than an overestimate, of the field strength.

10.4. DIRECTIONS OF FURTHER INVESTIGATION

This report is based on the first stage and a portion of the sec-

ond stage of an investigation of the long-term strength properties of compacted Beaumont clay. As an additional part of the second stage of this investigation, further consolidated-undrained ($\bar{R}$) triaxial shear tests are being performed on specimens of the red clay from the IH 610 and Scott Street embankment. Some of these specimens have been consolidated from a slurry and some have been formed by packing soil into a mold at a moisture content slightly lower than the liquid limit. It is probable that the effective stress failure envelope produced by these tests will have a much lower cohesion intercept.

A series of direct shear tests are also in progress to measure the residual drained strength of the red clay from the IH 610 and Scott Street embankment. It is not clear at this time whether the residual effective stress shear strength parameters will correlate with the values back-calculated by Stauffer (1984).

A large number of Shelby tube samples have been obtained from and adjacent to the main slide at IH 610 and Scott Street. The results of the triaxial tests being performed on these samples should indicate whether the undisturbed strength of the clay is significantly different from the strength measured with specimens compacted in the laboratory. It should also be possible to determine whether the strength of the clay varies throughout the embankment.

It is anticipated also that another cyclically consolidated test will be performed in which the specimen will be subjected to a shear stress while the effective confining pressure is varied cyclically.

This loading condition comes closer to reproducing the loading experienced by soil in the embankment during cycles of wetting and drying.

10.5. FINAL OBSERVATIONS

The test data presented in this report represent the first study of the long-term shear strength of compacted Beaumont clay at low effective stresses. Indeed, it appears that there is very little information available on the drained strength of compacted fill composed of any highly plastic clay under realistic confining conditions. Vaughan et al. (1978) state that: "To the authors' knowledge, there has been no systematic study of the strength of compacted fills at the low effective stresses which govern slope stability." The results of this investigation represent the first step towards understanding the complicated phenomena which are causing long-term shallow embankment slides in Texas.

APPENDICES

APPENDIX A

Appendix A contains the individual test results for the triaxial shear tests performed on red clay from the embankment at IH 610 and Scott Street. Stress-strain relationships (over the full range of strains employed in a test and over the first 1.50 percent of strain) and stress paths (plotted on modified Mohr-Coulomb diagrams) are presented in the form of plots generated by the computer program RBARPLT for each test.

Results are included for:

- Tests B.1, B.2, B.3, B.4, B.5, 6.1, and 6.2 which were all performed under consolidated-undrained ($\bar{R}$) conditions.

- Test 6.3 which was performed under consolidated-drained (S) conditions (stress-strain relationships only).

- Test 6.5 in which the specimen was cyclically consolidated and then sheared under undrained conditions.

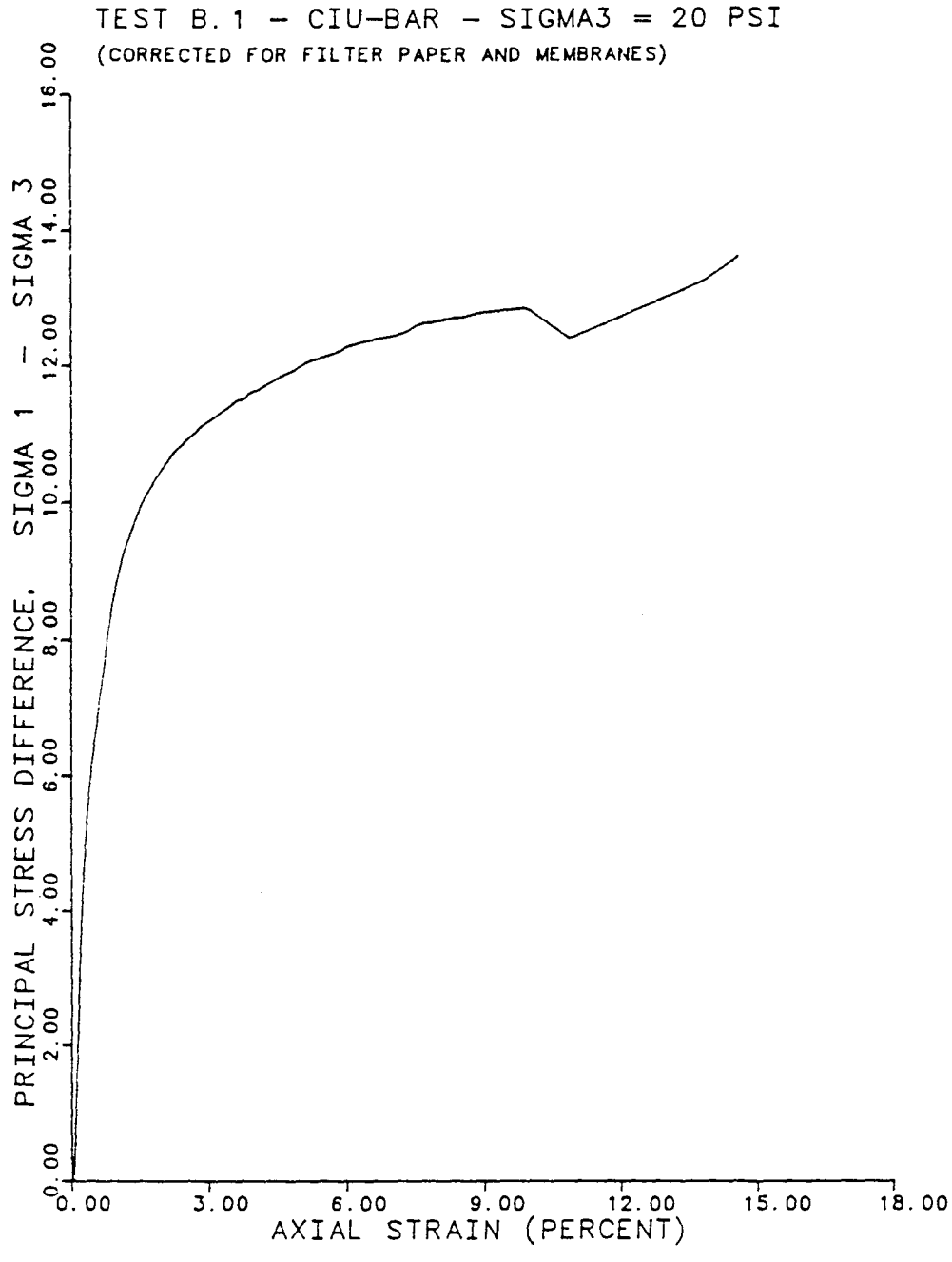

Fig. A.1 Stress-Strain Relationship from Test B.1 on Red Clay from IH 610 and Scott Street

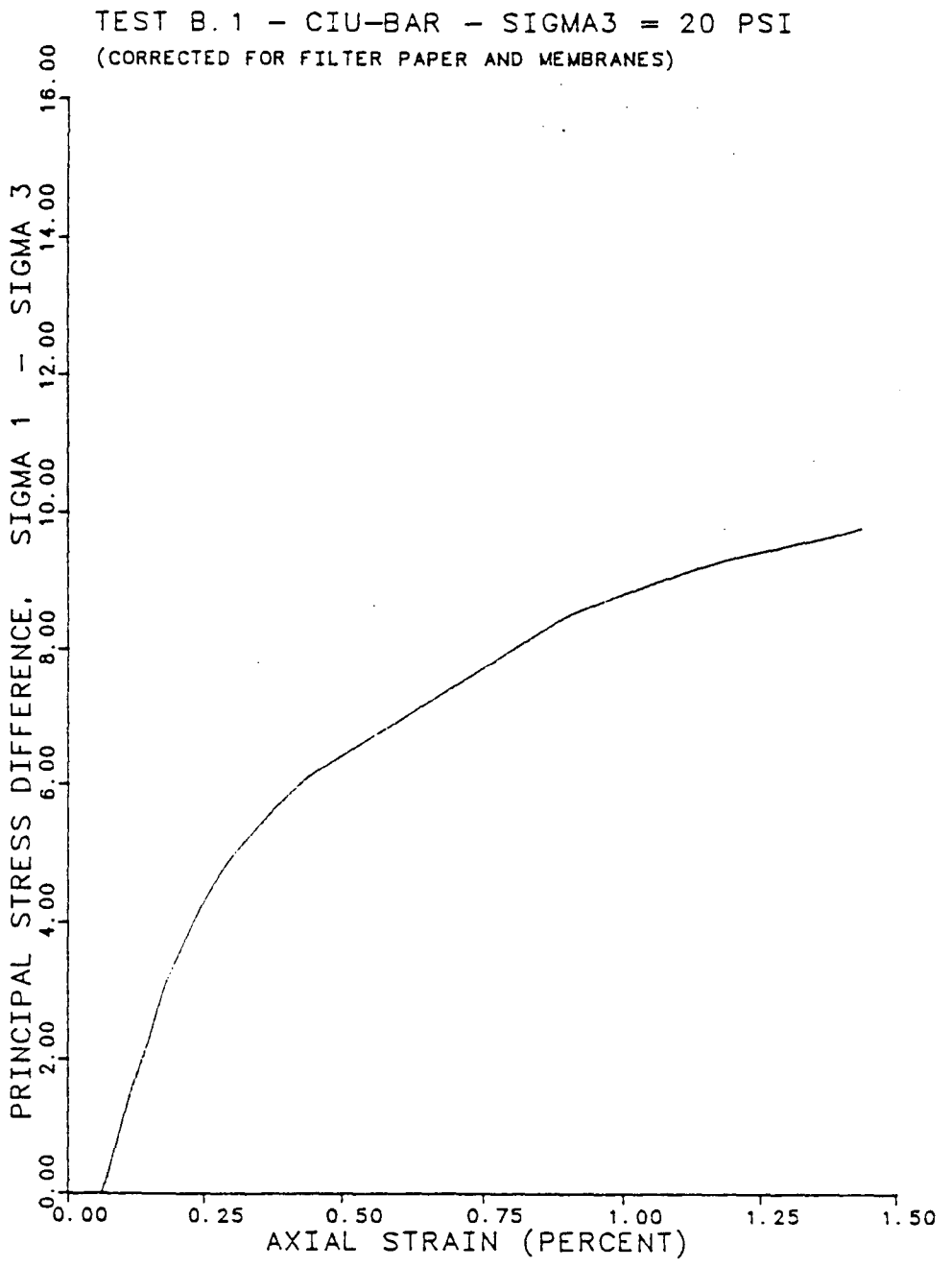

Fig. A.2 Stress-Strain Relationship at Low Strains from Test B.1 on Red Clay from IH 610 and Scott Street

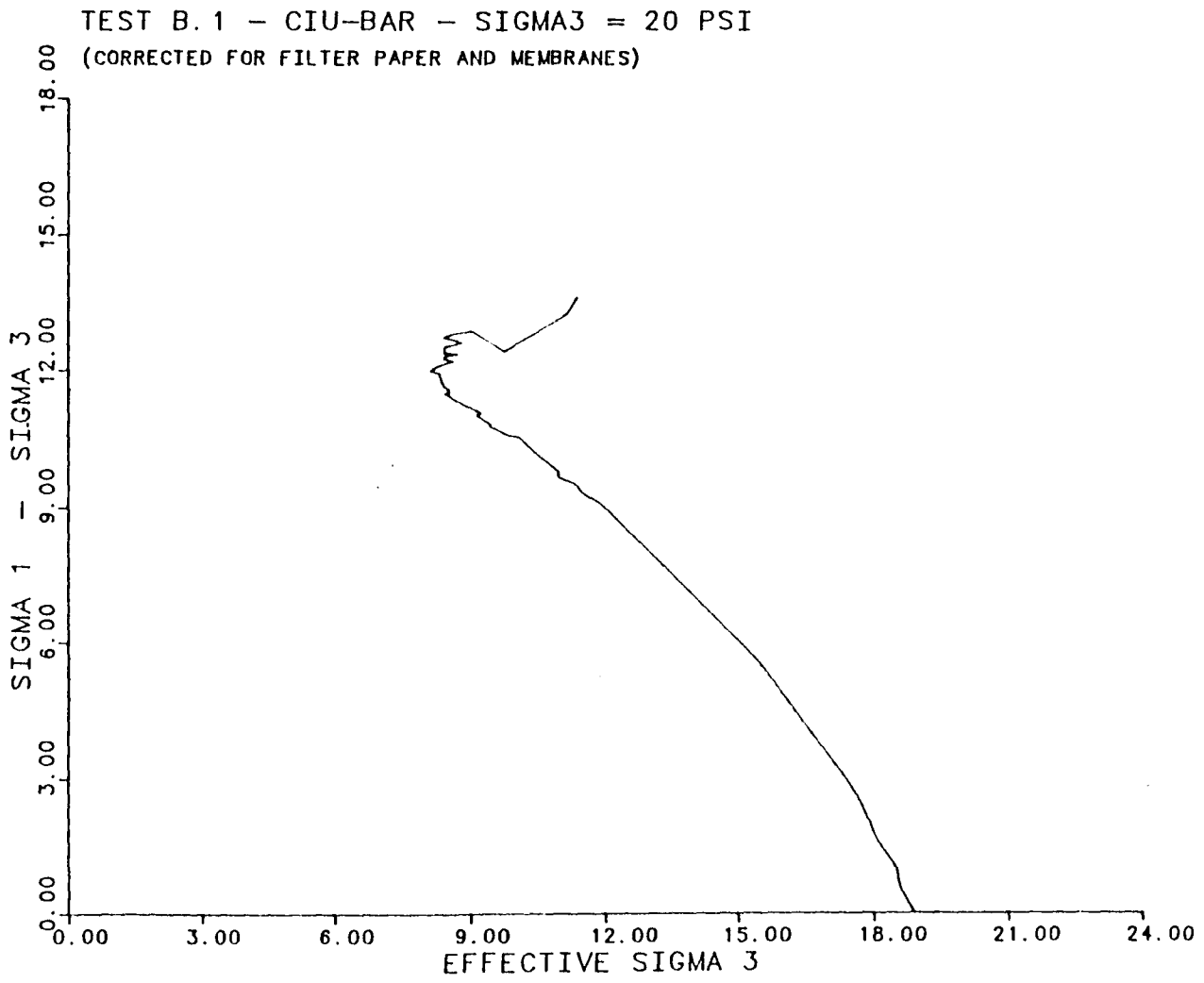

Fig. A.3 Effective Stress Path from Test B.1 on Red Clay from IH 610 and Scott Street

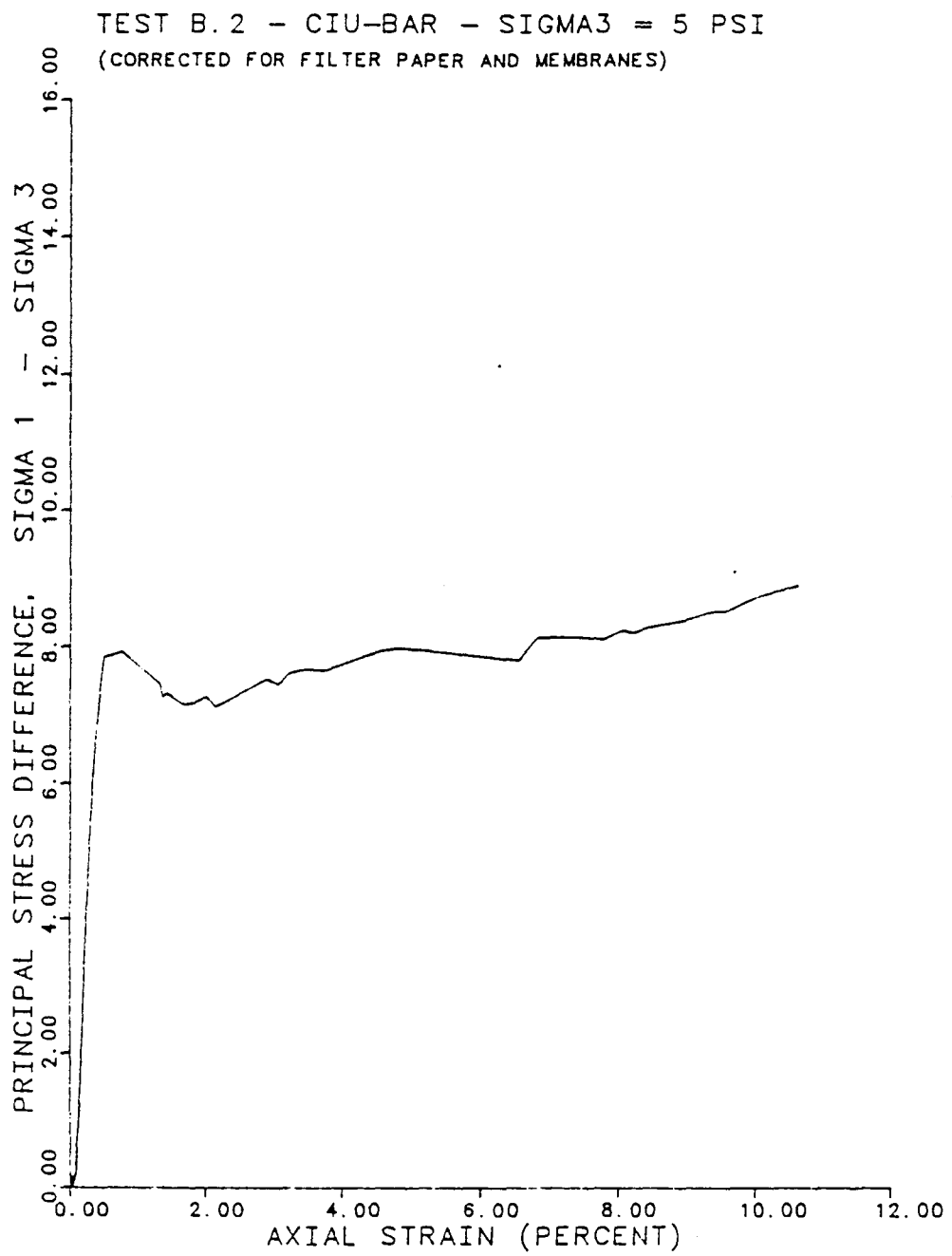

Fig. A.4 Stress-Strain Relationship from Test B.2 on Red Clay from IH 610 and Scott Street

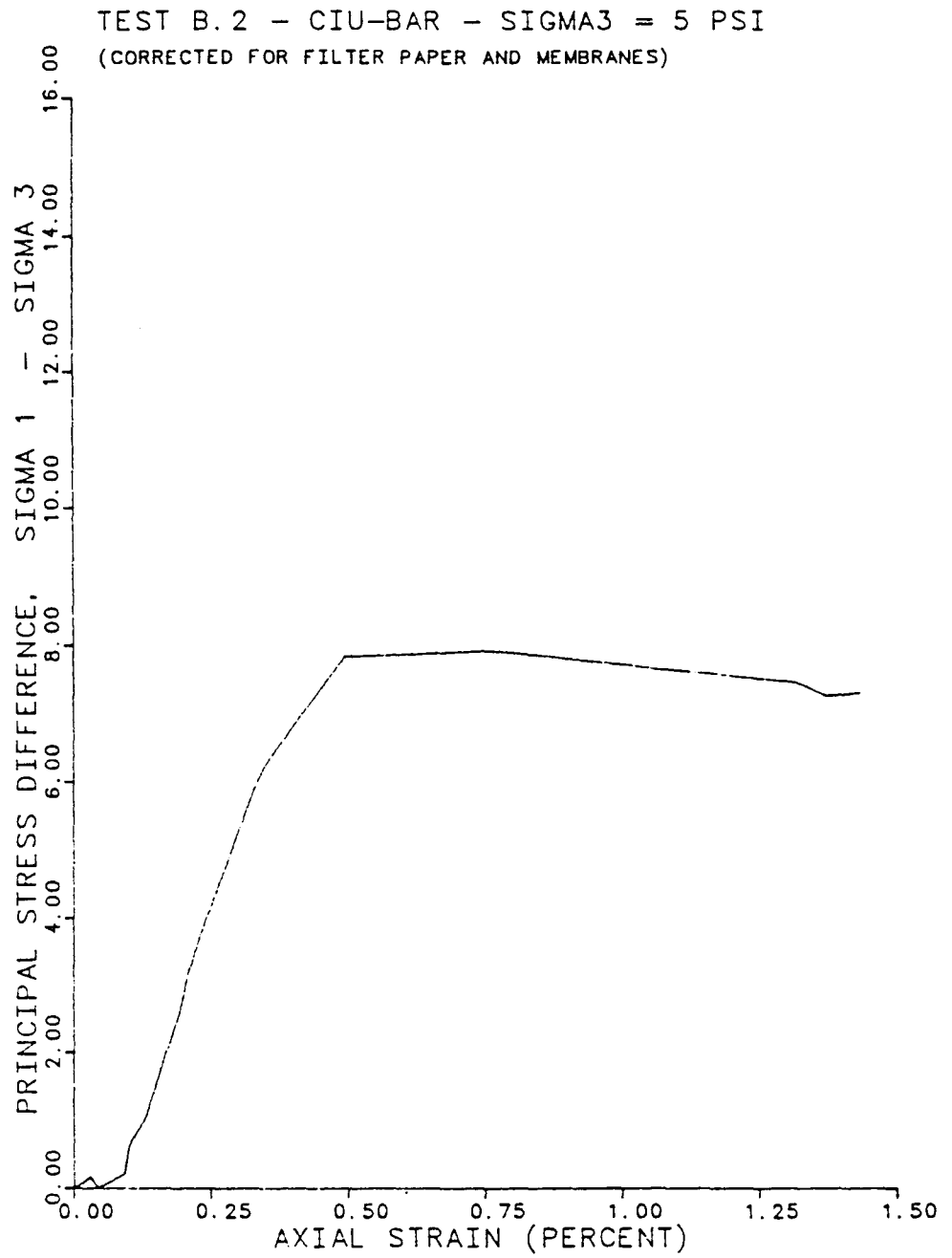

Fig. A.5 Stress-Strain Relationship at Low Strains from Test B.2 on Red Clay from IH 610 and Scott Street

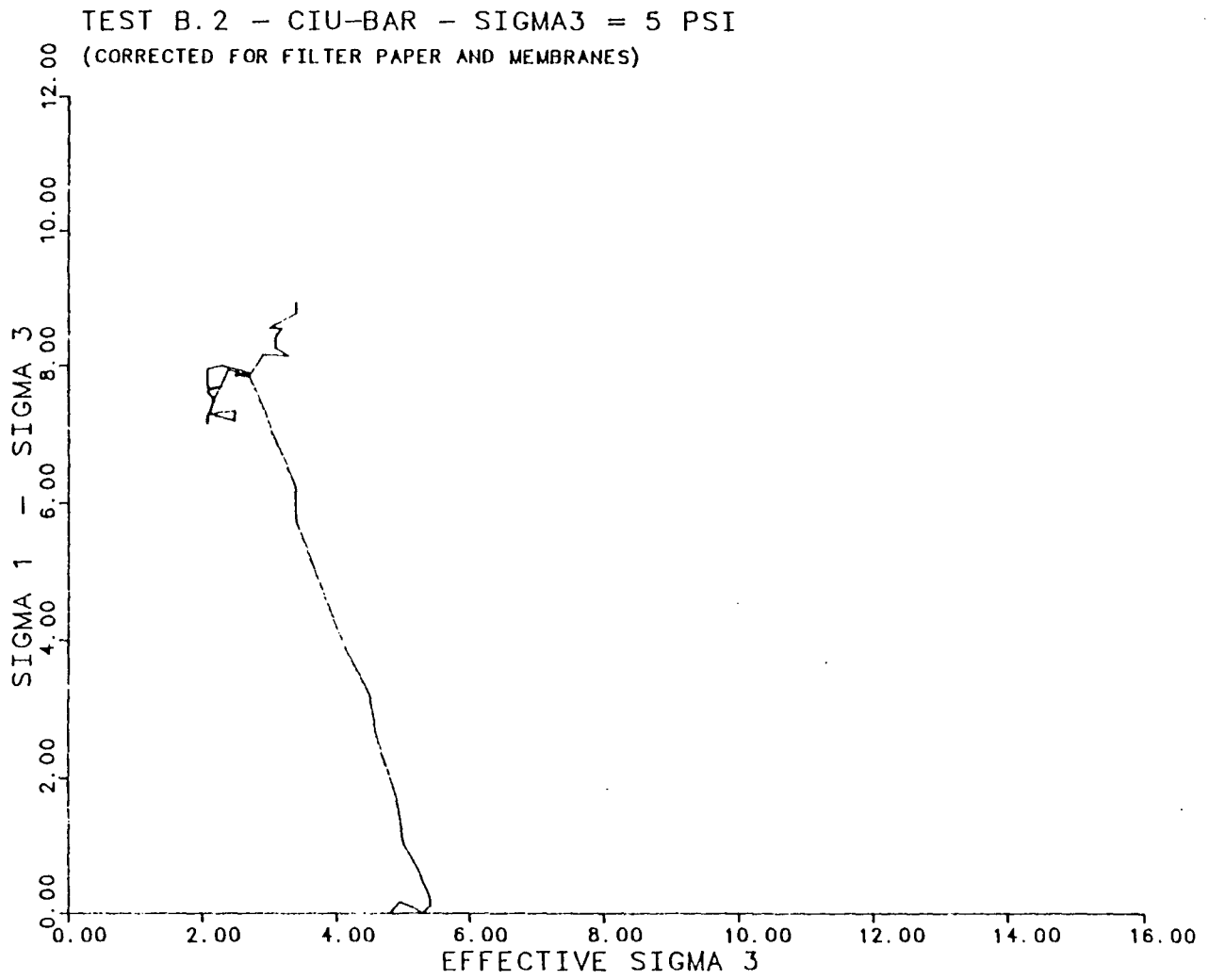

Fig. A.6 Effective Stress Path from Test B.2 on Red Clay from IH 610 and Scott Street

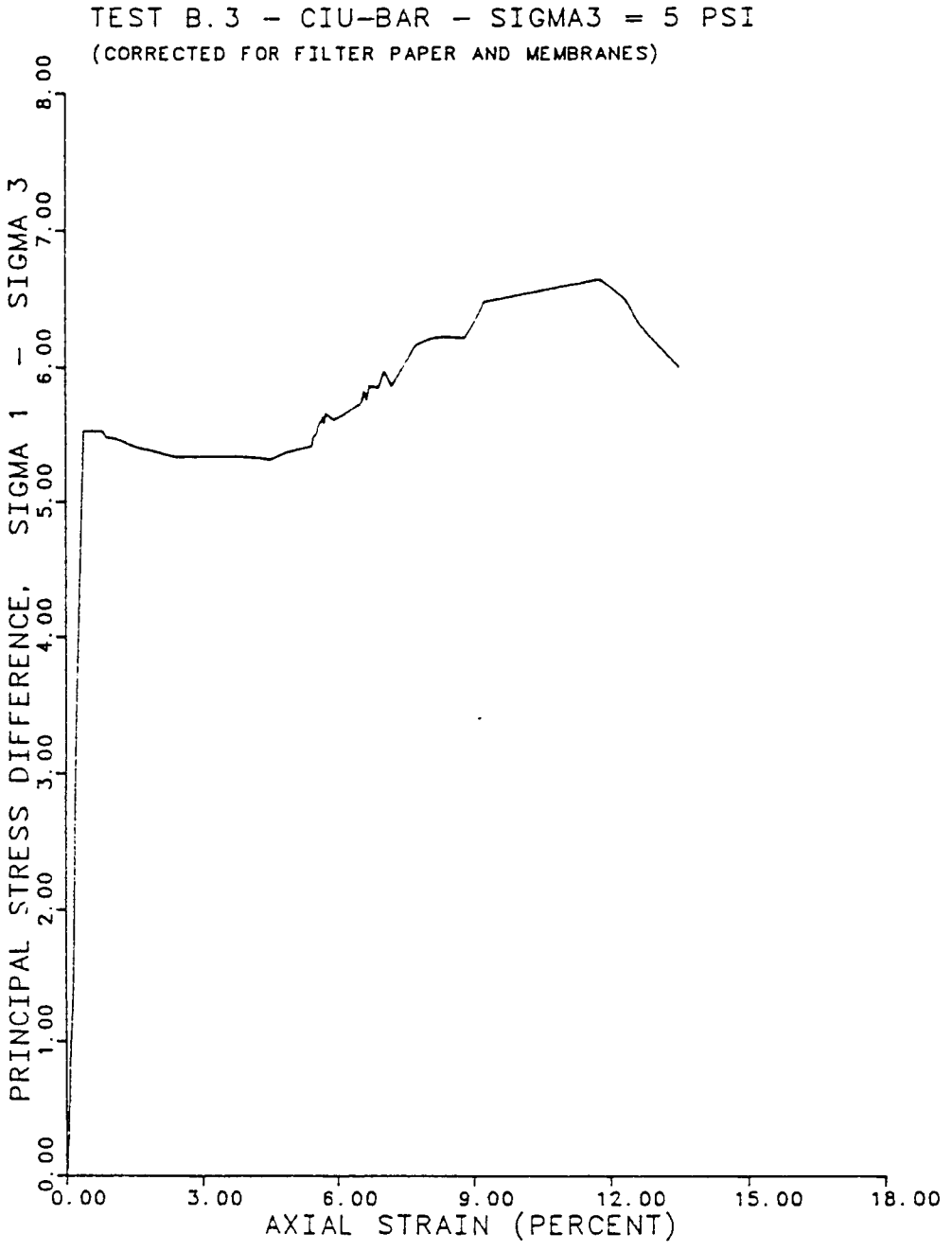

Fig. A.7 Stress-Strain Relationship from Test B.3 on Red Clay from IH 610 and Scott Street

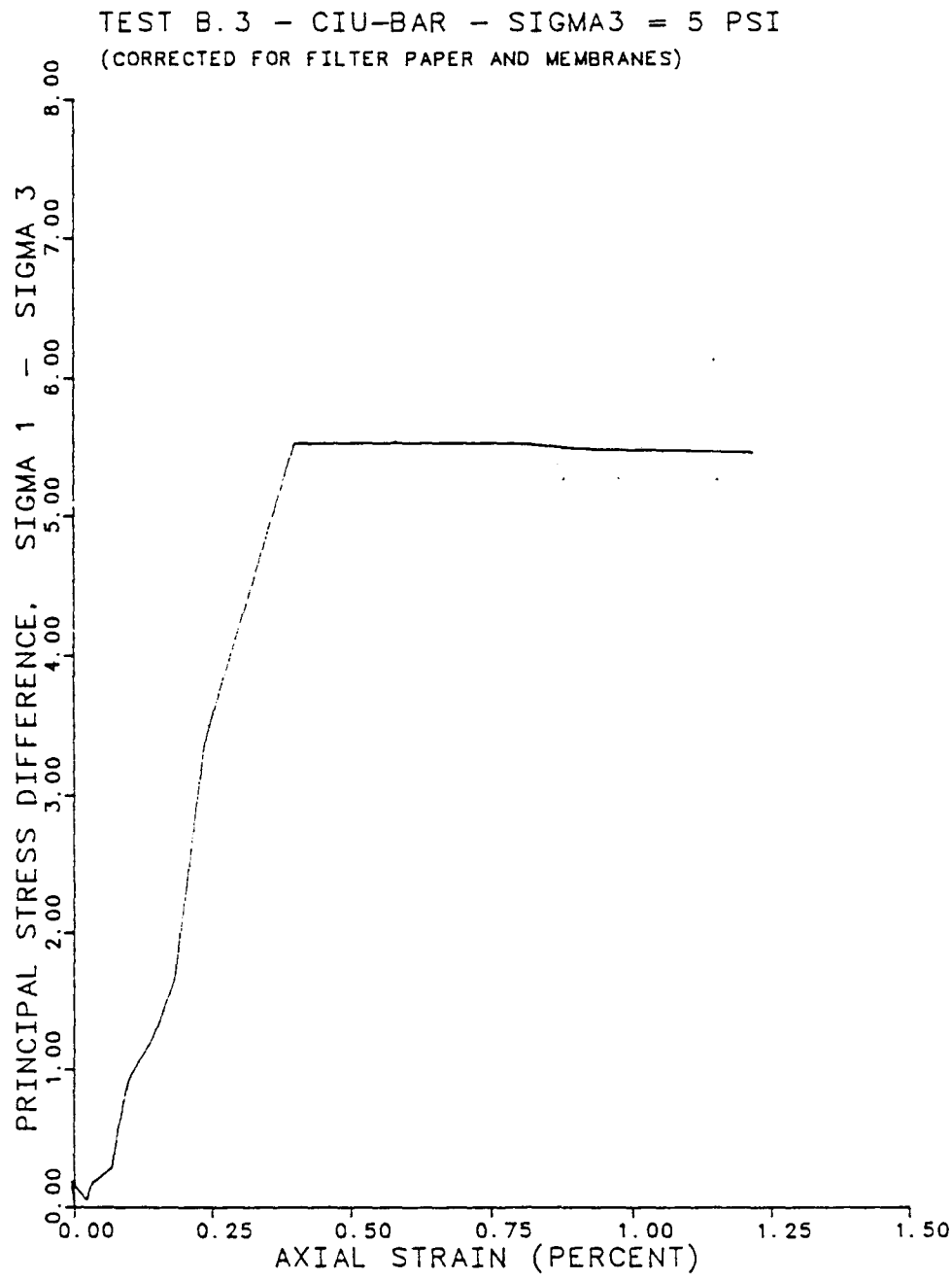

Fig. A.8 Stress-Strain Relationship at Low Strains from Test B.3 on Red Clay from IH 610 and Scott Street

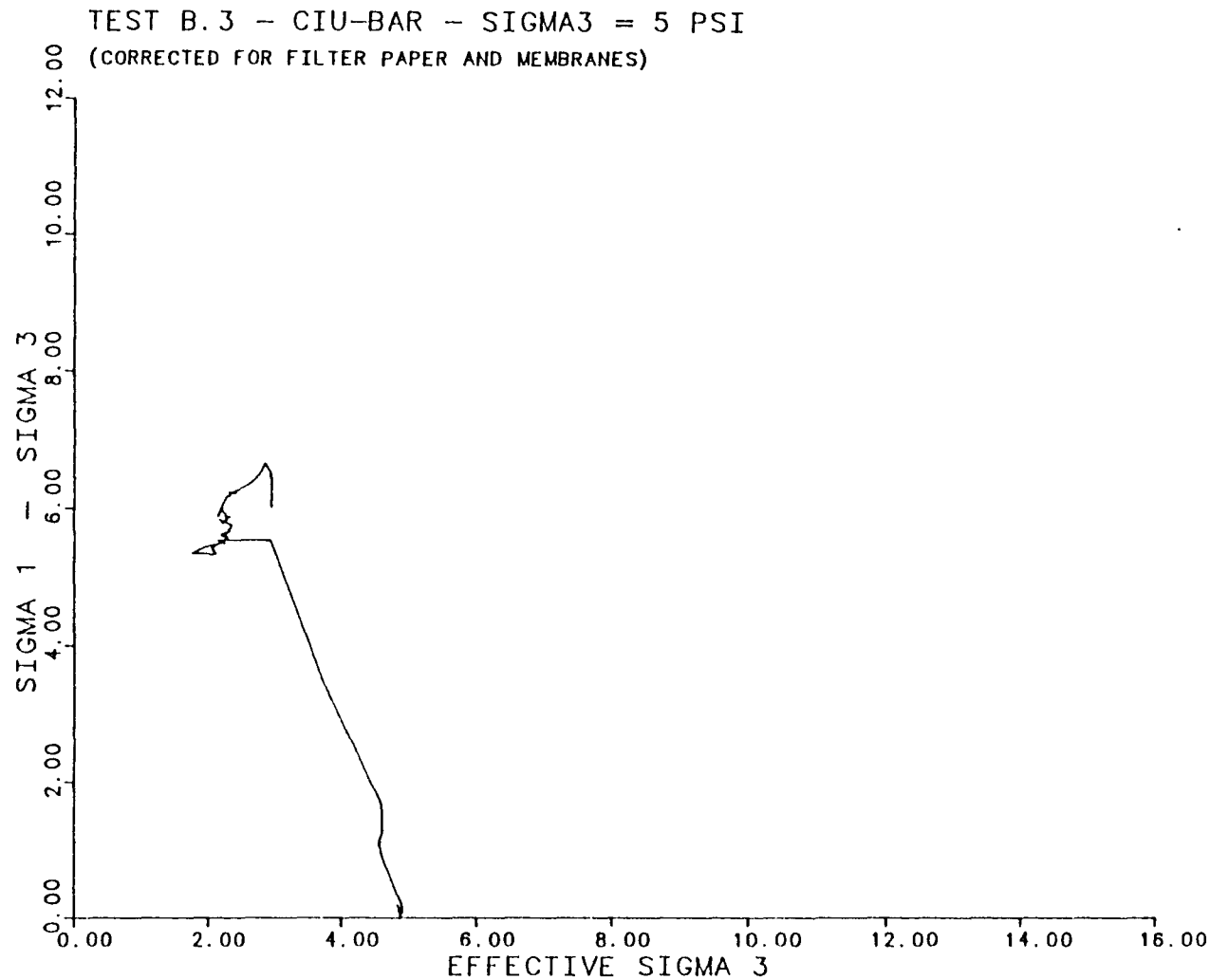

Fig. A.9 Effective Stress Path from Test B.3 on Red Clay from IH 610 and Scott Street

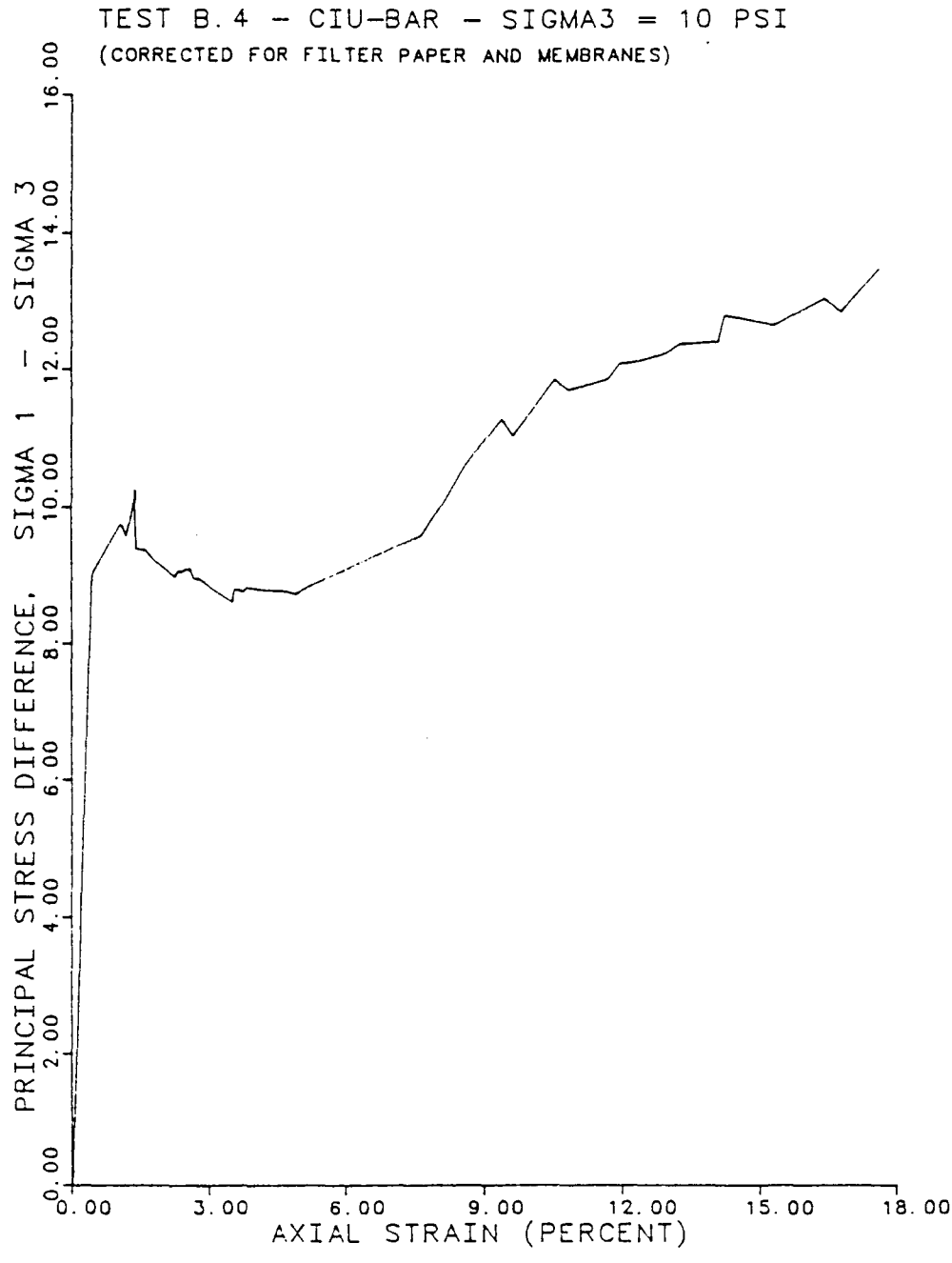

Fig. A.10 Stress-Strain Relationship from Test B.4 on Red Clay from IH 610 and Scott Street

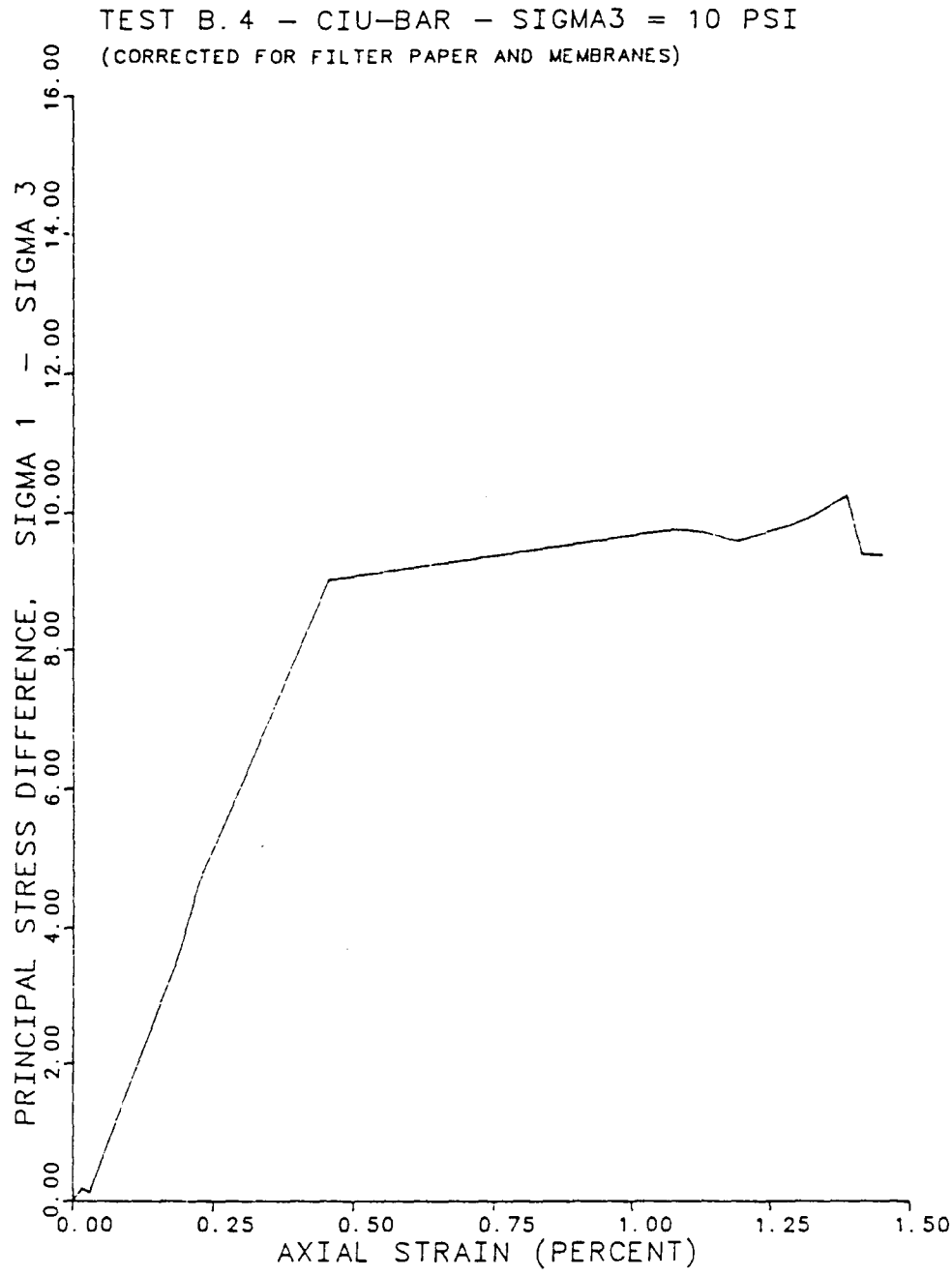

Fig. A.11 Stress-Strain Relationship at Low Strains from Test B.4 on Red Clay from IH 610 and Scott Street

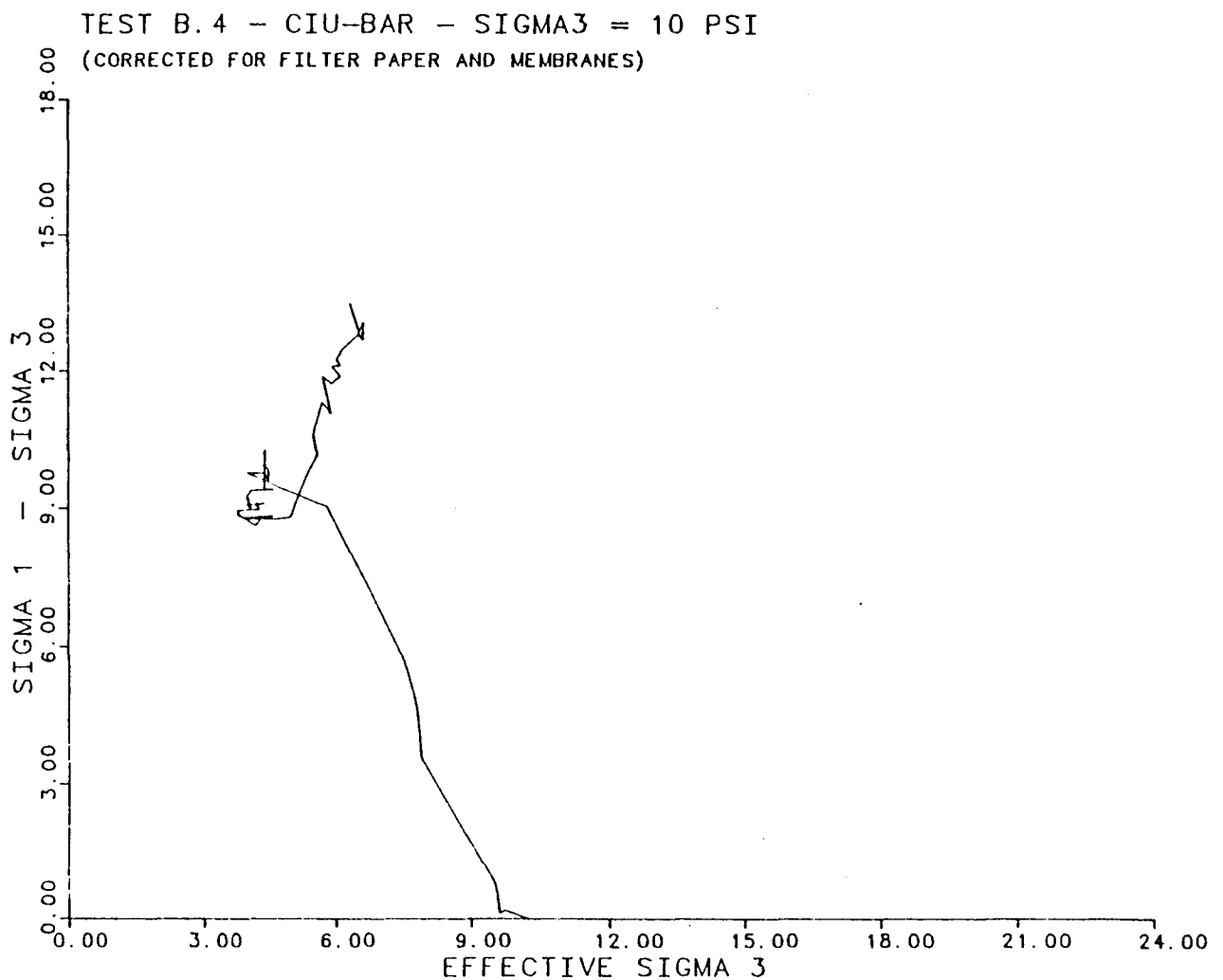

Fig. A.12 Effective Stress Path from Test B.4 on Red Clay from IH 610 and Scott Street

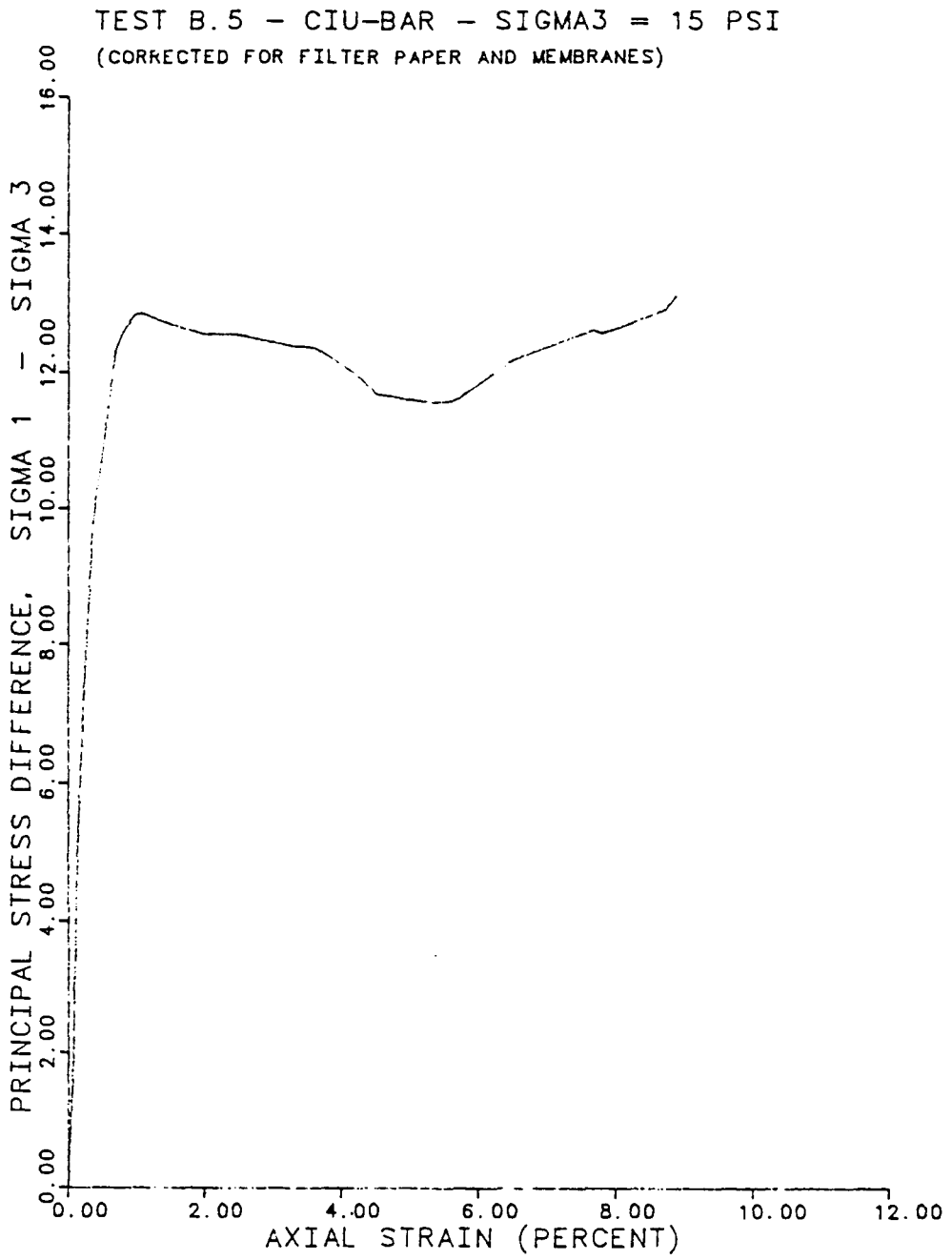

Fig. A.13 Stress-Strain Relationship from Test B.5 on Red Clay from IH 610 and Scott Street

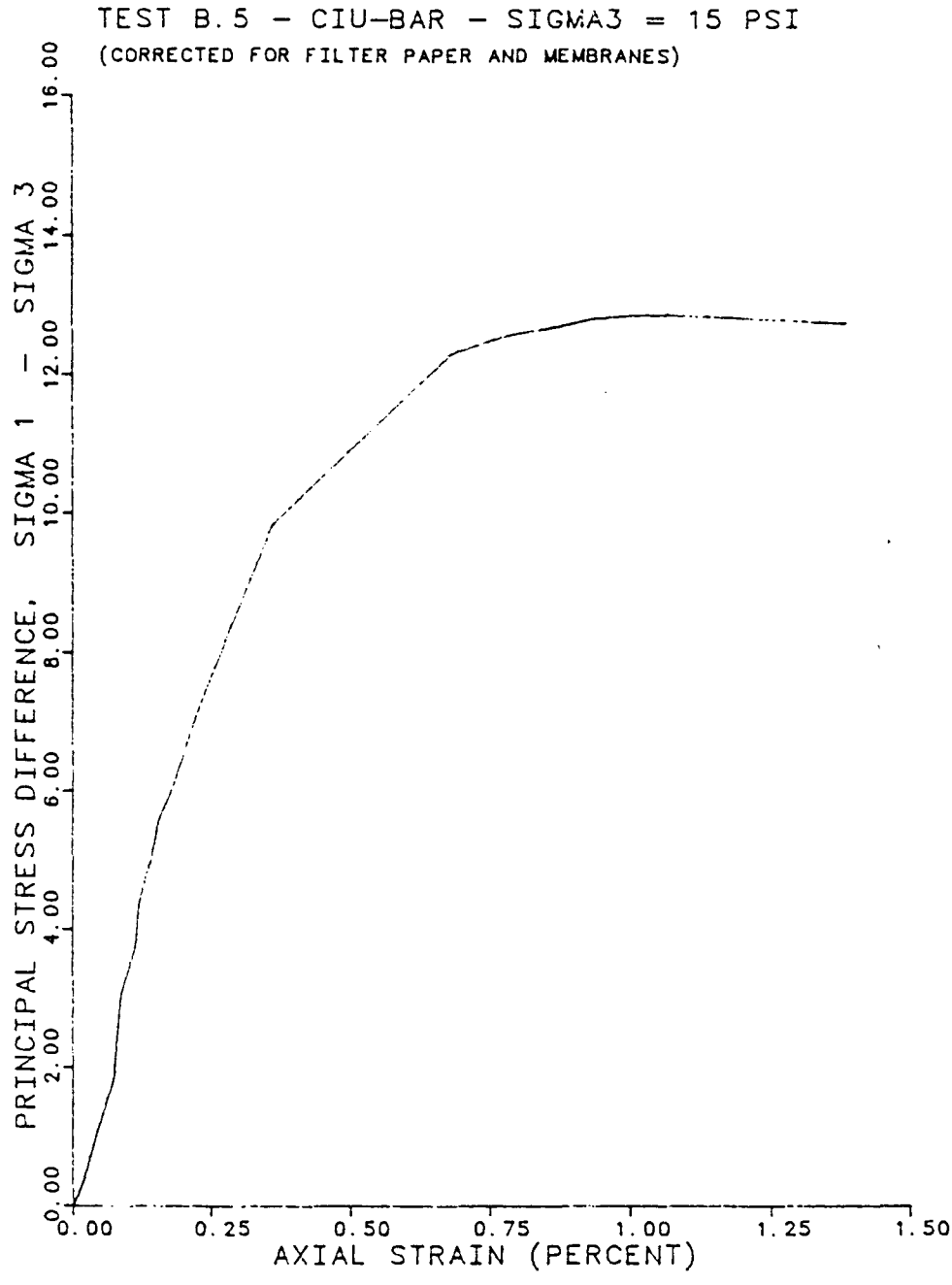

Fig. A.14 Stress-Strain Relationship at Low Strains from Test B.5 on Red Clay from IH 610 and Scott Street

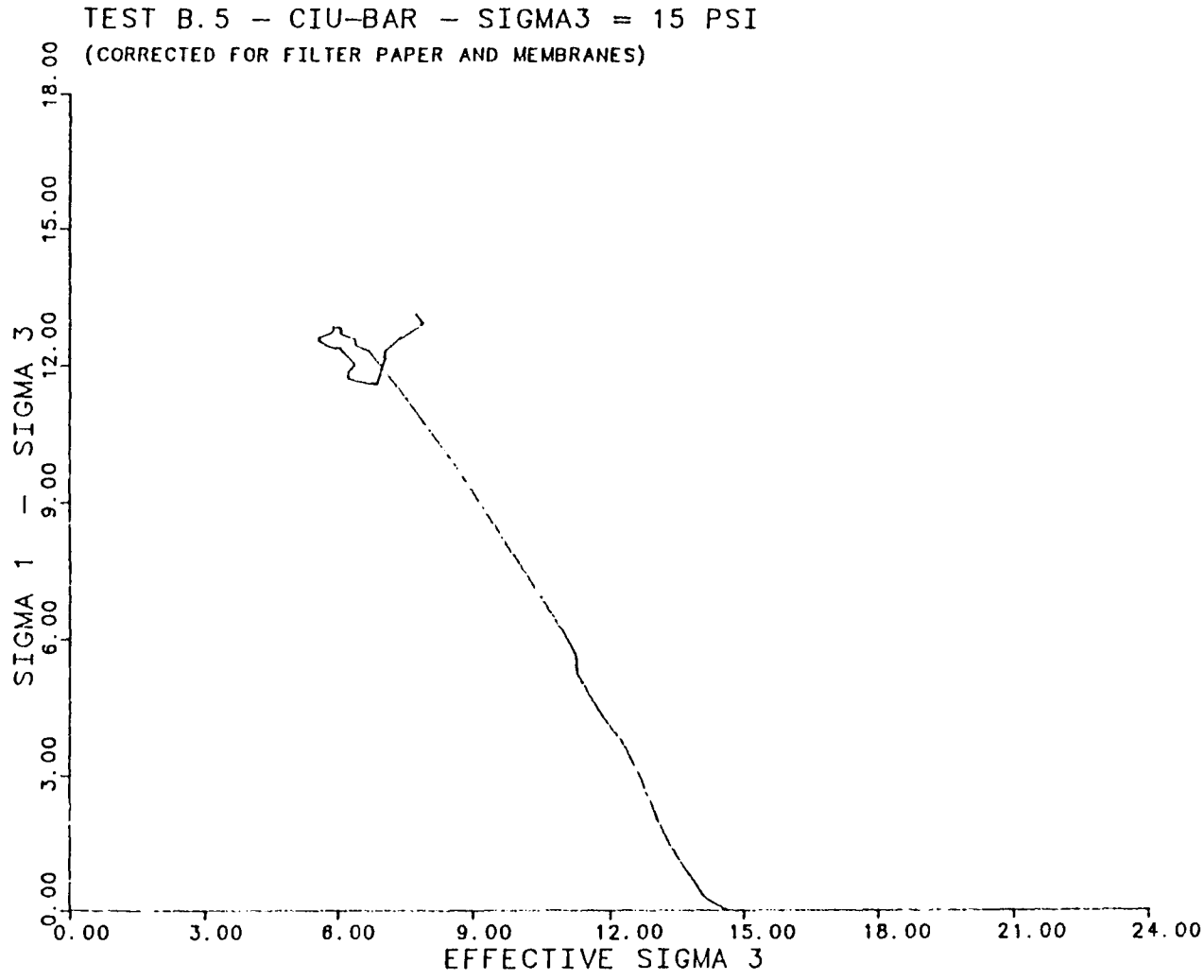

Fig. A.15 Effective Stress Path from Test B.5 on Red Clay from IH 610 and Scott Street

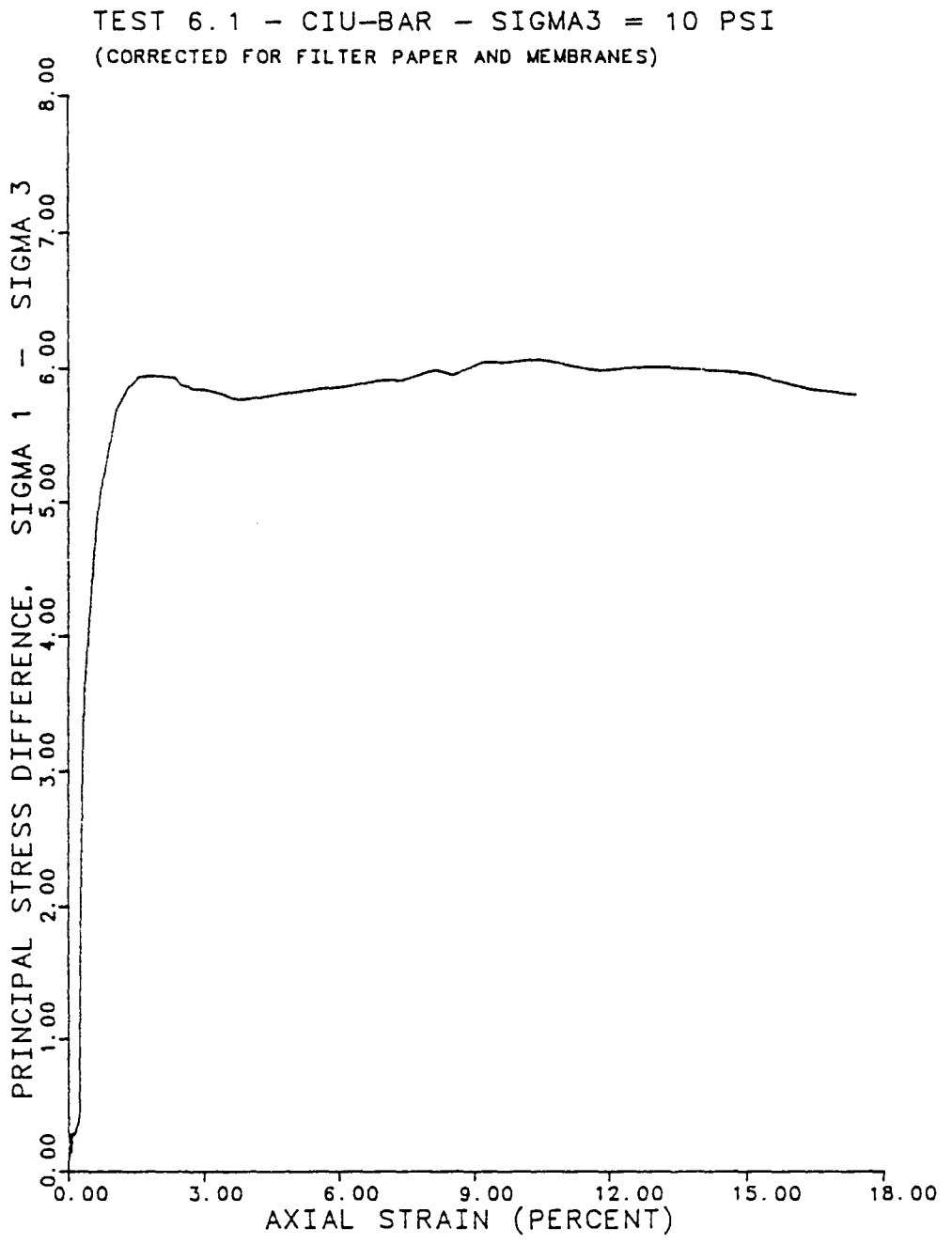

Fig. A.16 Stress-Strain Relationship from Test 6.1 on Red Clay from IH 610 and Scott Street

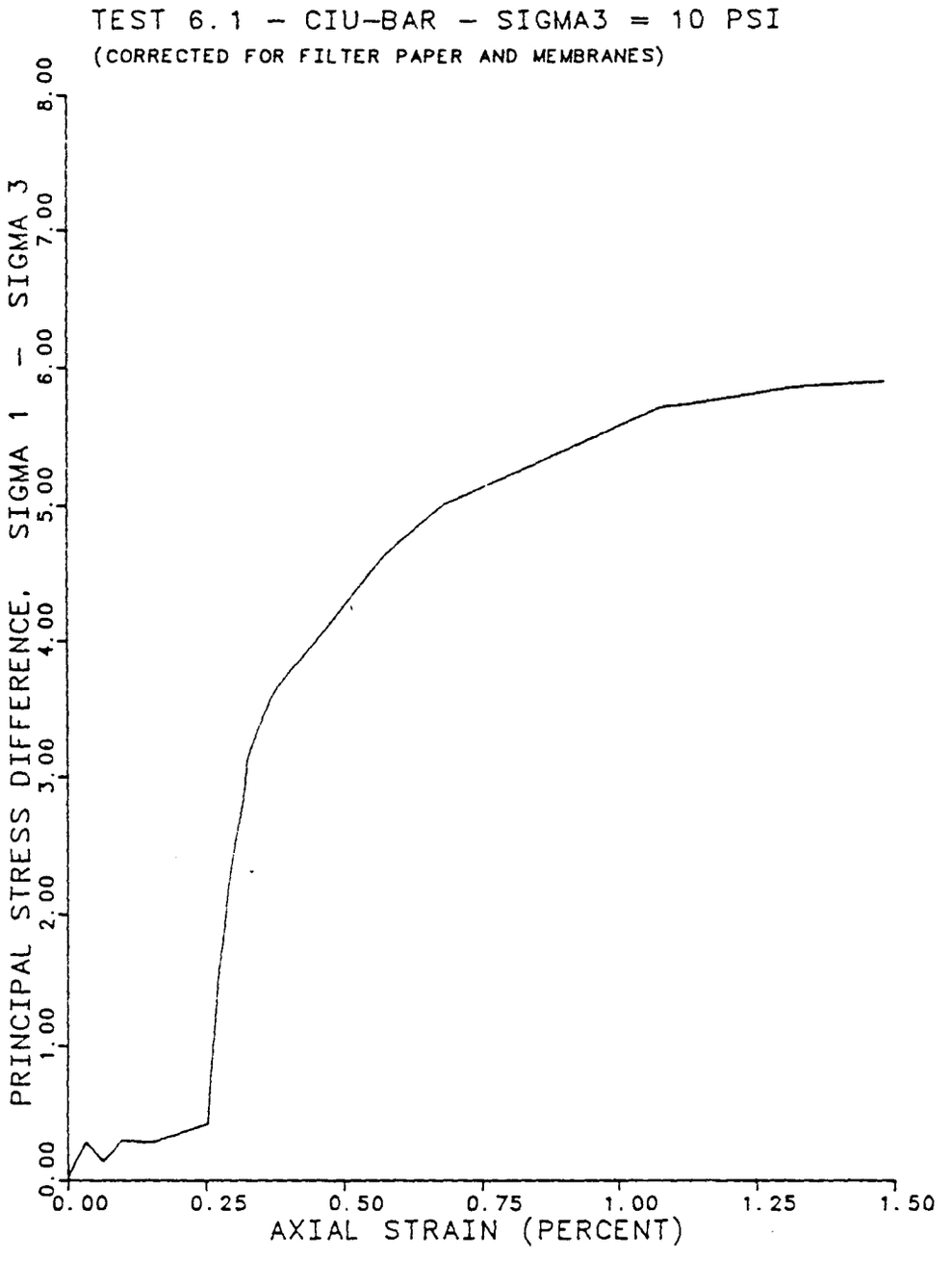

Fig. A.17 Stress-Strain Relationship at Low Strains from Test 6.1 on Red Clay from IH 610 and Scott Street

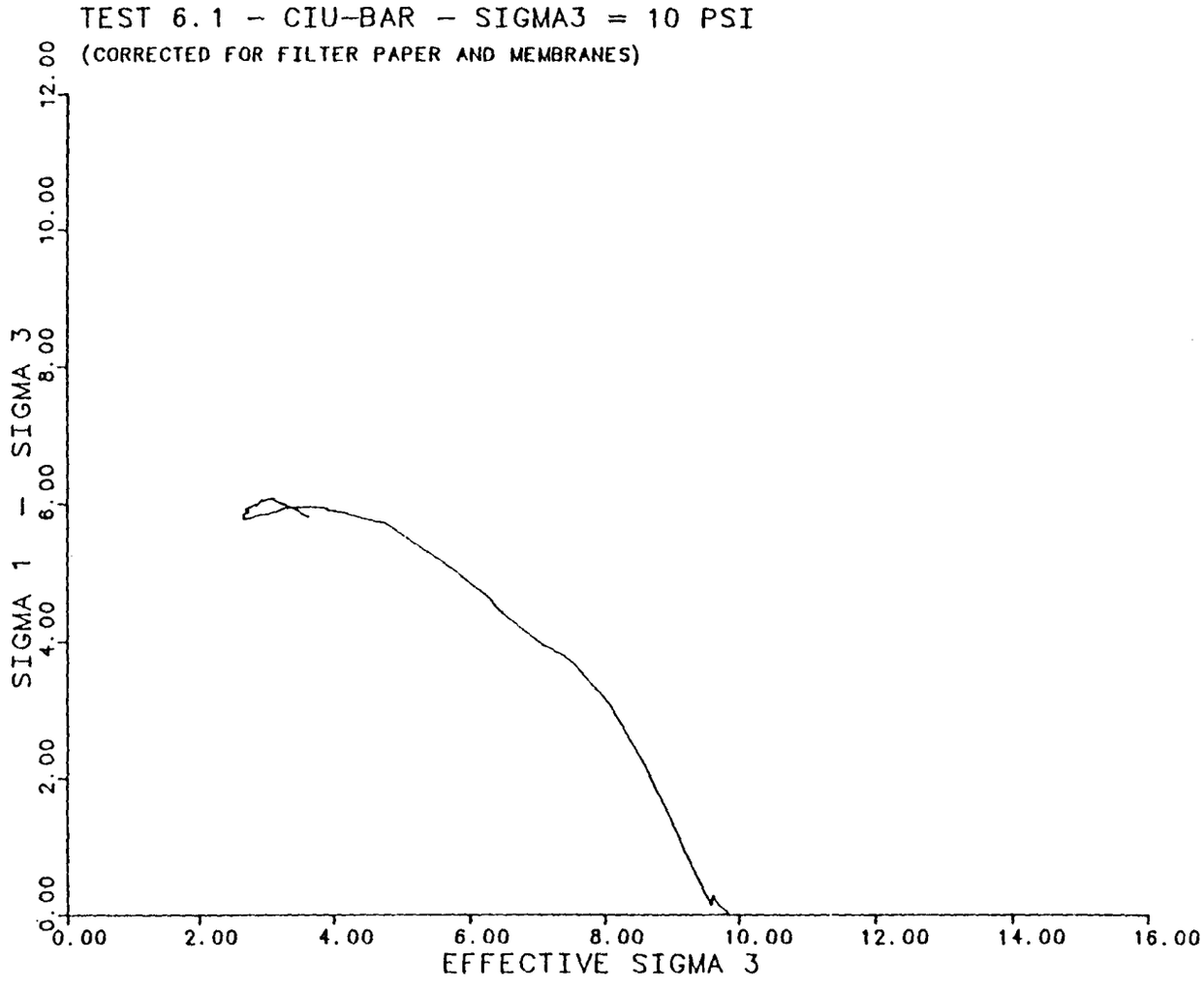

Fig. A.18 Effective Stress Path from Test 6.1 on Red Clay from IH 610 and Scott Street

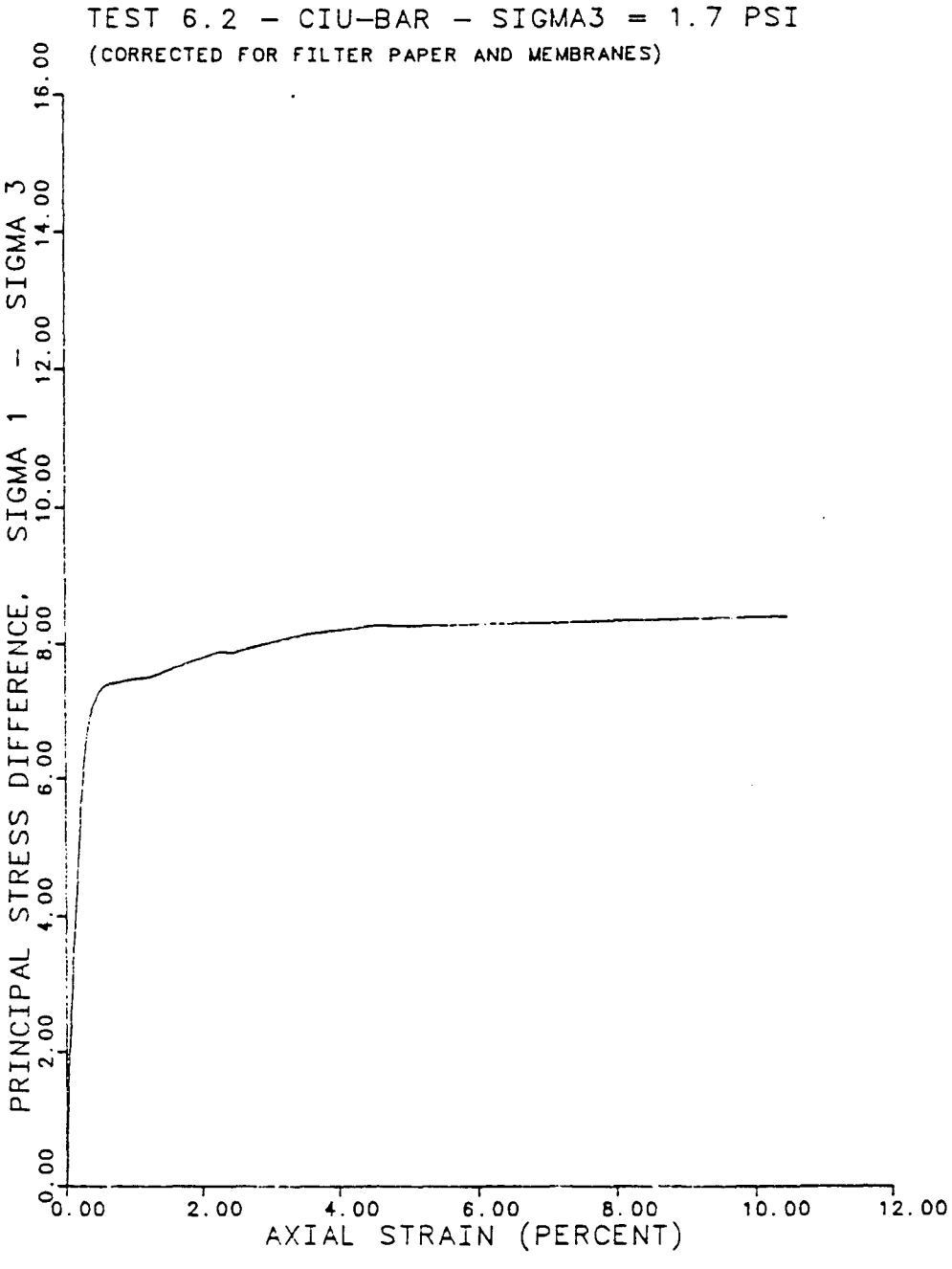

Fig. A.19 Stress-Strain Relationship from Test 6.2 on Red Clay from IH 610 and Scott Street

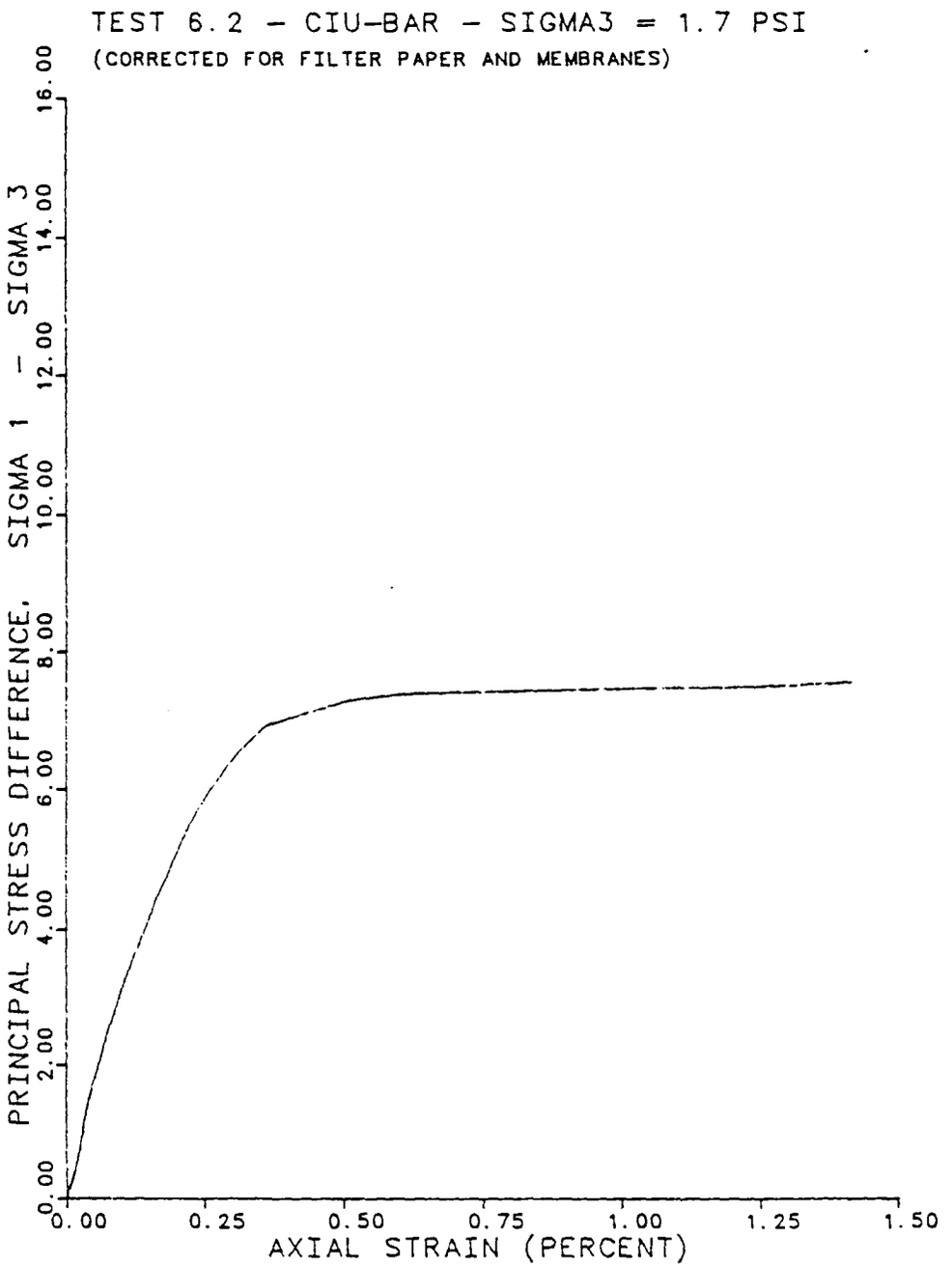

Fig. A.20 Stress-Strain Relationship at Low Strains from Test 6.2 on Red Clay from IH 610 and Scott Street

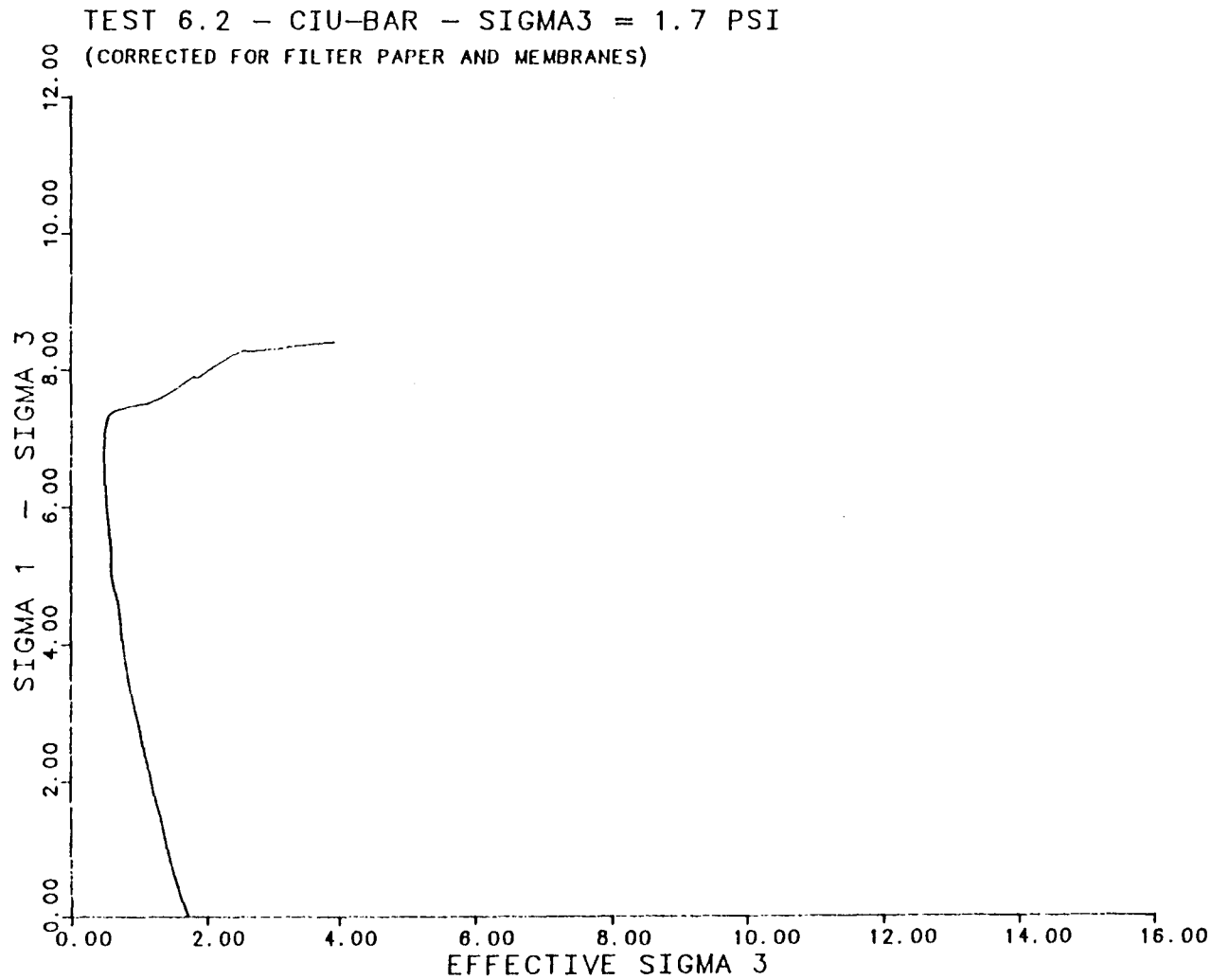

Fig. A.21 Effective Stress Path from Test 6.2 on Red Clay from IH 610 and Scott Street

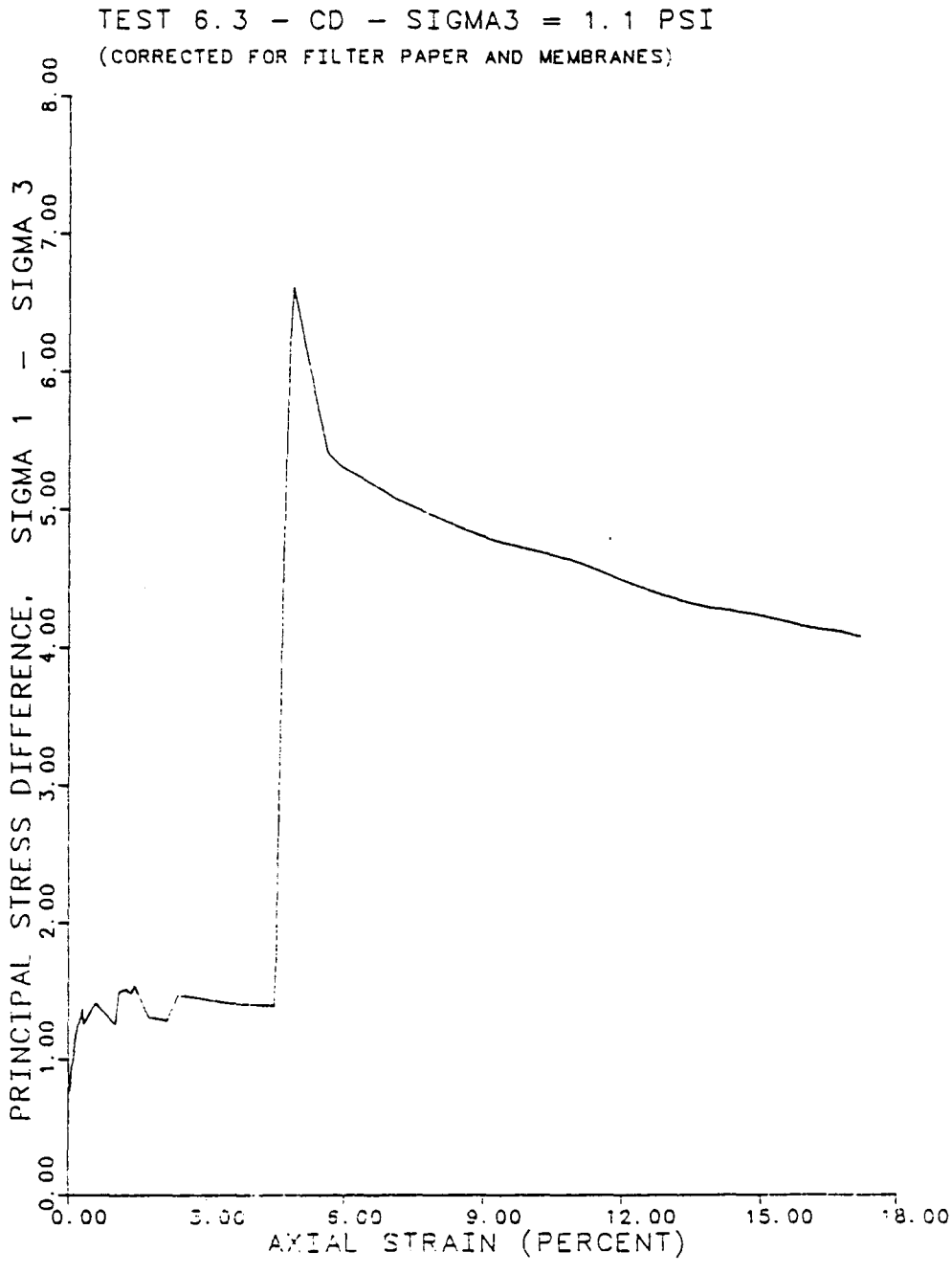

Fig. A.22 Stress-Strain Relationship from Test 6.3 (Consolidated-Drained) on Red Clay from IH 610 and Scott Street

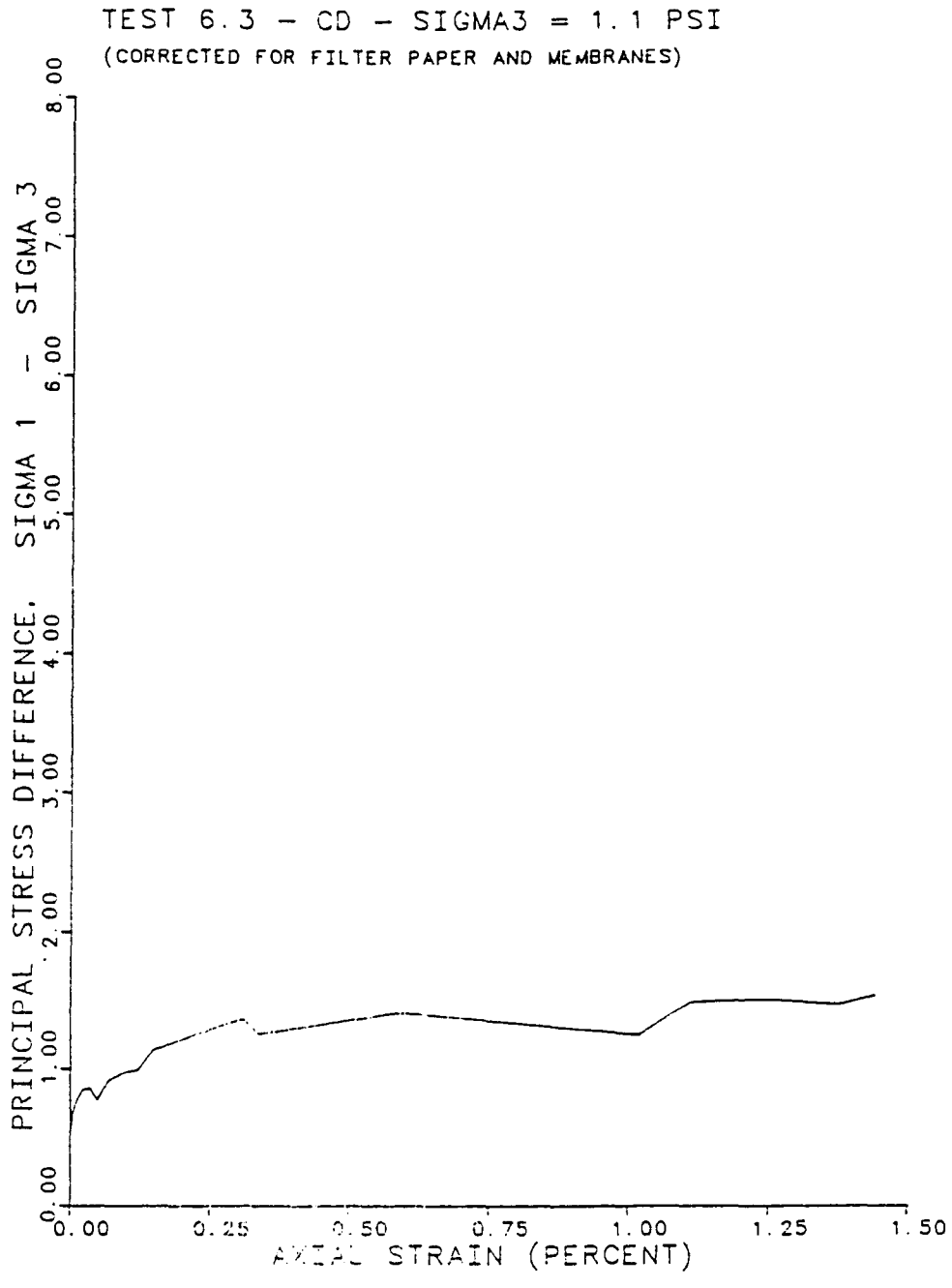

Fig. A.23 Stress-Strain Relationship at Low Strains from Test 6.3 (Consolidated-Drained) on Red Clay from IH 610 and Scott Street

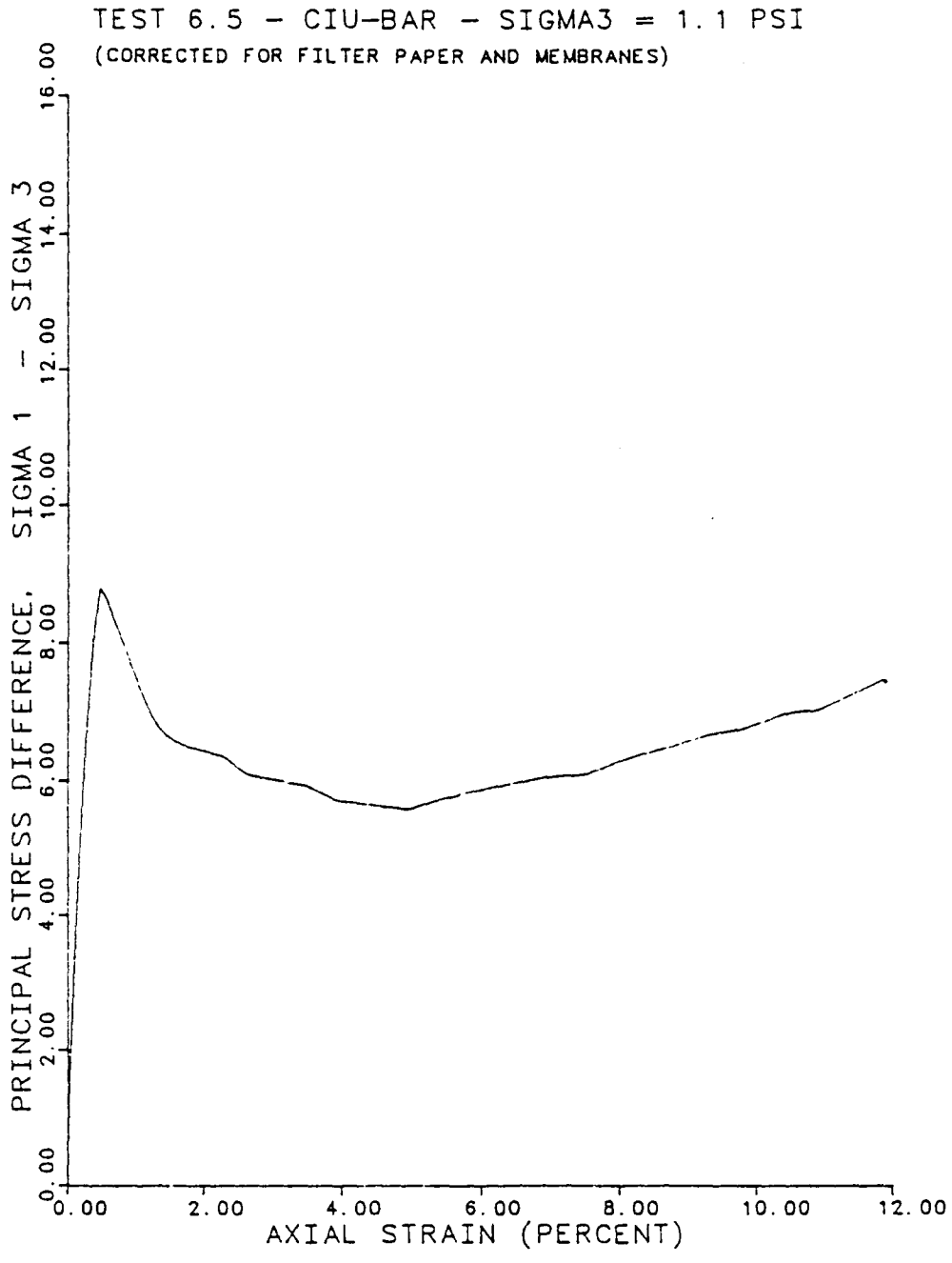

Fig. A.24 Stress-Strain Relationship from Test 6.5 on Red Clay from IH 610 and Scott Street

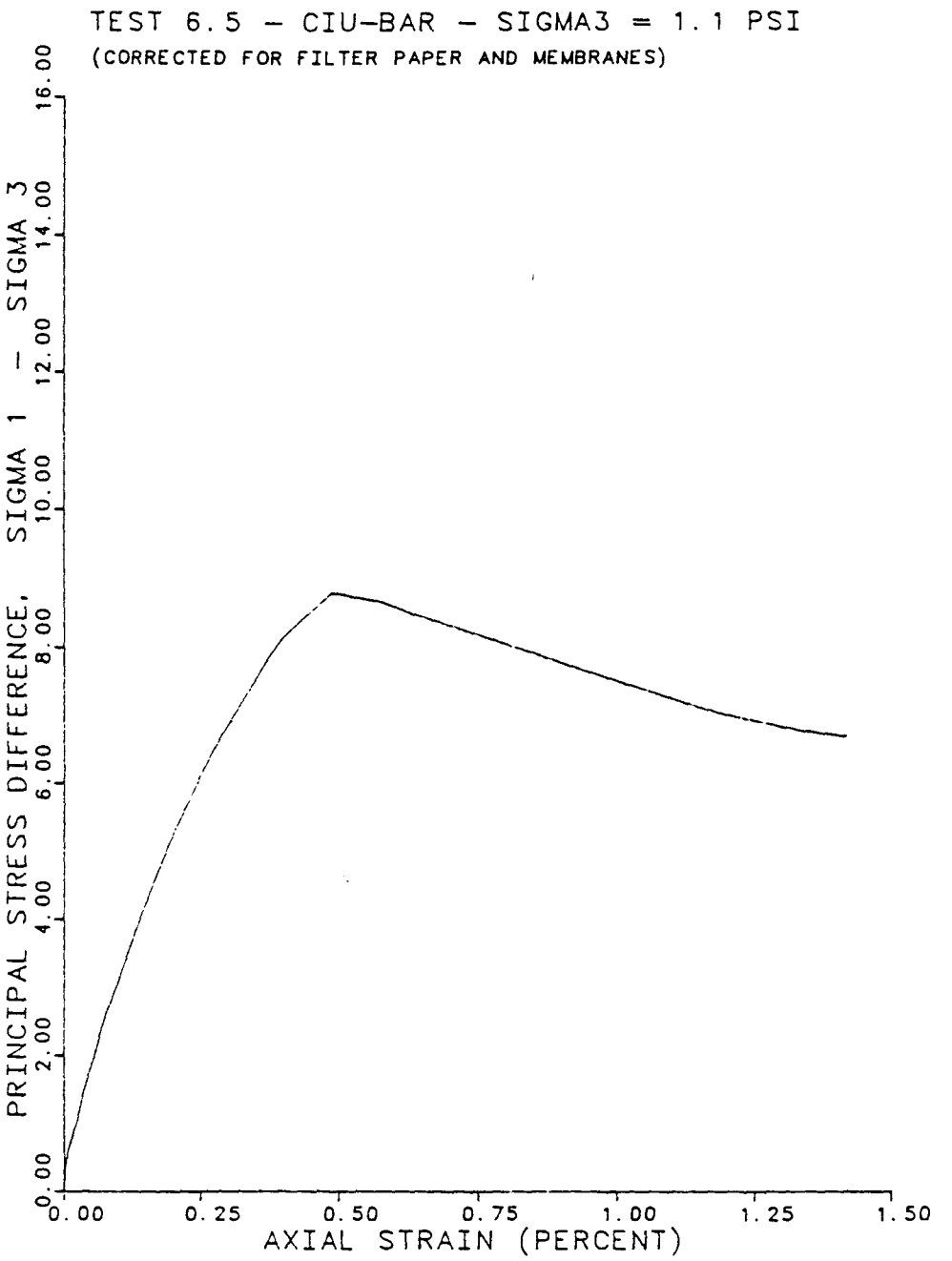

Fig. A.25 Stress-Strain Relationship at Low Strains from Test 6.5 on Red Clay from IH 610 and Scott Street

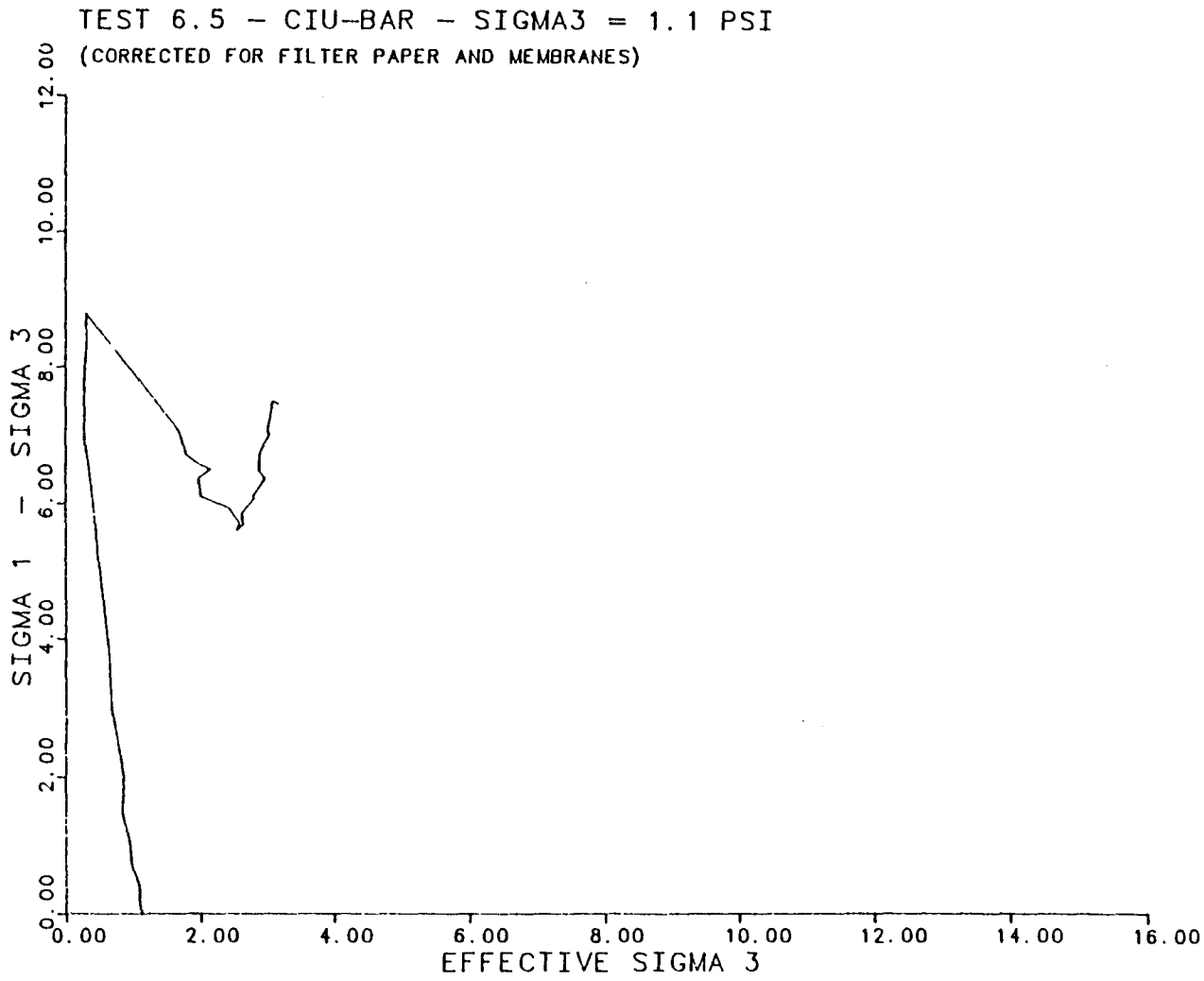

Fig. A.26 Effective Stress Path from Test 6.5 on Red Clay from IH 610 and Scott Street

APPENDIX B

Appendix B contains the individual test results for the consolidated-undrained ($\bar{R}$) triaxial shear test (6.6) performed on brown clay from the embankment at SH 225 and SH 146 (SW Quadrant). Stress-strain relationships (over the full range of strains employed in the test and over the first 1.50 percent of strain) and the stress path (plotted on a modified Mohr-Coulomb diagram) are presented in the form of plots generated by the computer program RBARPLT for the test.

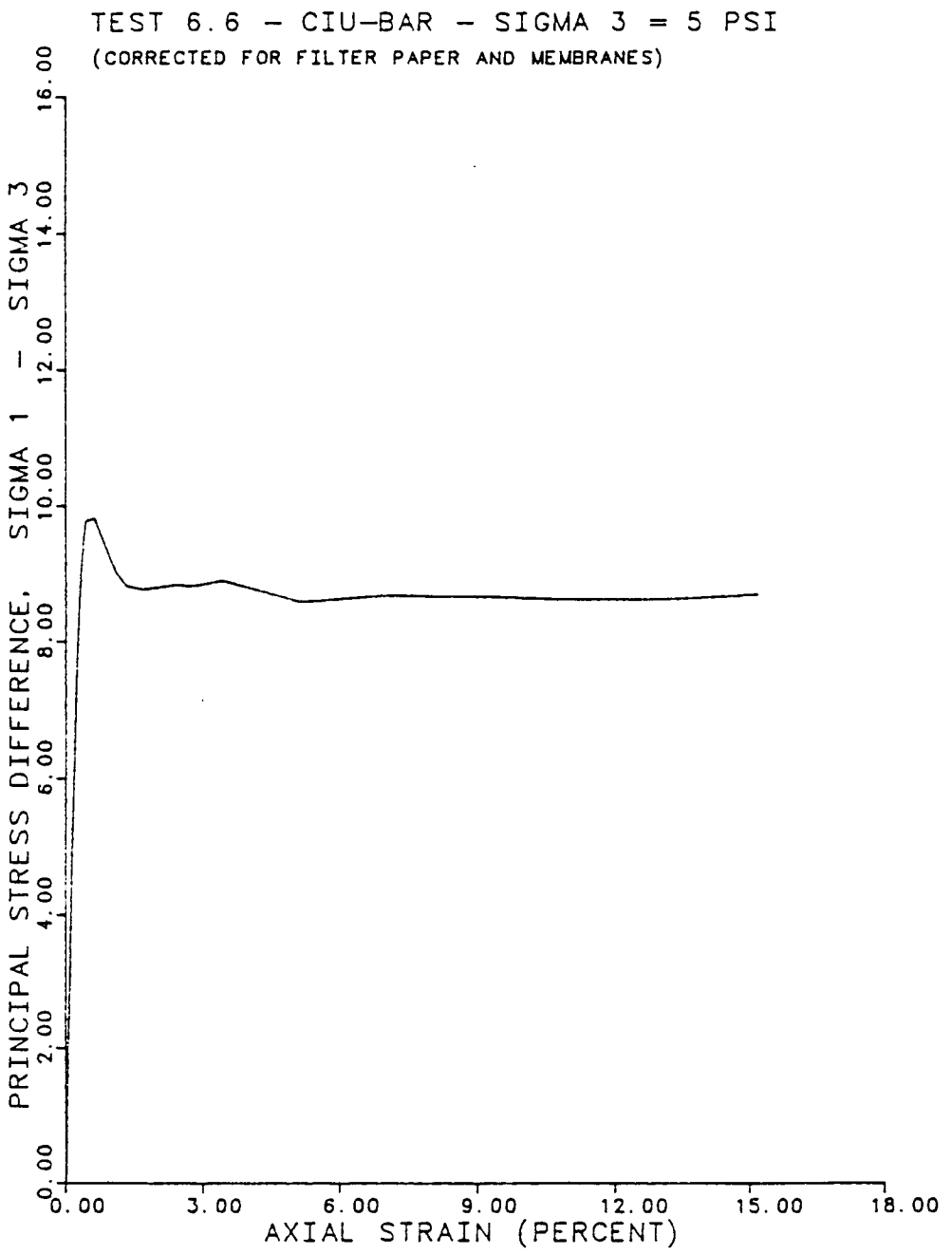

Fig. B.1 Stress-Strain Relationship from Test 6.6 on Brown Clay from SH 225 and SH 146 (SW Quadrant)

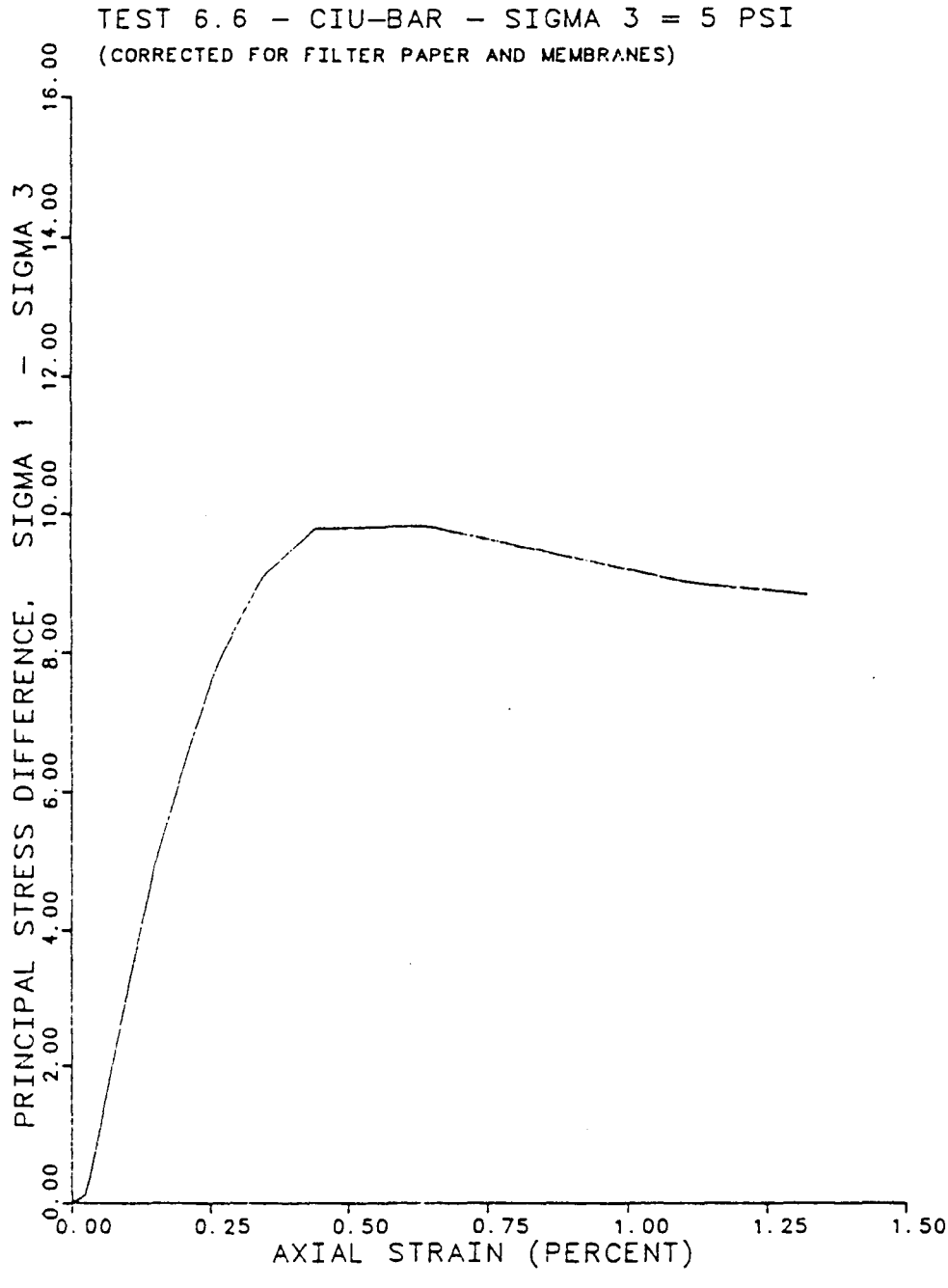

Fig. B.2 Stress-Strain Relationship at Low Strains from Test 6.6 on Brown Clay from SH 225 and SH 146 (SW Quadrant)

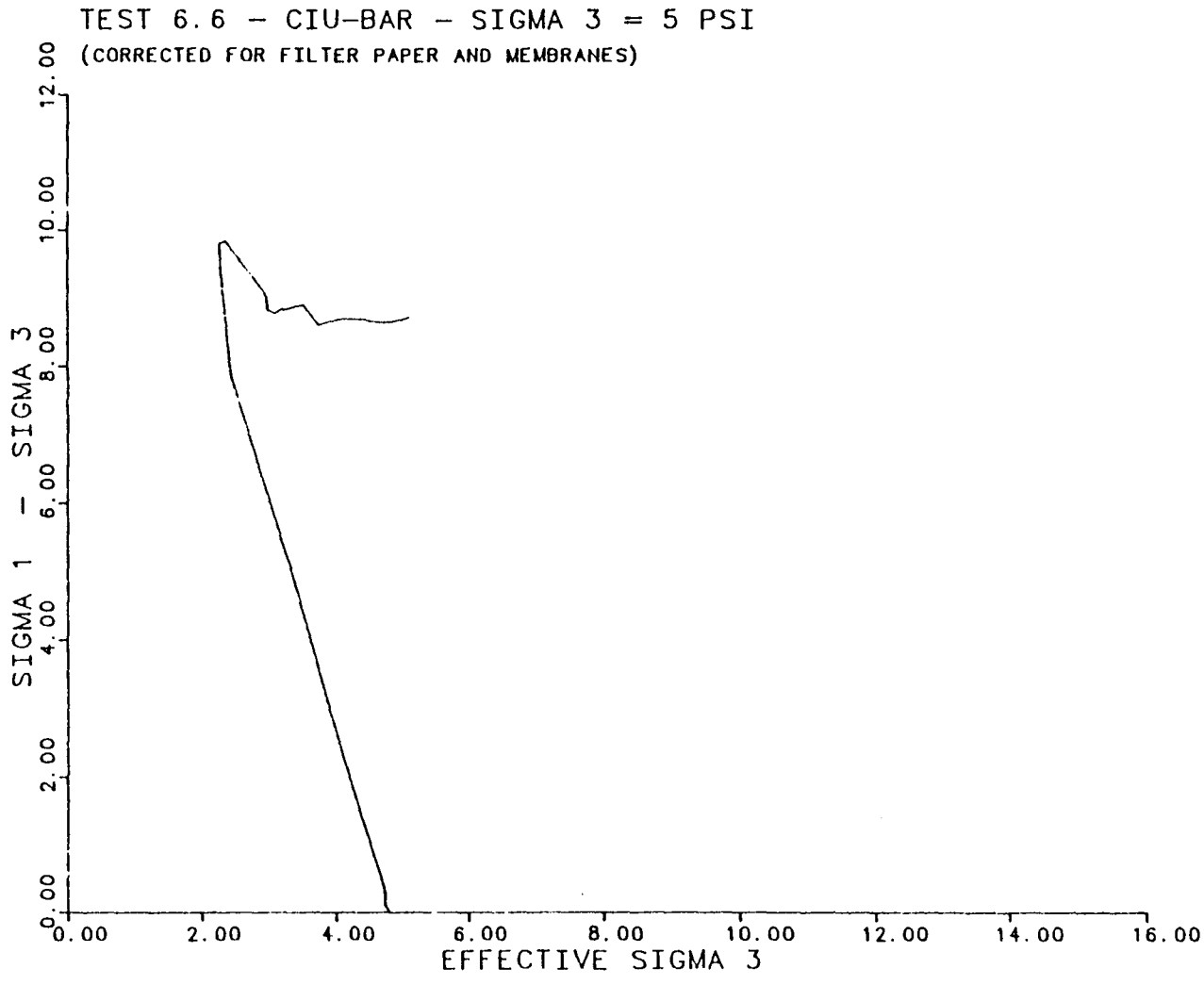

Fig. B.3 Effective Stress Path from Test 6.6 on Brown Clay from SH 225 and SH 146 (SW Quadrant)

APPENDIX C

Appendix C contains the individual test results for the triaxial shear tests performed on grey clay from the embankment at IH 610 and Scott Street. Stress-strain relationships (over the full range of strains employed in a test and over the first 1.50 percent of strain) and stress paths (plotted on modified Mohr-Coulomb diagrams) are presented in the form of plots generated by the computer program RBARPLT for each test.

Results are included for:

- Tests B.6, B.7, 6.4, and 6.8 which were all performed under consolidated-undrained ($\overline{R}$) concitions.

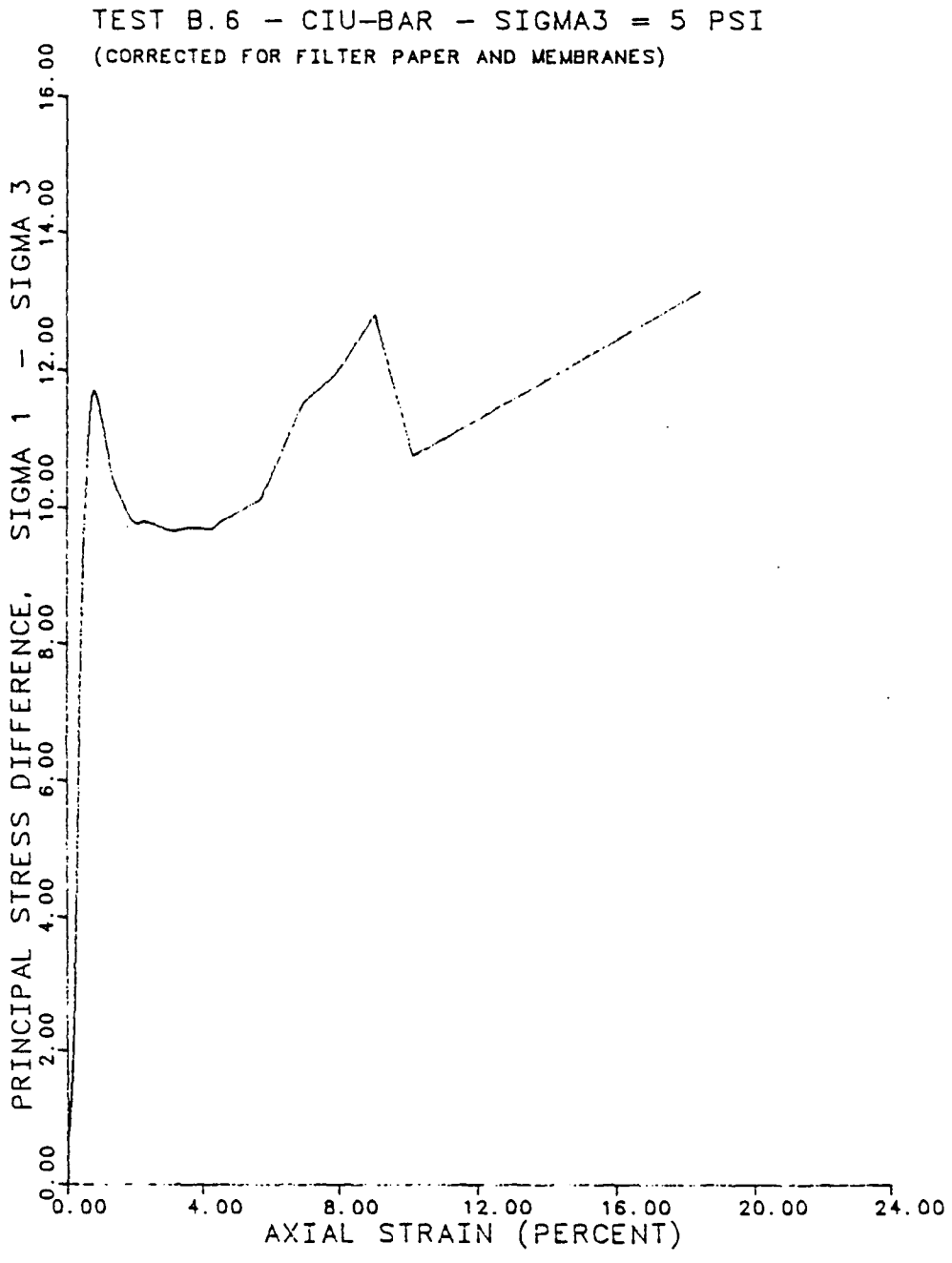

Fig. C.1 Stress-Strain Relationship from Test B.6 on Grey Clay from IH 610 and Scott Street

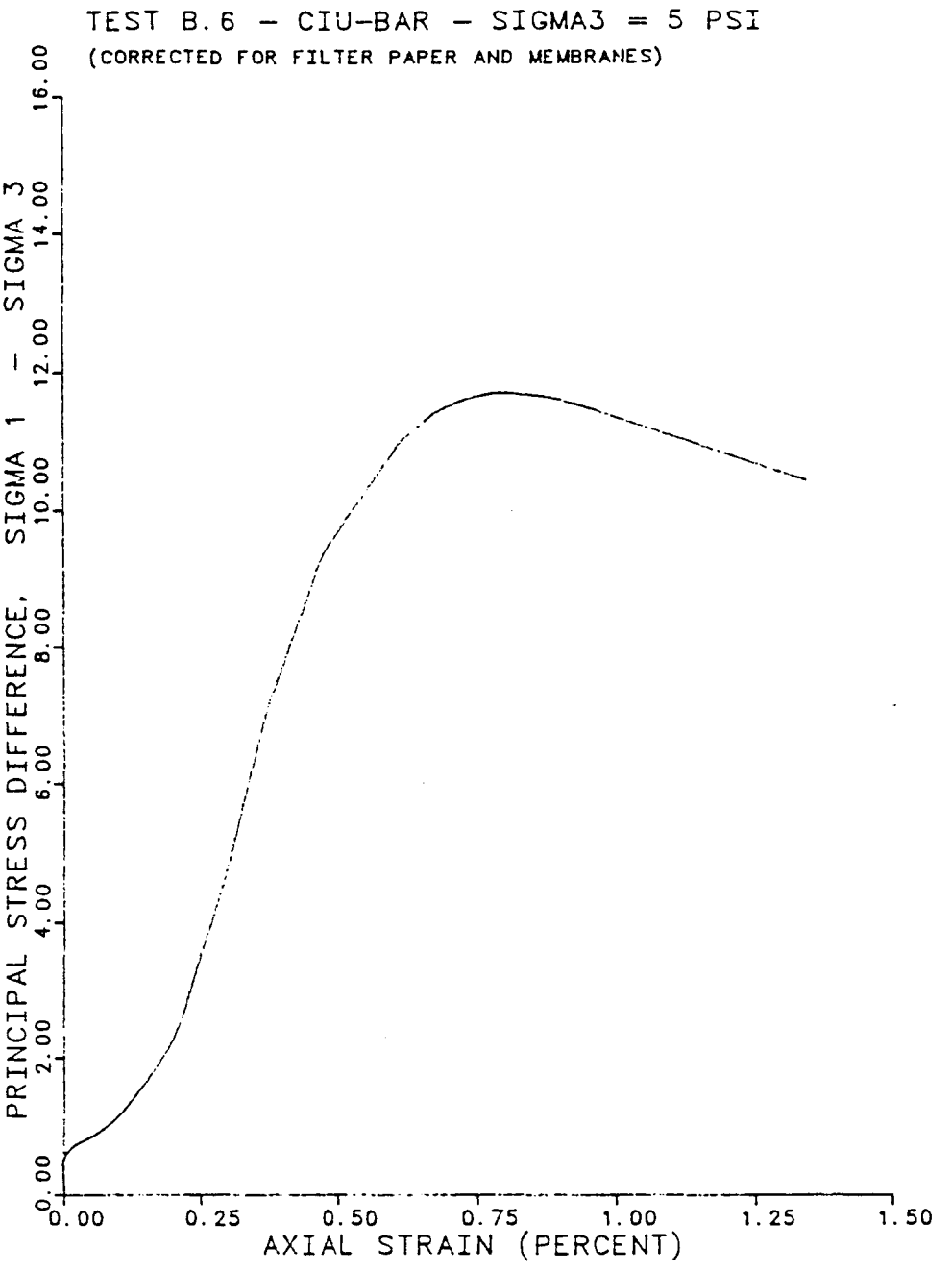

Fig. C.2 Stress-Strain Relationship at Low Strains from Test B.6 on Grey Clay from IH 610 and Scott Street

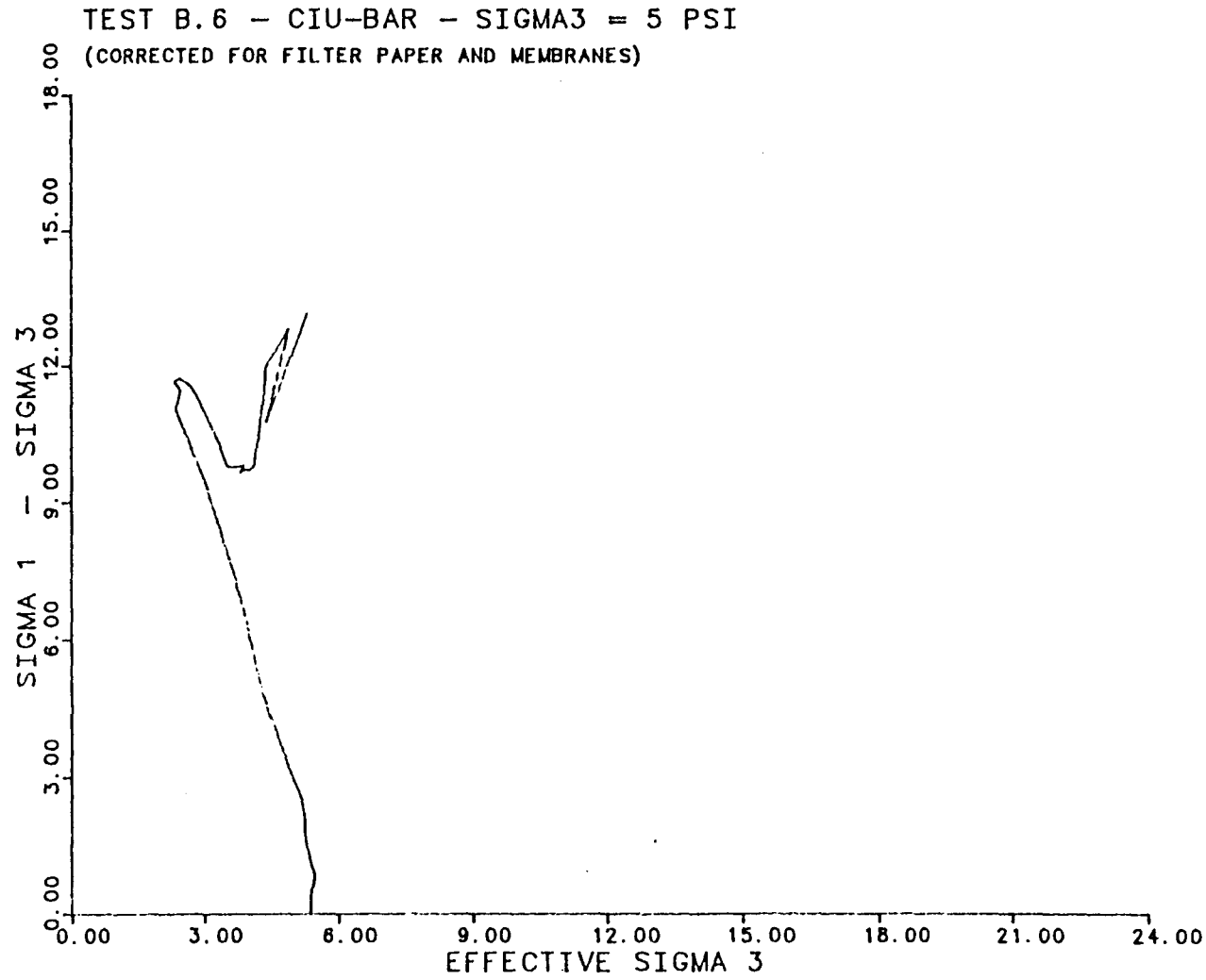

Fig. C.3 Effective Stress Path from Test B.6 on Grey Clay from IH 610 and Scott Street

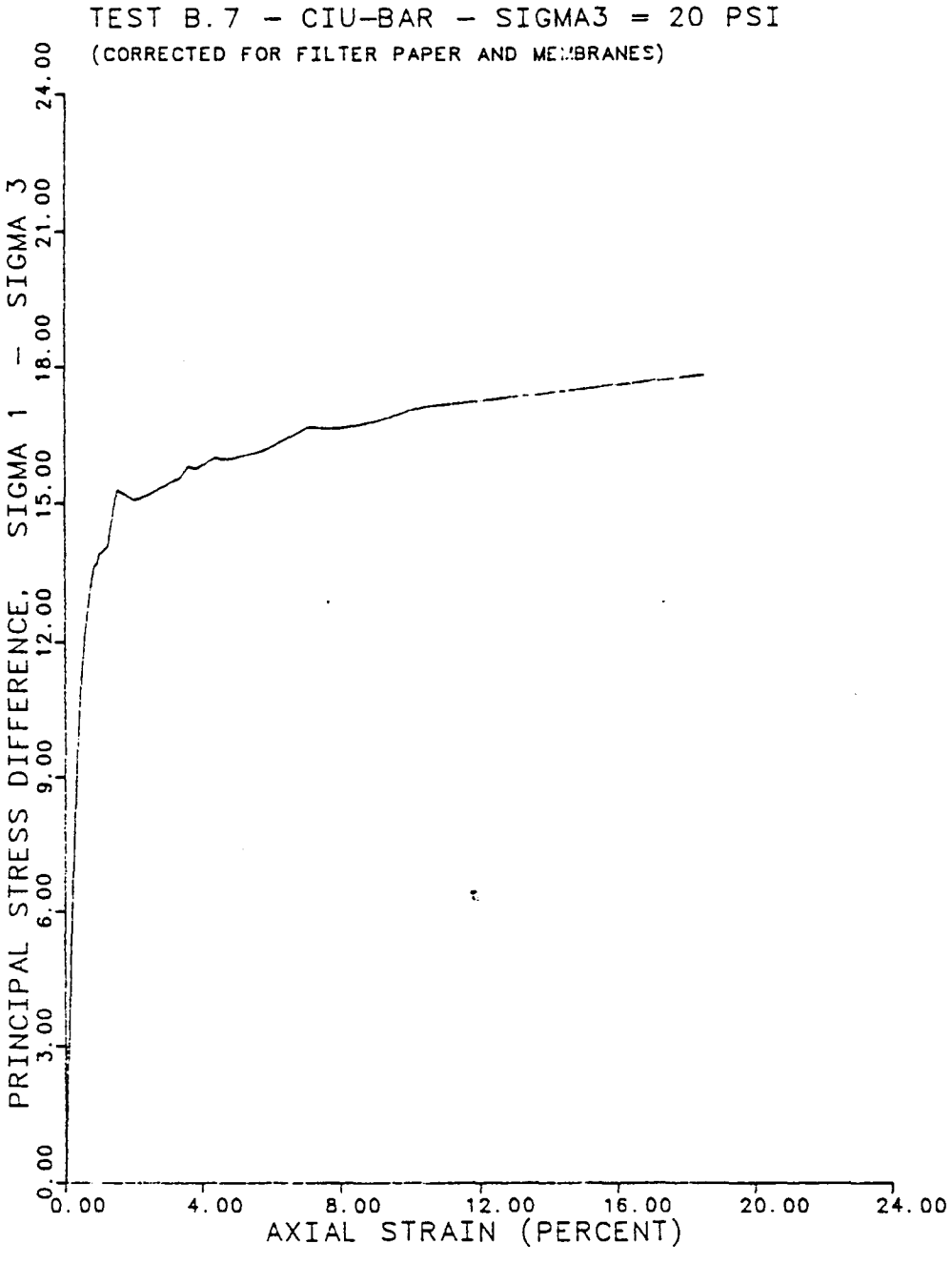

Fig. C.4 Stress-Strain Relationship from Test B.7 on Grey Clay from IH 610 and Scott Street

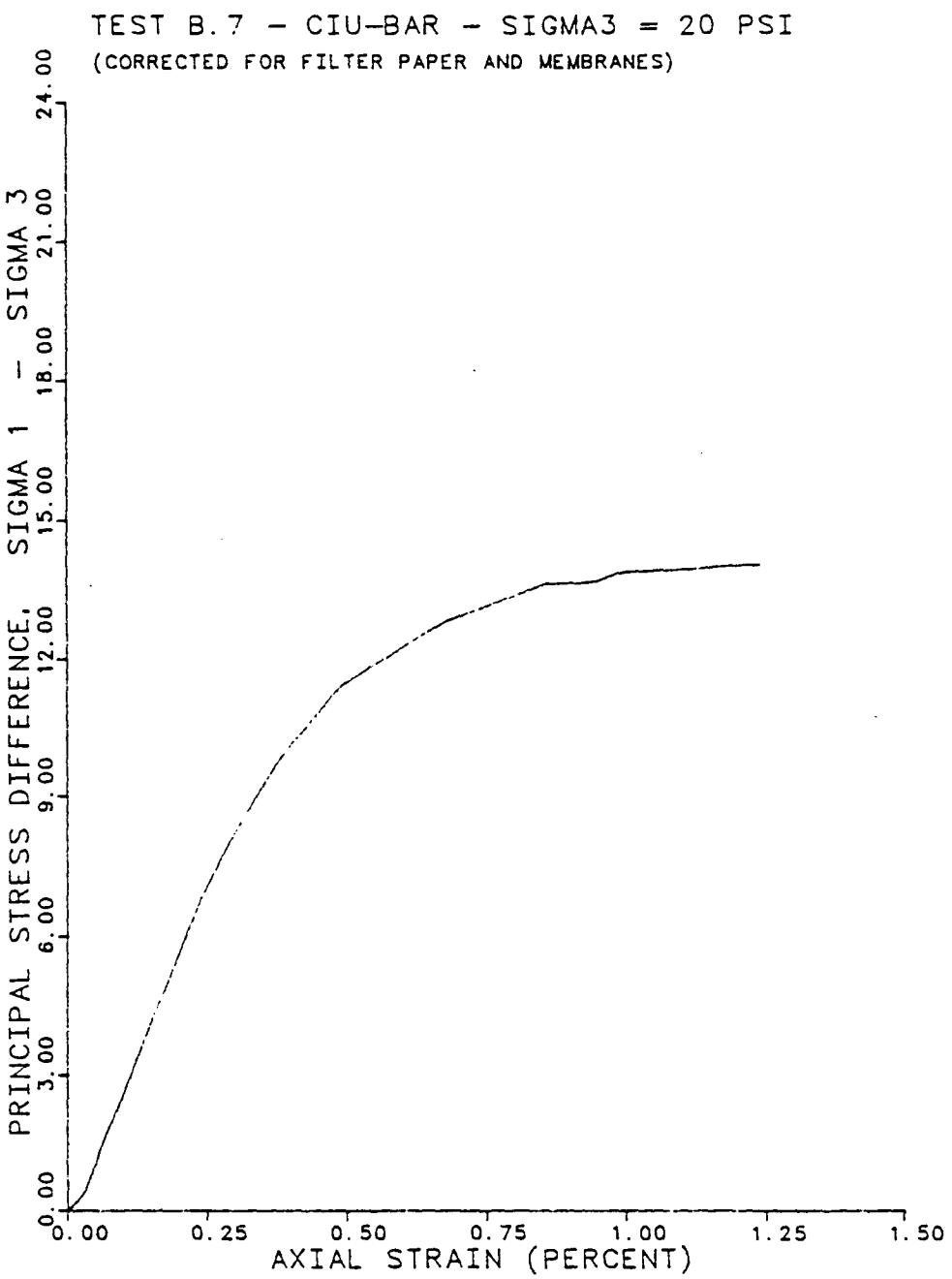

Fig. C.5 Stress-Strain Relationship at Low Strains from Test B.7 on Grey Clay from IH 610 and Scott Street

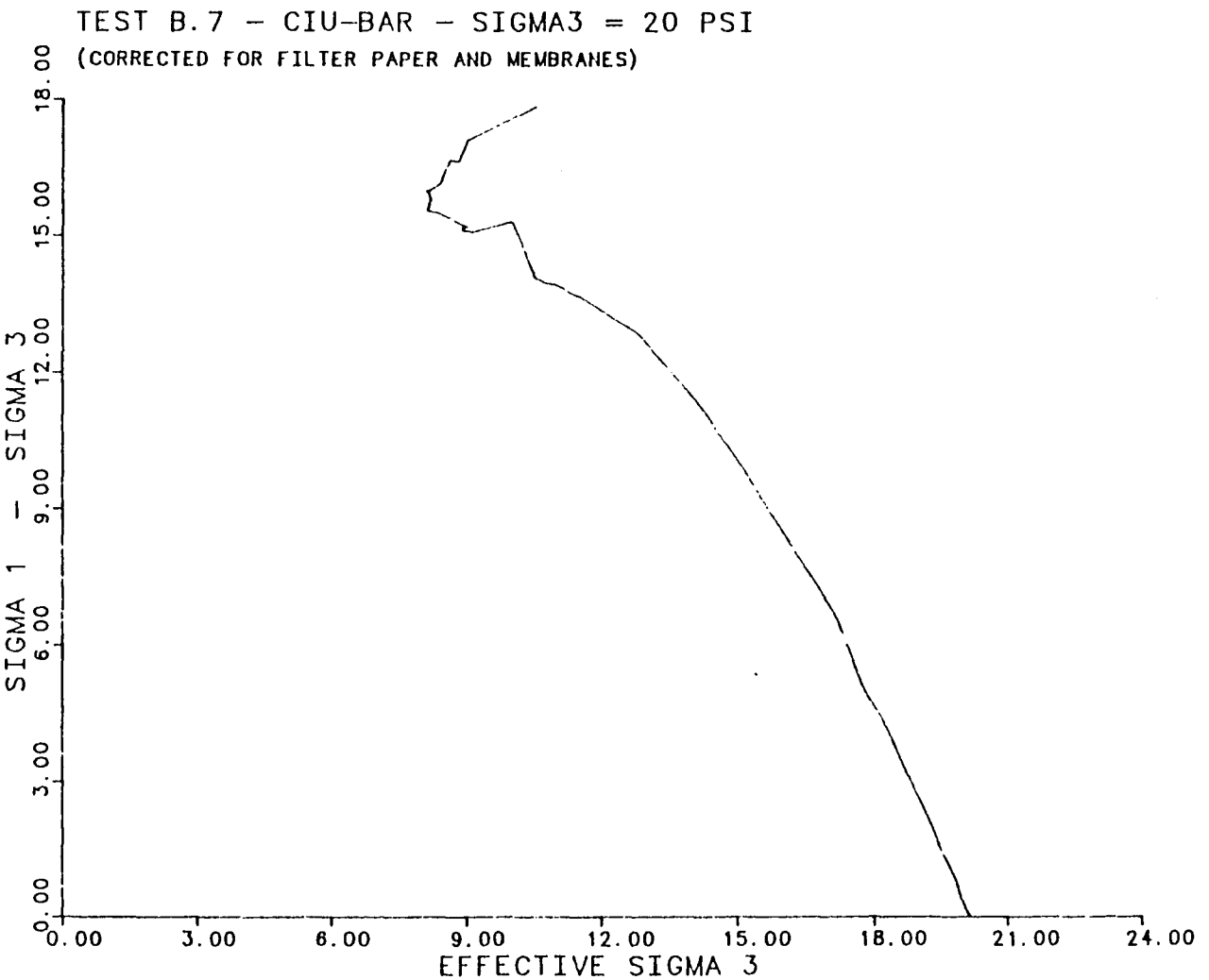

Fig. C.6 Effective Stress Path from Test B.7 on Grey Clay from IH 610 and Scott Street

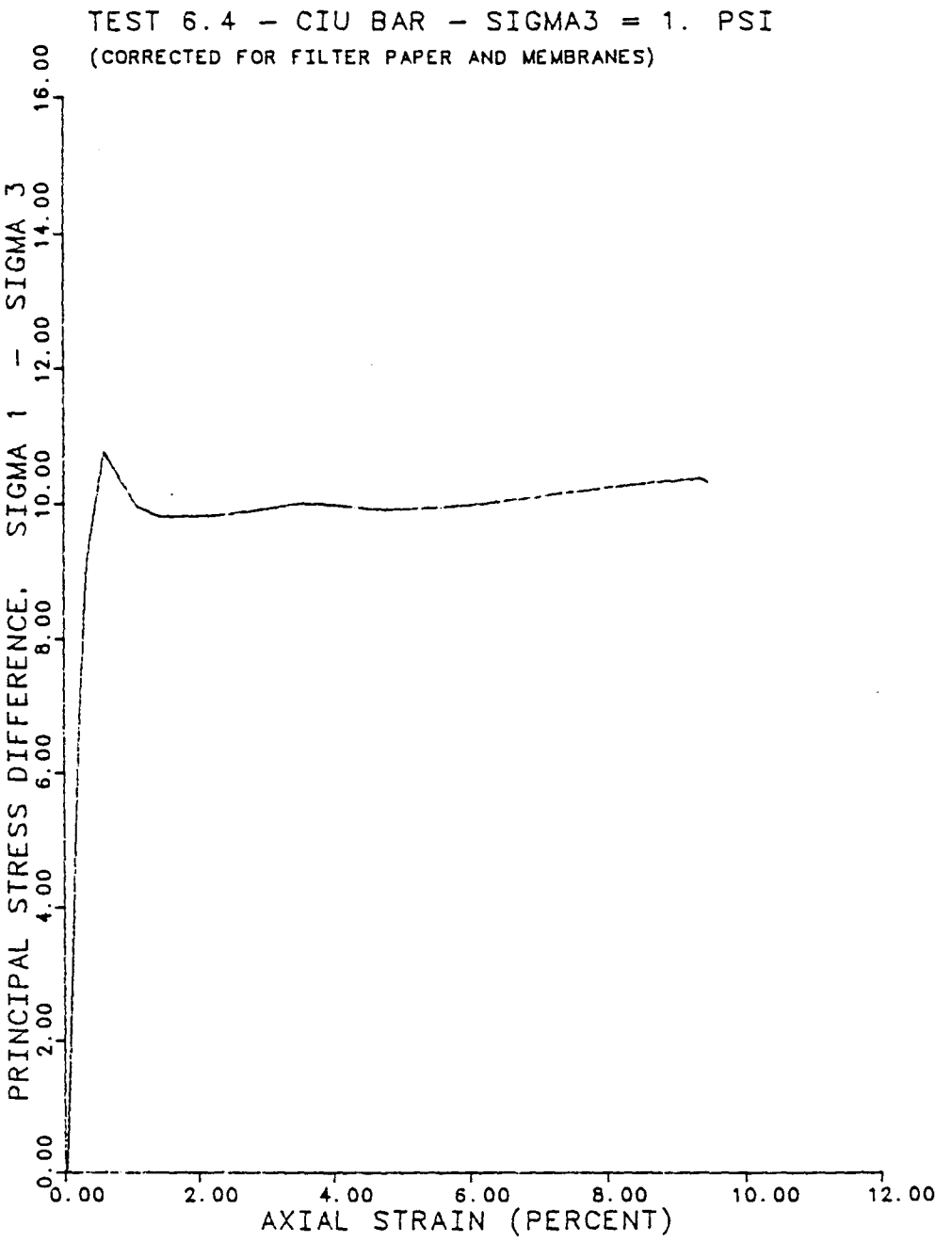

Fig. C.7 Stress-Strain Relationship from Test 6.4 on Grey Clay from IH 610 and Scott Street

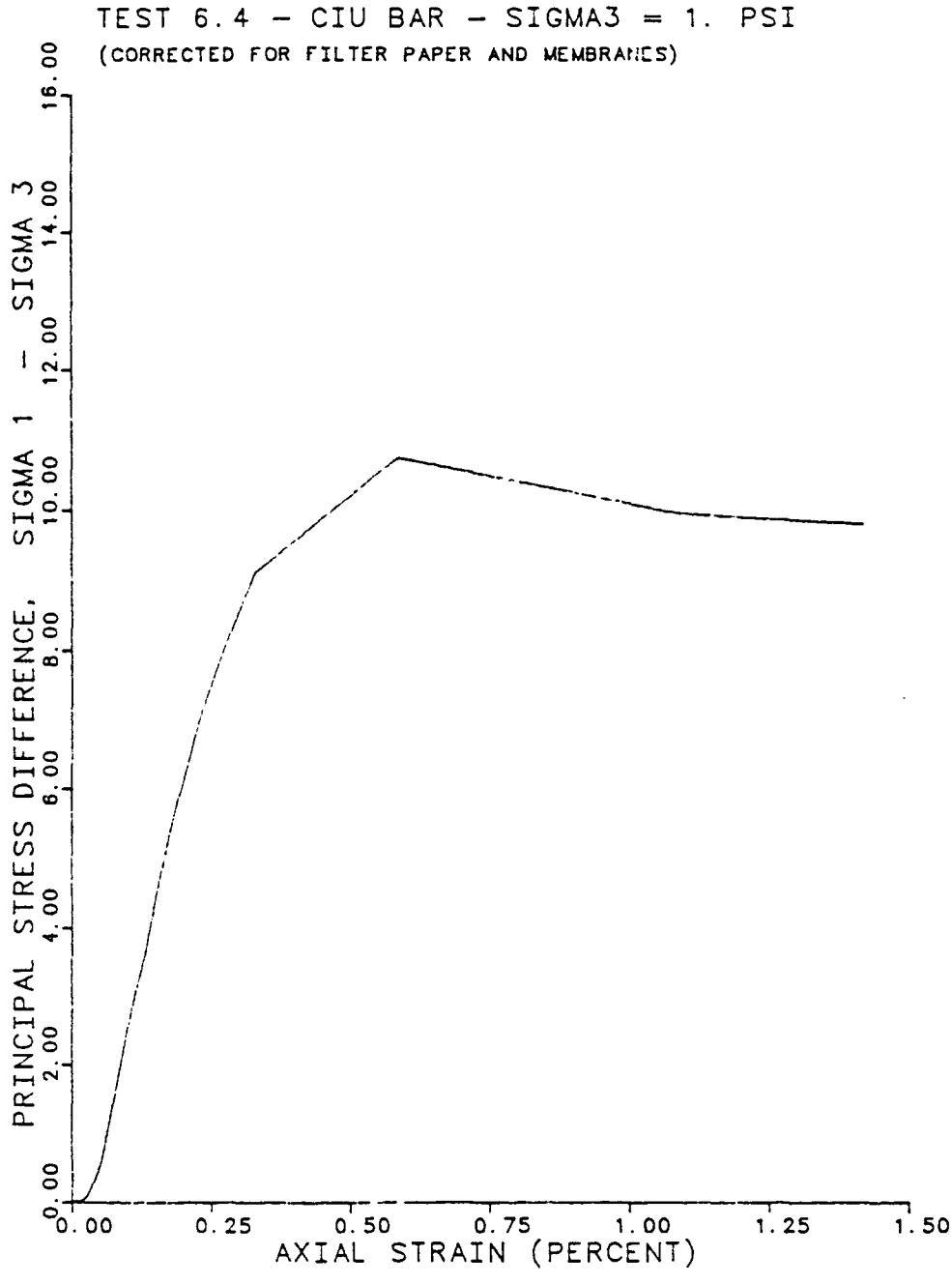

Fig. C.8 Stress-Strain Relationship at Low Strains from Test 6.4 on Grey Clay from IH 610 and Scott Street

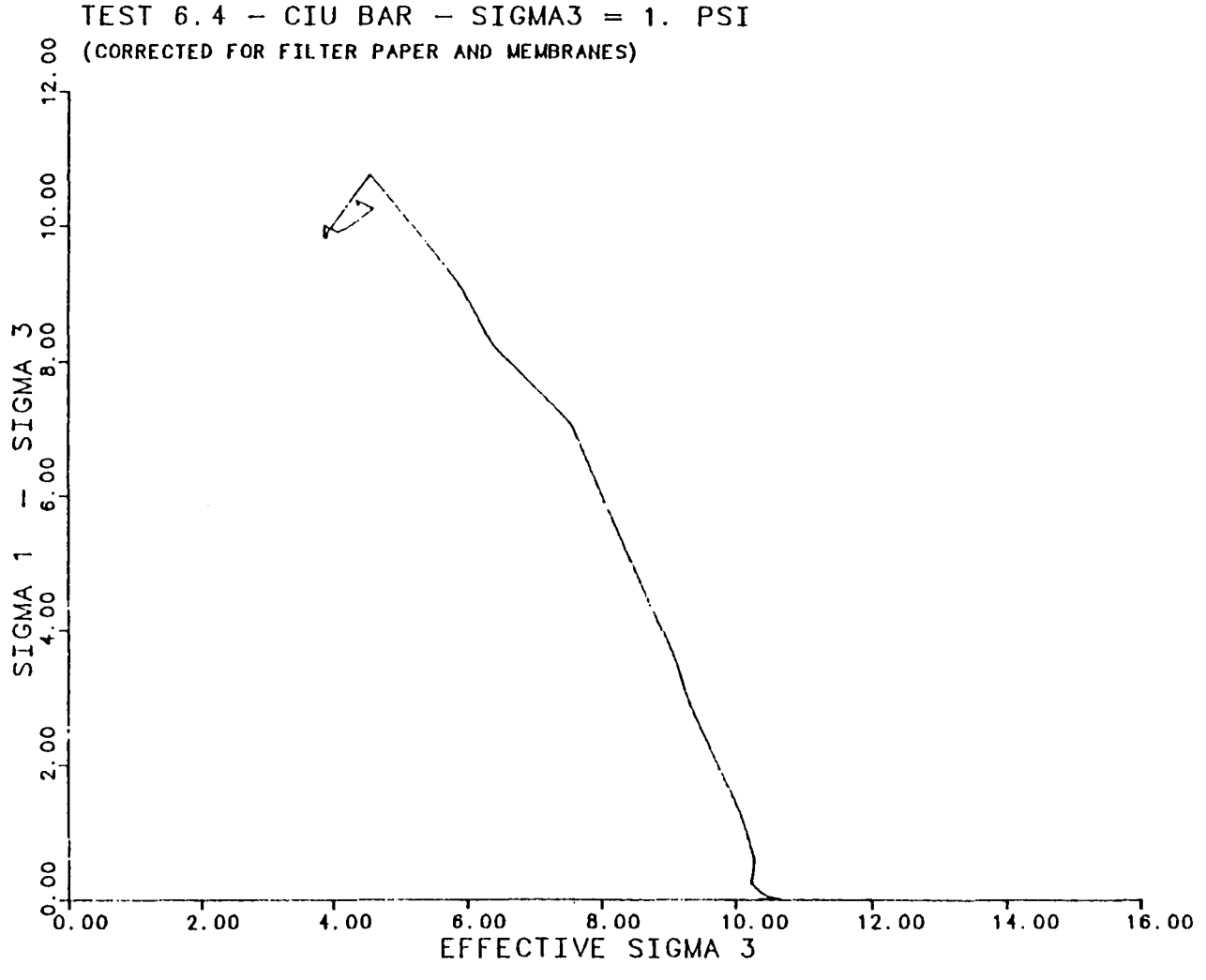

Fig. C.9 Effective Stress Path from Test 6.4 on Grey Clay from IH 610 and Scott Street

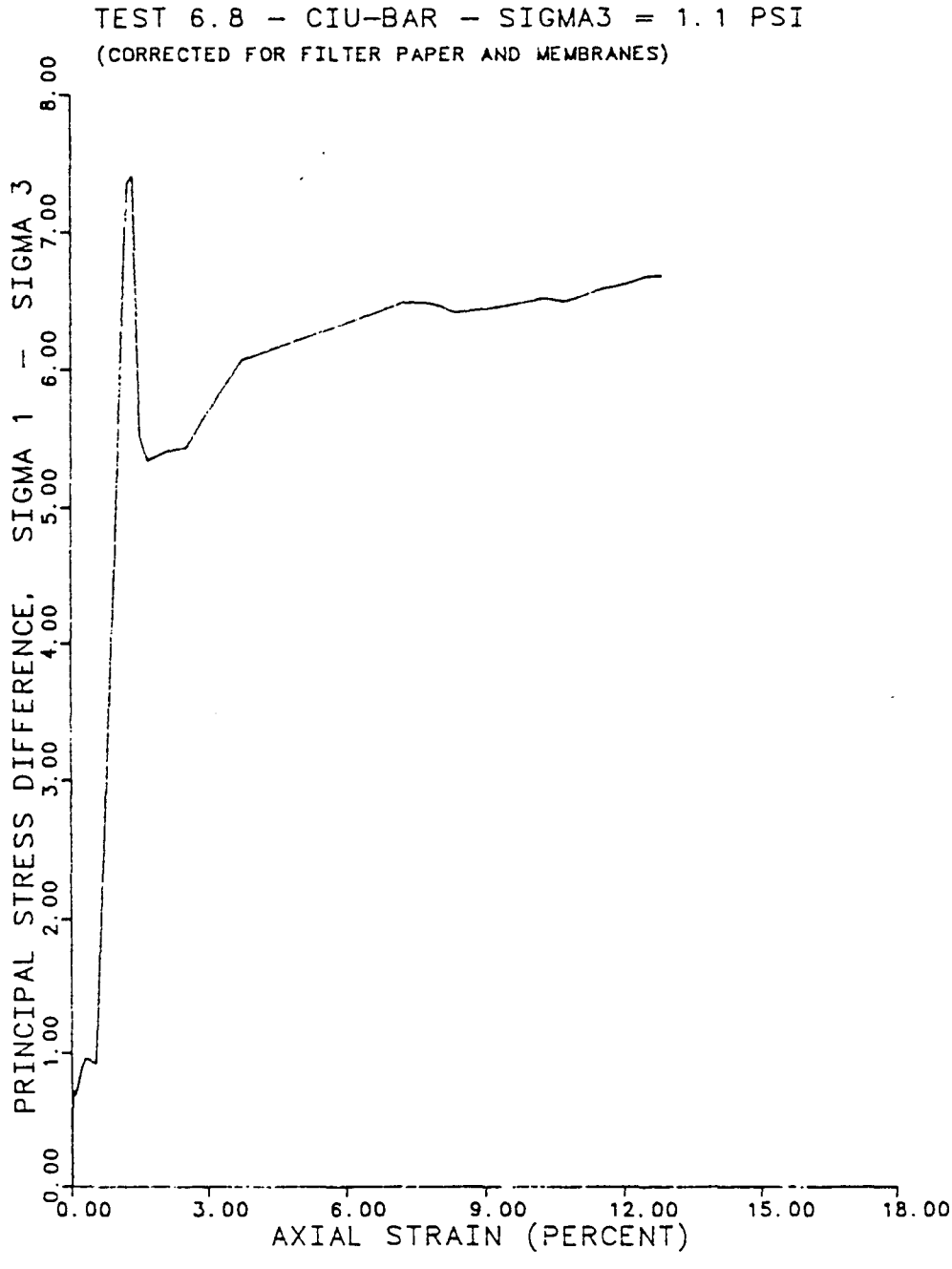

Fig. C.10 Stress-Strain Relationship from Test 6.8 on Grey Clay from IH 610 and Scott Street

Fig. C.11 Stress-Strain Relationship at Low Strains from Test 6.8 on Grey Clay from IH 610 and Scott Street

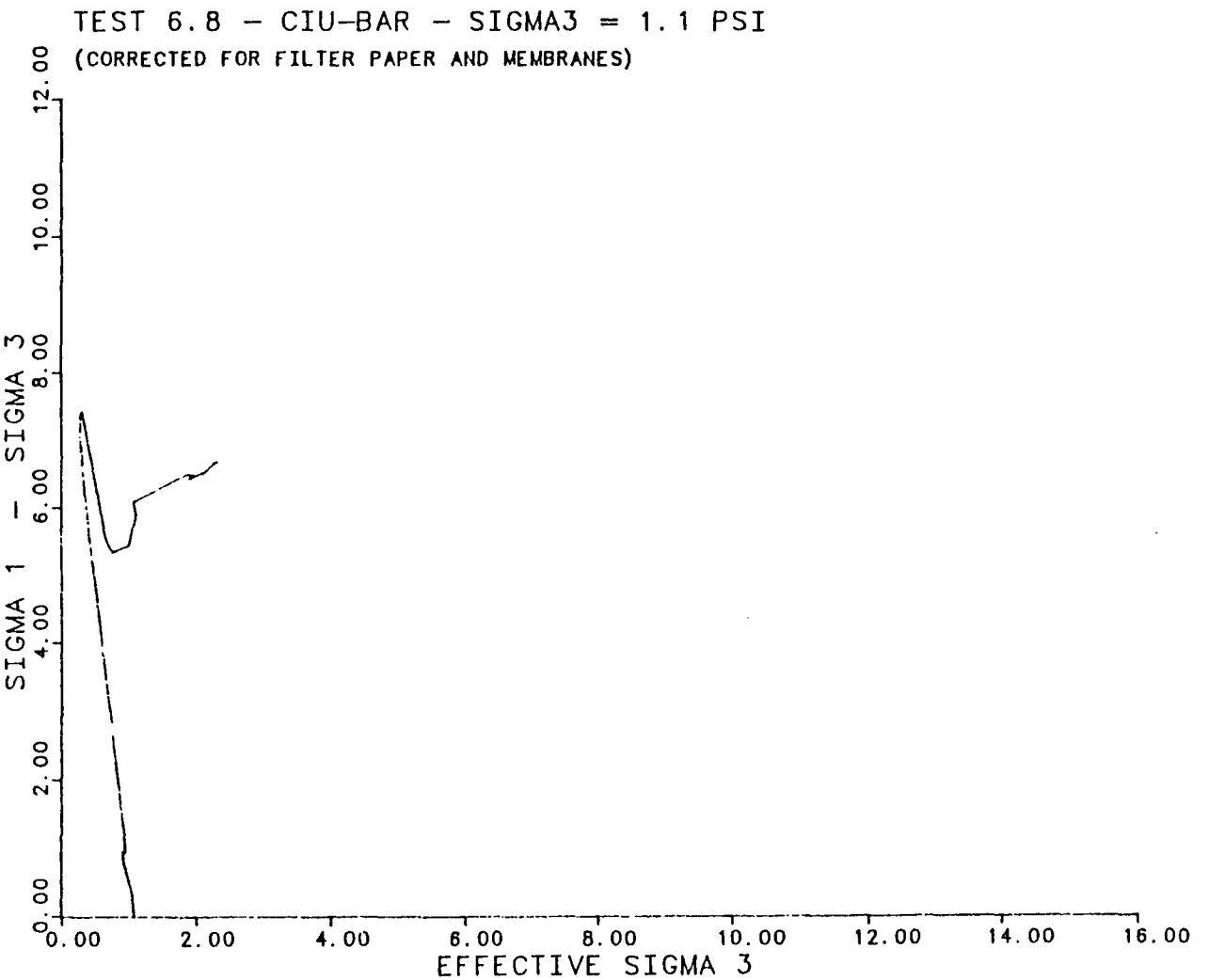

Fig. C.12 Effective Stress Path from Test 6.8 on Grey Clay from IH 610 and Scott Street

BIBLIOGRAPHY

ASTM (1982), Annual Book of ASTM Standards: Part 19, American Society for Testing and Materials, Philadelphia, 710 p.

Bishop, A.W. and Henkel, D.J. (1962), The Measurement of Soil Properties in the Triaxial Test, Second Edition, Edward Arnold, London, 1962, 228 p.

Bishop, A.W. and Gibson, R.E. (1963), "The Influence of the Provisions for Boundary Drainage on Strength and Consolidation Characteristics of Soils Measured in the Triaxial Apparatus," ASTM Special Technical Publication No. 361, pp. 435-451.

Blight, G.E. (1963), "The Effect of Nonuniform Pore Pressures on Laboratory Measurements of the Shear Strength of Soils," ASTM Special Technical Publication No. 361, pp. 173-184.

Bjerrum, L. and Simons, N.E. (1960), "Comparison of Shear Strength Characteristics of Normally Consolidated Clays," Proceedings, American Society of Civil Engineers Research Conference on Shear Strength of Cohesive Soils, pp. 711-726.

Carothers, H.P. (1965), "Engineered Foundations in Expansive Clay," Engineering Effects of Moisture Changes in Soils, Concluding Proceedings, International Research and Engineering Conference on Expansive Clay Soils, Texas A&M Press, College Station, Texas.

Chan, C.K. and Duncan, J.M. (1966), "A New Device for Measuring Volume Changes and Pressures in Triaxial Tests on Soils," University of California, Institute of Transportation and Traffic Engineering, Berkeley, California.

Deming, P.W. (1982), "Cyclic Loading of Clay Specimens in the Triaxial Test," M.S. Thesis, The University of Texas at Austin.

Duncan, J.M. and Seed, H.B. (1965), "Errors in Strength Tests and Recommended Corrections," Report No. TE 65-4, Department of Civil Engineering, University of California, Berkeley, Calif., 1965.

Gibson, R.E. (1953), "Experimental Determination of the True Cohesion and True Angle of Internal Friction in Clays," Proceedings, Third International Conference on Soil Mechanics and Foundation Engineering, Switzerland, 1953, Vol. I, pp. 126-130.

Holtz, W.G. and Lowitz, C.A. (1957), "Compaction Characteristics of Gravelly Soils," ASTM Special Technical Publication No. 232, 67 p.

Mitchell, J.K. (1976), Fundamentals of Soil Behavior, Wiley, New York, 422 p.

Paster, M. (1981), "Static and Cyclic Stress-Strain Behaviour of a Normally Consolidated Clay," M.S. Thesis, The University of Texas at Austin.

Skempton, A.W. (1954), "The Pore Pressure Coefficients A and B," Geotechnique, Vol. 4, No. 4, pp. 143-147.

Sowers, G.F. (1979), Introductory Soil Mechanics and Foundations: Geotechnical Engineering, Fourth Edition, MacMillan, New York, 621 p.

Stauffer, P.A. (1984), "An Examination of Earth Slope Failures in Texas," M.S. Thesis in progress, The University of Texas at Austin.

Tamez, E. (1957), "Some Factors Affecting the Dynamic Compaction Test," ASTM Special Technical Publication No. 232, 67 p.

Taylor, D.W. (1948), Fundamentals of Soil Mechanics, Wiley, New York, 700p.

Texas SDHPT (1978), Manual of Testing Procedures, Texas State Department of Highways and Public Transportation, Austin, Texas.

United States Bureau of Reclamation (1963), Earth Manual, First Edition revised, Washington, D.C., 783 p.

United States Department of Agriculture, Soil Conservation Service (1976), Soil Survey of Harris County, Texas.

United States Department of The Navy (1982), Design Manual: Foundations and Earth Structures, NAVFAC DM-7.2, Department of The Navy, Naval Facilities Engineering Command, Alexandria, Va., p.46.

Vaughan, P.R. (1977), Panel Discussion: Session 3, Proceedings, Ninth International Conference on Soil Mechanics and Foundation Engineering, Tokyo, 1977, Vol. 3, pp. 411-413.

Vaughan, P.R., Hight, D.W., Sodha, V.G., and Walbancke, H.J. (1978), "Factors Controlling the Stability of Clay Fills in Britain," Proceedings, Conference on Clay Fills, Institution of Civil Engineers, pp. 205-217.